Synthesis, Characterisation and *In Vitro* Studies of Metal Complexes of Some Selected Antimalarial Drugs

By

Peter Adewale AJIBADE

Department of Chemistry
University of Zululand
Private Bag X1001
KwaDlangezwa 3886

November 2005

Synthesis, Characterisation and *In Vitro* Studies of Metal Complexes of Some Selected Antimalarial Drugs

By

Peter Adewale AJIBADE (Student No.: 010001)

B.Sc. (Hons), M.Sc. Chemistry (Ibadan, Nigeria)

Being a thesis submitted to the Faculty of Science and Agriculture in fulfilment of the requirements for the award of the degree of

Doctor of Philosophy in Chemistry

of the

University of Zululand

Promoter: Prof G. A. Kolawole
Department of Chemistry
University of Zululand
Private Bag X1001
KwaDlangezwa 3886

November 2005

CERTIFICATION

This is to certify that this thesis is a record of original research carried out by Peter Adewale AJIBADE under my supervision at the Department of Chemistry, Faculty of Science and Agriculture, University of Zululand, South Africa.

Date

Supervisor
G. A. Kolawole
B.Sc. (Hons), M.Ed. (Evaluation), PhD (Ibadan)
C.Chem. FRSC (London)
Professor of Inorganic Chemistry
University of Zululand, RSA

DEDICATION

The memories of the heart bring double happiness. There is the joy of the original receiving and the joy of the present recollection. With heartfelt thanks, this work is dedicated to my wife, Benedicta A. Ajibade, my brother Rev. Fr P. A. Ajibade and my entire family and to those from whom I have learned.

Acknowledgement

I thank my supervisor, Prof G.A. Kolawole, for his invaluable contribution to the success of this study, for his guidance and support throughout the duration of the entire work and for his encouragement in the first instance to come and study at the University of Zululand. My thanks also go to Prof. N. Revaprasadu and other staff and colleagues in the department for efforts rendered in various ways and the moments we shared together and all my friends in the University especially Bayo, Precious, Mandisa, Zama, Samke, Mamakhethe, Lolo, Phumu and Gogo Rueben. I also thank the University of Zululand for giving me the opportunity to study here and use the university facilities.

I wish to thank Prof. Paul O'Brien, Head of the School of Chemistry, the University of Manchester, UK for hosting me in his group and for his constructive suggestions. I also thank other members of his group and staff, with special reference to Drs Madeleine Helliwell and James Raftery, for the crystallographic data collection and Joanna Woluska for the EPR data. I also wish to acknowledge Prof. Reto Brun of the Swiss Tropical Institute, Switzerland and his assistant, Marcel Kaizer for screening the complexes against isolates of *Plasmodium falciparum*. I wish also to place on record my gratitude to Mr. Boateng Dampte, my chemistry teacher in the secondary school who inspired me to love chemistry.

I express my sincere gratitude to the University of Ado-Ekiti, Nigeria for granting me leave to undertake this study and the entire staff and students of the Department of Chemistry, University of Ado-Ekiti. Special thanks to Prof. Akin Oyebode for giving

executive approval to the study leave and Prof. O. Olaofe, Dr. E. I. Adeyeye, Prof. Adegun and Niyi Afolabi for their assistance in various ways. I also thank the National Research Foundation (South Africa) and the Royal Society (UK) for financial support.

My heartfelt thanks goes to my parents, Chief and Mrs J. O. Ajibade for their prayer and concern, my brother Rev. Fr. P. A. Ajibade for his prayer, love and support, my uncle Mr Kayode Osho for financial support and every member of my family for their love and support. Most tenderly, I thank my wife Benedicta A. Ajibade for her love, prayer and most especially for her sacrifice in enduring three years of loneliness and cold nights. Your love and support is a driving force for me!

Abstract

This project deals with the synthesis, characterisation and *in vitro* studies of metal complexes of antimalarial drugs. The synthetic techniques were based on the modification of antimalarial drugs by the introduction of metal ions into the molecular structure of the drugs. Thirty two metal complexes derived from chloroquine, amodiaquine, trimethoprim, sulfadiazine, tetracycline and pyrimethamine have been synthesised using the following metal ions: Co(II), Cu(II), Zn(II), Mn(II), Ni(II), Pt(II), Pd(II), Co(III), Fe(III), Ru(III) and VO(II). The complexes were characterised by melting point / decomposition temperature, solubility, conductivity measurement, elemental analyses, UV-Vis and IR spectroscopy, mass spectrometry, magnetic susceptibility measurement and EPR. Six of the complexes and sulfadiazine ligand were also characterised by single X-ray crystal studies.

The complexes were screened *in vitro* against four isolates of *Plasmodium falciparum* at various stages of the parasites development. The results showed that three of the metal complexes, cobalt(III)amodiaquine, cobalt(III)quinacrine and iron(III)amodiaquine are more active *in vitro* against the parasites in comparison to chloroquine the first drug of choice for treatment of chloroquine falciparum malaria in Africa.

Contents

List of Figures

List of Tables

List of Abbreviations

DMSO	dimethysulfoxide
DMF	N,N′-dimethylformamide
en	ethylenediamine
CQ	chloroquine
CQB	chloroquine base
AQ	amodiaquine
TMP	trimethoprim
QNC	quinacrine
TCQ	tetracycline
SD	sulfadiazine
PRM	pyrimethamine
UV	ultraviolet
IR	infrared
NMR	nuclear magnetic resonance
TGA	thermo gravimetric analysis
MS	mass spectrometry
EPR	electron paramagnetic resonance
μ	Magnetic moment
B.M.	Bohr magneton

CHAPTER ONE

1.0 INTRODUCTION AND LITERATURE REVIEW

1.0.1 Introduction

Malaria infections are caused by intracellular parasites of the genus *Plasmodium* that are transmitted by anopheles mosquitoes (Figure 1). The mosquito is found in the region lying roughly between Latitudes 60 °N and 40 °S and in an environmental temperature of between 18 and 29 °C with suitable humidity. Despite more than a century of efforts to eradicate or control malaria, the disease remains a major and growing threat to public health and economic development of countries in the tropical and subtropical regions of the world (Figure 2) where 2.4 billion people, approximately 40% of world's population, live[1].

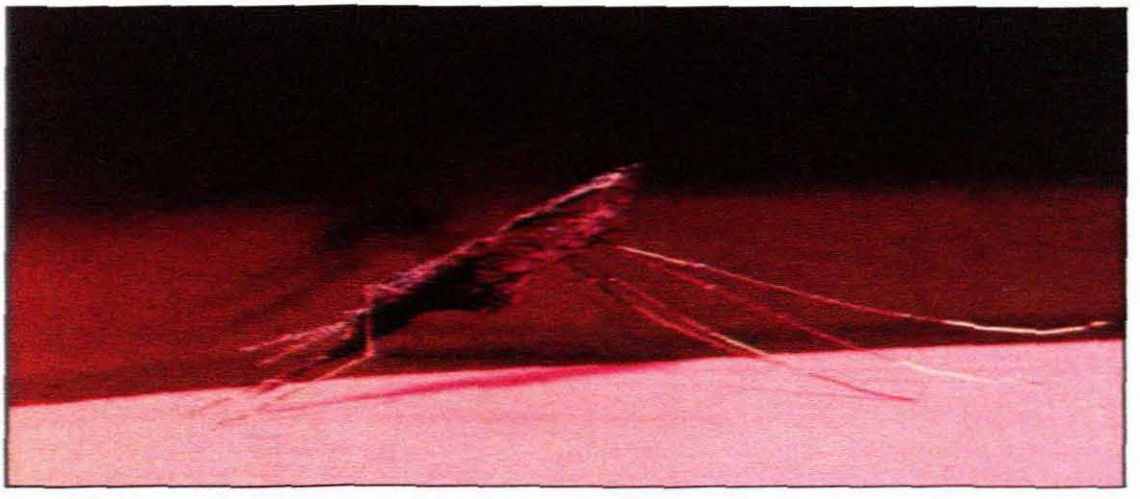

Figure 1: A female anopheles mosquito[2]

Malaria has been around since ancient times. The early Egyptians wrote about it on papyrus, and the former Greek physician, Hippocrates, described it in detail. It devastated invaders of the Roman Empire. In ancient Rome, as in other temperate climates, malaria

lurked in marshes and swamps. People blamed the unhealthiest in some areas on rots and decay that wafted out on the foul air, or, as the Italians were to say, "*Mal aria*" or bad air. In 1880, scientists discovered the real cause of malaria, the one-celled *Plasmodium* parasite, and 18 years later, they attributed the transmission of malaria to the anopheles mosquito[3].

There are an estimated 300-500 million cases, up to 2.7 million deaths and 44 million Disability Adjusted Life Years (DALYS) each year. The DALY provides a means to measure the burden that is more informative than crude measures of mortality and prevalence. It is fast becoming the standard used to compare the burdens of different diseases.

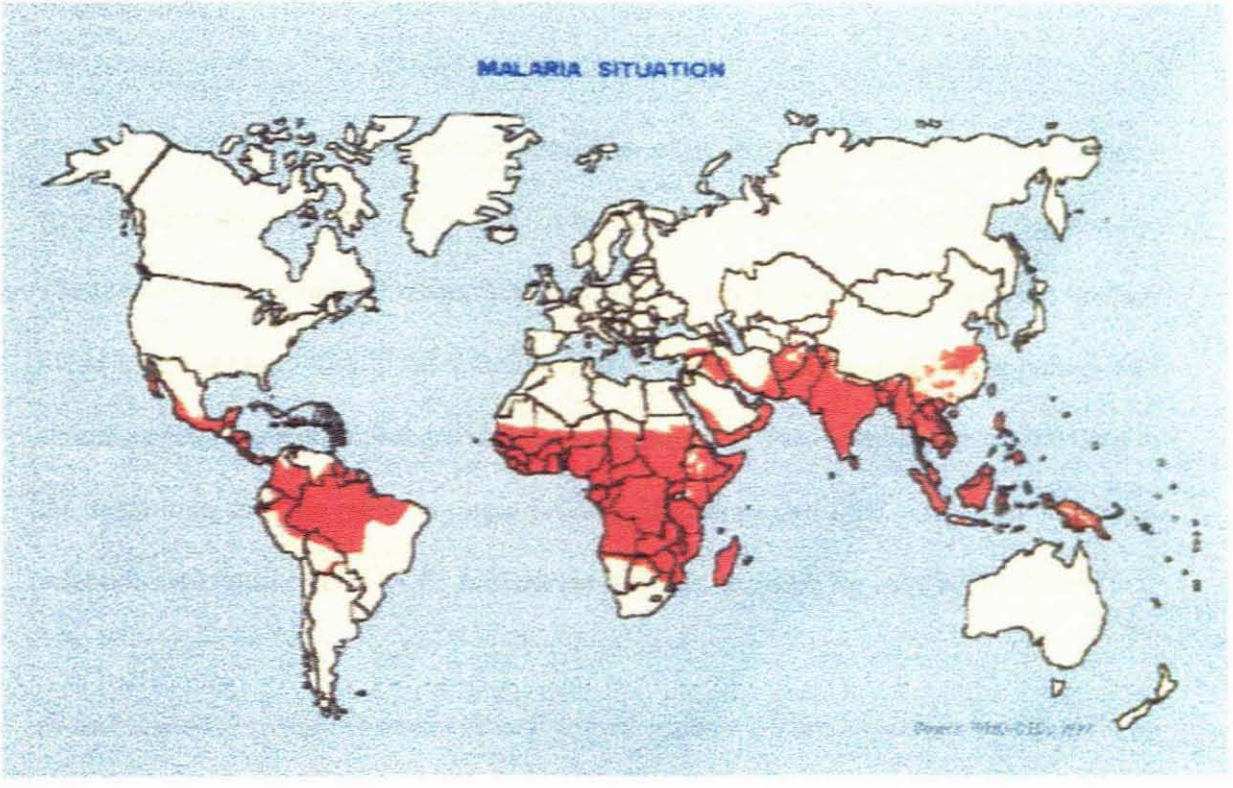

Figure 2: Geographical distribution of malaria (source: WHO)

The mortality levels are greatest in sub-Saharan Africa, where children under five years account for 90% of all deaths due to malaria. The economic devastation caused by malaria reflects in health-care costs, lost workdays and schooldays, and other direct and indirect costs. Retardation of the rate of long-term national, regional, and continental economic growth because of malaria has been appreciated only recently. In countries with endemic malaria, the annual economic growth rates over 25-year period were 1.5% lower than other countries. This implies that the cumulative effect of the lower annual economic output in a malaria endemic country was a 50% reduction in per capital GNP compared to non-malarious country. Recent studies suggest that the number of malaria cases may double in 20 years if new methods of control are not devised and implemented[4].

More than 100 different species of *Plasmodium* exist, and they produce malaria in many types of animals and birds, as well as in humans. Four species of the parasite, namely, *Plasmodium falciparum, Plasmodium malariae, Plasmodium vivax and Plasmodium ovale* infect humans. The differentiation of the species depends on the morphology and staining of the associated changes in the containing cells. Two or more species can live in the same area and can infect a single individual at the same time. The most important infections are those caused by *P. falciparum* and this accounts for over 90% of cases[5].

Plasmodium falciparum is responsible for most malaria deaths, especially in Africa. The infection can develop suddenly and produce several life-threatening complications. *P.*

vivax, the most geographically widespread of the species, produces less severe symptoms. Relapses can occur for up to 3 years, and chronic disease is debilitating. Once common in temperate climates, *P. vivax* is now found mostly in the tropics, especially throughout Asia. *Plasmodium malariae* infections produce typical malaria symptoms but also persist in the blood for very long periods, possibly decades, without ever producing symptoms. A person with asymptomatic *P. malariae* can infect others either through blood transfusion or mosquito bites. *P. malariae* has been wiped out from temperate regions, but it persists in Africa. *Plasmodium ovale* is rare, can cause relapses, and generally occurs in West Africa.

Malaria transmissions within humans are through the bites of females of certain species of anopheles mosquitoes. In rare cases, a person may contract malaria through contaminated blood, or a mother may infect a foetus during pregnancy. There are about 400 species of anopheles mosquitoes; only 60 of them transmit malaria under natural conditions, and only 30 are of major importance. The *Anopheles gambiae* complex and *Anopheles fenestus* are the most efficient vectors for *P. falciparum* transmission. The highest rates of sporozoites development are in *An. gambiae*, the species that is widespread throughout tropical Africa[6]. The factors that aid malaria transmissions are host immunity, the number (density), human-biting habits, and longevity of anopheline mosquito vectors. Malaria transmission is directly proportional to the density of the vector, the square of the number of human bites per day per mosquito, and the 10^{th} power of the probability of the mosquito surviving for one day[7]. Resistance to antimalarial drugs

and insecticides, the decay in public health infrastructures, population movements, political unrest, and environmental changes are also contributing to the spread of malaria.

1.0.2 Life Cycle of Malaria Parasite

The entire developmental life cycle of anopheles mosquito (Figure 3) was identified in 1948, half a century after the discovery of anopheles as the transmitting agent for malaria. In anopheles mosquito, *Plasmodium* reproduces sexually (by merging of the parasite's sex cells). In human, the parasite reproduces asexually (by sex division), first in liver cells and then, repeatedly, in red blood cells. The parasite undergoes development in the female's mosquito, which requires blood meal to mature her eggs. When it bites a human, it injects the primitive form of the malaria parasite called sporozoites into the circulating blood. The sporozoites moved to the liver where they develop to young parasites called merozoites after about twelve days. The merozoites released into blood circulation to infect red blood cells[8]. The parasites in the red blood cells develop into two forms, sexual and asexual forms. The sexual form called gametocytes (male and female) goes into a biting mosquito and develops to sporozoites, which infect humans. The asexual forms develop in the individual where it causes clinical malaria disease.

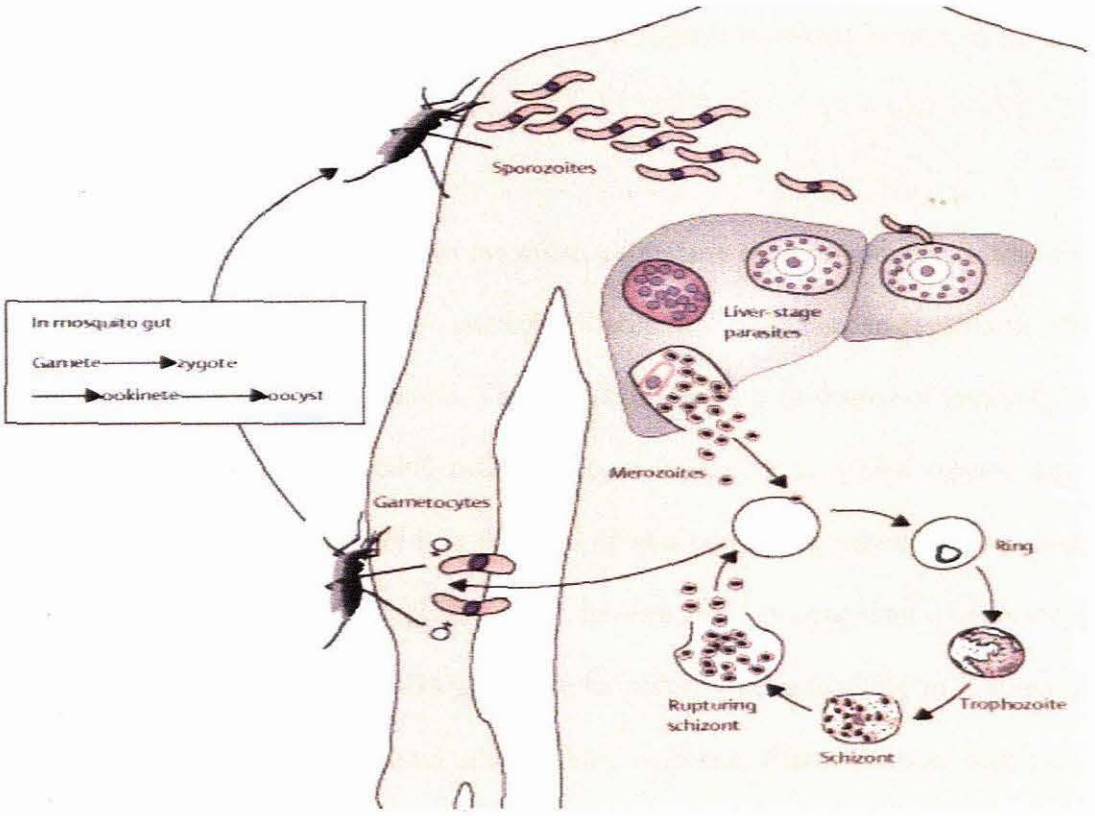

Figure 3: Life cycle of malaria parasite[9]

1.0.3 Epidemiology

Malaria is defined variably as acute febrile illness in endemic areas, with or without parasitaemia, depending upon local capability for parasitological confirmation. Malaria infection can result in asymptomatic parasitaemia; clinical malaria (febrile episodes, parasitaemia); severe malaria (anaemia, neurological syndromes) and mortality[10]. Acute severe illness can lead to cerebral malaria, with high fatality rate. The ominous signs for children with acute malaria are coma, severe anaemia and respiratory distress. Pregnant women with malaria are at risk of hypoglycaemia due to parasite metabolism in red blood cells. The impacts of malaria on pregnant woman and her foetus were recently

established. In particular, low birth weight and subsequent increased infant and childhood mortality result from infected placenta[6].

The epidemiological patterns govern the effect of malaria on a community. Malaria in a population may be either stable or unstable. Stable malaria occurs in regions in which there is constantly repeated infection. The population has a high degree of immunity and epidemics do not occur. Unstable malaria occurs in regions in which transmission is intermittent; for example, where it is seasonal or in a population inadequately protected by drug suppression in entomological control. In such areas, the population has a varying degree of immunity and epidemics are liable to occur. The endemicity in a given area depends on the insect transmission and the host response. Endemic areas classified as hypoendemic, hyperendemic, mesoendemic and holoendemic depending on the findings in the population concerning parasitaemia and spleen rates in relation to age groups.

1.0.4 Immunity

Immunity in malaria is due to cellular, humoral, and racial or inherited factors in the blood. Research show that the concentration of gamma globulin in the newborn African infant is considerably higher than corresponding values reported in Europe. Furthermore, in "stable" areas, malarial infection contributes significantly to the maintenance of high G-globulin levels in all subjects after the first years of life. G-globulin prepared from the sera of adults immune to malaria has a consistent therapeutic effect when administered to West African children suffering from heavy *Plasmodium falciparum* infection[11].

The immune status of the individual and population plays the most important role in the clinical response to infection and transmission. Maternally derived antibody offers limited and short-duration protection to the newborn[12] in heavily endemic areas; over 30% of children acquire parasites by 3 months of age. Researchers have identified humoral antibodies to sporozoites, intra-hepatic parasites, merozoites, malaria toxins, parasite antigens on infected red blood cells (RBCs), intra-erythrocytic parasites, and, within the mosquito, to parasite fertilization. Cell-mediated immunity plays a role in the liver and RBC invasion and parasite development. Even with repeated infection, protective immunity is incomplete. Individuals in malarious areas frequently have parasitaemia and antibodies without symptoms, and this is age-dependent. There is a recent evidence for a genetic basis for antibody and cellular responses to malaria proteins[13].

It is now generally accepted that acquired malarial immunity depends upon the preserve of circulating antibody, which is associated with the 7S G-globulin fraction (IgG). The possible role of a B-cell antigen in the hyper-gammaglobulinemia associated with malaria and trypanasomiasis was discussed[14]. An indirect florescent antibody technique has been evolved which has demonstrated the presence of malarial antibodies in the sera of infected persons. It has also been demonstrated that an indirect haemagultination test could serve as a measure of protective immunity[15]. The fluorescent antibody technique has also revealed that a number of different species of mammalian plasmodia possess common antigen. This is of interest in view of the finding that East African strains of *P. falciparum* were found to be responsive to treatment with "immune" West African G-

globulin. In contrast, gamma globulin from West African failed to show marked protective activity in chimpanzees infected with drug-resistant strain of *falciparum* malaria from South East Asia. Three main types of *P. falciparum* antigens: labile, resistant and stable are described by McGregor and Wilson[16] by investigating their storage properties. Botchier and Cohen[17] showed that chronic malarial infection leads to synthesis of antibodies with wide cross reactivity, and felt that this might be encouraging from the point of view of malaria vaccine production.

The mechanism of defence of malaria, the cellular and the humoral, are probably interdependent. It is postulated that certain hereditary red cell traits protect against the lethal effects of malaria. These include haemoglobin S, haemoglobin C, and haemoglobin E, thalassaemia and glucose-6-phosphate dehydrogenase deficiency. The only convincing evidence to date concerns sickle cell (SS) haemoglobin and G-6-phosphate deficiency. The high incidence of a gene lethal in its homozygous expression (SS) in many parts of tropical Africa was difficult to explain. But Beat[18] and Allison[19] independently suggested that this might be due to selective advantage against the lethal effects of *P. falciparum* malaria and the loss of hormonal genes due to this cause outweighing the loss of the S gene in sickle-cell anaemic patients.

1.0.5 Treatment of Malaria

The ideal drug for treating malaria should be active at all stages of the life cycle of all plasmodia strains, act selectively on the parasite and be easy to employ on all individuals without side effects. None of the available drugs meets this ideal. For this reason,

treatment of malaria requires a perfect understanding of the mode of action and the advantages and disadvantages of each drug. There are two main groups of antimalarial drugs based on their point of impact. They are schizontocides and gametocytocides.

The schizontocides act on the endoerythrocytic forms of *P. falciparum*. They combat the clinical symptoms and have a prophylactic effect when administered in sufficient amounts. The gametocytocides act on the potentially sexual forms, the gametocytes, which are capable of ensuring transmission of the disease to anopheles thus maintaining malarial endemicity. They also combat hepatic tissue forms, thus protecting the individual against recrudescence induced by some species such as *P. ovale* and *P. malariae*. Unfortunately, they are poorly tolerated, dangerous and difficult to manage.

1.1.0 Classification of Antimalarial Drugs

Antimalarial drugs are generally classified on three main bases: biological, chemical and combination therapy.

1.1.1 Biological Classification

Antimalarial drugs are broadly grouped into five classes according to the life cycle (Figure 4) of the parasite on which they act[20].

- ***Tissue Schizontocides (Casual prophylaxis)***

They act on the hepatic cells (pre-erythrocytic stage) to prevent the invasion of the red blood cells e.g. primaquine, proguanil, cylcoguanil embonate, pyrimethamine, trimethoprim, some sulphonamides (sulfalene, sulfadoxine,

sulfadiazine and sulfamethoxy-pyridiazine) and sulphones (dapsone and acedapsone) and tetracycline in combination.

❖ ***Tissue Schizontocides (anti-relapse)***

They act on secondary tissue forms (exo-erythrocytic stages of *P. vivax* and *P. ovale*) to achieve radical cure e.g. primaquine, pamaquine

❖ ***Blood Schizontocides (Clinical Cure)***

They act on red blood cells (erythrocytic stage) commonly associated with clinical malaria. They usually act on the sexual erythrocytic forms of *P. vivax*, *P. ovale* and *P. malariae*, but not directly on the mature gametocytes of *P. falciparum*. Examples are quinine, chloroquine, amodiaquine, mefloquine and trimethoprim/sulfadoxine (e.g. Fansidar).

❖ ***Gametocytocides***

These drugs destroy all sexual forms, including those of *P. falciparum* and developmental stages of malarial parasites, e.g. primaquine.

❖ ***Sporontocides***

They prevent or inhibit the formation of oocysts and sporozoites in anopheles mosquitoes that fed on carrier of gametocytes. They interfere with the transmission of malaria though they may have no direct action on gametocytes in the human host e.g. proguanil, pyrimethamine.

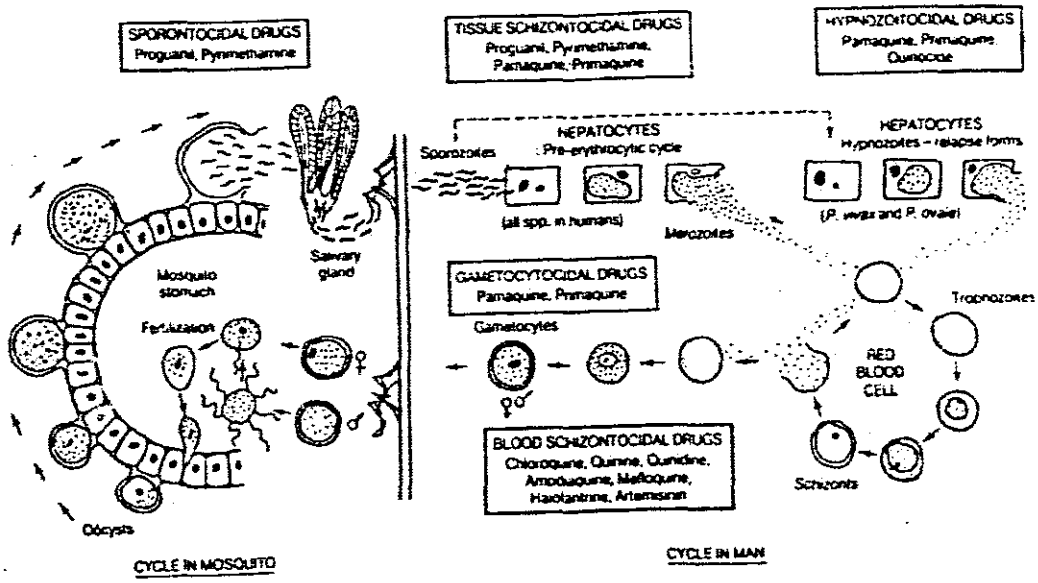

Diagram of antimalarial compounds at different stages of the development of the malaria parasite in Anopheles mosquitos and in the human host [Redrawn by David Warhurst after David Payne]

Figure 4: Antimalarial drugs at the different stages of the development of the malaria parasite[21]

1.1.2 Chemical Classification

Chemically antimalarial drugs are classified as:

- 4-aminoquinolines
- 8-aminoquinolines
- Dihydrofolate reductase inhibitors
- Sulphonamides
- Sulfones
- Antibiotics
- Quinine methanol
- Phenanthrene methanol
- Pyridine methanol

- ❖ Sesquiterpene lactone
- ❖ Acridines
- ❖ Miscellaneous compounds.

1.1.3 Combination Therapy

Antimalarial combination therapies are aimed at increasing the efficacy, shorten duration of treatment, hence increasing compliance, and decrease the risk of resistance of parasites to drugs arising from mutation during therapy. The notion that combination regimens might reduce build-up of resistance is based on work done with mycobacterium infection. The most common antimalarial combination drugs are listed below:

- ❖ Pyrimethamine-Sulfadoxine
- ❖ Pyrimethamine-Sulfadiazine
- ❖ Pyrimethamine-Sulfadoxine-Mefloquine
- ❖ Quinine-Pyrimethamine-Sulfadoxine
- ❖ Quinine-Tetracycline
- ❖ Chloroquine-Doxycline

1.1.4 Structure of Some Antimalarial Drugs

4-Aminoquinolines

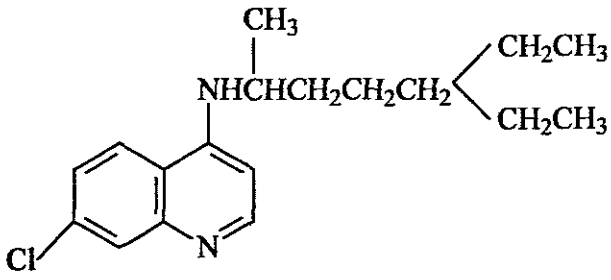

1. Chloroquine

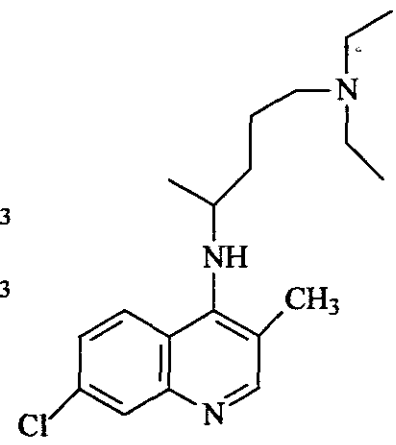

2. Sontoquine

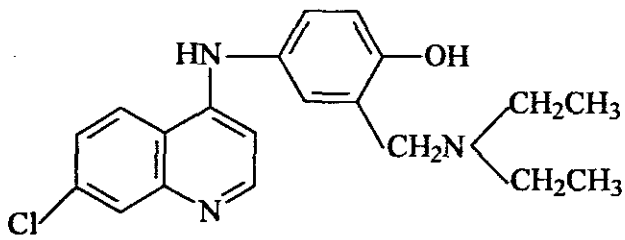

3. Amodiaquine

9-Aminoacridine

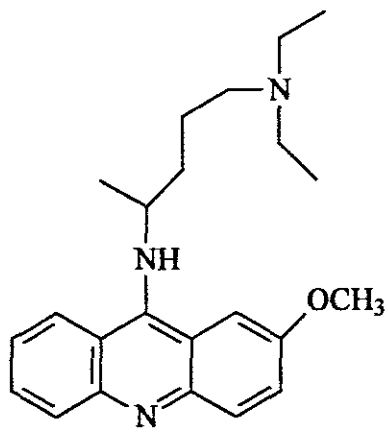

4. Mepacrine

8-Aminoquinolines

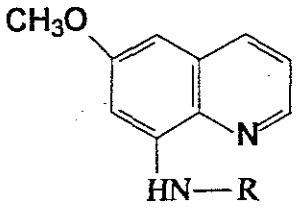

R= —CH(CH$_2$)NH$_2$
|
CH$_3$

5. Primaquine

R = —(CH$_2$)$_5$NHCH(CH$_3$)$_2$

6. Pentaquine

R= —CH(CH$_2$)$_3$N(CH$_2$CH$_3$)$_2$
|
CH$_3$

7. Pamaquine

Dihydrofolate Reductase Inhibitors

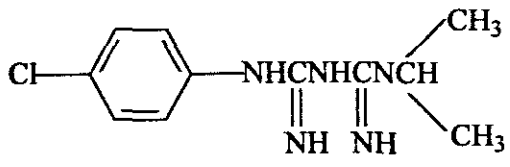

8. Proguanil

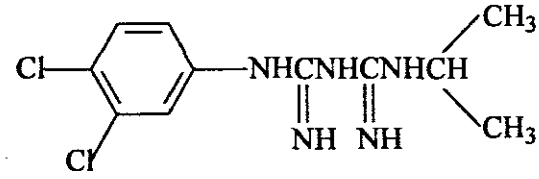

9. Chloroproguanil

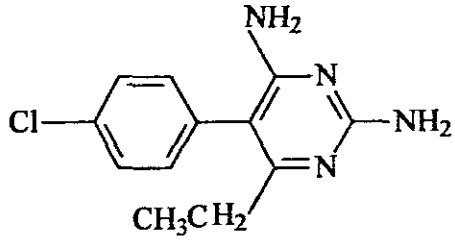

10. Pyrimethamine

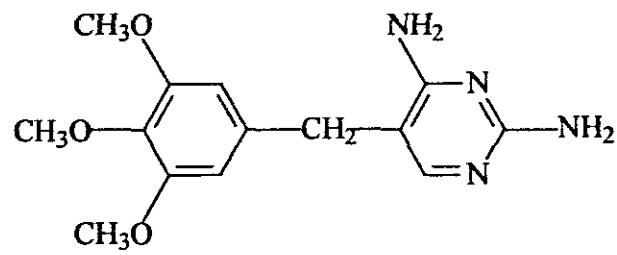

11. Trimethoprim

Sulfonamides

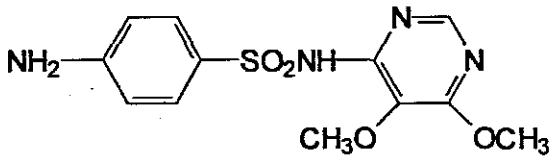

12. Sulfadoxine

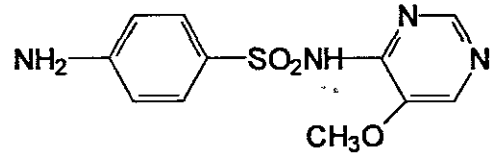

13. Sulfalene

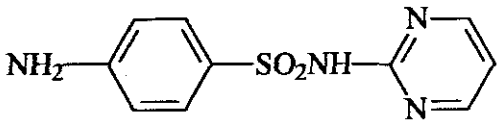

14. Sulfadiazine

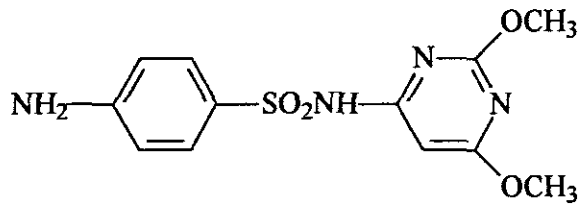

15. Sulfadimethoxine

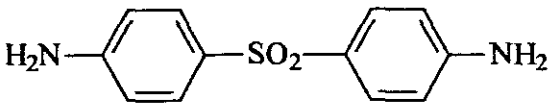

16. Dapsone

Antibiotics

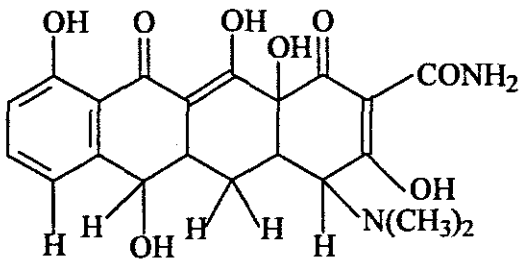

17. Tetracycline

Quinoline-methanol

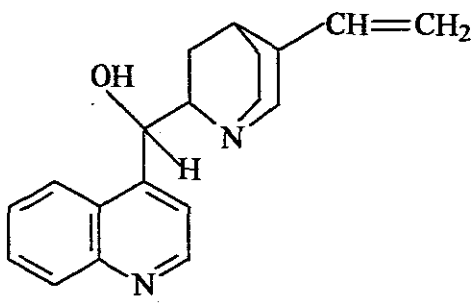

18. Quinine

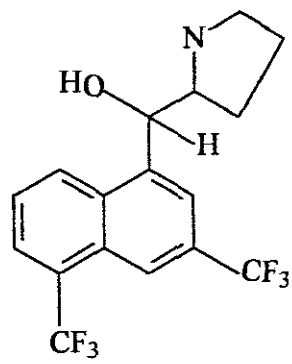

19. Mefloquine

Phenanthrene Methanol

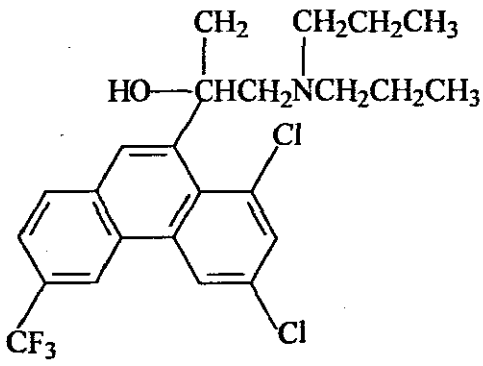

20. Halofantrine

Sesquiterpene lactones

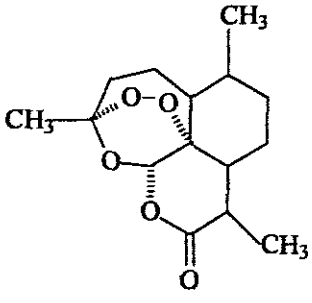

21. Qinghaosu (Artemisinin)

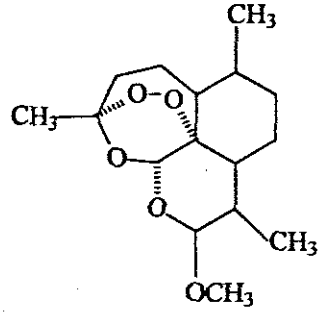

22. Artemether

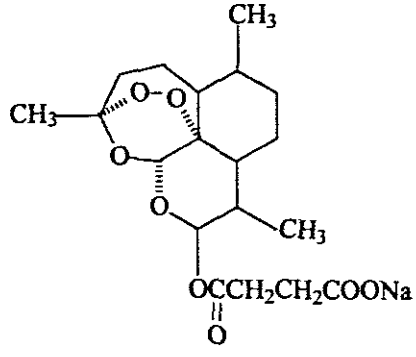

23. Sodium artesunate

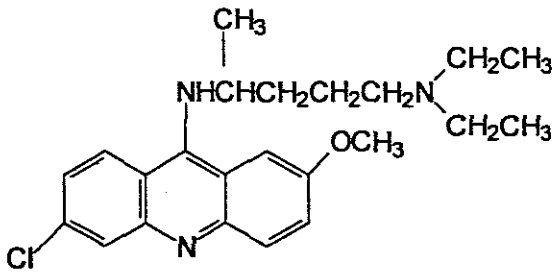

24. Acridines

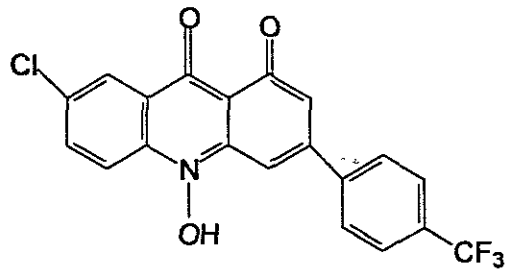

25. Floxacrine

1.2.0 Antimalarial Chemotherapy: A Chemical Perspective

The benzene ring occurs in the molecular structure of almost all antimalarials. In some instances, atoms other than carbon, may replace one or more of the carbon atoms of the benzene ring to form a heterocycle. The heteroatom of importance in the chemistry of antimalarials is nitrogen. Thus, pyridine and quinoline are bases of an important group of antimalarials.

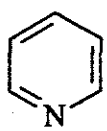

Pyridine

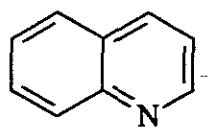

Quinoline

Other polycyclic compounds on which a number of antimalarials are built are acridine and phenanthrene.

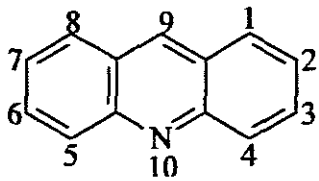

Acridine

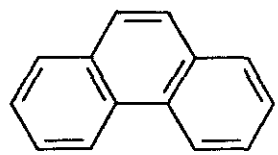

Phenanthrene

Three groups of antimalarials are also built on non-cyclic structures. These are the biguanides, the sulfones, and the sulfonamides.

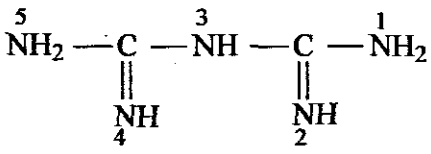

Biguanides

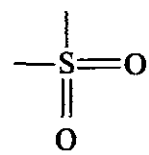

Sulfones

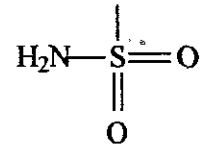

Sulfonamides

The existing antimalarial drugs are described in relation to their chemical structure and their biological activity.

Cinchona Alkaloids

Quinine (**18**), the most important compound of this group, has a complex chemical structure composed of the quinoline ring (with a methoxy group at the 6 position), the quinolidine complex ring with an attached vinyl group and connecting link in the form of a hydroxylated methylene group. Any alteration in the chemical structure of quinine changes the pharmacological action of the compound. Although the correct structure of quinine was suggested in 1908, Woodward and Doering[22] achieved synthesis of this compound only in 1944. However, when evidence showed that the quinoline nucleus could be a useful component of an antimalarial drug[23] and Woodward and Doering method of synthesis was such that this was not a commercially viable method to meet a supply of reasonably priced synthetic quinine, chemists explored less complex synthetic routes. A complete stereoselective synthesis was achieved by Balkovec, *et al.*[24] only in 2001.

8-Aminoquinolines

The search for synthetic antimalarials led to the replacement of one methyl group of methylene blue by dialkylaminoalkyl side chain and the demonstration that it had a high activity on avian malaria led to the discovery of pamaquine (7)[25]. In the first synthetic antimalarial, the 6-methoxyquinoline was combined with the basic side chain. Although the 6-methoxy substituent on the quinoline nucleus is not essential for high activity, all of the clinically useful 8-aminoquinolines (pamaquine, rhodoquine, pentaquine (6), isopentaquine, primaquine (5) and quinocide) contain it. Only primaquine is now widely used mainly as a gametocytocides and antirelapse drug. The compounds may produce adverse side effects such as pain and haemoglobin anaemia and these, together with the need for frequent dosage, limit their value as prophylactic agents (i.e. as sporontocidal agents). A single dose of primaquine given to the host totally inhibits the sporogonic malarial cycle in the vector[26].

9-Aminoacrinides

The replacement of the quinoline ring of pamaquine by acridine in the hope of decreasing the toxicity and prolonging the action of the new compound, which was the best of some 12 000 compounds tested by German scientists between the two World wars, led to the synthesis of mepacrine (4)[27]. Although the quinoline ring of pamaquine had been expanded to form acridine, the aminoalkylamino side chain of pamaquine was found to be essential for activity. The presence of a methoxy group and of a chlorine atom endowed the compound with other desirable properties. Because the hydrogen atom assumes two alternative positions in the molecule, mepacrine has two structurally

isomeric forms, which exist in a dynamic equilibrium. Mepacrine was of unquestionable value during the 1940s, when quinine was not available; it is today obsolete, wholly replaced by other compounds.

4–Aminoquinolines

The presence of quinoline ring in the structure of quinine and mepacrine as well as the known therapeutic properties of 8-aminoquinolines were the logical precursors of further studies in antimalarial compounds and those with the basic dialkylaminoalkyl side chain in the 4 position showed some promise. Eventually two of them, chloroquine (**1**) and sontoquine (**2**),[28] were selected for further trials in North Africa. The Germans, on the ground that it was less toxic, gave the second preference. Chloroquine proved to be the most effective and least toxic among them. It contains the same alkyl chain as mepacrine but differs from the latter in having a quinoline instead of an acridine nucleus and lacking a methoxy radical. Further work on a wide variety of compounds was undertaken in the course of the American Wartime Survey[29]. All of the clinically useful drugs of this series have the chloro substituents at position 7, which seems connected with their specific antiplasmodial action. Amodiaquine (**3**), another member of this group, has a structural formula in which an anilino group replaces the alkylamino side chain. It was synthesised by Burckhalter, *et al.*[30] Its manner of antimalarial action is equal to that of chloroquine on strains of *P. falciparum* resistant to chloroquine. Amodiaquine base is less bitter than its salts and this is of interest in paediatric practise.

There are well over 200 derivatives of 4–aminoquinoline with varying degrees of antimalarial activity[31]. Among these, sontoquine is less toxic than chloroquine but also less active than some others are. Hydroxychloroquine has a lower chronic toxicity but all of them, including cycloquine, have little advantage over chloroquine. French chemists produced variation on the chloroquine side chain with the intention of extending the duration of the schizontocidal effect. This gives a series of bis-quinolylpiperazines of which amopyroquine, a pyrrolidine analogue of amodiaquine, is effective by mouth and parenterally against *P. falciparum* and *P. vivax* in humans. It can be a substitute for amodiaquine in intramuscular administration. The emergence of strains of *P. falciparum* resistant to chloroquine has stimulated interest in new analogues of the 4–aminoquinolines.

Biguanides

Research on new antimalarial drugs carried out in Britain during the Second World War[32] showed that sulfonamides have some antimalarial action. Thus, it was felt that these compounds could be introduced in other chemical structures. It was also thought that the activity of mepacrine was due to competition with riboflavin for some plasmodia enzyme systems. Pyrimidine derivatives carrying the dialkylamino groups (characteristic of mepacrine and pamaquine) were prepared which gave rise to a long and ingenious series of modifications. Each of the subsequent compounds was monitored for antiplasmodial actions. Results showed that while a pyrimidine ring provided a convenient means for assessing all the possible relationship between structure and activity, a ring system was not essential for activity. This led to the development of the

biguanide molecule as necessary structural framework around which active drugs might be prepared. Variations in the aryl substituents and in the terminal alkyl groups were introduced. Two compounds in which a benzene ring linked to a simple isopropyl amino group, through two amidine groups, proved to be more active.

The highest antiplasmodial action was found in proguanil (**8**), in which a biguanide chain has a cholorophenyl ring and a simple alkyl group (isopropyl) attached at each end. It was more active than quinine on avian malaria and had little toxicity in laboratory animals. It acted as antimalarial agent by interfering with the nuclear division of its erythrocytic cycle through an inhibitory action of dihydrofolate reductase[33]. Proguanil is one of many plasmodicidal drugs of this series. The 3,4–dichlorobenzene analogue yielded chloroproguanil (**9**), which was more active than proguanil. The bromo analogue of proguanil also had high activity and a more persistent action because of its less rapid excretion. A number of other compounds such as nitroguanil, a relative of guanylurea, were prepared and showed a degree of activity but less than proguanil.

Proguanil exerts its antiplasmodial action indirectly through a metabolite produced by the host tissues. In human 60% of the parent compound passes through urine, 30% as triazine. Chloroproguanil is also metabolised to a triazine. The biologically active metabolite of proguanil is cylcoguanil, which bears a close structural relationship to pyrimethamine. The value of cylcoguanil, the dihydrotriazine metabolite of proguanil, was explored by Thompson, *et al.*[34] who developed a long acting injectable preparation consisting of the pamoic acid salt (embonate) of the parent compound. The prolonged

action of this repository compound is attributable to the diffusion of the active portion of it (cylcoguanil) from a depot at the site of injection. Results showed that up to 50 % of the injected drug remains for two weeks and small amounts could be for months. However, absorption of the drug depends on the particle size of the preparation and on the degree of local reaction to it.

Diaminopyrimidines

Falco[35] and his colleagues in the USA discovered an additional potent group of pyrimidines that proved to have a pronounced antagonistic effect on folic acid (pteroylglutamic acid) in cultures of lactobacillus. The close structural relationship between 2,4–diamino–5–parachlorophenoxypyrimidine and the biguanide in their biologically active cyclic form led to the proliferation of a variety of allied compounds; those with a 5–phenyl substituent were the most active. Substitution of an alkyl group in 6 position of the pyrimidine also increased the activity and, in the case of 5–parachlorophenyl derivatives, a high peak of antiplasmodial activity was obtained in animal trials with the 6–ethyl compound, given the generic name pyrimethamine (**10**).

Pyrimethamine and the active metabolite of proguanil have structural analogy. Their antiplasmodial effect is due to the inhibition of dihydrofolic reductase, an enzyme that is essential for folate synthesis by the parasite, a process involved in the early formation of nucleic acids. Pyrimethamine proved to be many times more active than proguanil. The basis for selective action of pyrimethamine is differential binding to dihydrofolic reductase in different species of plasmodia and the mammalian hosts and the

extraordinary sensitivity to this action of the nuclear division of the malaria parasite at the time of the development of schizont in the erythrocytes and in the liver tissues. Pyrimethamine and proguanil are plasmodistatic rather than plasmodicidal drugs, leaving the elimination of the parasites whose growth are arrested to the natural defence mechanisms of the body.

The development of pyrimethamine was a brilliant feat of organic synthesis guided by biochemical considerations and (as some authors stressed) closer to Ehrlich's "magic bullet" than any other antimalarials[36]. Several insoluble salts of pyrimethamine have been prepared with the aim of obtaining extended action. Additional chemical modifications of the 2,4–diamino–5–benzylpyrimidine structures led to the production of a 3,4,5–trimethoxybenzyl derivative known as trimethoprim (**11**), which showed a high degree of inhibition of bacterial dihydrofolate reductase and only a slight decrease in binding to the mammalian. Trimethoprim alone has activity against certain species and strains of human plasmodia, but it is less effective than pyrimethamine. Host factors appear to play a part in the action of this compound with other antimalarials

Sulfones and Sulfonamides

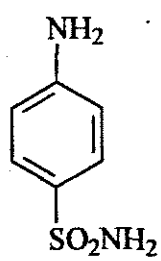

26. ***Sulfanilamide***

Two types of compounds can be derived by substitution of the sulfonamide group or the amino group in sulfanilamide. The most active sulfonamides belong to the first type, the amide group being replaced by a group with heterocyclic ring. Some members of this series include sulfadiazine (**14**), sulfadimidine and sulfamethizole. Other compounds of this type were then developed that were found to strongly bind to plasma proteins and very slowly excreted; they are sulfamethoxy-pyridiazine, sulfalene (**13**), sulfadimethoxine (**15**) and sulfadoxine (**12**)[37].

The second type, in which the amino group is masked, needs to activate in the body by removing the substituent groups since the free amino group is essential for antibacterial action. These compounds split off in the intestine and the active substance is slowly liberated. The antiplasmodial action of sulfonamides was reported as early as 1937,[38] and many derivatives of these compounds were used with varying success against human malaria and experimentally in avian, rodent and simian infections. The slow rate and short duration of action and the need for high and potentially toxic doses were responsible for the suspension of these drugs. However, the advent of resistance of *P. falciparum* to 4–aminoquinolines in the 1960s has revived the interest in the sulfones and sulfonamides.

The sulfonamides of interest in the management of malaria are the long-acting compounds with a half-life in the blood of between 60 and 200 hours. Examples are sulfadiazine, sulfadimethoxine, sulfamethoxy-pyridiazine, sulfadoxine and sulfalene. The value of these drugs stems from the fact that they obviate the need for frequent

administration. The series of sulfones is represented by 4,4–diaminodiphenylsulfone (e.g. dapsone (**16**)). Several derivatives of dapsone were developed recently but there is no evidence that they are significantly better than the parent compound. The results of the experimental treatment of human malaria transmitted to owl monkeys showed that combination of sulfonamide such as sulfadiazine with pyrimethamine enhances the action of the latter 32 folds. In addition, the action of sulfadiazine is enhanced hundred folds when infection is by strains not resistant to either of the two-drugs[39]. In contrast to this result, the activity of the same drug combination on strains resistant to pyrimethamine was often disappointing. It is likely that this might occur in cases of falciparum malaria in man when the infecting strain is highly resistant to antifolates drugs. This is in accordance with the finding that sulfonamides and sulfones have modest schizontocidal action against *P. falciparum* when used alone. At present, the combination of long-acting sulfonamides with antifolic compounds such as pyrimethamine is widely used for treatment of falciparum malaria resistant to 4–aminoquinolines.

Antibiotics

Antibiotics are chemicals, extracted from organisms (such as moulds, bacteria, and yeasts), that inhibit growth or destroy other microorganisms and used to treat many diseases in human and animals, and in small amounts, to speed the growth of poultry and livestock. Antibiotics can function in many ways to prevent the growth or to destroy a disease-causing organism. Since the discovery of penicillin in 1928 by Chain and Flory (results published in 1941),[40] several antibiotics have been isolated, purified and synthesized. Among them, the tetracyclines are a family of closely related antibiotics,

first obtained from *Streptomycin aureofaciens*. More compounds are still being added to the group of tetracyclines (**17**). The classification of antibiotics is complex and controversial. Their modes of action are very specific, following three main mechanisms of operations: inhibition of synthesis of bacterial wall, increased permeability of cytoplasmic membranes, and interference with intracellular protein or nucleic acids synthesis. There is some correlation between the mode of action and the general spectrum of activity of antibiotics[41].

In 1952, Coatney and Greenberg had listed 31 antibiotics, of which tetracycline, chloramphenicol, gliotoxin, fumigacin, tyrothricin and some others had some antiplasmodial activity[42]. Tetracycline and chloramphenicol had a slow therapeutic action on human malaria and a partial causal prophylactic effect on avian malaria. Lincomycin, an antibiotic isolated from an oil *streptomyces*, is unlike any other major compound of this group. A number of synthetic derivatives (e.g. clindamycin) have been prepared and used widely for the treatment of various bacteria infections. However, the consensus is that only the tetracycline and lincomycin groups of antibiotics have any significant antiplasmodial action. Interest in lincomycins was stimulated by demonstration of their activity against infections with chloroquine-resistant or dapsone-resistant strains of *P. berghei*. Further studies in sporozoites-induced and blood-induced infections with *P. cynomolgi* in rhesus monkey showed that clindamycin had significant activity against early and late tissue schizont, resulting in prevention of radical cure in a large proportion of infected animals. This compound and another derivative of chlorinated lincomycin were able to cure trophozoites-induced infections at well-tolerated dosages, and both

compounds were equally effective against pyrimethamine-sensitive strains. Some of the new compounds were effective in infections with a highly resistant strain of *P. falciparum* in owl monkeys. Tetracycline combined with quinine acts as suppressant in human malaria and of value as an additional cure of chloroquine-resistant falciparum infections. In addition, chloroquine-resistant falciparum malaria can be treated with clindamycin alone or as a combination therapy.

1.2.1 Antimalarial Drugs from Plants

Artemisinin (Qinghaosu), (**21**) is an antimalarial principle isolated from *Artemisia annua.* The compound has the structure of sesquiterpene lactone with an internal peroxide linkage. There are many methods by which artemisinin could be synthesized in the laboratory but the preferred method is that of Avery, *et al.*[43]and other derivatives are synthesized by chemical reduction of the lactone ring[44]. These derivatives are lipid-soluble ethers, artemether (**22**) and arte-ether and the water-soluble sodium hemisuccinate and sodium artesunate (**23**). Artemisinin and its derivatives could be administered orally or intramuscularly. The drug is mainly used for the treatment of falciparum cerebral malaria. Adverse effects include embryo toxicity, bone marrow depression and depression of reticulocyte counts in humans.

These are traditional medicinal plants used for malaria therapy. Most of the antimalarial drugs currently available to treat malaria are quinoline derivatives modelled on the quinine molecule, found in the bark of cinchona trees. Among the modern antimalarial compounds isolated from plants artemisinin is the most important. This substance comes

from *Artemisia annua*, a plant used for thousands of years to treat malaria. Some other plants that have been screened are febrifugine from *Dichloroea febrifugal*,[45] *simaroubaceous*,[46] *aristolochia species, Cornus florida, Cissampelos pareira, Cooperia pedunca, croton species, Datisca glomerata, Eryngium foetidum, gentiana species,* and *Hymenocallis caribaea*[47].

1.2.3 Malaria Vaccine

Vaccination lessens, or completely eradicates, the occurrence of clinical diseases. There are various stages in the life cycle of plasmodium for which antigens have been described that could lead to the development of immunogenic epitopes. The various stages which have been targeted for immune response are the pre-erythrocytic stage, when the parasite is in liver cells; the asexual stage, when the parasite infects red blood cells; and the sexual stage. The last stage involves vaccines that elicit antibodies which prevent the development of the sexual stage within the midgut of the mosquito[48]. Thus, as the burden of antimalarial drug-resistance increases, the possibility of vaccine development is also considered. However, vaccine research over the past three decades has been characterized by insufficient funding, a serious underestimation of the complexity of the parasite, faith in technology above scientific understanding, lack of appropriate model, and above all a lack of the immune mechanism underlying protection[49]. One of the major vaccines to undergo large-scale clinical trials is SPf66 developed by Pattaroyo,[50] but it did not show any efficacy[51]. The most advanced development to date is the RTS'S, based on a particulate construct of the circumsporozoite protein fused to hepatitis B antigen but clinical trials showed protection only to a strain homologous to that used in the vaccine

design[52]. Among blood-stage molecules, MSP1, alone or combined with MSP2, has been included in several human trials. However, the inhibition of merozoites invasion obtained with monoclonal antibodies has not been induced to date by immunization[53]. Vaccine development against both falciparum and vivax malaria is ongoing[54]. The decision on which parasite antigens are to undergo clinical development is difficult. Criteria for development include evidence showing that the antigen serves a function critical to the parasite, is associated with naturally acquired immunity, or is protected in animal models[55].

1.3.0 Antimalarial Chemotherapy: A Historical Perspective

While malaria cannot rival tuberculosis and epilepsy as a literary disease, it proved to be a deciding factor even in modern wars. There was no progress in controlling malaria until modern times except the discovery at an unknown period of the curative values of cinchona bark. Linnaeus called the tree from which quinine was extracted cinchona although the term probably derived from the name of the Countess Anna of Chinchon[56]. Cinchona bark was introduced into Europe in the late 1630's[57] by returning missionary Jesuits, thus the new "drug" was known as the Countess', Jesuits or Fathers' powder but was slow to make its way into clinical use. Opposition to the use of cinchona bark was caused in part by the difficulty in establishing the right dose level. The response of a fever to cinchona, however, provided the first specific diagnostic tool for malaria. In 1735, the French Government sent an expedition to South America led by Condamine to find the miraculous "fever tree". Condamine found the tree in Peru, wrote a treatise "*Sur l'arbre du Quinquina*" and provided illustrations and plant samples for Linnaeus, who in

1742 renamed the plant as "Cinchona" (a misspelling of Chinchón)[57]. By 1790, the Spanish set up a monopoly to improve quality and to control supplies that they obtained from South America. Two French chemists, Pierre Pelletier and Joseph Caventou, in 1820 isolated two active alkaloids from cinchona, quinine and cinchonidine. This was followed by the production of a number of pure alkaloids from cinchona species. Commercial production of quinine began in 1821 and numerous attempts to synthesize quinine consumed the attention of chemists for many years. It was not until 1944 that Robert Woodward and William Doering[22] were able to synthesise quinine and a complete stereoselective synthesis were only achieved by Balkovec, *et al.* in 2001[24]. By the 1800's the French, British and Dutch all had colonies in malaria-infested areas. The lack of sufficient cinchona bark prompted them to attempt to develop cinchona plantations in areas other than South America. In a strange twist of fate, the Dutch ended up controlling the cinchona trade and had its plantations in Java. At the outbreak of the Second World War, Java was producing more than 20 million tons of cinchona bark a year. The drug had a chequered career and is still in use today.

Since the 1820's physicians were able to recognize the signs and symptoms of malaria and could cure the disease but they still did not understand the causative organism or the method of transmission. Marshy areas of land were firmly established in the mind of civilized man as the site of the disease and the swamp theory became widespread and was responsible for the two names of the disease in common use today – malaria (bad air) and paludism (marsh disease). The discovery of malarial pigment was the first clue to solving the problem. The Roman physician Lancis, in 1761 described a black pigment in the

human spleen and brain but did not associate it with malaria. It was Meckel in 1847 that observed black granules in the blood and spleen of a patient with the actual disease, vectors and control. In 1880, Lavern in Algeria discovered and described malaria parasites in human blood. The meticulous work of Ross in 1897 – 1898 demonstrated the complete cycle of bird malaria, followed by Grassi, Bignami and Bastian Elli who described the cycle of human malaria parasites in anopheles mosquitoes. When research showed that mosquitoes were the vector of malaria, hope rose to the possibility of eliminating the disease. Classical methods of drainage were added to the treatment of stagnant water surfaced with petroleum products and Paris green in order to destroy mosquito larvae. Biological controls were also attempted by introducing larvae-eating fish into ponds where mosquitoes bred. However, these methods were too expensive on a wide scale application.

The prospect changed completely with the advent of DDT, dichlorodiphenyl trichloroethane, the first insecticide to retain its toxic properties for a considerable time after application. The insecticide opened up the possibility of attacking mosquitoes on a broad front largely because of its residual effect, the comparative ease with which it could be applied and its low cost. At that time, it was thought that reducing the numbers of mosquitoes in human's immediate environment might break the chain of malaria and, in 1955; the World Health Assembly[58] launched a global eradication programme. Two other residual insecticides, chlorinated hydrocarbons, hexachlorocyclohexane and dieldrin, were produced but their use were discontinued because of toxicity to human and the development of resistance by mosquitoes. The newer insecticides, (e.g.

organophosphates and carbonates) have shorter residual life and are more expensive. During the first decade of the malaria eradication campaign, too much emphasis was on the use of residual insecticide spraying as the main method of attack on the mosquito. The appearance and spread of resistance to the insecticides was a great disappointment. Thus, the malaria problem remains and the main hope now lay with chemotherapy.

Quinine, the first of the antimalarials, is still being used to treat certain strains of drug - resistant malaria. Originally meant for treatment of all fevers, but sometimes used as an analgesic, the induction of labour (in abortion) and the treatment of muscle cramps. Resistance to quinine was not reported for many years although failure of the drug to act or the malabsorption of the drug by the host has been recorded. In the search for new synthetic agents after the isolation of quinine, methylene blue showed modest antimalarial activity in 1891 when Guttmann and Erich cured patients infected with *P. malariae*. Further work led, in 1929, to the first member of 8-aminoquinolones, pamaquine (plasmoquine), developed in Germany by Schliemann and his colleagues[59]. Mepacrine (quinacrine), a 9-aminoacridine, was the next promising compound to emerge in the 1930's out of more than 300 acridines that were examined. The drug came into prominence during the 1939 – 45 World War when quinine was in a very short supply[60].

The presence of the quinoline nucleus in quinine, mepacrine and 8–aminoquinolines encouraged further work that led to the development of the 4–aminoquinolines, chloroquine. Initially rejected and thought to be too toxic for any practical use in humans, but results since 1946, through rediscovery and re-evaluation, has made it the drug of

choice for malaria treatment throughout the world. Although chloroquine remains, the major antimalarial drug in use today, but since Marberti first reported resistance in 1960 from Venezuela and later detected in South East Asia, there has been high incidence of resistance. Further research led to the development of the biguanide from which proguanil proved to be the most active compound known up to that time. This was followed by the development of the pyrimidines from which pyrimethamine and trimethoprim are effective antimalarials. The mode of action of proguanil, cylcoguanil, pyrimethamine and trimethoprim is now well documented[61]. Closely associated with the history of these compounds are the sulphonamides and sulphones. Interest in the sulphonamides as antimalarials began with the discovery that the sulphonamide–containing dyes had antimalarial activity.

Artemisinin (qinghaosu) is an antimalarial principle isolated from *Artemisia annua* by Chinese Scientists in 1972[62]. This novel compound has the structure of sesquiterpene lactone with an internal peroxide linkage. *A. annua* is an herb used in traditional Chinese medicine. Artemisinin has been used for ages in the treatment of both chloroquine-sensitive and chloroquine-resistant strains of *P. falciparum*. Recently several new highly efficacious compounds in humans have been reported. In spite of all these drugs, there is a global increase in the incidence of malaria, an increase in the resistance to almost all antimalarial drugs, a decrease in funding of antimalarial drug development programmes and an uncertain prospect for the current generation of malaria vaccines. Moreover, the role of chemotherapy in combating the drug resistant strains of *P. falciparum* worsened

by the scant knowledge about the precise mechanism by which the parasites operate within the vector and human subjects.

Chloroquine-resistant *P. falciparum* parasite has deranged the antimalarial programmes of most countries that are malaria endemic. It has also worsened the economic burden of malaria on the world's poorest nations. The phenomenon of chloroquine-resistance, first reported almost simultaneously in both South East Asia and South America in 1961, detected initially in East Africa[63] has now become a major public health problem in most West African countries as well. The after-effect of the spread of *P. falciparum* resistance has been a resurgence of the disease with 2.7 million deaths annually, 90% of these deaths comes from Africa South of the Sahara alone.

1.3.1 Biochemistry of Malaria Parasites and Evaluation of Antimalarial Action

There are many difficulties facing studies on the biochemical requirements of human plasmodia because of the obligatory intracellular life of malaria parasites. Work on the plasmodia of birds, rodents and monkeys provides insight about malaria parasites in human. A great amount of information has been gathered on the nature and distribution of various substances in the life stages of plasmodia and on their nutritional requirements and metabolic pathways. The relevance of these studies to the development of chemotherapeutic substances cannot be over emphasised[64].

The main reactions involved in plasmodia metabolisms are: phosphorylation of glucose, which provides the energy required; oxidative processes, which are maintained by the

oxy-haemoglobin of the lost cell; enzyme breakdown of the globulin portion of haemoglobin into amino acids and peptides and synthesis of lipids. Among inorganic substances, investigation of the uptake and utilization of phosphorus by plasmodia has received particular attention because of the role of this element in the formation of the nucleic acids, DNA and RNA. Typical protozoan mitochondria are present in plasmodia and are the probable site of action of enzyme. Mitochondria supply the parasites with the energy that they require, particularly during their extra cellular existence.

As for protein metabolism, it appears that the main source of amino acids utilized by malaria parasites is red cell haemoglobin. The first step is cleavage, which liberates amino acids and haemozoin (malaria pigment). Among the free amino acids in the serum, L–methionine and L–isoleucine are essential for the growth of mammalian plasmodia in addition to several other amino acids. Tetrahydrofolic acid is a co-factor in this process, thus antifolates as antimalarials block this and other folic acid-dependent reactions (e.g. DNA synthesis). Nucleic acid metabolism in plasmodia is similar to that of other similar organisms and both DNA and RNA are synthesized during nuclear development and division. All enzymes necessary for the biosynthesis of foliate co-factors occurred in several species of plasmodia[65].

Sulfonamides and antifoliates act as antimalarials by interfering with the synthesis of foliate co-factors by the enzymes of the parasites; the sulfonamides inhibit dihydropteroate synthesis and the antifolates, such as pyrimethamine, bind plasmodia dihydrofolate reductase. Chloroquine and other 4–aminoquinolines interact with

nucleoproteins of the parasite, but this does not appear to be their primary mode of action. Primaquine and its congeners appear to act through interference with mitochondria respiratory processes. Present knowledge of biochemical changes during growth in malaria parasites obtained chiefly through the cultivation of erythrocyte forms of animal plasmodia *in vitro*. Recent successes in maintaining long-term *in vitro* cultures of *P. falciparum* are bound to open new vistas in the understanding of the various aspects of the metabolism of this and other species, and so improve the prospects of chemotherapy.

It is obvious that understanding of the metabolic processes of plasmodia may offer much guidance in the evaluation of potential antimalarial compounds. Most of the early test procedures carried out on *P. relictum* and *P. cathemerium* of canaries, later *P. lophurae* and *P. gallinacean* of duckling and chicks, were widely used. The discovery of *P. berghei* opened the possibility of tests in rodents[66]. Various species of simian malaria parasites were used for further evaluation of drugs and their physiological disposition in animals closer to humans. For the study of the chemotherapeutic effects on both blood and tissue, stages[67] *P. cynomolgi* and *P. knowlesi* of rhesus monkeys (*Macaea mulatta*) were of particular value. Recently both normal and drug–resistant strains of *P. vivax* and *P. falciparum* have been adapted to owl monkeys *(Aotus trivirgatus)* for drug evaluation[68]. All promising antimalarial compounds undergo tests for acute and chronic toxicity by various routes of administration to show the effects on the most valuable organs. The final evaluations of promising and least harmful potential antimalarials is

carried out either on volunteers with induced malaria or naturally infected subjects in hospital or in the field.

1.3.2 Drug Resistance in Malaria

Malaria chemotherapy has relied on a handful of drugs each with inherent pharmacological limitations, of which parasite resistance has been the most damaging. Antimalarial drug resistance has emerged as one of the greatest challenges facing malarial control in modern times. Drug resistance is responsible for the spread of malaria to new areas and re-emergence of malaria in areas where the disease had been eradicated. It also played a significant role in the occurrence and severity of epidemics in some parts of the world[69]. The factor limiting success in the use of antimalarial drugs as prophylactic or for curative purposes is the varying response of different strains of the parasite to drugs. The selection of each drug in use is based on one or more specific actions against the malarial parasite when administered to the patient in the appropriate dosage. The failure of this recognized action may be due to insufficient dosage or its active metabolite has not reached the parasite or the drug has reached the parasite but the parasite has become adapted to the introduced chemical environment and, by surviving, has entered the state of drug resistance[70].

The ability of a parasite strain to survive or to multiply despite the administration and absorption of a drug, given in doses equal to or higher than those usually recommended but within the limits of tolerance of the subjects, is defined as drug resistance[68]. For this definition to be applicable, the drug must gain access to the parasite or the infected red

blood cell for the duration of the time necessary for its normal action. It requires presence of malaria parasitaemia in a patient who has received an observed treatment dose of an antimalarial drug and simultaneous demonstration of adequate blood drug and metabolite. Although drug resistance embraces all species of malaria parasites and all acceptable dosages of blood or tissue schizontocides, gametocytocides and sporontocides, in practice, it is related to the effect of blood schizontocides on falciparum malaria and most often to chloroquine resistance. While drug resistance can cause treatment failure, not all treatment failure is due to drug resistance. Factors contributing to drug failure include incorrect dosing, non-compliance with duration of dosing regimen, poor drug quality, drug interactions, poor or erratic absorption, and misdiagnosis.

1.3.3 Mechanisms of Antimalarial Resistance

Resistance occurs through spontaneous mutations that confer reduced sensitivity to a given drug or class of drugs. For some drugs, only single point mutation is required to confer resistance while for other drugs multiple mutations appear to be required. Single malaria isolates consist of heterogeneous populations of parasites that can have widely varying drug response characteristics, from highly resistant to completely sensitive[71] and within a geographical area, malaria infections demonstrate a range of drug susceptibility. The establishment of resistance in the population with time can be very stable; persisting long after removing specific drug pressure. The biochemical mechanism of resistance has been well described for chloroquine,[72] the antifoliates combination drugs,[73] and atovaquone[74].

1.3.4 Factors Aiding the Spread of Drug Resistance

The most significant factor that contributes to the advent, spread, and intensification of drug resistance is biological. Data obtained on the response of sensitive parasites to antimalarial drugs *in vitro* and the pharmacokinetic profiles of common antimalarials showed that a residuum of parasites is able to survive treatment[75]. Parasite clearance after treatment is by the immune system under normal biological circumstances. Factors that decrease the effectiveness of the immune system in clearing parasite residuum after treatment also appear to increase survivorship of parasites and facilitate development and intensification of resistance. This mechanism has been suggested as a significant contributor to resistance in South-East Asia, where parasites are repeatedly cycled through populations of non-immune individuals,[76] the same mechanism may also explain poorer treatment response among young children and pregnant women[77].

Many antimalarial drugs are chemically related, thus development of resistance to one can facilitate development of resistance to others. Chloroquine and amodiaquine are both 4–aminoquinolines and cross-resistance between these two drugs is well known[78]. Development of resistance to mefloquine may also lead to resistance to halofantrine and quinine. Antifolate combination drugs have similar action and widespread use of sulfadoxine/pyrimethamine for treatment of malaria may lead to increased parasitological resistance to other antifolate combination drugs[79]. There is an interesting theory that development of resistance to a number of antimalarial drugs among some *Plasmodium falciparum* parasites produces a level of genetic plasticity that allows the parasite to rapidly adapt to a new drug, even when the new drug is not chemically related to drugs

previously experienced[80]. Another major factor facilitating the development of resistance is mismatched pharmacokinetics. For example, the elimination half-life of pyrimethamine is between 80-100 hours, while for sulfadoxine it is 100-200 hours, leaving an extended period when sulfadoxine is "unprotected" by synergy with pyrimethamine[81]. This sort of mismatched pharmacokinetics is more apparent in the mefloquine-sulfadoxine-pyrimethamine combination used in Thailand because mefloquine has an elimination half-life of 336-432 hours[82]. Other factors that aid development of antimalarial drug resistance therefore include overall drug pressure, inadequate drug intake, pharmacokinetic and pharmacodynamic properties of the drug or drug combination, and drug interactions[83].

1.3.5 Geographical Distribution of Antimalarial Drug Resistance

The geographical distribution of chloroquine-resistant falciparum malaria has increased greatly since 1957 when it was first suspected in Thailand and later found in patients in Colombia in 1960[84]. Ever since resistant strains have appeared in much of South-East Asia to such an extent that the majority of infections are chloroquine-resistant the same has also occurred in those parts of South America where malaria eradication programmes have not been successful. Recent evidence indicates that there has been a considerable geographical extension in the distribution of chloroquine-resistant malaria (Figure 5). Since resistance to chloroquine emerged more than 30 years ago,[85] the parasites have developed resistance to most of the widely used antimalarial drugs including quinine,[86] and mefloquine[87].

Chloroquine-resistant *Plasmodium* was first confirmed in Africa in 1979[89] and later reported in Cameroon,[90] Benin,[91] and Nigeria[92]. The rate of resistance *in vivo* to chloroquine in Ibadan, Nigeria increased from 5% in 1987 to 35% in 1990[93]. Failure of chloroquine and proguanil,[94] with mefloquine[87] and clinical failures of halofantrine[95] and quinine[96] have occurred in Africa. In regions where *P. falciparum* is resistant to chloroquine, combination therapy has been employed in the management of the chloroquine-resistant species. The emergence and spreading of parasite resistance to antimalarial drugs indicates that novel compounds need development by identification of novel chemotherapeutics agents. The frightening spread of the parasite resistance has led the World Health Organisation to predict that without new antimalarial drug intervention, the number of cases of malaria will have doubled by the year 2010. Hence, the search for new antimalarial therapies is a high-priority for the control of the disease.

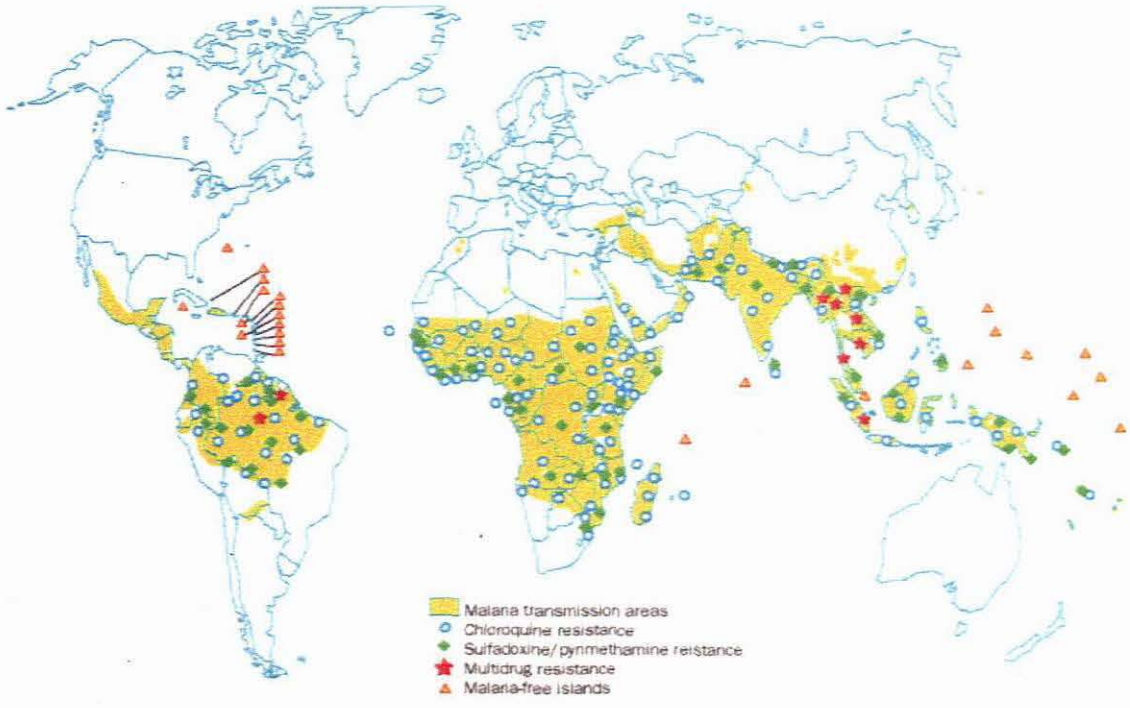

Figure 5: Geographical distribution of antimalarial drug resistance[88]

1.3.6 Foci of Antimalarial Drug Development

In the search for novel chemotherapeutic agents, two major approaches are currently gaining tremendous attentions. The first approach involves building on compounds of known efficacy while the second approach centres on proteases search. In the first approach, the three different methods used are:

- ❖ Synthesis of novel derivatives of quinine and other alkaloid-based antimalarial drugs.
- ❖ Synthesis of novel derivatives and development of artemisinin-based drugs.
- ❖ Synthesis and evaluation of metal complexes of existing antimalarial drugs.

The second approach involves identification of some proteases used by the malaria parasite in cracking down haemoglobin. The approach combines results from *Plasmodium* genome sequencing with combinatorial chemistry and synthesis to make molecules that can target the essential proteases used by the parasites. This approach is based on two major methods:

- Synthesis of plasmepsins inhibitors.
- Cracking of plasmodium genome.

1.3.7 Chemotherapy

Chemotherapy is defined as the use of chemical agents to destroy infectious organisms without simultaneously destroying the host. It is a relatively modern phenomenon. Before 1900, only three specific chemical remedies were known, mercury (for syphilis-but often with disastrous results), cinchona bark (for malaria), and ipecacuanha (for dysentery). Modern chemotherapy began with the work of Ehrlich with his discovery in 1907 of the curative properties of a dye called Trypan Red I when used against experimental trypanosomiasis and with his discovery in 1909 of salvarsan as a remedy for syphilis. Ehrlich introduced the term "chemotherapy", and in his research sort what he called the "magic bullet"; that is, chemicals that would be toxic to infectious microorganisms but harmless to humans[97].

1.3.8 Metals in Medicine

Metals have played an important role in medicine for years; many are essential in human diet in varying amounts and some are used in the medical profession as invaluable

diagnostic tools. These include radioactive and magnetic techniques using a variety of exotic elements to explore the inner structure of the human body without the need for invasive procedures. In ancient history Cu, Au, Fe and Zn were used for various purposes while in the early 20th century Paul Ehrlich successfully used arsenic compound (arsphenamine or salvarsan) for the treatment of syphilis, and in other developments $K[Au(CN)_2]$ was used for tuberculosis and Sb compounds for leishmaniasis[98]. The use of metal complexes capable of enhancing biological activity has become a vibrant and growing area of research among inorganic chemists and biologists over the last few decades resulting in a variety of exciting and invaluable drugs such as *cis*-platin[99]. Researches are being undertaken in fields such as cancer, arthritis and cardiovascular medicine. Recently, it was shown that most of the elements of the periodic table up to and including bismuth (Z = 83) are potentially useful in the design of new drugs and diagnostic agents[100]. Development of inorganic drugs is broadly divided into two categories: diagnostics and therapeutics. As diagnostics, researches are been undertaken in radiopharmaceutical (γ, β^+), MRI and X-ray contrast agents. As therapeutics, inorganic compounds are used as chelating agents, as radiopharmaceuticals (α, β, Auger e-, NC), and as chemotherapeutics: anticancer agents, metal-mediated antibiotics, antibacterial, antiviral, antiparasitic, treatments of rheumatoid arthritis and radiosensitizers[101-103].

1.3.9 A Review of Metal-Based Malaria Chemotherapy

Sanchez-Delgado, *et al.*[104] reported the synthesis, *in vitro* and *in vivo* studies of Rh and Ru chloroquine complexes: [Rh(COD)(CQ)Cl] and $[RuCl_2(COD)]_2$. The Ru complex was five times more active than chloroquine *in vitro* while the Rh and Ru complexes reduces

parasitaemia by 73% and 94% *in vivo* without any sign of acute toxicity being observed for up to 30 days after treatment. Dudeja, *et al.*[105] reported the complexes of chloroquine with a number of M(II) ions, $[VOL(H_2O)SO_4]$ and $[ML(H_2O)Cl_2]$ (M = Co, Ni, Cu; L = chloroquine). Navarro, *et al.*[106,107] reported the synthesis, *in vitro* and *in vivo* studies of gold-chloroquine complexes which were considerably more active than chloroquine diphosphate against chloroquine-sensitive and chloroquine-resistant strains of *P. falciparum in vitro* and *in vivo* but no clear structure activity correlations were established for the complexes. Dadachova[108] studied ^{198}Au(I)-labelled gold chloroquine $[^{198}Au(PPh_3)]PF_6$ and explored the possibility of using radio-labelled metal complexes with therapeutic radioisotopes for treatment of chloroquine-resistant malaria. Obaleye, *et al.*[109] studied the activity of Fe(II) and Ni(II) complexes of chloroquine against *P. yoelii nigeriensis*.

Wasi, *et al.*[110,111] reported the synthesis and *in vitro* evaluation of some metal complexes of amodiaquine and primaquine and concluded that the antiparasitic activity of the two drugs is independent of their coordination to any metal. Dermatin, *et al.*[112] reported the synthesis and crystal structure of $[CoCl_2(TMP)_2]$ (TMP = trimethoprim) with Co atom lying on a 2-fold axis and bonded by two chloro and two pyrimidinium N atoms in a tetrahedral environment. Naldini, *et al.*[113] reported the synthesis, magnetic susceptibilities and X-ray structure of $[Cu_2(OOCCH_3)_4(TMP)_2(C_6H_6)_2(CH_3OH)]$ and Zoroddu, *et al.*[114] reported the synthesis and X-ray structures of $[Rh_2(OOCCH_3)_4(TMP)_2(C_6H_6)_2(CH_3OH)]$ and $[Rh_2(OOCCH_3)_4(PYRM)_2]$ (PYRM = pyrimethamine). Muthiah and Robert,[115] reported the synthesis and crystal structure of cadmium complex of trimethoprim,

$[CdBr_2(TMP)_2(H_2O)_2]$ while Simo, *et al.*[116] also studied the interaction of Cu(II), Zn(II) and Cd(II) with trimethoprim and reported the crystal structures of $[Zn(TMP)_2Cl_2]$ and $[Cd(TMP)Cl_2(MeOH)]_n$.

Yamashita, *et al.*[117] reported the synthesis of Au, Ag, Zn, Mn and Mg derivatives of sulfadiazine, sulfamethizole and sulfasomidine while Lal[118] studied the formation constants of some metal complexes with three sulpha drugs and found that stabilities decrease according to the Irving-Williams order $Cu^{2+}>Zn^{2+}>Co^{2+}>Mn^{2+}$ for sulfadiazine, sulfamerazine and sulfadimidine. Guindi and Gaval[119,120] studied the acid dissociation constants and the thermodynamic equilibrium constants of sulfadiazine, sulfamerazine and sulfasomidine with Cu(II), Zn(II), Co(II), Ni(II) and Cu(II). Goel[121] reported Fe(III), VO(II), Co(II), Ni(II) and Cu(II) complexes of Schiff bases derived from sulfadiazine and sulfadimidine with 5-substituted salicyladehydes. Menabue and Saladium[122] reported the synthesis, structural and spectroscopic investigation of Co(II), Ni(II), Zn(II) and Cd(II) complexes of sulfadiazine (SD) and the single crystal X-ray structure of the Cd complex, $[Cd(SD)_2].H_2O$. In other studies Mukherjee, *et al.*[123] studied the equilibrium constants of complex formation of Co(II), Ni(II), Cu(II), and Zn(II) with sulfadiazine while Pamley, *et al.*[124] studied the chelation behaviour of Schiff base derived from sulfadiazine and pyridine-2-carboxaldehyde with cobalt(II), nickel(II), copper(II) and zinc(II). Omar[125] studied the potentiometric and thermogravimetric of some mixed-oxine sulpha drugs ternary complexes.

Tsumaki, *et al.*[126] were the first to study the metal complexes of quinine. This was followed by the study of Niyogi and Rieders[127] that studied the chelation as a method of exclusion screening for drugs. Tsangaris and Baxevaniclis[128] reported complexes of quinine with Cu(II), Ni(II), Co(II) and Cr(III) chlorides while Farooq and Malik[129] reported complexes of quinaldine, quinine, brucine and codeine. Gupta, *et al.*[130] studied the IR spectra of quinine and its complexes with Cu, Ag, Hg, Fe and Co salts. This was followed by the reported synthesis of complexes of cinconidine and quinine with VO, Fe, Co, Cu by Dudeja, *et al.*[131] Missling, *et al.*[132] reported organometallic complexes of Ru(II), Rh(III), Ir(III), and Au(I) with cinchona alkaloids. Hubel, *et al.*[133,134] studied coordination of transition metal to four potential donor sites of quinine and later studied Pd(II) and Pt(II) complexes of quinine derivatives and carried out *in vitro* tests.

Organometallic compounds incorporating chloroquine with a ferrocene nucleus localized at different sites have also been reported and their antiparasitic activities studied. Biot, *et al.*[135-138] reported the synthesis, characterisation, *in vitro* and *in vivo* studies of ferrochloroquine and ferrocenic mefloquine and quinine complexes. Some of the chloroquine derivatives showed high potent antimalarial activities *in vivo* on mice infected with *P. berghei* N. and *P. yoelii* NS and 22 times more potent against schizontocides than chloroquine *in vitro* against a drug-resistant strain of *P. falciparum*. Itoh, *et al.*[139] reported twelve novel ferrocenyl sugars and their biological properties towards the malaria parasite. The results obtained suggest that ferrocenyl sugars may become a leading compound for the management of malaria. Delhaes, *et al.*[140,141] reported the synthesis, *in vitro* and *in vivo* studies of novel organometallic complexes of

antimalarial drugs. The ferrochloroquine analogues are up to 20 times more active than chloroquine *in vitro* and *in vivo* against *P. bergei* N, *P. vinckei* and *P. falciparum*.

Blackie, *et al.*[142] reported the synthesis and *in vitro* antimalarial activities of Rh and Au derivatives of chloroquine and a series of ferrocenyl-4-amino-7-chloroquine. The complexes showed improved efficacy against chloroquine-resistant strains of *P. falciparum* with respect to chloroquine but a threefold drop in efficacy occurred in moving from the chloroquine-sensitive to the chloroquine-resistant strain.

Some aromatic chelators have also been reported as potential chemotherapeutic agents for malaria. Scheibel and Stanton[143] studied the effect of aromatic chelators on the growth of *P. falciparum* and found that alkythiocarbamates and 8-hydroxyquinoline chelates selectively inhibit glycolysis within parasitized erythrocytes at pharmacologic doses. Sharma, *et al.*[144] reported the discovery of Schiff-base and amine phenol gallium(III) and iron(III) complexes with potent antimalarial activity *in vitro*. Two complexes of Ga(III) are novel reciprocal agents, one possessing selective cytotoxic activity towards chloroquine-resistant parasites while the other showed selective activity toward chloroquine-sensitive strains. Tsafack, *et al.*[145] studied the mode of action of iron chelators and found that it was limited by factors related to drug permeation and parasite susceptibility to metal deprivation. In this study, iron-chelating isonicotinoyl and benzoyl hydazones were applied on *P. falciparum* cultures and assessed their antimalarial properties. The agents were used both individually and in combination with deferoxiamine (DFO). They concluded that the application of iron chelators as

antimalarials might be of therapeutic value. Cole, *et al.*[146] studied the inhibition of β-haematin (haemozoin) formation by metalloporphyrins and found that the complexes were six times more efficacious than the free ligand, protoporphyrins IX, in preventing β-haematin formation and four times as efficacious as chloroquine. In a related study, Goldberg, *et al.*[147]reported a new class of metal(III) chelates amenable to metallopharmaceutical development as antimalarials. The study showed that racemic mixtures of Al(III), Fe(III) or Ga(III) chelates killed intra-erythrocytic malaria parasites in stage-specific manner.

From the foregoing, it is evident that lots of work has been done on syntheses of metal complexes of a number of malaria drugs and their biological screening has produced very encouraging results. However, till date, no known metal complex has been employed in the management of chloroquine-resistant malaria unlike in other diseases reviewed earlier. This could be due to the reluctance of pharmaceutical companies to produce metal-containing drugs for mass usage, as would be the case in the management of malaria.

1.4.0 Aims of the project

1. To synthesize metal complexes of selected antimalarial drugs (trimethoprim, chloroquine, sulfadiazine, tetracycline, amodiaquine and quinacrine).
2. To characterize these complexes
3. To carry out *in vitro* studies against isolates of *P. falciparum.*

1.4.1 Objectives of the project

In 1955, a book entitled *Man's Mastery of Malaria*[148] reflected the generally held views of that time. Half a century later, malaria kills 2-3 million people annually,[149] with children younger than five years of age in sub-Saharan Africa accounting for 90% of cases. One African child dies from malaria every 30 sec,[150] and rarely has scientific optimism been so misplaced. With the advent of resistance to chloroquine and DDT, malaria re-emerged in many parts of the world. In recent years, the burden of disease and death has increased substantially in malaria-endemic countries,[151] and transmission has spread to new areas[152]. The major causes of this resurgence are the development of resistance to affordable drugs[153] and insecticides,[154] deterioration of national control programmes,[155] increasing human migration,[156] and tourism[157]. The rise in malaria deaths contrasts with falls in the causes of mortality in children in many developing countries[158].

The main objective of this study therefore is to contribute to efforts being made to search for novel chemotherapeutic drugs against the resistant strains of *P. falciparum*. In the search for novel drugs against chloroquine-resistant malaria parasites, the modification of chloroquine by coordination to a metal centre has attracted considerable attention in recent years. This study is based on the making of metal complexes of a selection of known antimalarial drugs. The synthetic strategy involves modification of the activity of antimalarial drugs through the incorporation of a transition metal into the molecular structure. Since the modification in the chemical structure of any drug changes the pharmacological action of the drug, it is envisaged that this would lead to novel pharmacological models of antimalarial agents. The synthetic procedures would combine

inorganic synthesis guided by biochemical considerations. Coordinating these drugs to various metal centres might increase their half-life and enhance gradual release of the parent drugs into the blood stream. Consequently the drugs might be retained in the blood stream long enough to obstruct the parasites from gulping haemoglobin. The electronic changes that are anticipated when drugs are coordinated to metal ions, and the subtle changes that occur as the metals are varied, might be able to "deceive/confuse" the parasites and hence enhance the efficacy of the drugs.

CHAPTER TWO

2.0 EXPERIMENTAL

2.1 Chemicals and Solvents

The drugs, chemicals and solvents used in this study were of analytical grade and used as obtained from Aldrich without further purification.

Drugs:

Ethylenediamine, chloroquine diphosphate, amodiaquine hydrochloride, sulfadiazine sodium salt, quinacrine hydrochloride, pyrimethamine, trimethoprim and tetracycline.

Chemicals:

N,N′-Dimethydithiocarbamate, 2,2′-bipyridine, cobalt(II) chloride hexahydrate, cobalt(II) acetate tetrahydrate, copper(II) chloride monohydrate, copper(II) acetate monohydrate, zinc(II) chloride hexahydrate, zinc(II) acetate tetrahydrate, iron(III) chloride hexahydrate, potassium tetrachloroplatinate(II), potassium tetrachloropalladate(II), manganese(II) chloride hexahydrate, ruthenium(III) chloride, rhodium(III) chloride, nickel(II) chloride hexahydrate, and nickel(II) acetate tetrahydrate.

Solvents:

Ethanol, methanol, toluene, benzene, acetonitrile, tetrahydrofuran, dimethysulfoxide, N,N′-dimethyformamide, acetone, diethylether, and petroleum ether,

2.2.0 Physical measurements

2.2.1 UV-Visible Spectroscopy

The electronic spectra of the complexes in solution were run in the range 180-1100 nm on Perkin Elmer λ20 spectrophotometer. The samples were placed in quartz cuvettes of 1 cm path length. The solvents used varied and it depends on the solubility of the complexes in a particular solvent and its stability. In all cases, HPLC grade solvents were used for solution measurements. The spectra of some of the complexes were also run in the solid state by the incorporation of an integrating sphere to the λ20 spectrophotometer and using $CaCO_3$ as reference.

2.2.2 Infrared spectroscopy

Infrared spectra were collected on Perkin Elmer Paragon 1000 FT-IR spectrophotometer equipped with caesium iodide window (4000-250 cm^{-1}) as KBr pellets.

2.3.3 Thermo gravimetric Analysis

Thermo gravimetric analysis on some of the complexes and the ligands (antimalarial drugs) were done under nitrogen atmosphere between room temperature and 800 °C using a Perkin Elmer Pyris 6 TGA with a sample weight of 5-15 mg and temperature gradient of 5 °C per min.

2.2.4 Atomic Absorption Spectroscopy

Metal analyses were carried out on Varian AA spectrometer. About 0.2 g of each complex was digested with 2.0 cm^3 of 50 % of water/nitric acid. The digest was rinsed quantitatively into a 100 ml standard flask and made up to the mark with deionised water.

2.2.5 Magnetic Susceptibility Measurements

The Gouy method, using Sherwood Scientific MXI model Evans magnetic balance, was used to determine the room temperature magnetic susceptibilities of the complexes. Diamagnetic corrections were estimated from Pascal's constant[159] and $Hg[Co(SCN)_4]$ was used as the calibrant.

2.2.6 X-ray Crystallography

The data sets for the single-crystal X-ray studies were collected with Mo Kα radiation at 100 K on a Bruker SMART APEX CCD diffractometer equipped with an Oxford Cryosystems low temperature device. A semi-empirical absorption correction was applied using SADABS[160] with variable maximum and minimum transmissions respectively for each complex. The structures were solved by direct methods using SHELXS-97 and completed by iterative cycles ΔF syntheses, using the SHELXTL package[160]. Hydrogen atoms were included in calculated positions and the structures were refined using full-matrix least-squares refinement against F^2.

2.2.7 Mass Spectrometry

The electrospray mass spectra were recorded on a Micromass platform mass spectrometer and a Kratos concept IS instrument, using N,N′-dimethyformamide and methylsulfoxide as solvents.

2.2.8 Conductivity

The molar conductance of the complexes was determined in either DMF or DMSO using Jenway PCM3 conductivity meter with a cell constant of 1.05.

2.2.9 Melting Point

The melting point and decomposition temperature of both the ligands and complexes were recorded on Gallenkamp apparatus.

2.2.10 Electron Paramagnetic Resonance (EPR)

The EPR measurements were done on a Bruker 200D X-band spectrometer employing 100 kHz modulation, magnetic field markers from an NMR gauss meter and an external microwave frequency counter.

2.3.0 Preparation of the complexes

2.3.1 Synthesis of *trans*–$[Co(en)_2Cl_2]Cl$

The compound was prepared by following a literature procedure with slight modification.[161] 80.0 g (0.337 mol) of $CoCl_2 \cdot 6H_2O$ was dissolved in 250 mL of deionised water and 32.75 mL of ethylenediamine in 250 mL of water was added. Oxygen gas was

passed into the solution for 10 h after which 175 mL of concentrated hydrochloric acid was added and stirred continuously for 30 min. The solution was evaporated on a water bath until a crust formed over the surface and then left at room temperature overnight before bright-green square plates of the hydrochloride of the *trans*–form were filtered off. These were washed with ethanol and diethylether and dried at 110 °C to remove the hydrochloric acid. A dark green powder-like substance was obtained. The reaction can be represented by the following equations:

$$4CoCl_2 + 8en + 8HCl + O_2 \longrightarrow 4\textit{trans}\text{–}[Co(en)_2Cl_2]Cl{\cdot}HCl + 2H_2O$$

2.3.2 Conversion of the *trans*– to *cis*– form

The *trans*– form was converted to the *cis*–form by dissolving the *trans*–$[Co(en)_2Cl_2]Cl$ in a minimum amount of water. The solution was evaporated to dryness on a water bath. The unchanged *trans*–form was washed with a little cold water.

2.4.0 Synthesis of Cobalt(III) complexes of Antimalarial Drugs

The *trans*– and *cis*–$[Co(en)_2Cl_2]Cl$ prepared in 2.3.1 and 2.3.2 above were used to synthesise Co(III) complexes of chloroquine, amodiaquine, quinacrine, trimethoprim and tetracycline.

2.4.1 Synthesis of Cobalt(III) complexes of Chloroquine

Chloroquine diphosphate was converted to the base prior to use in the synthesis. The conversion was done following a literature procedure.[162] The complex was prepared by

dissolving 1.60 g (5 mmol) of chloroquine base in 40 mL of ethanol and 1.43 g (5 mmol) of *trans*–$[Co(en)_2Cl_2]Cl$ in 40 mL of ethanol was added gradually and refluxed for 24 h. The solution turned green after 30 min and this colour was maintained throughout the duration of the reaction. The resulting solution was filtered hot to remove any un-reacted starting material. The filtrate was cooled to room temperature and filtered with sintered glass crucible. The green product obtained was washed with ethanol, diethylether and dried under vacuum. The *cis*–complex was prepared in a similar way except that the *cis*-form was used and 3 h into the reaction, the initial purple solution changes to green. The final product obtained was green and dried over $CaCl_2$.

2.4.2 Synthesis of Cobalt(III) complex of amodiaquine

The complex was prepared by dissolving 2.144 g (5 mmol) of amodiaquine in 60 mL of ethanol and a solution of 1.43 g (5 mmol) of *trans*–$[Co(en)_2Cl_2]Cl$ was added bit by bit. The bright yellow solution of amodiaquine turned completely green 20 min after the *trans*–form was added to it. The solution was refluxed for 12 h, cooled to room temperature and filtered. The green product was washed with ethanol and diethylether and dried over $CaCl_2$. The *cis*–form was also used in the same mole ratio as above. When the yellow solution of amodiaquine was mixed with the purple solution of *cis*–$[Co(en)_2Cl_2]Cl$, the mixture turned purplish yellow but changed to light green 30 min later and this green colouration was maintained throughout the duration of the reaction. The green product was filtered, washed with ethanol and diethylether and dried over $CaCl_2$. The procedures above was repeated using 10 mmol of amodiaquine to 5 mmol of *trans*–/*cis*–$[Co(en)_2Cl_2]Cl$.

2.4.3 Synthesis of Cobalt(III) complexes of Quinacrine

The *trans* complex was prepared by dissolving 2.365 g (5 mmol) of quinacrine in 60 mL of ethanol and adding 1.43 g (2.5 mmol) of *trans*–$[Co(en)_2Cl_2]Cl$ in bits. The solution turned yellowish green and it was refluxed for 12 h, cooled, filtered and washed with ethanol and diethylether and dried over $CaCl_2$. The *cis* complex was prepared in the same mole ratio as the *trans*–form. The final product, in both case, was yellowish purple.

2.4.4 Synthesis of Cobalt(III) complexes of trimethoprim

The *trans* complex was prepared by dissolving 1.438 g (5 mmol) of trimethoprim in 80 mL of ethanol followed by the addition of 1.456 g (5 mmol) of *trans*–$[Co(en)_2Cl_2]Cl$ in bits. The green solution was refluxed for 12 h, cooled, filtered, washed with ethanol and diethylether and dried over $CaCl_2$. The complex was also prepared in a 2:1 mole ratio using 1.438 g (5 mmol) of trimethoprim and 0.728 g of *trans*–$[Co(en)_2Cl_2]Cl$. The *cis* complex was also prepared as above in 1:1 and 2:1 mole ratios. The final product in each case was light green.

2.4.5 Synthesis of Cobalt(III) complexes of Tetracycline

The *cis*– and *trans*– forms of tetracycline were prepared by dissolving 1.111 g (2.5 mmol) of tetracycline in 60 mL of ethanol followed by the addition of 0.7175 g of *trans*–*/cis*– $[Co(en)_2Cl_2]Cl$ in bits. In both cases, the brown solution obtained was refluxed for 12 h, cooled, filtered and washed with ethanol and diethylether and dried over $CaCl_2$.

2.5.0 Synthesis of Metal Complexes of Sulfadiazine

The metal(II) (M = Co, Cu, Zn, Fe, Mn, Pd, Pt(II), Ru, Cr, Ni, and VO) complexes of sulfadiazine were synthesised and characterised.

2.5.1 Cobalt(II) complexes of sulfadiazine

2.723 g (10 mmol) of sodium salt of sulfadiazine was dissolved in 50 mL of water. This was followed by drop-wise addition of 1.186 g, (5 mmol) of $CoCl_2 \cdot 6H_2O$ or 1.245 g, (5 mmol) of $Co(CH_3COO)_2 \cdot 4H_2O$ in water with constant stirring at 40 °C for about 3 h. A pink precipitate was formed, filtered and washed with water, methanol and diethylether successively and dried under vacuum over $CaCl_2$. Suitable crystals for X-ray analyses were obtained by dissolving 0.238 g, (1 mmol) of $CoCl_2 \cdot 6H_2O$ in 30 mL of methanol and layered with 0.545 g, (2 mmol) sodium salt of sulfadiazine in 50 mL of methanol in a 150 mL conical flask. The mixture was allowed to stand at room temperature for two weeks after which tiny needle-like pink crystals formed. The crystals of sulfadiazine were obtained from a solution of methanol.

2.5.2 Synthesis of Copper(II) complexes of sulfadiazine

The copper complexes were made from $CuCl_2 \cdot 2H_2O$ 0.852 g, (5 mmol), $CuSO_4 \cdot 5H_2O$ 1.248 g, (5 mmol), or $Cu_2(CH_3COO)_4 \cdot 2H_2O$ 1.269 g, (5 mmol). The complexes were prepared by dissolving 2.723 g (10 mmol) of sodium salt of sulfadiazine in 50 mL of deionised water or methanol followed by dropwise addition of each of the copper salt respectively. The brown solution obtained in each case was stirred continuously at about

40 °C for about 3 h. The brown precipitate formed in each case was filtered under vacuum and washed with either water or methanol.

2.5.3 Synthesis of Zinc(II) complexes of sulfadiazine

The zinc complexes were made by dropwise addition of 5 mmol of $ZnCl_2 \cdot 6H_2O$ (1.222 g) or $Zn(CH_3COO)_2 \cdot 4H_2O$ (1.278 g) in 30 mL of deionised water to a solution containing 2.723 g (10 mmol) of sodium salt of sulfadiazine in 50 mL of water. The colourless solution obtained was stirred continuously at about 40 °C for 1 h. The white precipitate formed was filtered under vacuum, washed with water and dried over $CaCl_2$.

2.5.4 Synthesis of Iron(III) complex of sulfadiazine

2.723 g (10 mmol) sodium salt of sulfadiazine was dissolved in 50 mL of deionised water followed by the addition of 1.3515 g (5 mmol) of $FeCl_3 \cdot 6H_2O$ in 30 mL of water. The brown precipitate formed was stirred continuously for 3 h, filtered under vacuum, washed with water and dried over $CaCl_2$.

2.5.5 Synthesis of Manganese(II) complex of sulfadiazine

2.723 g (10 mmol) of sulfadiazine sodium salt was dissolved in 50 mL of deionised water followed by the addition of 0.990 g (5 mmol) of $MnCl_2 \cdot 4H_2O$ in 30 mL of deionised water. The mixture was stirred for about 3 h at 40 °C. The cream-coloured precipitate formed was filtered under vacuum, washed with water and dried over $CaCl_2$.

2.5.6 Synthesis of Palladium(II) complex of sulfadiazine

0.571 g (1.75 mmol) of K_2PdCl_4 was dissolved in 10 mL of deionised water followed by slow addition of 0.953 g (3.5 mmol) of sodium salt of sulfadiazine in 40 mL of deionised water. The mixture was stirred at 40 °C for 1 h. The yellow product was filtered under vacuum, washed twice with water and dried over $CaCl_2$.

2.5.7 Synthesis of Platinum(II) complex of sulfadiazine

0.726 g (1.75 mmol) of K_2PtCl_4 was dissolved in minimum amount of deionised water followed by slow addition of 0.953 g (3.5 mmol) of sodium salt of sulfadiazine in 40 mL of deionised water. The mixture was stirred at 40 °C for 1 h. The yellow product was filtered under vacuum, washed twice with water and dried over $CaCl_2$.

2.5.8 Synthesis of Ruthenium(III) complex of sulfadiazine

0.261 g (1 mmol) of $RuCl_3 \cdot 3H_2O$ was dissolved in 10 mL of deionised water followed by a slow addition of 0.545 g (2 mmol) of sodium salt of sulfadiazine in 40 mL of deionised water. The mixture was stirred at 40 °C for 3 h. The yellow product was filtered under vacuum, washed twice with water and dried over $CaCl_2$.

2.5.9 Synthesis of Nickel(II) complex of sulfadiazine

1.1886 g (5 mmol) of $NiCl_2 \cdot 6H_2O$ was dissolved in 15 mL of deionised water followed by slow addition of 2.723 g (10 mmol) of sodium salt of sulfadiazine in 50 mL of deionised water. The mixture was stirred at 40 °C for 1 h. The green product was filtered under vacuum, washed twice with water and dried over $CaCl_2$.

2.5.10 Synthesis of Oxovanadium(IV) complex of sulfadiazine

1.310 g (5 mmol) of $VOSO_4 \cdot 5H_2O$ was dissolved in 15 mL of deionised water followed by a slow addition of 2.723 g (10 mmol) of sodium salt of sulfadiazine in 50 mL of deionised water. The mixture was stirred at 40 °C for 1 h. The product was filtered under vacuum, washed twice with water and dried over $CaCl_2$.

2.6 Synthesis of Metal Complexes of Trimethoprim

Cobalt(II), copper(II), platinum(II), palladium(II), nickel(II), manganese(II) and iron(III) complexes of trimethoprim were synthesised by direct reaction between the metal salts and the drugs in a variety of solvent.

2.6.1 Synthesis of Cobalt(II) complex of trimethoprim

2.930 g (10 mmol) of trimethoprim was dissolved in 80 mL of methanol followed by a slow addition of 1.190 g (5 mmol) of $CoCl_2 \cdot 6H_2O$ in 20 mL of methanol. The resulted blue solution was refluxed for 3 h and the solution left to evaporate slowly at room temperature. Blue crystals formed overnight from the solution.

2.6.1.2 Cobalt(II) complex of trimethoprim

A second complex of cobalt(II) trimethoprim was synthesised from $Co(CH_3COO)_2 \cdot 4H_2O$. The complex was synthesised by dissolving 0.586 g (2 mmol) of trimethoprim in 35 mL of methanol followed by slow addition of 0.498 g (2 mmol) of $Co(CH_3COO)_2 \cdot 4H_2O$ in 65 mL of methanol. The resulting pink solution was refluxed for 3 h, layered with 65 mL of

toluene and covered with cotton wool to undergo slow evaporation at room temperature. Pink crystals were formed after a week.

2.6.2 Synthesis of Copper(II) complex of trimethoprim

1.465 g (5 mmol) of trimethoprim was dissolved in 60 mL of methanol followed by slow addition of 0.998 g (5 mmol) of $Cu_2(CH_3COO)_4 \cdot 2H_2O$ in 100 mL of methanol. The resulting green solution was refluxed for 1 h, layered with 120 mL of toluene, and transferred into the refrigerator. Green crystals formed after three days.

2.6.3 Synthesis of Platinum(II) complex of trimethoprim

1.453 g (3.5 mmol) of K_2PtCl_4 was dissolved in a minimum amount of deionised water followed by a slow addition of 1.026 g (3.5 mmol) of trimethoprim in 60 mL of methanol. The mixture was stirred at 40 °C for 1 h. The brown product was filtered under vacuum and washed twice with water.

2.6.4 Synthesis of Palladium(II) complex of trimethoprim

1.142 g (3.5 mmol) of K_2PdCl_4 was dissolved in 10 mL of deionised water followed by a slow addition of 1.026 g (3.5 mmol) of trimethoprim in 60 mL of methanol. The mixture was stirred at 40 °C for 1 h. The yellow product was filtered under vacuum and washed twice with methanol.

2.6.5 Synthesis of Nickel(II) complex of trimethoprim

0.498 g (2 mmol) of $Ni(CH_3COO)_2 \cdot 4H_2O$ was dissolved in 70 mL of methanol followed

by a slow addition of 0.586 g (2 mmol) trimethoprim in 35 mL of methanol. The resulting green solution was refluxed for 1 h and the solution left to evaporate slowly at room temperature. Green crystals suitable for X-ray analysis formed after one week.

2.6.6 Synthesis of Manganese(II) complex of trimethoprim

0.513 g (1.75 mmol) of trimethoprim was dissolved in 40 mL of methanol followed by a slow addition of 0.346 g (1.75 mmol) of $MnCl_2 \cdot 4H_2O$ in 20 mL of methanol. The resulting cream-coloured solution was refluxed for 2 h. The product was filtered and the filtrate left to evaporate slowly at room temperature. Both the initial product and the product from the evaporated filtrate were analysed. The complex obtained from the filtrate analysed pure.

2.7 Metal Complexes of Amodiaquine.

2.7.1 Synthesis of Iron(III) Complex of amodiaquine with dithiocarbamate

0.541 g of $FeCl_3 \cdot 6H_2O$ was dissolved in 20 mL of methanol followed by the addition of 0.858 g (2 mmol) of amodiaquine in 30 mL of methanol. The mixture was stirred at about 50 °C for 30 min after which 0.143 g (1 mmol) of N,N′-dimethydithiocarbamate in 20 mL of methanol. This mixture was stirred for 3 h and the product was filtered under suction. The filtrate was left to evaporate slowly at room temperature. Products from the filtrate and the precipitate were analysed to determine their composition. The precipitate analysed pure.

2.7.2 Synthesis of Iron(III) Complex of amodiaquine with 2,2-bipyridine

0.541 g of $FeCl_3 \cdot 6H_2O$ was dissolved in 20 mL of methanol followed by the addition of 0.858 g (2 mmol) of amodiaquine in 30 mL of methanol. The mixture was stirred at about 50 °C for 30 min after which 0.156 g (1 mmol) of 2,2′-bipyridine in 20 mL of methanol was added. The mixture was stirred for 3 h and filtered under suction. The filtrate was left to evaporate slowly at room temperature. Products obtained from the filtrate and precipitate were analysed to determine their composition. The precipitate analysed pure.

2.8. Synthesis of Platinum(II) complex of Chloroquine

0.836 g (2 mmol) of chloroquine base was dissolved in 50 mL acetone followed by dropwise addition of 0.830 g of Na_2PtCl_4 in minimum amount of water. The mixture was stirred at room temperature for 2 h, filtered under suction and washed with acetone. The filtrate was left to evaporate slowly at room temperature and precipitates were formed after three days. The pure complex was obtained from the filtrate.

2.9 Synthesis of Iron(III) complex of pyrimethamine with dithiocarbamate

0.541 g of $FeCl_3 \cdot 6H_2O$ was dissolved in 20 mL of methanol followed by the addition of 0.498 g (2 mmol) of pyrimethamine in 50 mL of methanol. The mixture was stirred at about 50 °C for 30 min after which 0.143 g (1 mmol) of N,N'-dimethydithiocarbamate in 10 mL of methanol. This mixture was stirred for 3 h and filtered under suction. The filtrate was left to evaporate slowly at room temperature. Both the product from the filtrate and precipitate were analysed to determine their composition. The precipitate analysed pure.

2.9.1 Synthesis of Iron(III) complex of pyrimethamine with trimethoprim

0.541g of $FeCl_3 \cdot 6H_2O$ was dissolved in 20 mL of methanol followed by the addition of 0.497 g (2 mmol) of pyrimethamine and 0.58 g (2 mmol) of trimethoprim in 60 mL of methanol. The mixture was refluxed for 3 h and filtered under suction. The filtrate was left to evaporate slowly at room temperature. Both the product from the filtrate and precipitate were analysed to determine their composition. The precipitate analysed pure.

2.9.2 Synthesis of cobalt(II) complex of pyrimethamine with trimethoprim

0.238g of $CoCl_2 \cdot 6H_2O$ was dissolved in 20 mL of methanol followed by the addition of 0.497 g (2 mmol) of pyrimethamine and 0.58 g (2 mmol) of trimethoprim in 60 mL of methanol. The mixture was refluxed for 3 h and filtered under suction. The filtrate was left to evaporate slowly at room temperature. Both the products from the filtrate and the precipitate were analysed to determine their composition. The precipitate analysed pure.

CHAPTER THREE

3.0 Results and Discussion

3.1.0 *Trans*– and *cis*–$[Co(en)_2Cl_2]Cl$

The *trans*– and *cis*– $[Co(en)_2Cl_2]Cl$ was synthesised as starting material for the synthesis of cobalt(III) complexes of the antimalarial drugs. The *trans*–complex was green in colour while the *cis*–form was purple. The complexes were characterized by elemental analysis, UV-Vis, magnetic susceptibility measurement, IR and conductivity measurements. Elemental Analysis: *trans*– $[Co(en)_2Cl_2]Cl$; $CoC_4H_{16}N_4Cl_3$ (molar mass, 285.49); [Found (Calc.)] Co, 21.17 (20.64); C, 16.85 (16.83); H, 5.69 (5.65); N, 19.68 (19.63), % yield = 78%, μ = 0.59 B.M.

Elemental Analysis: *cis*–$[Co(en)_2Cl_2]Cl$; [Found (Calc.)] Co, 21.17 (20.64); C, 16.85 (16.83); H, 5.69 (5.65); N, 19.68 (19.63), % yield = 89%, μ = 0.45 B.M.

3.1.1 Electronic spectra of Cobalt(III) complexes

The visible absorption spectra of cobalt(III) complexes consist of transitions from $^1A_{1g}$ ground state to other singlet states. It is possible to observe spin-allowed, d-d bands in the visible region of the spectra of low-spin cobalt(III) complexes because of the small value of 10Dq, (Δ), which is required to induce spin-pairing in the cobalt(III) ion[163]. Thus, the strong field ligands that do not cause the low-energy charge-transfer bands, often dictate the spectra of low-spin complexes. Consequently the two absorption bands found in the visible spectra of regular octahedral cobalt(III) complexes represent transition to the upper states $^1T_{1g}$ and $^1T_{2g}$, i.e. $^1A_{1g} \rightarrow {}^1T_{1g}$ and $^1A_{1g} \rightarrow {}^1T_{2g}$. These transitions correspond to the electronic promotion $t^6_{2g} \rightarrow t^5_{2g}e^1_g$ with the promoted electron retaining its spin

state. The orbital multiplicity of the $t^5_{2g}e^1_g$ configuration is 6 and so corresponds to two orbital triplet terms $^3T_{1g}$ and $^3T_{2g}$. On the other hand, if the promoted electron changes its spin, the orbital multiplicity is again 6 but the two T terms are now spin triplets, $^3T_{1g}$ and $^3T_{2g}$ given rise to a spin forbidden $^1A_{1g} \rightarrow {}^3T_{1g}$.

3.1.2 Electronic Spectra and Magnetic properties of *trans*– and *cis*– $[Co(en)_2Cl_2]Cl$

The electronic spectra of the *trans*– and *cis*– $[Co(en)_2Cl_2]Cl$ is shown in Figure 6. The *trans*–isomer showed marked splitting of $^1T_{1g}$ level due to substantial difference between en and Cl in the spectrochemical series[164]. Three bands were observed for the *trans*–isomer while the *cis*–isomer showed two bands; each complex has one well-defined band which occurred at about 625 nm for the *trans* isomer and at 540 nm for the *cis* isomer while the other band(s) is/are relatively less prominent. The observed bands in the *cis*–isomer are relatively broader than those of the *trans*–isomer because the *cis*-form lacks a center of symmetry[165].

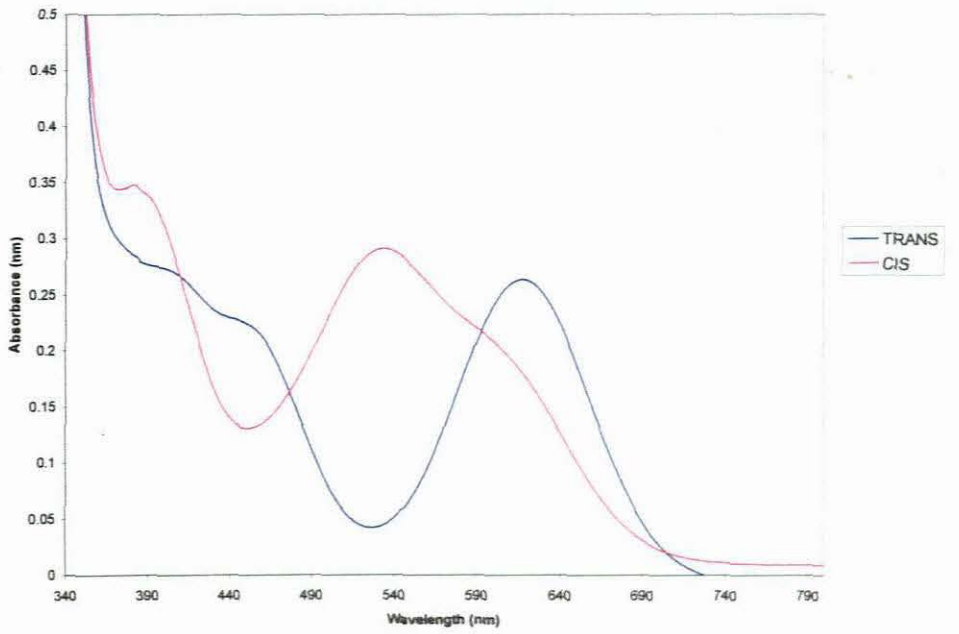

Figure 6: Solution spectra of *cis*/*trans*–$[Co(en)_2Cl_2]Cl$ in DMF

The effective magnetic moment of the *trans* form is 0.59 B.M. while that of the *cis* is 0.45 B.M. Cobalt(III) complexes are expected to be diamagnetic. The effective magnetic moments appear slightly higher than what is expected of low-spin octahedral d^6 configuration. This is most likely due to spin-orbit coupling since the complexes analyzed pure.

3.1.3 Infrared spectroscopy

The IR can be used to distinguish between the *trans* and *cis* isomers by comparing the spectra in the region 1700-1500 cm^{-1} (δNH_2), 950-850 cm^{-1} (CH_2 rocking), and 610-500 cm^{-1} (νM—N) as well as the Co—Cl stretching frequency at 400-300 cm^{-1}

respectively[166,167]. The *trans* forms belong to point group C_{2h}, in which only u vibrations (antisymmetric with respect to the center of symmetry) are infrared active. On the other hand, the *cis* forms belong to the C_2 point group, in which all the vibrations are infrared active. Thus, the *cis*-isomer exhibits more bands than the *trans*-isomer. The *trans* gave one band at 1553 cm^{-1} while the *cis* gave two bands at 1535 cm^{-1} and 1501 cm^{-1} for the NH_2 bending frequency. The *trans* form also showed a very sharp νCo—N band at 587 cm^{-1} and νCo—Cl at 294 cm^{-1}. On the other hand, the νCo—N in the *cis*-isomer is split into two occurring at 587 and 574 cm^{-1} while νCo—Cl also showed two sharp bands of comparable intensity at 293 and 269 cm^{-1}.

3.2.0 Cobalt (III) complexes of Antimalarial Drugs

3.2.1 Cobalt (III) complexes of Chloroquine

Chloroquine diphosphate was converted to the base ($C_{18}H_{26}N_3Cl$) prior to use. The white powder obtained analysed pure. Elemental analysis for $C_{18}H_{26}N_3Cl$, molar mass 319.88; [Found (Calc.)]: C, 68.06 (67.59); H, 8.24 (8.19); N, 13.23 (13.14); yield = 65%. The Co(III) chloroquine complexes were synthesized by reacting chloroquine base with the *trans*- or *cis*-$[Co(en)_2Cl_2]Cl$ in ethanol as described in Section 2.4.0. The complexes were formulated as $[Co(en)_2(CQ)Cl]Cl_2$, (CQ = chloroquine) and both complexes retain the green and purple colour of the starting material. Elemental analysis: [Found (Calc.)]: $CoC_{22}H_{34}N_7Cl_4$, molar mass, 597.30; Co, 9.29 (9.87); C, 43.01 (43.65); H, 6.31 (6.99); N, 16.50 (16.20). Microanalyses revealed that chloroquine base did not coordinate with the *cis*-$[Co(en)_2(CQ)Cl]Cl_2$. The proposed structure of the complex isolated is given in Figure 7.

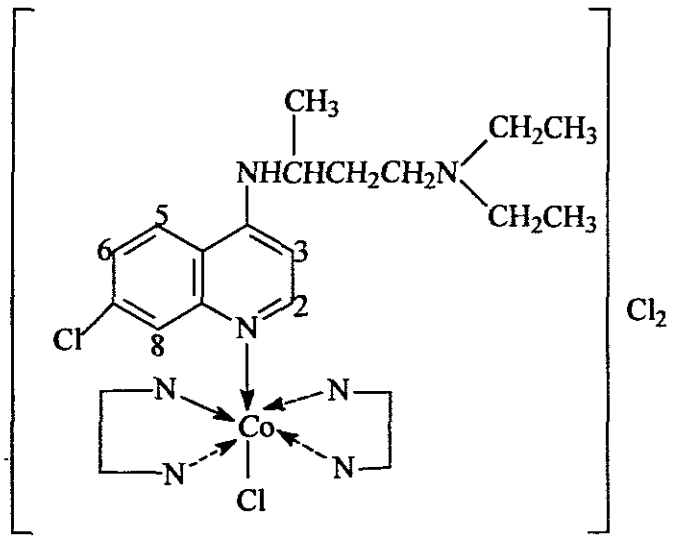

Figure 7: Proposed structure for Co(III) complex of chloroquine

3.2.1.1 Electronic Spectra and Magnetic properties of *trans*–$[Co(en)_2(CQ)Cl]Cl_2$

The electronic spectra of *trans*–$[Co(en)_2(CQ)Cl]Cl_2$ in water and DMF (Figure 7) show slight difference that may be due to the interaction of the solvent with the complex. The spectra are typical of octahedral low-spin complex. In DMF, two weak bands occur in the visible region; a band at 16,666 cm^{-1} (600 nm) is assigned to $^1A_{1g} \rightarrow {}^1T_{1g}$ and the second band at 17,543 cm^{-1} (570 nm) assigned to $^1A_{1g} \rightarrow {}^1T_{2g}$. The corresponding prominent band in water occurs at 15,873 cm^{-1} (630 nm), devoid of the fine structures observed in DMF, is assigned to $^1A_{1g} \rightarrow {}^1T_{1g}$. However, two additional well-separated bands were observed at about 26,666 cm^{-1} (375 nm), a shoulder, and 21,276 cm^{-1} (470 nm). It would appear that these last two bands were shifted to the red in the spectrum run in DMF. A magnetic moment of 0.47 BM was obtained for the complex that confirmed that it is a low-spin cobalt(III) complex.

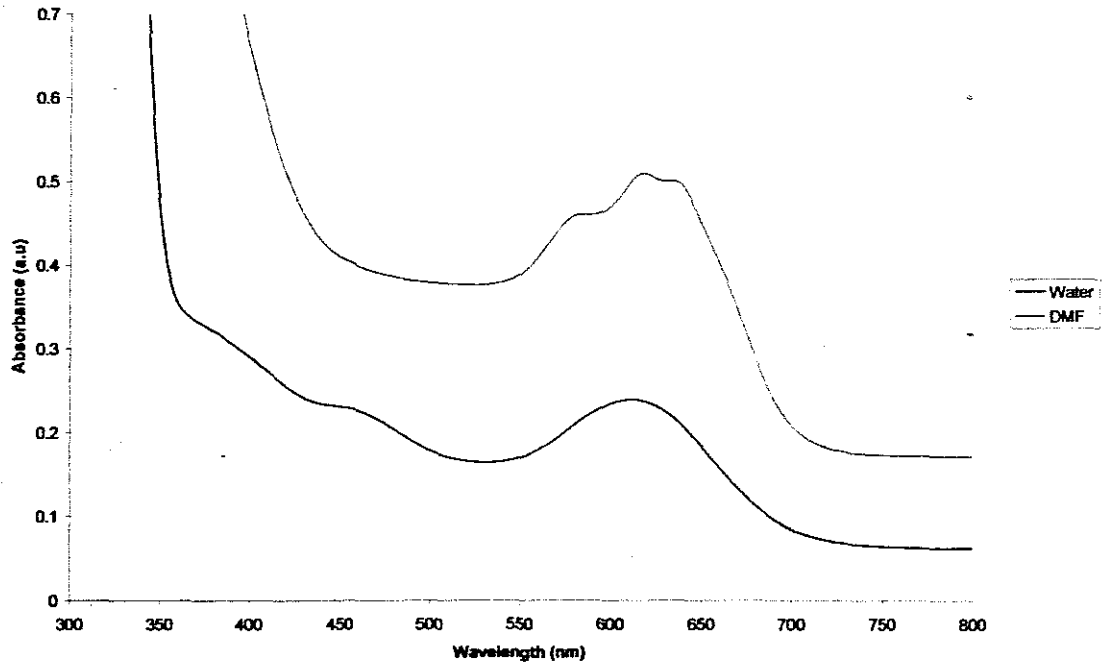

Figure 8: Solution Spectra of trans–$[Co(en)_2(CQ)Cl]Cl_2$

3.2.1.2 Infrared Spectra of *trans*–$[Co(en)_2(CQ)Cl]Cl_2$

Chloroquine base possesses three potential donor sites: the endocyclic nitrogen of the quinoline ring, the secondary amino nitrogen and the tertiary amino nitrogen. The IR of the free chloroquine base was compared with that of the complex (Figure 9) to determine the donor site at which the drug coordinated to the cobalt. Three absorption bands at 3475, 3271 and 3242 cm^{-1} showed that the N—H of the chloroquine base as well as the NH_2 of the en were intact. This observation was further strengthened by the sharp absorption band at 887 and 807 cm^{-1} due to N—H deformation.

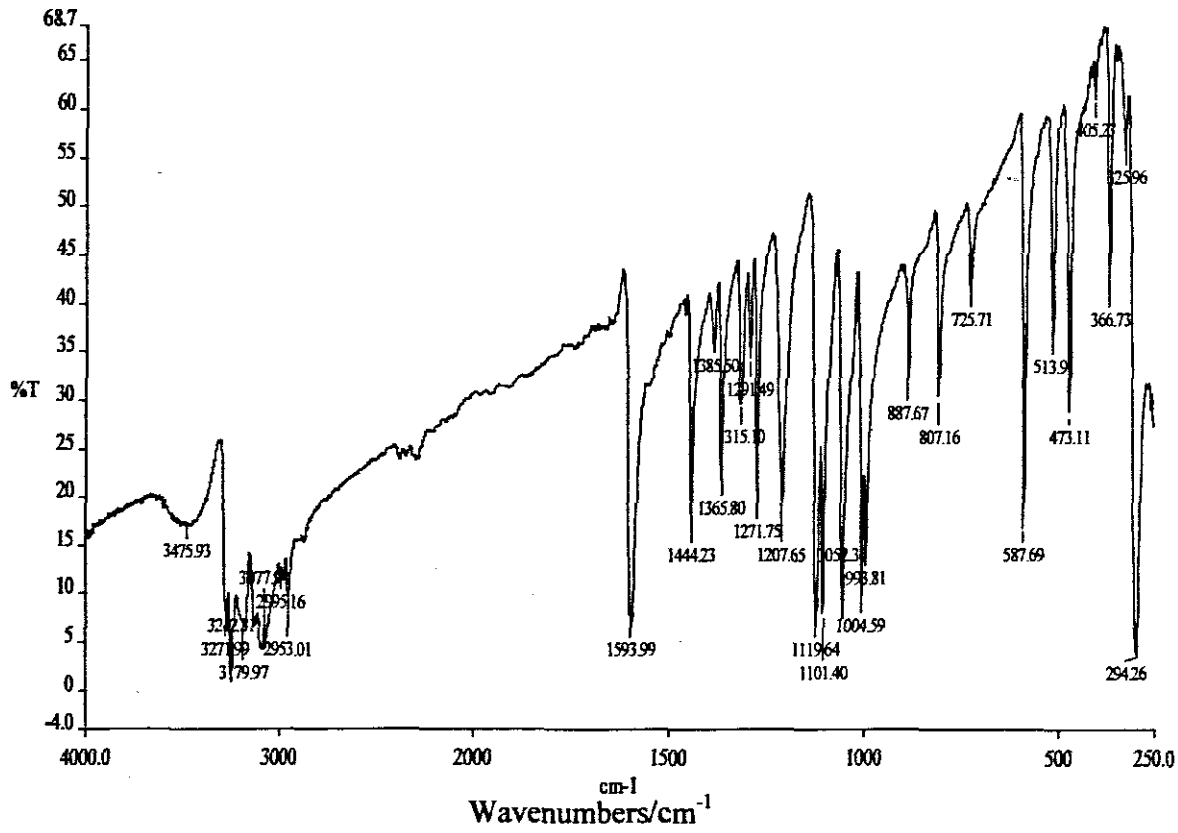

Figure 9: Infrared spectrum of *trans*–$[Co(en)_2(CQ)Cl]Cl_2$

The ν(C=N) which occurs at 1575 cm^{-1} with medium intensity in the chloroquine base shifted to a very sharp band at 1593 cm^{-1} with strong to medium intensity. This shows that chloroquine bond preferentially with the quinoline N atom. The C—N bands for the tertiary amino N atom that occurred at 1365 cm^{-1} remained virtually unchanged in the complex. Three Co—N bands can be assigned at 587 cm^{-1} (due to Co—N of en), 473 cm^{-1} (Co—N of the quinoline N(1)) and another at 513 cm^{-1} may be due to slight differences in the orientation of the two molecules of en in the complex. The νCo—Cl occurred as a single sharp band at 294 cm^{-1}.

3.2.1.3 ^{1}H nmr and mass spectrometry of *trans*–$[Co(en)_2(CQ)Cl]Cl_2$

The variation of the chemical shift in the ^{1}H nmr spectrum of the complex was compare with that of the chloroquine base (Table 1).

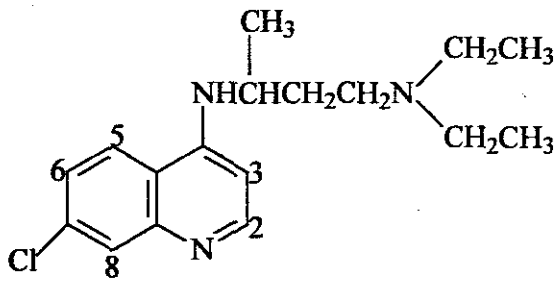

Figure 10: Chloroquine base

Table 1: ^{1}Hnmr of *trans*–$[Co(en)_2(CQ)Cl]Cl_2$

Position	Chloroquine / ppm	$[Co(en)_2CQCl]Cl_2$ / ppm
H2	7.80	9.20
H3	6.57	6.77
H5	7.40	7.52
H6	8.20	8.40
H8	8.35	8.40

The results showed that the protons in the complex shifted downfield with respect to the chloroquine base. The largest shift variation occurred for the H(2) which is at the vicinity of the endocyclic N-atom of chloroquine which the IR confirmed coordinated to Co atom. This further confirms the point at which the drug is bonded to the metal.

In the mass spectrometry of the Co(III)chloroquine complex, a peak was observed at m/z = 320 which corresponded to the loss of $[Co(en)_2Cl]$ from the molecule. The base peak

occurred at m/z = 249, which was due to a further fragmentation at the tertiary amino nitrogen of the chloroquine base, that is a loss of $—N(CH_2CH_3)_2$ from chloroquine base. The peak at m/z = 161 is attributed to the aliphatic side chain of chloroquine base, $C_9H_{24}N_2$.

3.2.2 Cobalt (III) complexes of Amodiaquine

All amodiaquine complexes were green in colour, irrespective of whether the starting material was *trans–/cis–*$[Co(en)_2Cl_2]Cl$. Even though the complex was prepared at 2:1 mole ratio of amodiaquine to the starting material, the product was 1:1, formulated as *trans–*$[Co(en)_2(AQ)Cl]Cl_2$, (AQ = amodiaquine). Elemental analysis for $CoC_{24}H_{38}N_7OCl$, molar mass = 641.36. [Found (Calc.)]: Co, 9.37 (9.19); C, 45.52 (44.95); H, 5.78 (5.97); N, 15.22 (15.29). Attempts to prepare the complex in a 1:1 mole ratio failed as the elemental analysis gave essentially the starting material, *trans–/cis–*$[Co(en)_2Cl_2]Cl$. In addition, irrespective of whether the starting material was *trans* or *cis*, the final product was always *trans* (confirmed by the colour, the electronic spectral and the IR). The proposed structure for the compound formed is shown in Figure 11.

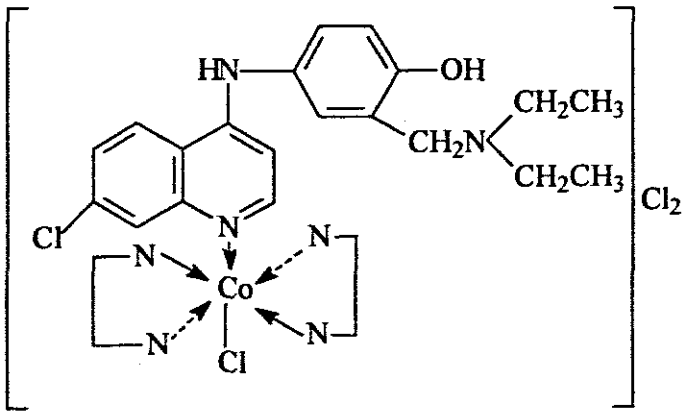

Figure 11: Proposed structure for $[Co(en)_2(AQ)Cl]Cl_2$

3.2.2.1 Spectral and Magnetic properties of $[Co(en)_2(AQ)Cl]Cl_2$

The solution and reflectance spectra of the complex (Figure 12 and 13) confirmed the initial observation in which the *cis* form changes to *trans* by turning from brown to green. An absorption maximum occurred at 25 000 cm^{-1} (400 nm), assigned to $^1A_{1g} \rightarrow {}^1T_{2g}$ and a second absorption occurred at 16 666 cm^{-1} (600 nm), which may be due to $^1A_{1g} \rightarrow {}^1T_{1g}$ transition. The second band appeared split to three bands at about 14, 285 -16 666 cm^{-1} (600-700 nm). The electronic spectra confirmed octahedral geometry formulated for the complex. In the solution spectrum, these bands split into two well defined bands and occurred at 16 666 cm^{-1} (600 nm) and 14 815 cm^{-1} (675 nm) respectively.

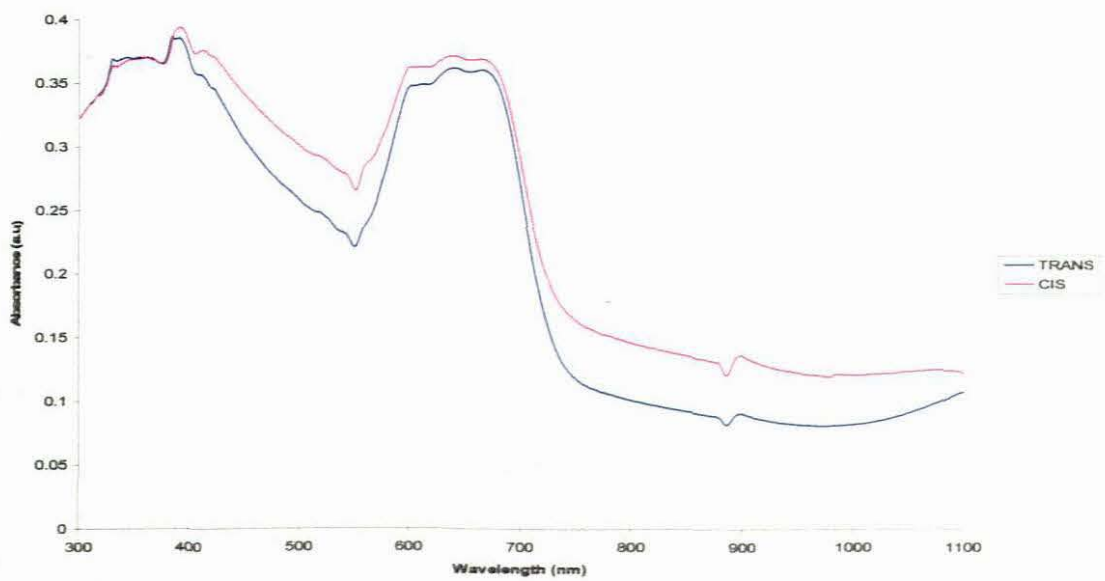

Figure 12: Reflectance Spectra of $[Co(en)_2(AQ)Cl]Cl_2$

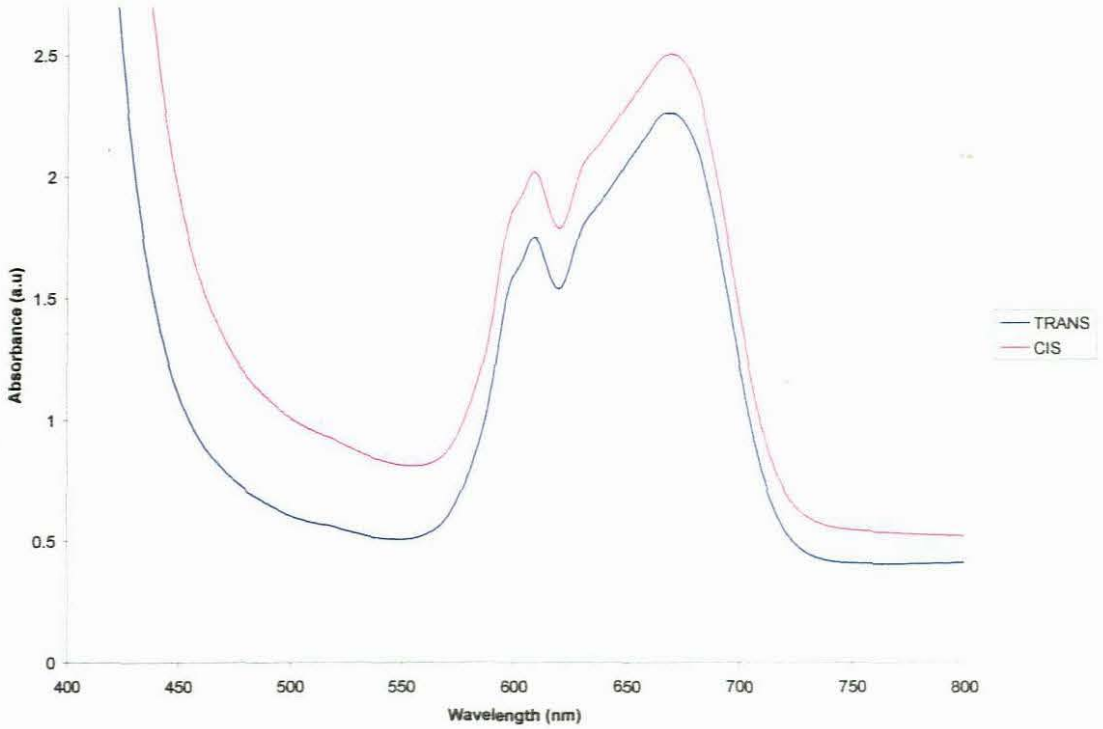

Figure 13: Solution Spectra of $[Co(en)_2(AQ)Cl]Cl_2$

3.2.2.2 Infrared Spectroscopy of $[Co(en)_2(AQ)Cl]Cl_2$

Amodiaquine, like chloroquine, possesses three potential donor sites. A comparison of the IR of the complex and the free ligand showed that there were extra absorption bands in the region 3093-3421 cm^{-1} in the complex. This could be attributed to the symmetric and asymmetric stretching frequencies of the NH_2 of en. In the drug the ν(C=N), which was occured at 1587 and 1618 cm^{-1} shifted marginally to 1582 and 1615 cm^{-1} in the complex. The νCo—N bands occurred at 587 and 512 cm^{-1} (due to Co—N of en), and at 474 cm^{-1} (due to Co—N of the quinoline N(1)). The νCo—Cl occurs as a single sharp band at 294 cm^{-1} (Figure 14) confirming that the complex bonded to one Cl atom in both *cis* and *trans* starting cobalt(III) complexes. Complexes prepared from *cis*- and *trans*-

$[Co(en)_2Cl_2]Cl$ produced similar IR spectra confirming that both isomers gave the same complex.

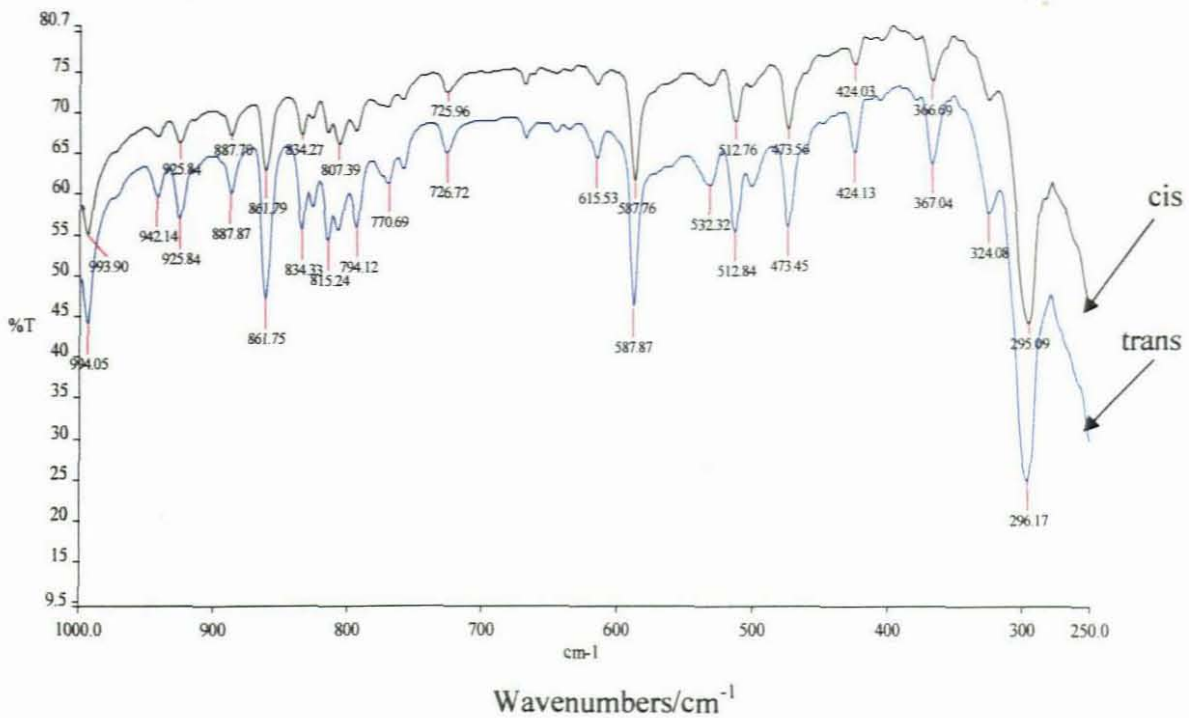

Wavenumbers/cm^{-1}

Figure 14: Infrared spectra of cis/trans- $[Co(en)_2(AQ)Cl]Cl_2$

3.2.3 Cobalt (III) complexes of Quinacrine

The Co(III) complex of quinacrine was synthesised from quinacrine and the starting precursor complexes. The complexes were synthesised in a 1:1 mole ratio using both *cis/trans*-$[Co(en)_2Cl_2]Cl$. Elemental analyses revealed that there was no coordination between quinacrine and the *trans*-$[Co(en)_2Cl_2]Cl$ whereas the reaction with the *cis* analogue appeared to have yielded a polymeric substance formulated as $[Co_2(QNC)(en)_4Cl_6]\cdot 2HCl$, QNC = quinacrine. Elemental analysis, $Co_2C_{31}H_{64}Cl_9N_{11}O$: Co, 11.83 (11.29); C, 34.62 (35.67); H, 5.94 (6.18); N, 14.82 (14.76); Cl, 31.27 (30.57).

Efforts are in progress to grow the crystals of the compound for structural analysis in order to ascertain the stoichiometry of the complex. Attempt is also ongoing for the nmr studies.

3.2.3.1 Spectra and Magnetic properties of Co(III) complex of quinacrine

The solution and reflectance spectra of the complex are presented in Figures 15 and 16.

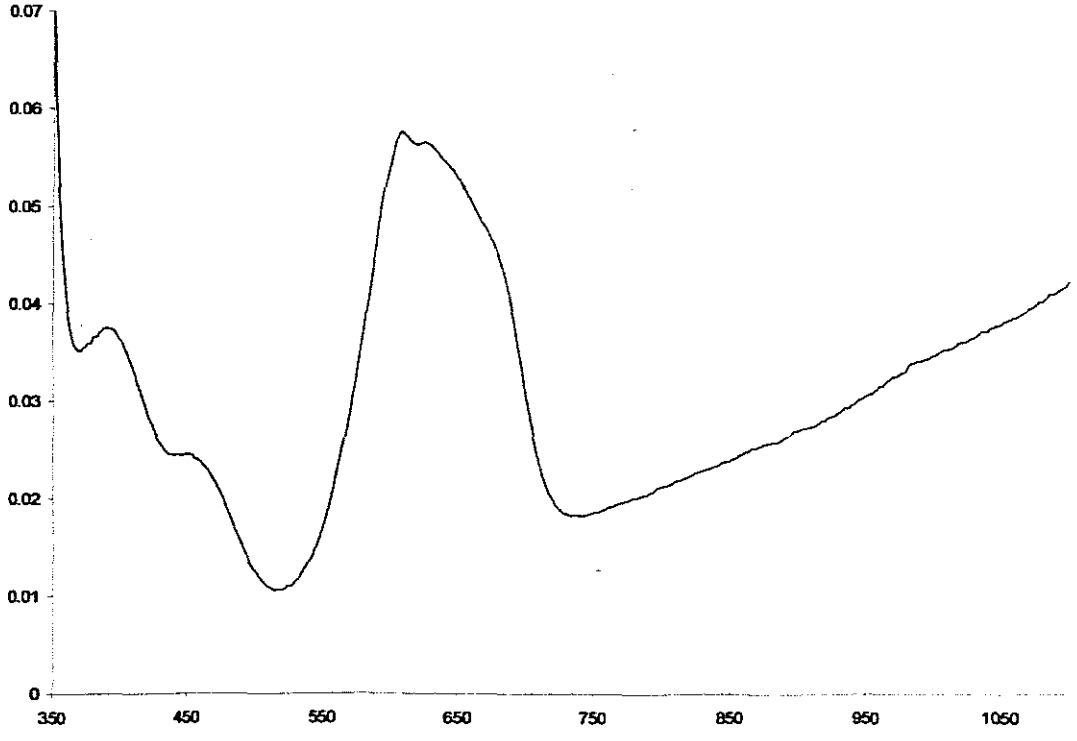

Figure 15: Solution spectrum of trans-Co(III)quinacrine in DMF

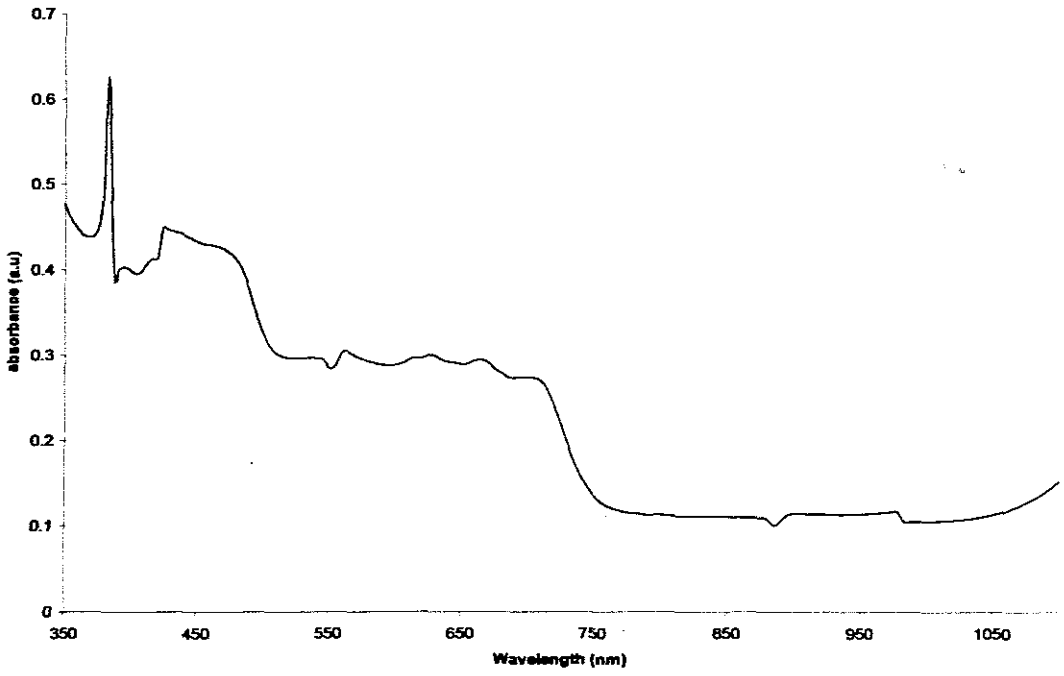

Figure 16: Reflectance spectra of Co(III)quinacrine

The solution spectrum of the complex showed absorption maxima typical of octahedral complex. In the solution spectrum, the complex showed absorption bands in the region 16,475 cm^{-1} (607 nm) that appear slightly split and can be assigned to $^1A_{1g} \rightarrow {}^1T_{1g}$. The second band occurred at about 25,840 cm^{-1} (387 nm) assigned to $^1A_{1g} \rightarrow {}^1T_{2g}$ with a third band at 21,787 cm^{-1} (459 nm). On the other hand the reflectance spectrum appears too complex to assign any geometry, presumably because of the non-monomeric nature of the complex. Apparently, the complex broke down to monomeric octahedral species in solution.

3.2.3.2 Infrared Spectra

The infrared spectrum of $[Co_2(QNC)(en)_4Cl_6]\cdot 2HCl$ is shown in Figure 17. Quinacrine possesses three potential donor sites through which it can coordinate to the metal ion. A

comparison of the IR of the complex with that of the ligand showed that quinacrine most probably coordinated through the endocyclic N atom. The band at 3393 cm^{-1} indicates that the N—H on the quinacrine is still free in the complex. The ν(C=N), which occurs at 1595 and 1634 cm^{-1} in the ligand with medium to sharp intensity, occurred as very sharp bands at 1587 and 1630 cm^{-1} in the complex. The νCo—N band due to en occurred as a rather weak bandat 588 cm^{-1}along with other overlapping bands. This seems to confirm the presence of Co—N band in different chemical environment. The band at 474 cm^{-1} is assigned Co—N of the endocyclic N(1). The Co—Cl occur as a single sharp band at 294 cm^{-1} (Figure 17).

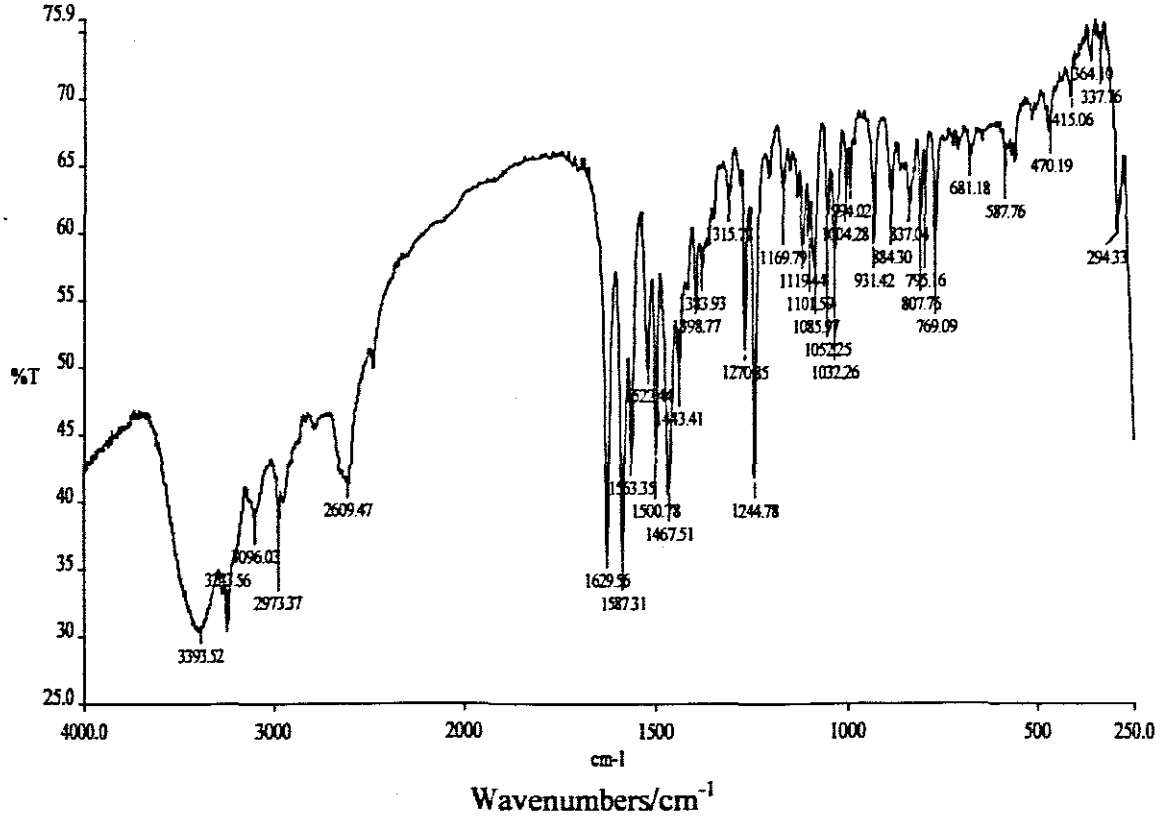

Figure 17: Infrared spectrum of Co(III) complex of quinacrine

3.2.4 Cobalt (III) complexes of Trimethoprim

The Co(III) complex of trimethoprim was synthesised from trimethoprim and *trans*– / *cis*– $[Co(en)_2Cl_2]Cl$ in methanol and ethanol. Microanalyses showed that there was no coordination in ethanol when the reaction was carried out in a 1:1 mole ratio. However, when the preparation was done at 2:1 mole ratio the *trans*–complex was isolated. The complex obtained is formulated as $[Co(en)_2(TMP)_2]Cl_3$, (TMP = trimethoprim), $CoC_{32}H_{52}N_{12}O_6Cl_3$ (molar mass, 866.13). Analysis: [Found (Calc.)]: Co, 6.80 (7.50); C, 44.56 (44.38); H, 6.00 (6.05); 19.12 (19.41). The proposed structure is shown in Figure 18.

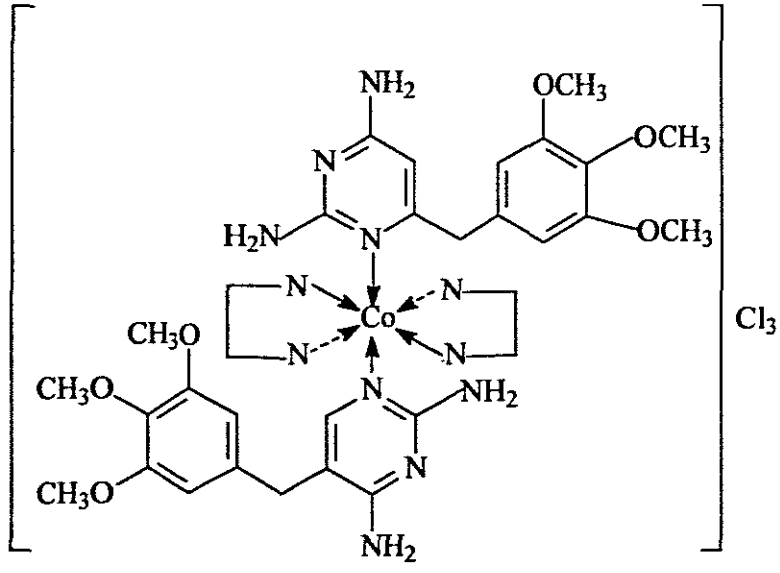

Figure 18: Proposed structure for $[Co(en)_2(TMP)_2]Cl_3$

The filtrate obtained from the preparation in methanol in a 1:1 mole ratio was concentrated and crystallised. Both products from the filtrate and the precipitate obtained from the reactions were analyzed. The precipitate analysed as un-reacted trimethoprim, $C_{14}H_{18}N_3O_3$; found (calc): C, 57.70 (57.92); H, 6.13 (6.25); N, 19.37 (19.30); whereas the

product obtained from the filterate analyzed as $[Co(en)_2(TMP)Cl]Cl_2$, $CoC_{18}H_{34}N_8O_3Cl_3$; Molar mass, 575.81. Elemental analysis: [Found (Calc.)]: C, 37.13 (37.55); H, 5.98 (5.95); N, 17.39 (19.46). The N is lower than the expected value. The proposed structure based on this analysis is shown in Figure 19.

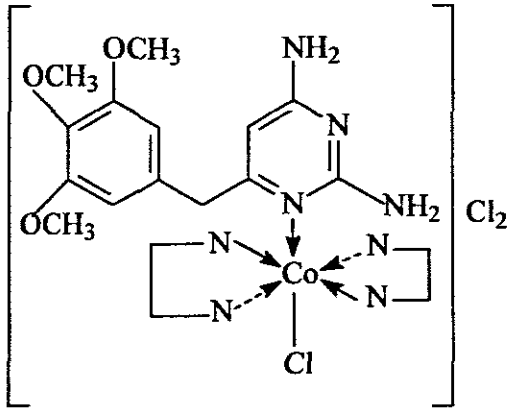

Figure 19: Proposed structure for $[Co(en)_2(TMP)Cl]Cl_2$

3.2.4.1 Electronics Spectra and Magnetic properties of Co(III) trimethoprim complexes

The electronic spectra of the complexes are shown in Figures 20 and 21. The complexes showed absorption bands in the region 14,706-16,129 cm^{-1} (680-620 nm) that appear split and can be assigned to $^1A_{1g} \rightarrow {}^1T_{1g}$. The second band occurred at about 22,222-25,000 cm^{-1} (450-400 nm) assigned to $^1A_{1g} \rightarrow {}^1T_{2g}$. The second absorption band is more intense in the 1:1 complex formed from methanol while the first band is much more intense in the 2:1 complex formed from ethanol. All the spectra are typical of octahedral complexes. A magnetic moment of 0.56 BM was obtained for $[Co(en)_2(TMP)Cl]Cl_2$ and 0.32 BM was obtained for $[Co(en)_2(TMP)_2]Cl_3$. This confirms that the complexes are low spin Co(III) complexes.

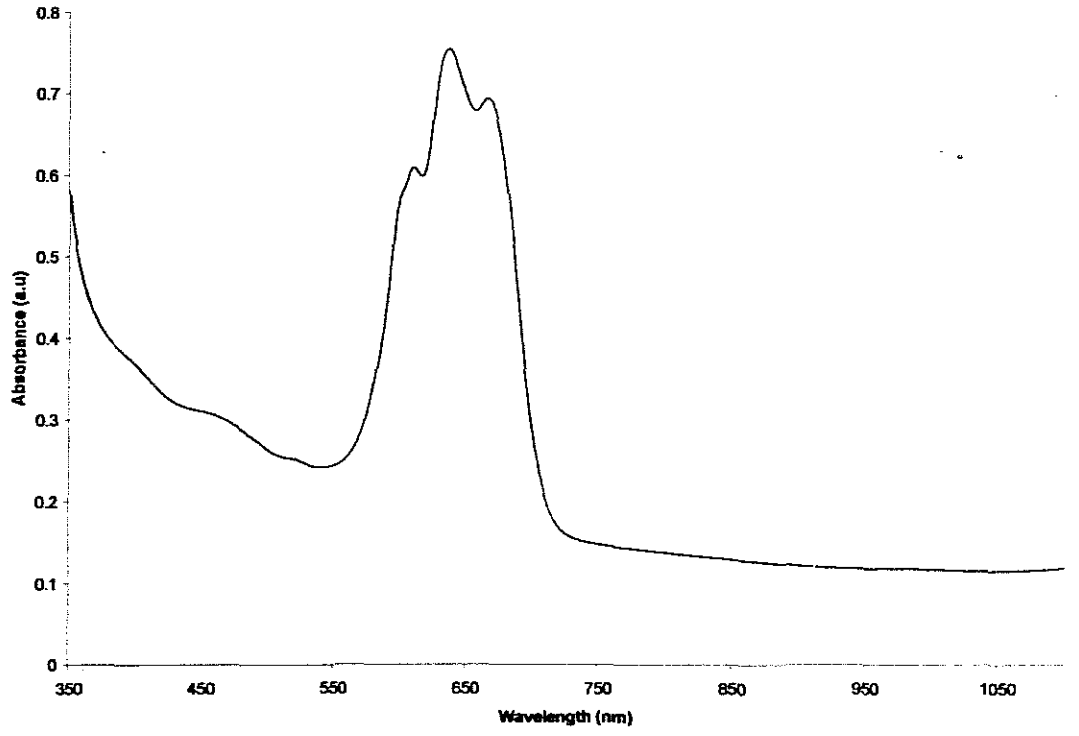

Figure 20: Solution spectra of $[Co(en)_2(TMP)_2]Cl_3$ in DMF

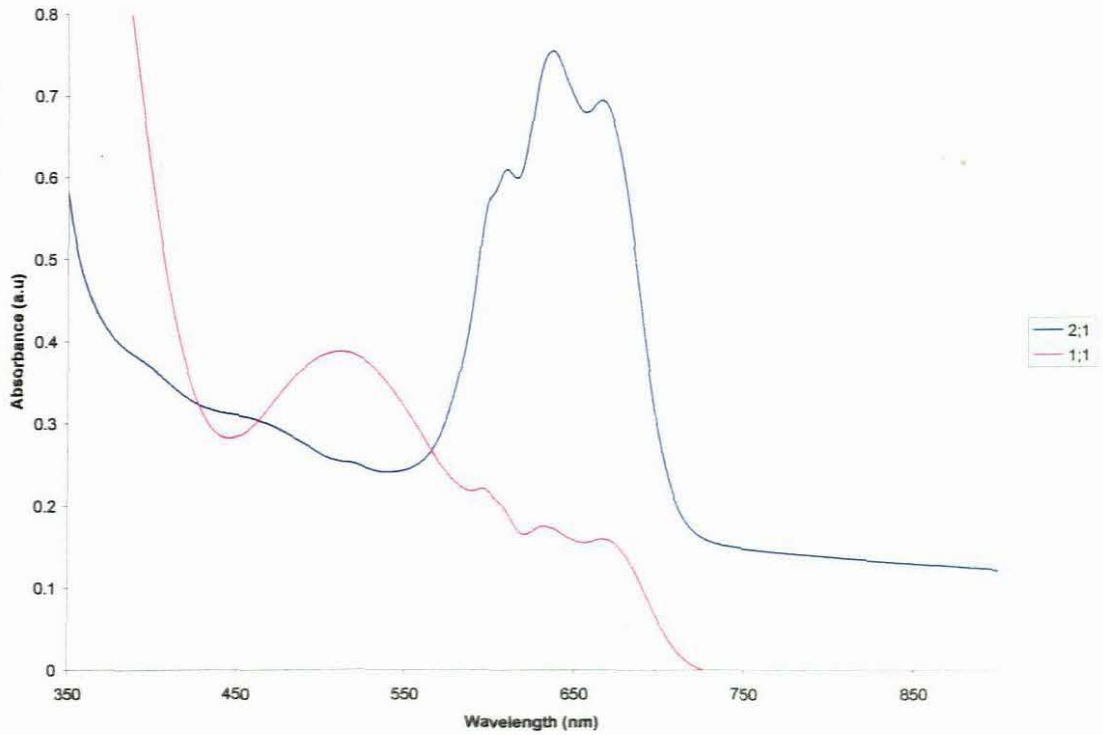

Figure 21: Solution spectra of Co(III)trimethoprim

3.2.4.2 Infrared Spectra of Co(III) complexes of trimethoprim

The infrared spectrum of *trans*-$[Co(en)_2(TMP)_2]Cl_3$ is shown in Figure 22 while selected IR bands of both $[Co(en)_2(TMP)_2]Cl_3$ and $[Co(en)_2(TMP)Cl]Cl_2$ are presented in Table 2.

Table 2: Selected IR bands for Co(III) complexes of trimethoprim

Formulation	$\nu(NH_2)$	$\nu(C{=}N)$	$\nu Co{-}N$ Quinoline N	$\nu Co{-}N$ (en)
Trimethoprim	3471vs 33318s	1632w 1565m		
$[Co(en)_2(TMP)_2]Cl_3$	3469vs 3318s	1642m 1590s	510vs	389vs
$[Co(en)_2(TMP)Cl]Cl_2$	3404m 3324m	1668w 1590vs	529vs	387s

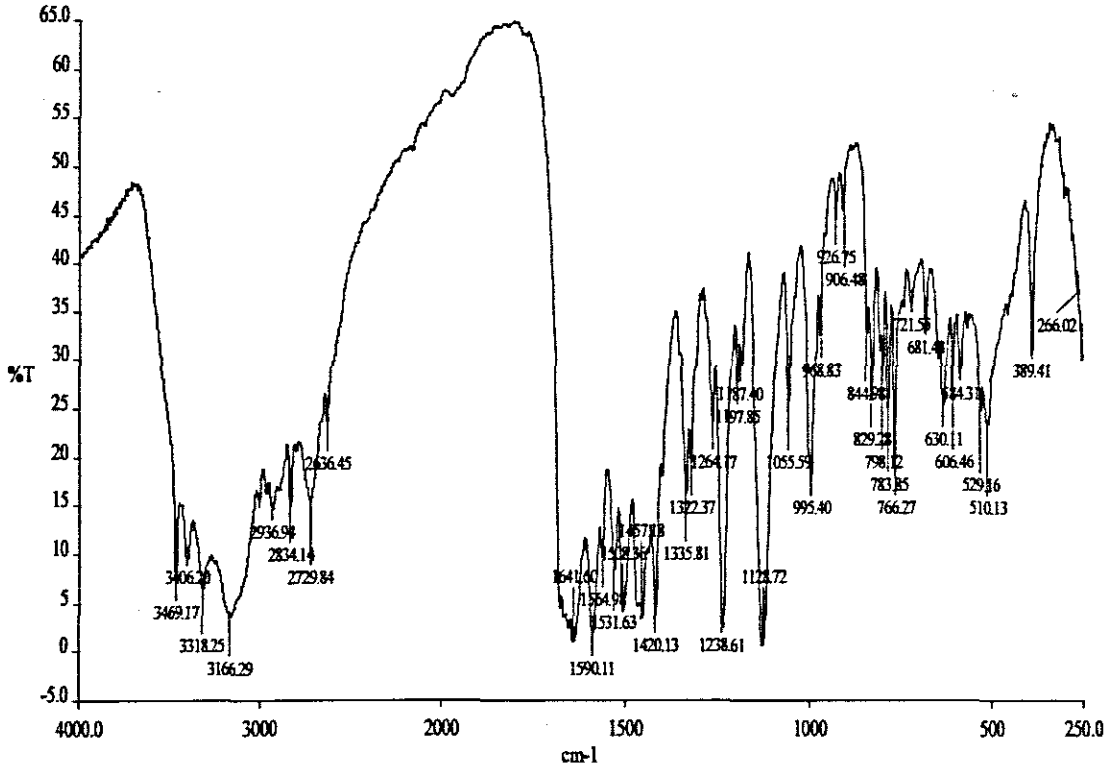

Figure 22: IR spectrum of $[Co(en)_2(TMP)_2]Cl_3$

Trimethoprim possesses seven potential donor sites; two pyrimidinyl N atoms, two NH_2 groups on the pyrimidinyl ring and three methoxy groups but the two pyrimidinyl N atoms and two NH_2 group on the pyrimidinyl ring are considered as the most likely point for coordination. The IR spectrum of the ligand was compared with the IR spectra in order to make tentative assignment of the bands. The extra bands that appear in the complexes in the region 3100 – 3500 cm^{-1} might be due to the presence of extra NH_2 group from en. The ν(C=N) shifted in both complexes as compared to trimethoprim and the Co—N bands are almost similar in both complexes.

3.2.5 Cobalt (III) complexes of tetracycline

The Co(III) complex of tetracycline (TCQ) was synthesised from tetracycline and the starting material, *cis*- and *trans*-$[Co(en)_2Cl]Cl_2$. The complex analyzed as $[Co(en)_2(TCQ)Cl]Cl_2$ (molecular formula $CoC_{26}H_{40}N_6Cl_3O_8$, molar mass = 729.93). For the complex from *cis* starting material, elemental analysis: [Found (Calc.)]: Co, 8.07, (8.07); C, 40.76 (42.78); H, 5.63 (5.52); N, 9.54 (11.53) and for the complex from *trans* starting material, elemental analysis: [Found (Calc.)]: Co, 8.41, (8.07); C, 41.45 (42.78); H, 5.58 (5.52); N, 8.38 (11.53). The two complexes were brown. The elemental analyses showed they are essentially the same compound. In both cases, the composition of carbon and nitrogen are lower than the expected values. There are two plausible explanations for the observed deviations; it is either the complexes formed through elimination of -$N(CH_3)_2$ from tetracycline or the complex is formed with lattice water molecule since the tetracycline free base used for the synthesis contain x molecules of water. Evidence from IR spectra of the complexes showed bands between 700-800 cm^{-1} that might be due to lattice water molecule but this does not necessarily mean that -$N(CH_3)_2$ has been eliminated. The structure of the complexes will be confirmed after the ^{1}Hnmr and ^{13}Cnmr or possibly the X-ray data of the complexes have been done.

3.2.5.1 Spectra and Magnetic properties of Cobalt(III)tetracycline complexes

The electronic spectra of the tetracycline complexes are shown in Figure 23 (a and b). The spectra confirm that both complexes were essentially the same, and strengthened the results from microanalyses.

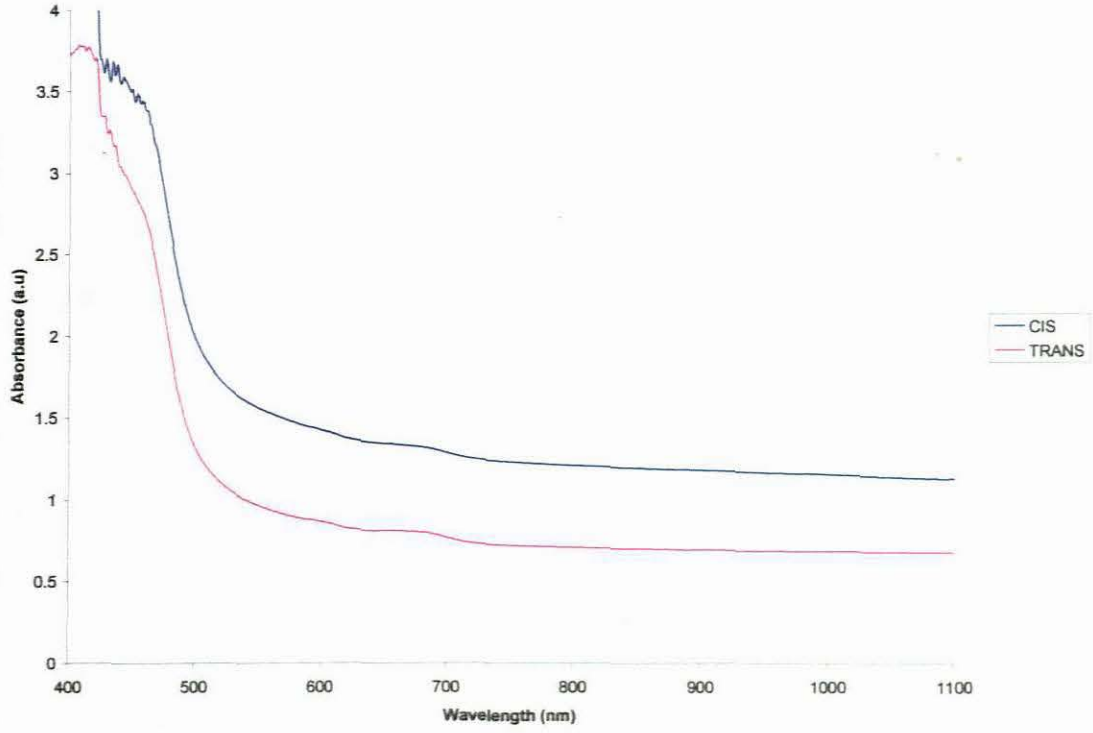

Figure 23a: Solution spectra of Co(III) tetracycline complexes in DMF

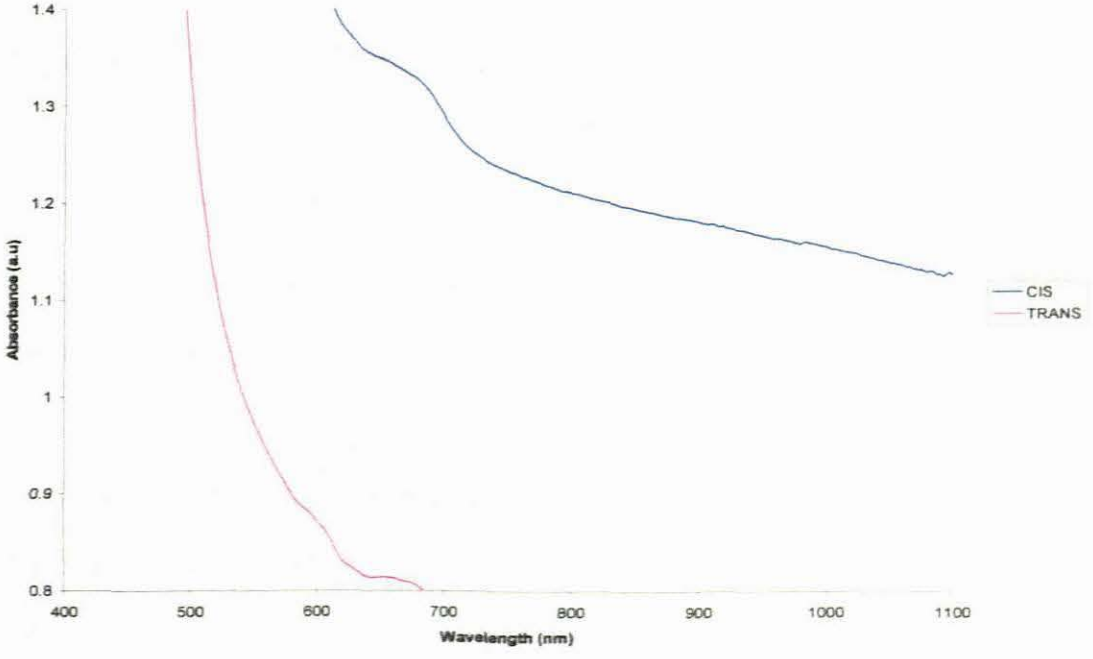

Figure 23b: Solution spectra of Co(III) tetracycline complexes in DMF

The complexes showed an absorption band at about 15,152 cm^{-1} (660 nm), Figure 23b which is assigned to $^1A_{1g} \rightarrow {}^1T_{1g}$ and the second band, a shoulder, occurs at about 23,529 cm^{-1} (425 nm) assigned to $^1A_{1g} \rightarrow {}^1T_{2g}$. The spectra look like a typical octahedral spectrum although the bands are not well defined.

3.2.5.2 Infrared Spectra of the Co(III) complex of tetracycline

The assignments of the IR bands are proposed based on the reported detailed study of IR and vibrational assignments for tetracycline and analogues and other studies of metal-tetracycline complexes[168]. The infrared spectra of both complexes are similar. The (v-OH + NH_2) of tetracycline at 3368 and 3434 cm^{-1} is collapsed in the complex yielding a broad band centered at approximately 3353 cm^{-1}. Another very weak band at about 3700 cm^{-1} with bands between 800-700 cm^{-1} may be an indication of lattice water in the complex. The Co—N is assigned to band at 509 cm^{-1}.

3.3 Metal Complexes of Sulfadiazine

The Co(II), Cu(II), Zn(II), Mn(II), Ni(II), Pd(II), Pt(II), Fe(III), Ru(III), and VO(II) complexes of sulfadiazine were synthesised as highlighted in paragraph 2.5.

3.3.1 Cobalt (II), Mn(II), Cu(II) and Zn(II), complexes of sulfadiazine

In the course of these syntheses, attempts were made to use different metal salts with the intention of establishing the effect of varying the counter-anion on the composition of the complexes, but irrespective of the metal salt used (halides, acetate, nitrate or sulfate),

results from elemental analyses showed that the products were essentially the same. In each case two solvent molecules were always accommodated within the coordination sphere of each complex. The complexes were formed by cation exchange between the metal salts and the sodium salt of sulfadiazine. The formation of the complexes may be represented by the general equation below.

$$MX_2{\cdot}nH_2O + 2\,Na(SD) \longrightarrow [Co(SD)_2(A)_2] + 2\,NaX + n\,H_2O$$

($X = Cl^-, NO_3^-, SO_4^-, CH_3COO^-$ and $A = H_2O, CH_3OH$, M = Co, Cu, Mn and Zn; SD = sulfadiazine).

The complexes were completely insoluble in water and non-coordinating solvents but easily dissolved in polar solvents with strong donor strength like DMF. The complexes were non-electrolytes in DMF with Λ_m values of 1.0 and 4.0 $\Omega^{-1}cm^2mol^{-1}$. The complexes were characterised by elemental analyses, UV-Vis and IR spectroscopy and magnetic susceptibility measurement. $[Co(SD)_2(CH_3OH)_2]$ and sulfadiazine were further characterised by single X-ray crystal analysis while the zinc complex was also characterised by mass spectrometry. The analytical data for the complexes are presented in Table 3. The octahedral geometry proposed for the complexes consists of a metal ion that coordinates to two molecules of sulfadiazine acting as bidentate ligands through one pyrimidinyl N and the sulfonamido N atoms on each sulfadiazine molecule. The fifth and sixth coordination spheres were occupied by two molecules of water or methanol depending on the solvent used in the synthesis. The proposed structure is shown in Figure 24.

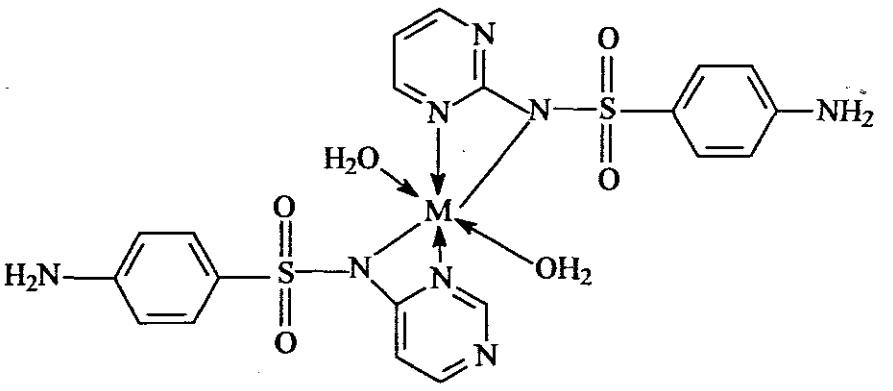

M = Co(II), Cu(II), Mn(II), Zn(II)

Figure 24: Proposed structure for some metal(II) complexes of sulfadiazine

Table 3: Analytical data for the Co(II), Cu(II), Mn(II) and Zn(II) complexes of sulfadiazine

Formulation	Molecular formula	Molar mass	% C	% H	% N	% M
$[Co(SD)_2(H_2O)_2]$	$CoC_{20}H_{24}N_8O_6S_2$	595.91	40.07 (40.33)	3.92 (4.06)	18.76 (18.82)	9.62 (9.90)
$[Co(SD)_2(CH_3OH)_2]$	$CoC_{22}H_{26}N_8O_8S_2$	653.55	42.44 (42.51)	4.01 (4.22)	17.92 (18.02)	9.35 (9.48)
$[Cu(SD)_2(H_2O)_2]$	$CuC_{20}H_{22}N_8S_2O_6$	598.11	40.56 (40.16)	3.37 (3.71)	18.78 (18.73)	10.64 (10.62)
$[Zn(SD)_2(H_2O)_2]$	$ZnC_{20}H_{22}N_8O_6S_2$	599.94	39.85 (40.04)	3.45 (3.70)	18.25 (18.68)	10.56 (10.90)
$[Mn(SD)_2(H_2O)_2]$	$MnC_{20}H_{22}N_8O_6S_2$	589.50	39.58 (40.75)	3.62 (3.76)	18.53 (19.01)	9.16 (9.32)

3.3.1.1 X-ray Crystallography of Co(II) sulfadiazine complex

The sample for the single crystal structure of the ligand was obtained from methanol.

The data sets for the single-crystal X-ray studies were collected with Mo Kα at 100 K on a Bruker smart APEX CCD diffractometer equipped with an Oxford Cryosystems low

temperature device. For the complex, the absorption correction applied used semi-empirical from equivalents with maximum and minimum transmission of 0.8450 and 0.7502 but there was no absorption correction for the ligand and maximum and minimum transmissions were 0.9708 and 0.9158. The structures were solved by direct methods using SHELXS-97 and completed by iterative cycles ΔF syntheses and full-matrix least-squares refinement against F^2. Crystallographic data are presented in Table 4.

3.3.1.2 The molecular structures of Co(II) sulfadiazine complex and sulfadiazine

The molecular structure of the complex, $[Co(SD)_2(CH_3OH)_2]$ and sulfadiazine with the atom-numbering scheme used are presented in Table 5 and their structures are shown in Figs. 25 and 26.

Table 4: Crystal data and structure refinement parameters

	$[Co(SD)_2(CH_3OH)_2]$	Sulfadiazine
Empirical formula	$C_{22}H_{26}CoN_8O_6S_2$	$C_{10}H_{10}N_4O_2S$
Formula weight	621.56	250.28
Temperature (K)	100(2)	100(2)
Wavelength (Å)	0.71073	0.71073
Crystal system	Monoclinic	Monoclinic
Space group	$P_2(1)/c$	$P_2(1)/c$
Unit cell dimensions		
a (Å)	7.1287(9)	13.6830(16)
b (Å)	9.0628(11)	5.8190(7)
c (Å)	20.287(3)	14.7950(17)
α (°)	90	90
β (°)	94.085	115.037(2)
γ (°)	90	90
Volume ($Å^3$)	1307.3(3)	1067.3(2)
Z	2	4
$D_{calc}(Mg/m^3)$	1.579	1.558
Abs. coefficient (mm^{-1})	0.871	0.299
F(000)	642	520
Crystal size (mm)	0.35x0.35x0.20	0.30x0.20x0.10
θ range for data (°)	2.01 to 26.36	1.64 to 28.32
Index ranges	-8<=h<=5, -11<=k<=11, -25<=l<=25	-17<=h<=18, -7<=k<=6, -19<=l<=16
Reflection collected	7253	6348
Independent reflections	7256 [R(int)=0.0000]	2492 [R(int)=0.0588]
Completeness to θ = 26.36	99.4%	94.0
Data/restraints/ parameters	7256/0/192	2492/0/166
Goodness-of-fit on F^2	1.093	0.947
R indices [I>2δ(I)]	R1 = 0.0433, wR2 = 0.1053	R1 = 0.403, wR2 = 0.0917
R indices (all data)	R1 = 0.0487, wR2 = 0.1081	R1 = 0.0549, wR2 = 0.0966

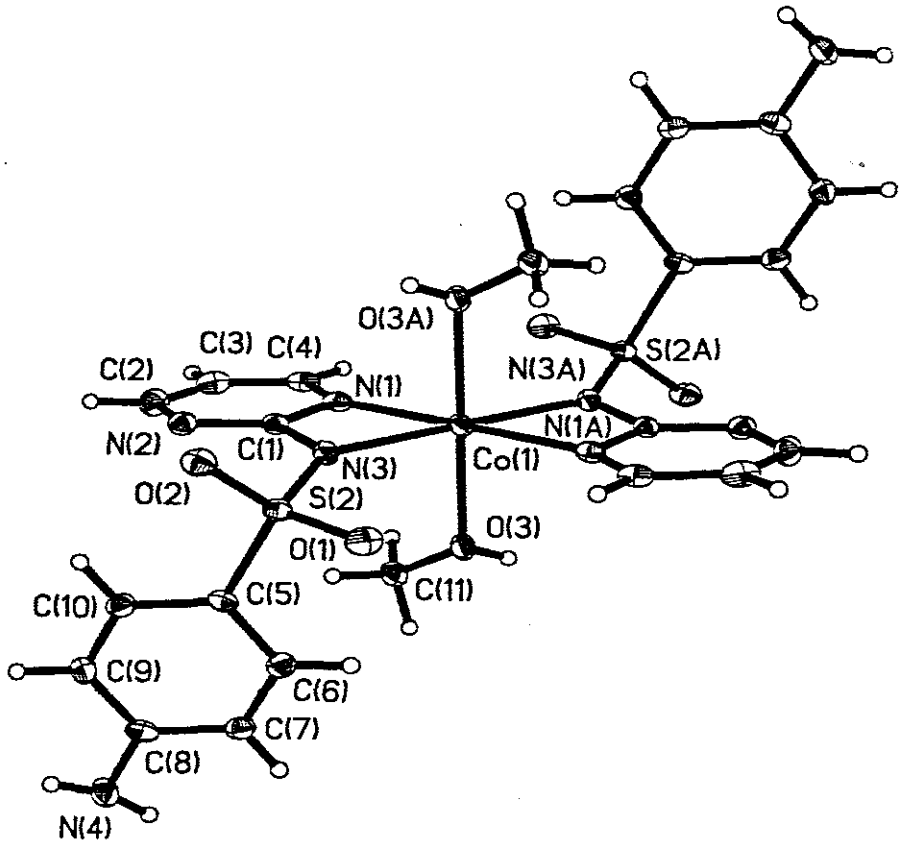

Figure 25: X-ray crystal structure of $[Co(SD)_2(CH_3OH)_2]$

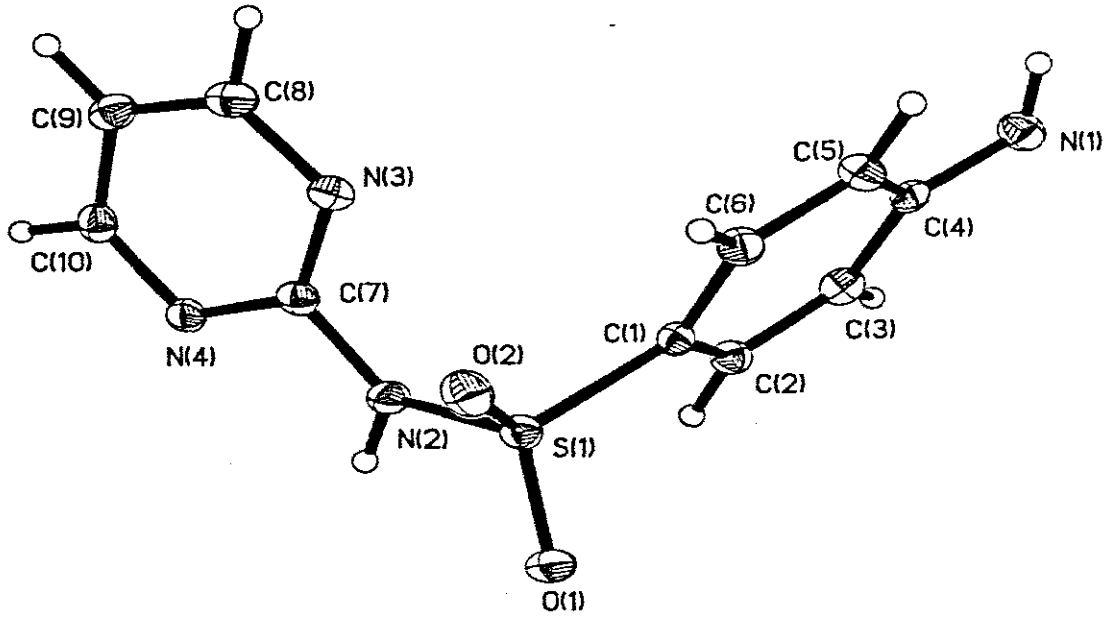

Figure 26: Molecular structure of sulfadiazine showing the numbering scheme.

Table 5: Selected bond lengths and angles of Co(II)sulfadiazine and Sulfadiazine

Bond lengths (Å)		Bond angles (°)	
Co(II)sulfadiazine			
Co(1)-N(3)	2.1163(15)	N(3A)-Co(1)-N(3)	180
Co(1)-N(1)	2.1166(15)	N(3A)-Co(1)-N(1A)	62.99(6)
Co(1)-O(3)	2.1377(13)	N(3)-Co(1)-N(1A)	117.01(6)
S(2)-O(2)	1.4411(14)	N(3A)-Co(1)-N(1)	117.02(6)
S(2)-O(1)	1.4420(13)	N(1)-Co(1)-N(1)	180.0
S(2)-N(3)	1.6025(15)	N(3A)-Co(1)-O(3A	91.16(6)
S(2)-C(5)	1.7593(17)	N(3)-Co(1)-O(3A)	88.84(6)
O(3)-C(11)	1.442(2)	N(1A)-Co(1)-O(3A)	89.26(5)
O(3)-H(5)	0.75(2)	N(1)-Co(1)-O(3A)	90.74(5)
N(1)-C(4)	1.329(2)	N(3A)-Co(1)-O(3)	88.84(6)
N(1)-C(1)	1.364(2)	C(3)-Co(1)-O(3)	91.16(6)
N(3)-C(1)	1.367(2)	N(1A)-Co(1)-O(3)	180
C(11)-H(11A)	0.9800	O(3A)-Co(1)-O(3)	107.12(8)
Sulfadiazine			
C(4)-N(1)	1.383(3)	C(6)-C(1)-C(2)	120.80(17)
C(7)-N(4)	1.345(2)	N(3)-C(7)-N(4)	127.15(17)
C(7)-N(2)	1.381(2)	N(3)-C(7)-N(2)	118.70(17)
N(2)-S(1)	1.6496(16)	N(4)-C(7)-N(2)	114.14(16)
O(1)-S(1)	1.4374(13)	O(1)-S(1)-N(2)	101.73(8)
O(2)-S(1)	1.4282(14)	O(2)-S(1)-C(1)	108.65(9)
C(1)-S(1)	1.7412(19)	O(2)-S(1)-O(1)	119.57(8)

In the complex, the sulfadiazine behaves like a bidentate anionic ligand due to the deprotonation of the H atom on the sulfonamide N. The central ion coordinated *via* the sulfonamido N and pyrimidine N on each of the sulfadiazine anion, with the fifth and

sixth coordination sites occupied by two molecule of methanol. This indicates that in the medium of the reaction, the N(1)—H proton is acidic. The crystal structure of the complex consists of discrete neutral $[Co(SD)_2(CH_3OH)_2]$ molecules (Fig. 25), which gives rise to network of chains by means of intermolecular hydrogen bonding (Fig. 27). The Co(II) atom has a distorted octahedral coordination in which the sulfadiazine ligand occupied asymmetric positions and the methanol molecules, sulfonamide N and the pyrimidine N of each sulfadiazine are *trans* to one another. Main distances and angles are given in Table 5. The bond length between Co(II) and each of the four planar coordinated N atoms is the same and also the bond length of the two axial coordinated O atoms of the methanol molecules are also the same. The bond distances and angles in this complex are slightly larger, in most cases, than those observed for Ag(I)[120], Zn(II)[121] and Cd(II)[122] sulfadiazine complexes. The packing of the $[Co(SD)_2(CH_3OH)_2]$ molecules in the crystal structure consists of parallel chains, which are formed by mutual interactions through hydrogen bonding between molecules. Each molecule interacts through sixteen hydrogen bonds with five neighbouring molecules (Table 6).

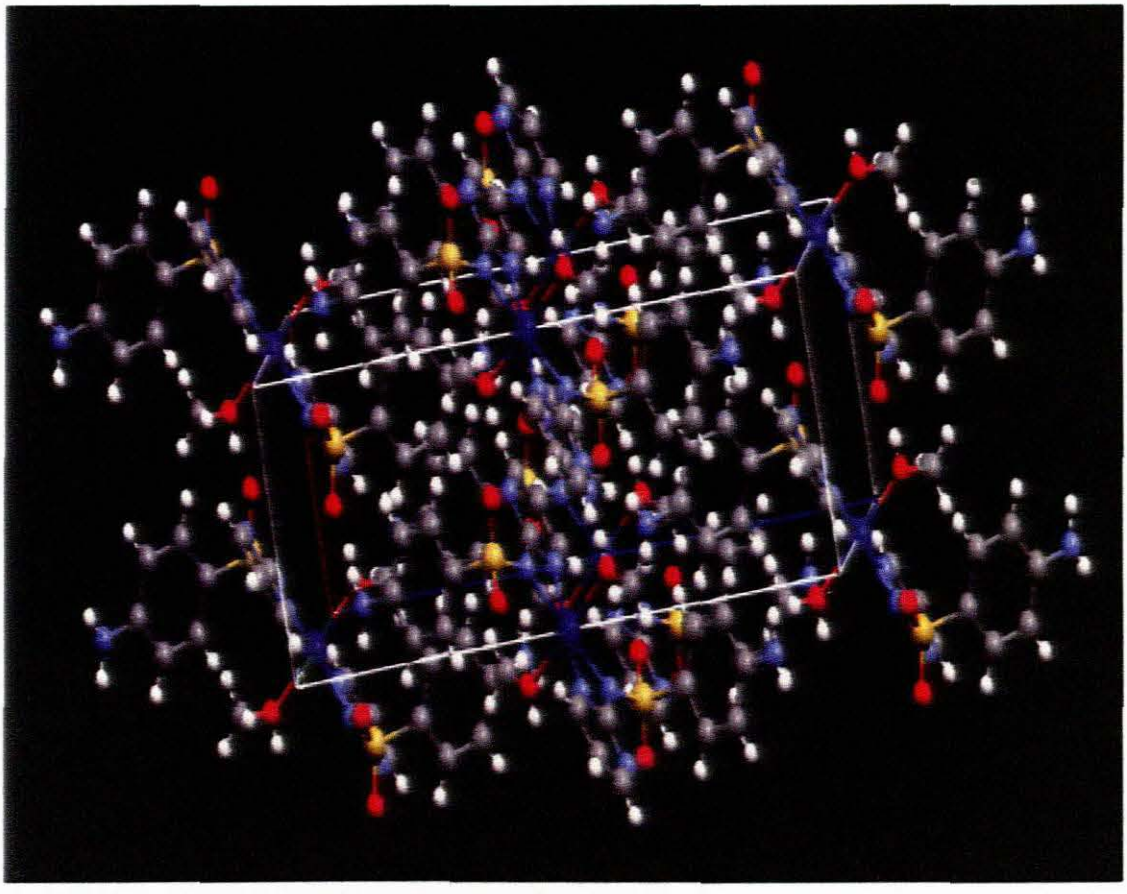

Figure 27 Parking diagram for $[Co(C_{10}H_9N_4O_2S)_2(CH_3OH)_2]$

Table 6: Position of atoms of hydrogen bonds

D-H···A	d (D-H)	d (H···A)	d (D···A)	‹(DHA)
N(4)–H(5N)...O(1)#2	0.92(2)	2.08(2)	2.993(2)	172.5(19)
N(4)–H(4N)...O(2)#3	0.85(2)	2.18(2)	3.021(2)	171.5(19)
O(3)–H(5)...O(2)#4	0.75(2)	2.69(2)	3.134(2)	119.6(19)
O(3)–H(5)...N(2)#4	0.75(2)	2.16(2)	2.876(2)	159.0(2)

Symmetry transformations used to generate equivalent atoms:
#1 –x, -y + 2, -z +1 #2 –x, y- ½, -z + ½ #3 -x +1, y-½, -z + ½

3.3.1.3 Infrared spectra of the complexes

In order to clarify the mode of bonding and the effect of the metal ion on the ligand, the IR spectra of the free ligand and the metal complexes were studied (Table 7) and assigned on the basis of careful comparison of their spectra with that of free ligand. The bands in the region 3450-3000 cm^{-1} due to symmetrical and asymmetrical stretching modes of NH_2 in the spectrum of the ligand undergo only slight change in spectra of the complexes. This is an indication that the NH_2 groups on the free ligand are not affected by the coordination to the metal ion. However, apparent shifts in the NH_2 frequencies are due to intermolecular hydrogen bonding, as revealed by X-ray structure of one of the complexes. The effect of the coordinated metal is noticeable on the SO_2 symmetrical and asymmetrical stretching modes that are shifted to lower wavenumbers while the ν(S—N) shifted to higher wavenumbers in all the complexes. These observations confirm the coordination of metal ions through the sulfonamido N atom.

Table 7. Selected IR data (cm^{-1}) for sulfadiazine and the complexes

Formulation	$\nu(NH_2)$	$\nu(NH_2)$	$\nu(SO_2)_{asym.}$	$\nu(SO_2)_{sym}$	ν(SN)	ν(MN)	ν(MO)
Sulfadiazine	3422vs 3355vs	1652vs	1325vs	1157vs	942s		
$[Co(SD)_2(CH_3OH)_2]$	3437vs 3347s	1625w	1267s	1129vs	987vs	596vs	390s
$[Co(SD)_2(H_2O)_2]$	3480vs 3248m	1652w 1621s	1263vs 1240vs	1124s	989	588vs	426s 390s
$[Cu(SD)_2(H_2O)_2]$	3448s 3368s	1631vs	1277ms	1126	971	526s	412s
$[Zn(SD)_2(H_2O)_2]$	3423vs 3355vs	1628s	1325vs 1264ms	1133s 1079s	977vs	388s	288s
$[Mn(SD)_2(H_2O)_2]$	3454s 3176s	1654vs	1326vs 1264s	1132s	946vs	345s	278s

Abbreviations: v = very; s = strong; m = medium; w = weak.

In addition to the three νN—H peaks observed in the sulfadiazine ligands that shifted to higher wavenumbers in the two Co(II) complexes, $[Co(SD)_2(H_2O)_2]$ showed a generally broader band with two additional bands at 3557 and 3787 cm^{-1} for the coordinated water possibly overlapping with the νNH_2 on the pyrimidine ring. The effect of the coordinated metal is also noticeable on the SO_2 symmetrical and asymmetrical stretching modes that are shifted to lower wavenumbers (by about 33-85 cm^{-1}) while the ν(S—N) shifted by about 47 cm^{-1} to higher wavenumbers in both complexes. These observations confirm the coordination of Co(II) through the sulfonamido N atom. The complexes show two νCo—N bands at about 731 cm^{-1} and 588 cm^{-1} and Co—O bands at 390-330 cm^{-1} respectively. $[Co(SD)_2(H_2O)_2]$ gave an additional intense band at 426 cm^{-1} which is completely absent in $[Co(SD)_2(CH_3OH)_2]$. The involvement of N and O in coordination is further strengthened by the appearance of bands at 590-297 cm^{-1} assigned to ν(Co-N + Co-O).

In the Cu(II) complex, multiple absorption bands in the regions 3750-3500 cm^{-1} can be attributed to the presence of coordinated water. This is further strengthened by the sharp band at 389 cm^{-1} assigned to Cu—O stretching frequency. There are little changes in both the symmetric and asymmetric stretching frequencies of SO_2 indicating that the SO_2 was not involved in coordination. The νS—N shifted in the complex as observed in the Co(II) sulfadiazine complexes. The bands at 578 and 526 cm^{-1} are assigned to Cu—N and the band at 412cm^{-1} assigned to the Cu—O. The band at 844 cm^{-1} is assigned to the wagging vibration of coordinated water. The rocking vibration of the coordinated water is assigned

to a band that appears at about 546 cm^{-1}. The Mn—N and Mn—O vibrations are assigned to bands at 345 and 278 cm^{-1} respectively.

3.3.1.4 Infrared spectroscopy and Mass spectrometry of $[Zn(SD)_2(H_2O)_2]$

The IR of the complex showed multiple absorption bands in the regions 3500-3200 cm^{-1} that can be attributed to the presence of coordinated water. There are little changes in both the symmetrical and asymmetrical stretching frequencies of SO_2 indicating that the SO_2 was probably not involved in coordination. The νS—N shifted in the complex as observed in the Co(II) sulfadiazine complexes. The Zn—N bands appear at 388 cm^{-1} and the Zn—O to a band at 288 cm^{-1}. The rocking and wagging vibrations of the coordinated water; $\rho_r(H_2O)$ and $\rho_w(H_2O)$ are assigned to the bands at 580 and 840 cm^{-1} respectively.

In the mass spectrometry of zinc(II) sulfadiazine, a peak observed at m/z = 562 corresponds to $[Zn(C_{10}H_9N_4O_2S)_2]^+$ indicating that water molecules has been lost from the complex. The base peak at m/z = 249 is due to the sulfadiazine, $C_{10}H_9N_4O_2S$. Some of the other peaks are assigned thus: m/z = 312, $ZnC_{10}H_9N_4O_2S$; m/z = 169, lost of pyrimidine from sulfadiazine and m/z = 147 is due to Zn(pyrimidine).

3.3.1.5 Electronic spectra and Magnetic Properties of the complexes

Magnetic susceptibility measurements were carried out on powdered samples at 297 K. The effective magnetic moments, 4.86 B.M. for $[Co(SD)_2(H_2O)_2]$ and 4.93 B.M. for $[Co(SD)_2(CH_3OH)_2]$, are in agreement with high-spin octahedral cobalt(II) complexes. For high spin d^7 systems, the ground term is ^4F with a low-lying ^4P excited term. Six-

coordinate octahedral or pseudo-octahedral species will exhibit three transitions[169]. The transitions are: υ_1, $^4T_{1g}(F) \rightarrow {}^4T_{2g}$; υ_2, $^4A_{2g}(F) \rightarrow {}^4T_{1g}$ and υ_3, $^4T_{1g}(F) \rightarrow {}^4T_1(P)$. The second transition is very weak and rarely observed. Tetrahedral species also exhibit three transitions and all three are observable. The electronic spectra of the complexes in DMF (Figure 28) confirmed their octahedral stereochemistry. The electronic spectra of the complexes in the visible region are similar. They show two bands of weak to medium intensity at 18,656 cm^{-1} and 22,988 cm^{-1} respectively. This may tentatively be assigned to $^4T_1g(F) \rightarrow {}^4T_2g$ and $^4T_1g(F) \rightarrow {}^4T_1(P)$ transitions.

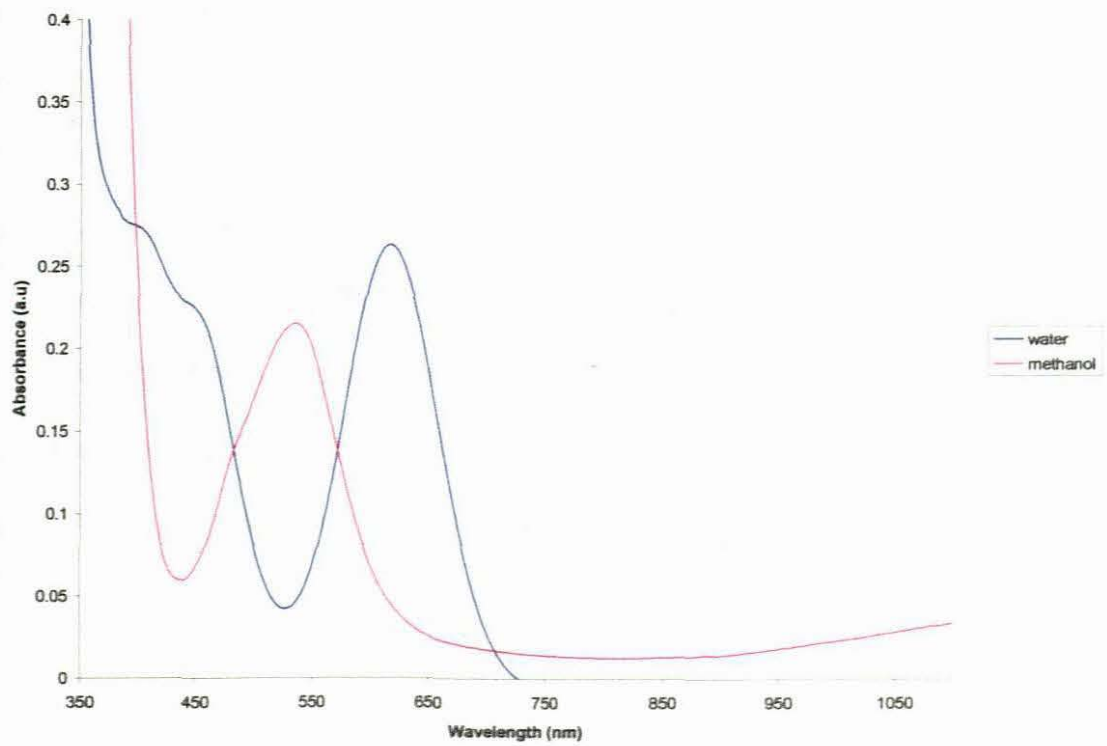

Figure 28: Solution spectra of Co(II) sulfadiazine in DMF

In octahedral Cu(II) complexes, a single absorption band in the visible spectrum corresponding to the $^2E_g \rightarrow {}^2T_{2g}$ transition is expected. But due to strong Jahn-Teller distortion, octahedral Cu(II) complexes often give broad bands resulting from several overlapping bands or, where the bands are resolved, up to three close bands[165]. The electronic spectrum of the Cu(II) sulfadiazine complex in Figure 29 shows a broad asymmetric band in the regions 19,047-16000 cm^{-1} (525-625 nm). This confirms the octahedral stereochemistry proposed for the complex.

A further confirmation of the stereochemistry obtained from the magnetic susceptibility measurements showed that the complex has an effective magnetic moment of 1.88 B.M. It could thus be concluded that the complex has a distorted octahedral geometry since the E ground term in octahedrally coordinated ion gives moments in excess of the spin-only value because of the mixing of the excited T term into the ground term, and the high value of λ (the spin-orbit coupling constant) makes the effect significant. Thus moments of magnetically dilute compounds are in the range 1.9-2.2 B.M., with compounds whose geometry approaches octahedral having moment at the lower end and those with geometries approaching tetrahedral having moment on the higher end [169].

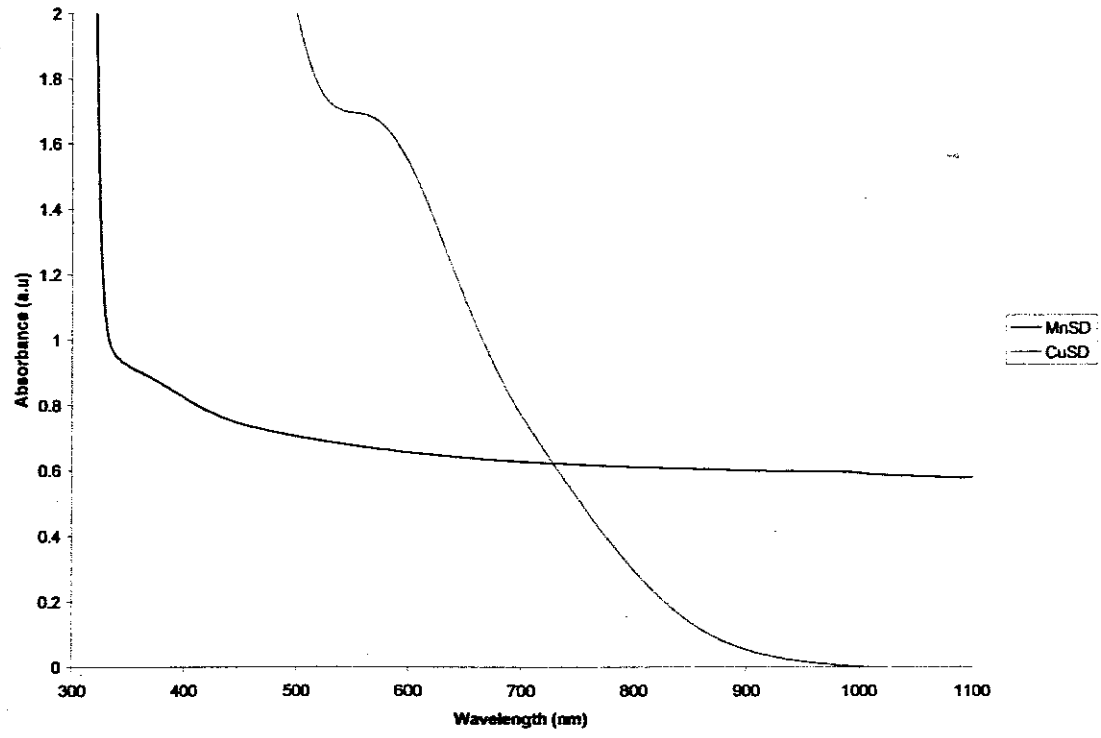

Figure 29: Electronic spectra of Cu(II) and Mn(II) sulfadiazine in DMF

High spin manganese(II) complexes are weakly coloured. It is rarely possible to identify many, if any, of the d—d bands of a Mn(II) complex with an organic ligand since even the very weak tail of UV organic absorption to the visible can obscure them. The Tanabe Sugano diagrams indicate that low-spin complexes might have rich d—d spectra if the d—d bands are not obscured by charge-transfer; very few of such complexes are known. For d^5 configuration, the ground term is the orbital singlet ^6S in high-spin complexes. It cannot be split by crystal field of any symmetry. The absence of any other spin sextet terms requires that all transitions in high spin d^5 complexes are spin-forbidden, as well as Laporte forbidden and therefore give very weak bands. Transitions from ^6S to spin doublet levels are highly forbidden and rarely observed. In octahedral field, the $(t_{2g})^4(e_g)^1$

and $(t_{2g})^2(e_g)^3$ each give rise to $^4T_{1g}$ and $^4T_{2g}$ states. The $(t_{2g})^3(e_g)^2$ configuration gives rise to the spin quartets: $^4A_{1g}$, $^4A_{2g}$, $^4T_{1g}$ and 2 ^4E_g. Thus, the $^4A_{1g}$, $^4A_{2g}$, and ^4Eg states have energies independent of any crystal field, and will appear as horizontal line[165]. The electronic spectra of the Mn(II) complex of sulfadiazine is presented in Figure 25. In the visible region, it gave a horizontal line and can thus be inferred that it is high spin Mn(II) complex with octahedral symmetry and very weak d—d transitions. A magnetic moment of 5.86 BM was obtained for the complex, thus further confirming that it is a high spin d^5 complex.

3.3.2 Ni(II), Pd(II), and Pt(II) complexes of Sulfadiazine

The Ni(II) complexes were made from $NiCl_2{\cdot}6H_2O$, $Ni(NO_3)_2{\cdot}6H_2O$ and $Ni(CH_3COO)_2{\cdot}4H_2O$ but results from elemental analyses indicated that they all yielded the same complex. The products were green in colour and were formulated as $[Ni(SD)_2(H_2O)_2]{\cdot}2H_2O$; yield = 78 %. Pd(II) and Pt(II) complexes were isolated from aqueous methanol mixture. The Pd complex is formulated as $[Pd(SD)(H_2O)(CH_3OH)]$; yield = 67% while the Pt complex is formulated as $[Pt(SD)(H_2O)Cl]$; yield, 76%. The analytical data for the complexes are presented in Table 8; their proposed structures are in Figure 30-32.

Table 8: Analytical data for Ni(II), Pd(II) and Pt(II) complexes of sulfadiazine

Formulation	Empirical formula	Molar mass	% C	% H	% N
$[Ni(SD)_2(H_2O)_2]\cdot 2H_2O$	$NiC_{20}H_{26}N_8O_8S_2$	629.29	38.44 (38.17)	3.63 (4.16)	17.94 (17.81)
$[Pd(SD)(H_2O)(CH_3OH)]$	$PdC_{11}H_{15}N_4O_4S$	405.74	32.42 (32.56)	3.51 (3.73)	13.60 (13.81)
$[Pt(SD)(H_2O)Cl]$	$PtC_{10}H_{11}N_4O_3SCl$	497.82	23.84 (24.13)	2.84 (2.23)	10.77 (11.25)

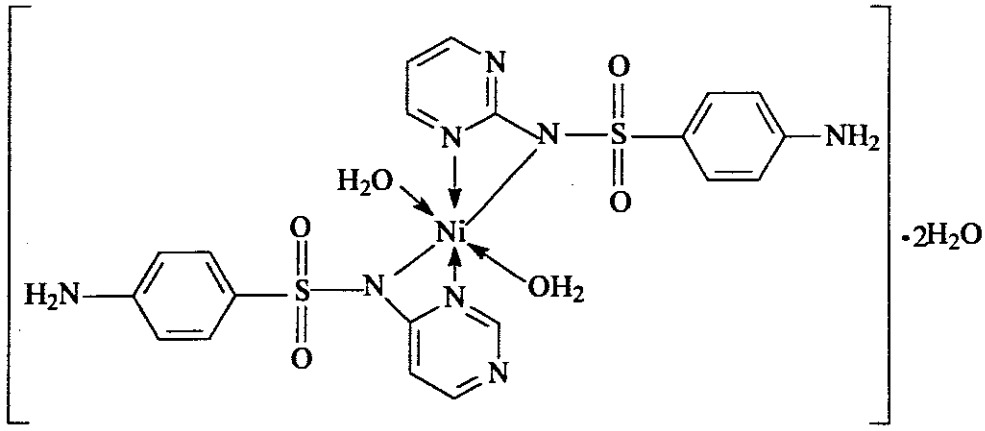

Figure 30: Proposed structure for Ni(II) sulfadiazine complex

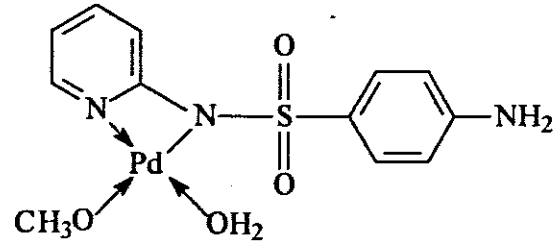

Figure 31: Proposed structure for Pd(II) sulfadiazine complex

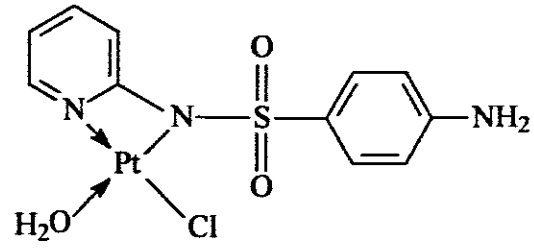

Figure 32: Proposed structure for Pt(II) sulfadiazine complex

3.3.2.1 Infrared spectra of Ni(II), Pd(II) and Pt(II) sulfadiazine

The selected IR data of the complexes and sulfadiazine are presented in Table 9.

Table 9: Selected IR data (cm^{-1}) for sulfadiazine and the complexes

Formulation	$\nu(NH_2)$	$\nu(NH_2$	$\nu(SO_2)$ asym.	$\nu(SO_2)$ sym.	ν(SN)	MN	MO
Sulfadiazine	3422vs 3355vs	1652vs	1262vs	1157vs	942s		
$[Ni(SD)_2(H_2O)_2]\cdot 2H_2O$	3468s 3369s	1630vs	1263ms	1125ms	966s	378s	342w
$[Pd(SD)_2(H_2O)_2]$	3342s 3322s	1630s	1258ms	1124s	970vs	511s	409s
$[Pt(SD)_2(H_2O)_2]$	3417s 3318s	1631vs	1260s	1124s	968vs	512s	423s

Abbreviations: v = very; s = strong; m = medium; w = weak

A comparison of the IR spectrum of the free sulfadiazine ligand and the complexes showed some slight changes in the regions 3500 – 3100 cm^{-1} in the complexes. These differences may be due to the interaction between the free NH_2 groups on sulfadiazine and the stretching, wagging and rocking vibrations of coordinated and lattice water respectively, or due to intermolecular hydrogen bonding. The rocking and wagging vibrations in the complexes due to O—H of water molecule occur between 804 and 511 cm^{-1} in the complexes. The spectra of the complexes showed that SO_2 was not directly coordinated to the metal ions because only a minimal shift was observed whereas the νS—N band shifted appreciably in the complexes with respect to the ligand indicating that the sulfonamido N was involved in bond formation. The νNi—N and νNi—O vibrations are assigned to bands at 378 and 345 cm^{-1} respectively. The νPd—N is assigned to a band at 501 cm^{-1} while coordinated water shows rocking and wagging vibrations at 796 and 511 cm^{-1} and the νPd—O band appearing at 409 cm^{-1}. The

νPd—Cl is assigned at 257 cm^{-1}. The Pt—N, Pt—O and Pt—Cl vibrations are assigned to the bands at 512, 423 and 284 cm^{-1} respectively.

3.3.2.2 Electronic Spectra and Magnetic properties of Ni(II), Pd(II) and Pt(II) Sulfadiazine complexes

In octahedral Ni(II) complexes, three spin-allowed transitions are expected because of the free-ion ground ^3F term and the presence of ^3P term. The d—d transitions $^3A_{2g}(F)\rightarrow{}^3T_{2g}(F)$, $^3A_{2g}(F)\rightarrow{}^3T_{1g}(F)$, $^3A_{2g}(F)\rightarrow{}^3T_{1g}(P)$ generally occurred within the ranges 7000-13000, 11,000-20,000 and 19,000-27,000 cm^{-1} respectively. In addition, two spin-forbidden transitions are usually quite prominent. The electronic spectrum of the Ni(II) complex of sulfadiazine is shown in Figure 33. The spectrum shows three bands. A broad band that peaks at about 9,091 cm^{-1} (1100 nm) can be assigned to $^3A_{2g}(F)\rightarrow{}^3T_{2g}(F)$, while a broad band that peaks at 15,432 cm^{-1} (648 nm) is assigned to $^3A_{2g}(F)\rightarrow{}^3T_{1g}(F)$. This occurs with a shoulder at about 12,845 cm^{-1} (778 nm). A third band (Figure 34) appears at 27,855 cm^{-1} (359 nm) which is assigned to $^3A_{2g}(F)\rightarrow{}^3T_{1g}(P)$. It can thus be inferred that the Ni(II) sulfadiazine complex has an octahedral geometry. The T ground term of tetrahedral Ni(II) complexes is expected to lead to a temperature-dependent orbital contribution to the magnetic moment, whereas the A ground term of the octahedral is not, although mixing of the excited $^3T_{2g}(F)$ term into the $^3A_{2g}(F)$ ground term is expected to raise its moment. The increase in the magnetic moment of the tetrahedral complexes lie in the range 3.2-4.1 BM whereas for octahedral complexes, it lies in the range 2.9-3.3 B.M. The effective magnetic moment of 2.98 B.M. was obtained for the Ni(II) complex and thus confirms the octahedral stereochemistry formulated for the complex.

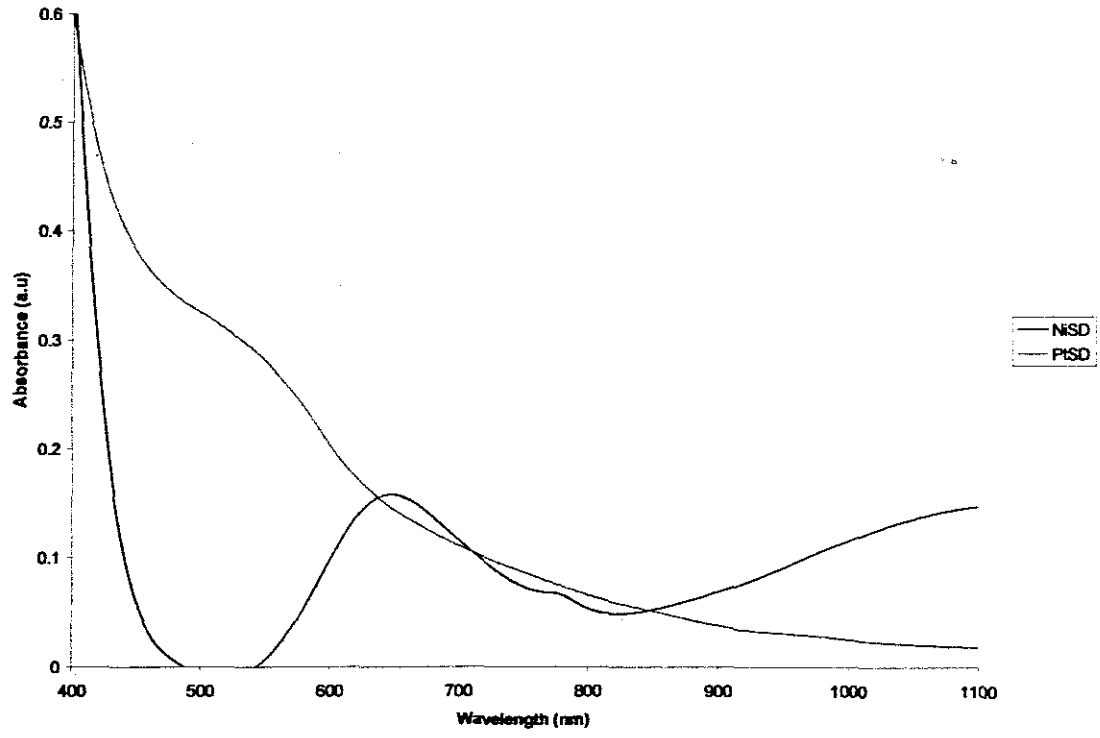

Figure 33: Solution Spectra of Ni(II) and Pt(II) sulfadiazine complexes

The effect of complexation on the splitting of the d orbitals is greater in the case of second and third than the first row transition elements, and the associated effect more marked for Pt and Pd and consequently, their complexes are diamagnetic and the vast majority of the complexes are planar. The electronic spectra of complexes of Pt and Pd, like any other square planar complexes, can be assigned easily. However, the situation is complicated in the Pt(II) series by the expectation that the d—p transitions will occur at comparable energies to LMCT transitions and a clear distinction between these two types of transition may be difficult. Absorption may be to states that are admixtures of LMCT and d—p. In the case of Pd(II), the separation between d—p and LMCT transitions is such that below 50,000 cm^{-1}, d—p transitions are not expected. Two closely spaced

$\pi x \rightarrow \delta^*M$ transitions ($^1A_{2u}$, $^1Eu(1)$) should be followed by a more intense $\delta x \rightarrow \delta^*M$ ($^1Eu(2)$). Transition from the non-bonding $\pi x a_{2u} \rightarrow b_{1g}\delta^*$ level yields an orbital-forbidden $^1B_{2u}$ state which may appear weak[165].

The electronic spectra of the Pd(II) sulfadiazine complexes is presented in Figure 34. The spectrum is typical of that expected for square planar complexes, which shows no discernible d—d absorption band but gives a series of fragmented bands between 400 - 300 nm that can be attributed to high spin orbit coupling. Magnetic moment of 0.24 BM confirms that the complex is diamagnetic. The electronic spectrum of Pt(II)sulfadiazine complex is shown in Figure 33 and 34. The spectrum show a very weak and broad d—d band at about 450-550 nm typical of square planar d^8 complexes. A magnetic moment of 0.32 B.M. confirms that the complex is also diamagnetic.

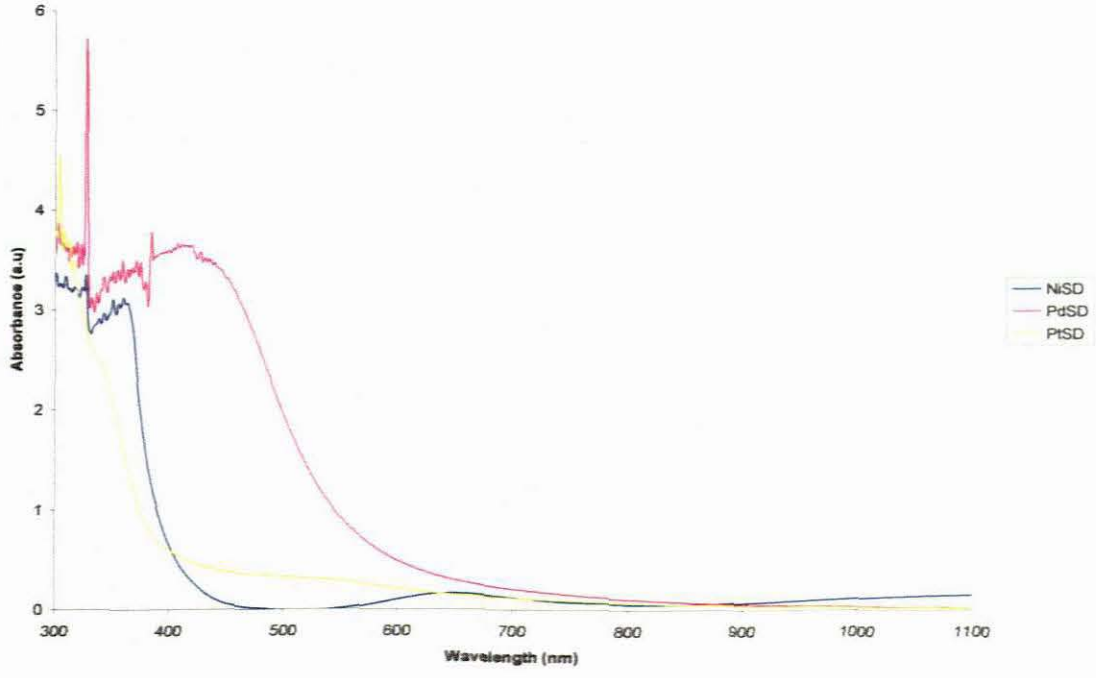

Figure 34: Solution spectra of Ni(II), Pd(II), and Pt(II) sulfadiazine complexes in DMF

3.3.3 Fe(III) and Ru(III) complexes of sulfadiazine

The complexes were isolated from water. A cream coloured product was obtained from iron(III) and is formulated as $[Fe(SD)_3]\cdot 3H_2O$; molar mass, 857.71; yield: 79%. A brown product was obtained for Ru(III) and is formulated as $[Ru(SD)_2(H_2O)Cl]$; molar mass, 653.07; yield: 85%. The analytical data for the complexes are presented in Table 10

Table 9: Analytical data for Fe(III) and Ru(III) sulfadiazine

Formulation	Empirical formula	% C	% H	% N	%S	% M
$[Fe(SD)_3].(H_2O)_3$	$FeC_{30}H_{33}N_{12}O_9S_3$	42.46	3.56	19.23	11.32	6.48
		(42.01)	(3.88)	(19.60)	(11.21)	(6.51)
$[Ru(SD)_2(H_2O)Cl]$	$RuC_{20}H_{20}N_8O_5S_2Cl$	37.14	3.59	17.21	9.63	
		(36.78)	(3.09)	(17.16)	(9.82)	

The complexes have octahedral geometry. In the Fe(III) complex, the metal ion is coordinated to three molecules of sulfadiazine and crystallises with three lattice water. Ru coordinates to two molecules of sulfadiazine and the octahedral arrangement around the metal ion is completed by a molecule of water and a chloride ion. The proposed structures for the complexes are given in Figures 35 and 36.

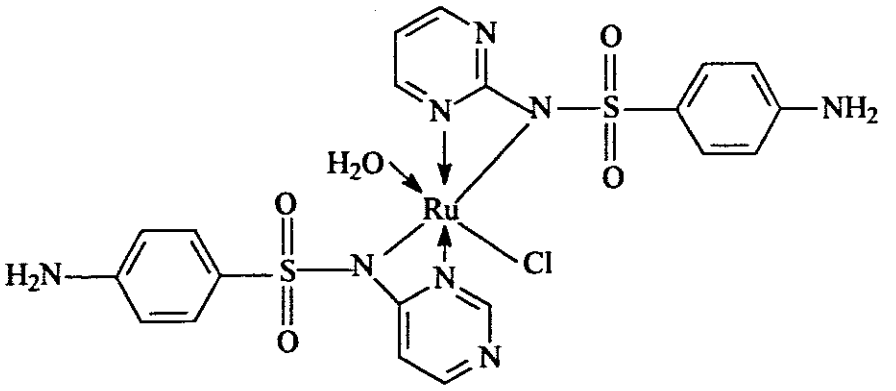

Figure35: Proposed structure of Ru(III)sulfadiazine

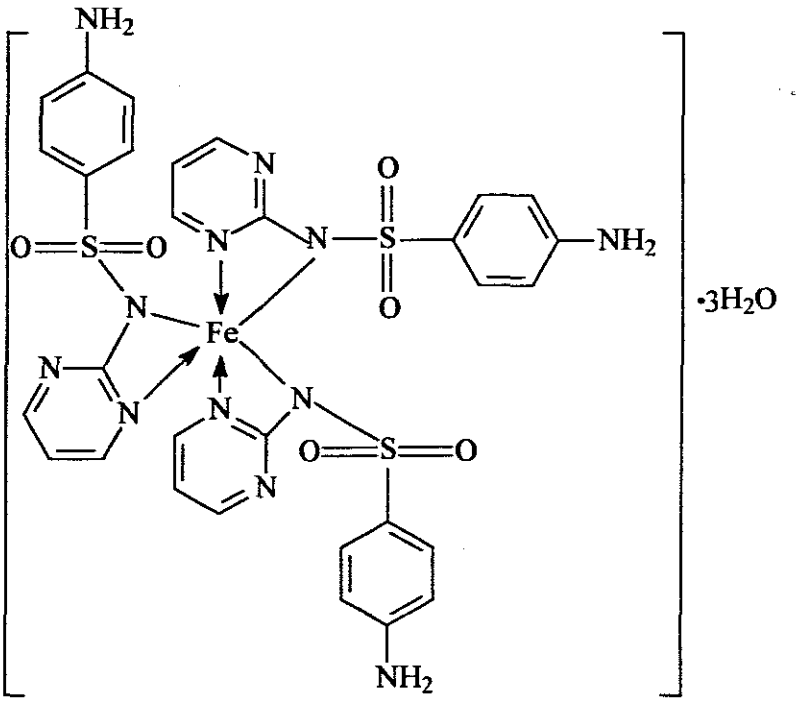

Figure 36: Proposed structure for Iron(III)sulfadiazine

3.3.3.1 Infrared spectra of Fe(III) and Ru(III) complexes of sulfadiazine

The bands in the region 3523-3270 cm^{-1} due to symmetrical and asymmetrical stretching modes of NH_2 in the spectrum of the ligand underwent appreciable change in the spectra of the complexes. This is a consequence of the coordination of the metal ion to the deprotonated sulfonamido N atom and most probably due to the interaction between the uncoordinated NH_2 groups on the complexes and the O—H stretching frequencies of coordinated water in the case of Ru(III) complex (Figure 37) and lattice water in the Fe(III) complex respectively. In addition to the three peaks observed in free sulfadiazine that shifted to higher wavenumbers in the complexes, there were several other bands probably due to the presence of more than one molecule of sulfadiazine. The effect of the

coordinated metal is also noticeable on the SO_2 symmetrical and asymmetrical stretching modes that shifted to lower wavenumbers in the spectrum of the complex. The Fe—N is assigned to a band at 519 cm^{-1}. Two bands of almost equal intensity at 575 and 550 cm^{-1} are assigned to Ru—N while the bands at 370 and 280 cm^{-1} are assigned to Ru—O and Ru—Cl respectively. The multiple absorption bands in the regions 600-250 cm^{-1} is most probably due to "librational modes" that are due to rotational oscillations of the lattice water molecules, restricted by interactions with neighbouring atoms.

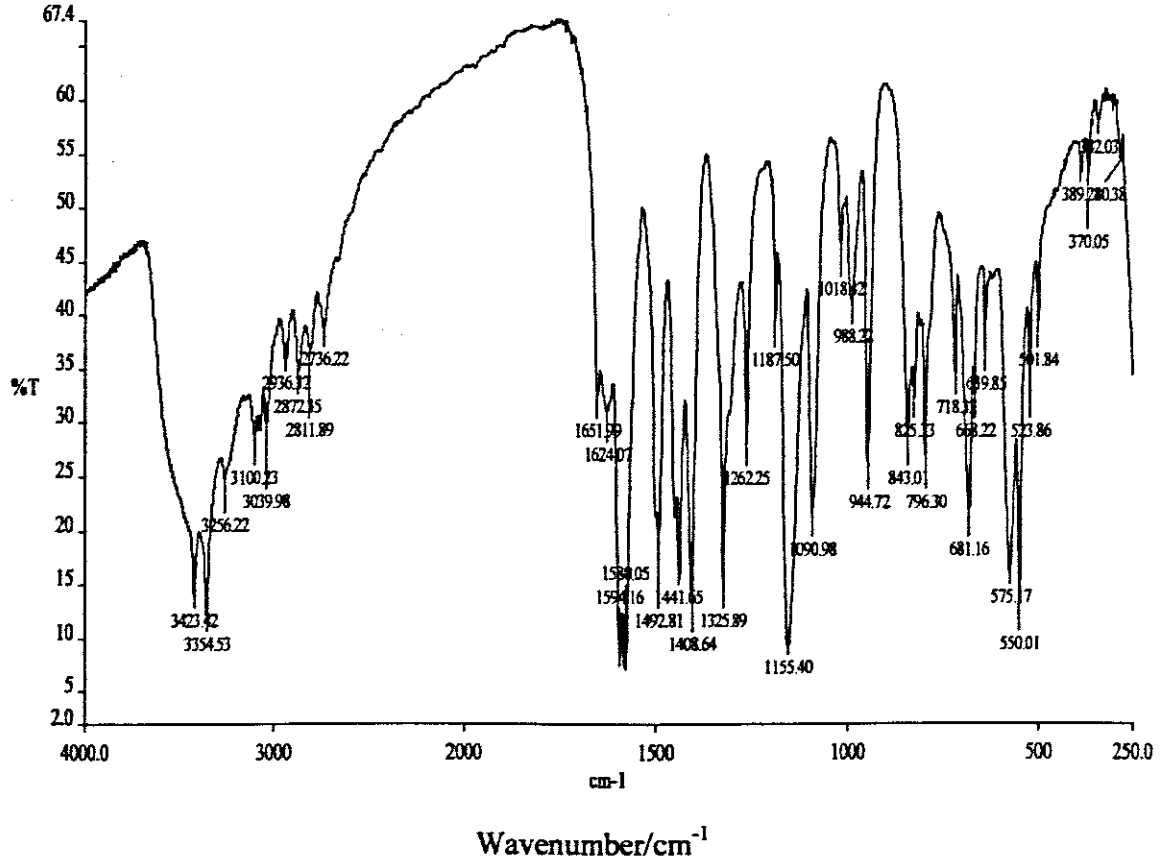

Wavenumber/cm^{-1}

Figure 37: IR spectrum of Ru(III) complex of sulfadiazine

3.3.3.2 Electronic Spectra and magnetic properties of Fe(III) and Ru(III) sulfadiazine complexes

Iron(III) is a moderately oxidizing ion and many of its complexes exhibit ligand to metal charge transfer transitions (L→MCT). In general, both L→ $^2t_{2g}$ and L→ ^2e_g transitions may be expected[165]. In most cases, the d—d absorption in octahedral complexes is rarely observed because the L→MCT absorptions obscure such weak band. Furthermore the *high-spin iron(III) complexes are not stabilized by crystal field.* Charge transfer transitions in Fe(III) complexes occur between 45,000 -26,000 cm^{-1} (222- 384 nm).

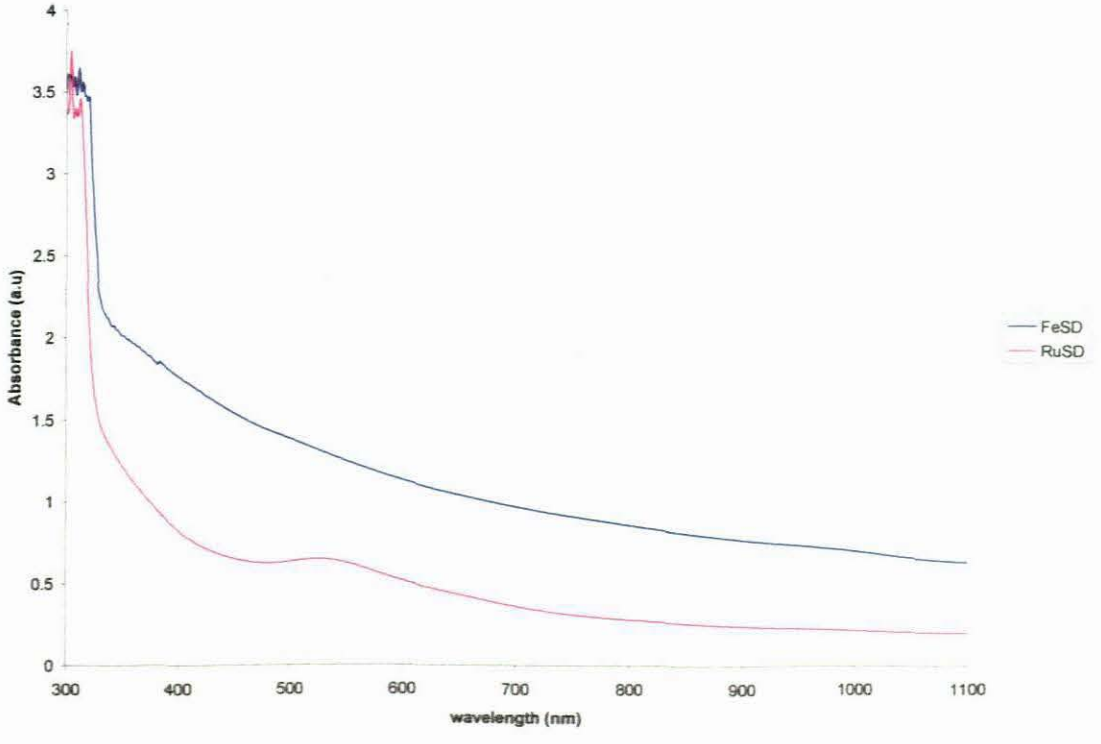

Figure 38: Solution spectra of Fe(III) and Ru(III) sulfadiazine complexes in DMF

High-spin iron(III) complexes, in general, have magnetic moments at room temperature close to 5.9 B.M. and somewhat in excess of 2.0 B.M. due to orbital contribution if they are low-spin. The electronic spectrum of the iron(III) sulfadiazine complex is shown in Figure 38. In the region 300-352 nm, the absorption in this region could be attributed to L→MCT. Another band appears at 26,042 cm^{-1} (384 nm) and is assigned to $^2t_{1u} \rightarrow {}^2t_{2g}$ charge-transfer transition. A magnetic moment of 5.4 B.M. for the complex indicates that it is high spin.

Ruthenium(III) complexes are almost invariably six coordinate unless doped in special lattices[165]. Charge transfer absorption often occurs at low energies while the crystal field parameter is quite large; thus d—d bands are frequently obscured[165]. Though the spin-orbit coupling coefficient is greater than for iron(III), intra-configurational transitions within $^2T_{2g}$ still lie at too low an energy to be conveniently identified. The two lowest absorptions, the spin-forbidden $^4T_{1g} \rightarrow {}^2T_{2g}$ and $^4T_{2g} \rightarrow {}^2T_{2g}$, can frequently be observed but most often as shoulders. The electronic spectrum of the Ru(III) complex (Figure 38 and 39) showed a very broad band at 20,000 – 18,000 cm^{-1} (500-550 nm) which could be assigned to $^4T_{2g} \rightarrow {}^2T_{2g}$.

The effective magnetic moments of 1.89 BM obtained for the complex showed that it is a low-spin octahedral complex with one unpaired electron. This is typical of second and third row transition metal complexes with odd number of unpaired electrons.

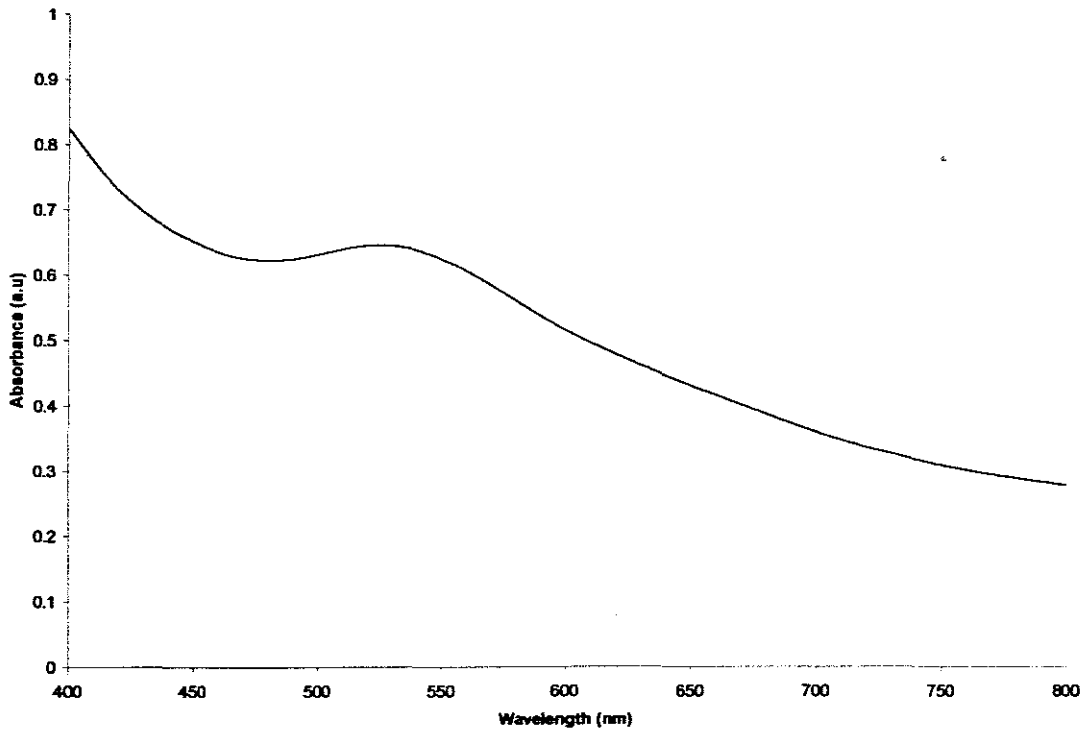

Figure 39: Solution spectrum of Ru(III) sulfadiazine complex in DMF

3.3.10 Oxovanadium(IV) complex of sulfadiazine

The product was blue in colour and is formulated as $[VO(SD)_2(H_2O)]\cdot H_2O$: $VOC_{20}H_{22}N_8O_6S_2$. Molar mass, 601.51; Yield: 95%. Elemental analysis: [Found (Calc.)]: C, 40.56 (39.94); H, 3.56 (3.69), N, 18.05 (18.63). The proposed structure for the complex based on the above formulation is shown in Figure 40.

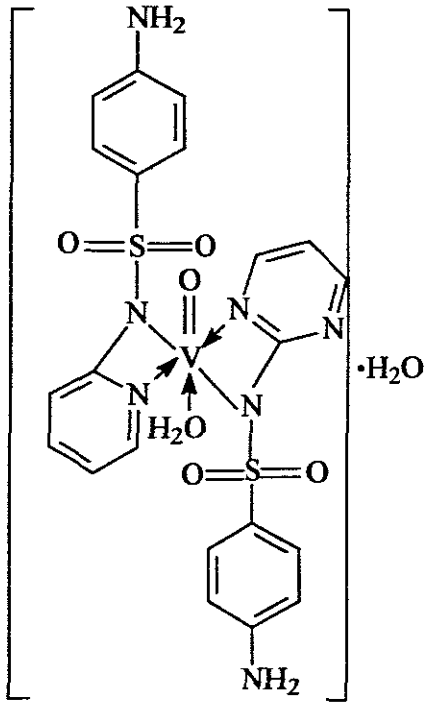

Fig.40: Proposed structure of VO(II)sulfadiazine

3.3.10.1 Electronic Spectra of Oxovanadium(IV) sulfadiazine complexes

The electronic spectra of VO(II) complexes are dominated by square pyramidal geometry and characterised by three d—d transitions in the range 8000 - 30,000 cm^{-1}. The first band (I) , ($b \rightarrow e^*_x$) lies in the range 11,000 – 16,000 cm^{-1}, the second band , II ($b_2 \rightarrow b_1^*$) occur in the range 14,500-19,000 cm^{-1} and the third band, III ($b_2 \rightarrow a_1^*$) occur in the range 21,000 – 30,000 cm^{-1}. The last band is frequently obscured by strong charge transfer transitions which typically occur in the blue or ultraviolet region of the electromagnetic spectrum[169]. It was clearly demonstrated by Patel *et al.*[169a] that changes do occur in band II as the symmetry of VO(II) complexes go from C_{2v} to C_{4v} and ultimately to octahedral symmetries. Several attempts have been made on detailed interpretation of the ligand field spectra of VO(II) complexes. The most commonly used

is the molecular orbital treatment of $[VO(H_2O)_5]^{2+}$ by Ballhausen and Gray[170]. By using this energy treatment, the π-bonding in the ion is thus essentially axial given rise to a double bond between the vanadium atom and the unique oxygen atom[171]. The electronic spectrum of VO(II) sulfadiazine complex is shown in Figure 41. The spectrum gave band III, 22,883 – 27,933 cm^{-1} (437 - 358 nm). The band is assigned to $b_2 \rightarrow a_1^*$ transitions. It could thus be concluded that the complexes most probably have a six-coordinate geometry[165] in DMF either due to solvent interaction or that the complex in the solid state was octahedral

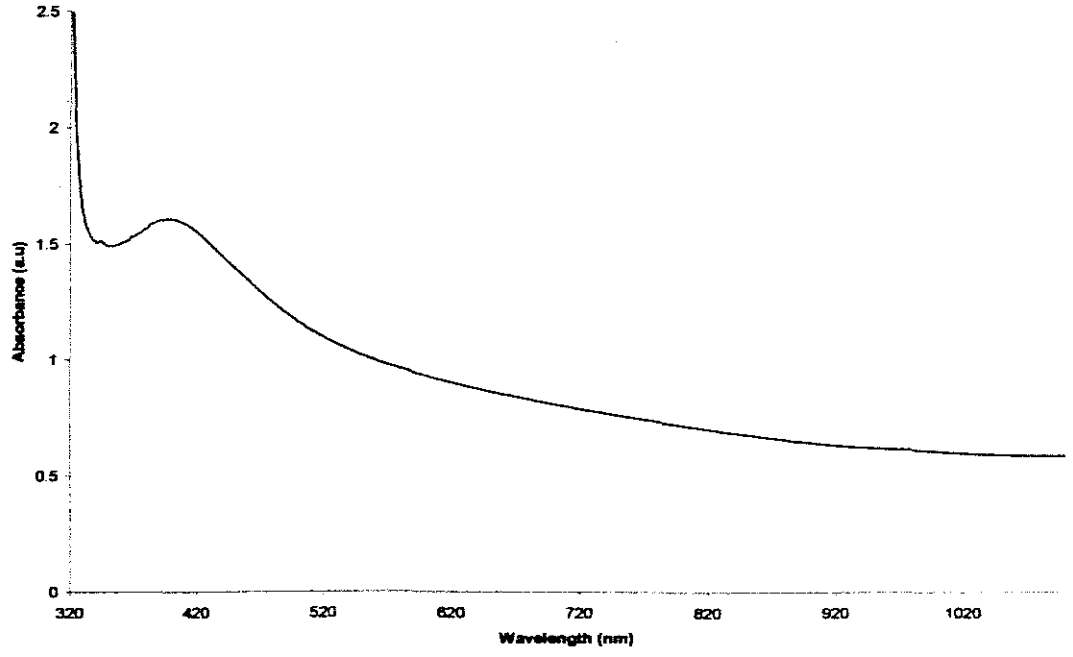

Figure 41: Solution spectrum of VO(II) sulfadiazine complex in DMF

3.3.10.2 Infrared Spectra of VO(II)sulfadiazine

The IR spectrum shows multiple absorption bands in the region 3422-3039 cm^{-1} indicating that the NH_2 is not involved in bond formation in the complex. The three very

sharp bands at 1652, 1590 and 1580 cm^{-1} are assigned to the C = N stretching frequencies. The V=O bond in VO(II) complexes can be regarded as a multiple covalent bond, the π component consisting of $p\pi$ electrons to oxygen of $d\pi$ orbitals of vanadium. The electron –accepting capacity of vadium(IV) markedly depends upon the ligands coordinated to the oxycation moiety. Depending upon the donor ability of ligand, by increasing the electron density in the metal, the $O(p\pi) \rightarrow O(d\pi)$ donation is reduced, lowering the V=O bond order. As a result the V=O stretching frequency will decrease. The VO^{2+} frequencies generally fall in the range 960 ± 50 cm^{-1}. The VO stretching vibration is assigned to the sharp band that appear at 945 cm^{-1}. This is most probably due to the effect of electron-donating groups coordinated to the metal leading to a weakening in the V=O bond[172]. The V—N is assigned to bands at 550 and 511 cm^{-1}.

3.4 Metal Complexes of Trimethoprim

Cobalt(II), copper(II), platinum(II), nickel(II), manganese(II) and iron(III) complexes of trimethoprim were isolated and characterized by elemental analysis, UV-Vis, IR, magnetic susceptibility measurement, conductivity, M.pt. /decomposition temperatures and some by mass spectrometry and single crystal X-ray crystallography.

3.4.1 Cobalt(II) complex of Trimethoprim

The complex was deep blue in colour and is formulated as $[Co(TMP)_2Cl_2]$: $CoC_{28}H_{36}N_8O_6Cl_2$, molar mass = 710.48. Elemental analysis, [Found (Calc.)]: C, 47.24 (47.34); H, 5.01 (5.11), N, 15.81 (15.77); Co, 8.35 (8.29). The single crystal data of the complex obtained showed that it was essentially the same as those reported by Dermatin,

et al. [112] but the unit cell parameters obtained for $[Co(TMP)_2Cl_2]$ are completely different from those reported by Dermatin, *et al.* [112] . Dermatin, *et al.* reported a crystallographic space group C_2/c for their complex whereas our complex adopts crystallographic space group P—1.

3.4.2.1 X-ray crystal structure

The molecular structure of the complex, $[Co(TMP)_2Cl_2]$, is shown in Figure 42 with the atom-numbering scheme used in Table 11, which also contains the most relevant bond distances and angles. The selected bond lengths and angles for the crystal structure are presented in Table 12. The complex displays crystallographic P-1 space group in which the Co atom lay on a two fold axis bonding two chlorine atoms and two trimethoprim molecules in a distorted tetrahedral environment. The trimethoprim acts as a monodentate ligand and bonds through the pyrimidine N(1). The Cl—Co—Cl bond angle of 111.38° is smaller than 118.1° reported in the literature. The packing diagram of the crystal structure is presented in Figure 43. The structure consists of two molecules of trimethoprim linked to each other by intermolecular hydrogen bonding. The hydrogen bonding parameters are presented in Table 13.

Table 11: Crystal Data and Structure Refinement for $[Co(TMP)_2Cl_2]$

Empirical formula	$C_{28}H_{36}Cl_2CoN_8O_6$
Formula weight	710.48
Temperature	100(2)K
Wavelength	0.71073A
Crystal system	Triclinic
Space group	P–1
Unit cell dimensions	
a (Å)	10.2097(7)
b (Å)	10.3469(7)
c (Å)	16.0179(10)
β (°)	106.3850(10)
γ (°)	96.9160(10)
Volume ($Å^3$)	1593.28(18)
Z	2
D_{calc} Mg/m^3	1.481
Absorption coefficient (mm^{-1})	0.761
F(000)	738
Crystal size (mm)	0.60 × 0.50 × 0.10
Theta range (°)	2.01 to 26.40
Reflections collected	12749
Independent reflection	6396 [R(int) =0.0216]
Completeness to Θ = 26.40	98.0 %
Refinement method	Full-matrix least-squares on F^2
Data/restraints/parameters/	6396 / 0 / 444
Goodness-of-fit on F^2	1.035
Final R indices [I>2sigma(I)]	R1 = 0.0320, wR2 = 0.0827
R indices (all data)	R1 = 0.0364, wR2 = 0.0855
Largest diff. Peak and hole	0.612 and –0.264 e. $Å^{-3}$

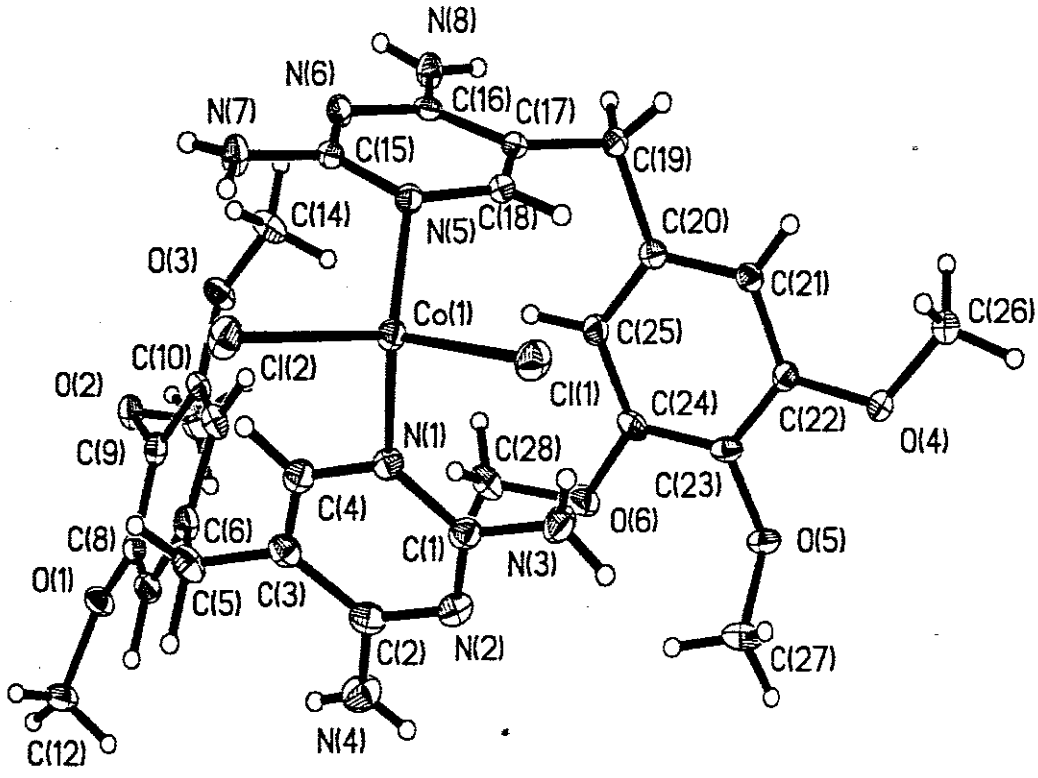

Figure 42: The X-ray crystal structure $[Co(TMP)_2Cl_2]$

Table 12: Selected bond length and angle for $[Co(TMP)_2Cl_2]$

Bond Length (Å)		Bond Angles (°)	
Co(1)–N(5)	2.0269(14)	N(5)–Co–N(1)	98.46(1)
Co(1)–N(1)	2.0328(15)	N(5)–Co–Cl(1)	114.58(4)
Co(1)–Cl	2.2528(5)	N(1)–Co–Cl(1)	111.48(4)
Co–Cl(2)	2.2852(5)	N(5)–Co–Cl(2)	113.40(4)
N(1)–C(4)	1.358(2)	N(1)–Co–Cl(2)	106.56(4)
N(1)–C(1)	1.359(2)	Cl(1)–Co–Cl(2)	111.380(18)
N(5)–C(15)	1.356(2)	C(4)–N(1)–Co(1)	116.14(12)
N(5)–C(18)	1.363(2)	C(1)–N(1)–Co(1)	128.12(12)
N(3)–C(1)	1.339(2)	C(15)–N(5)–Co(1)	123.07(11)
N(7)–C(15)	1.346(2)	C(18)–N(5)–Co(1)	116.50(11)

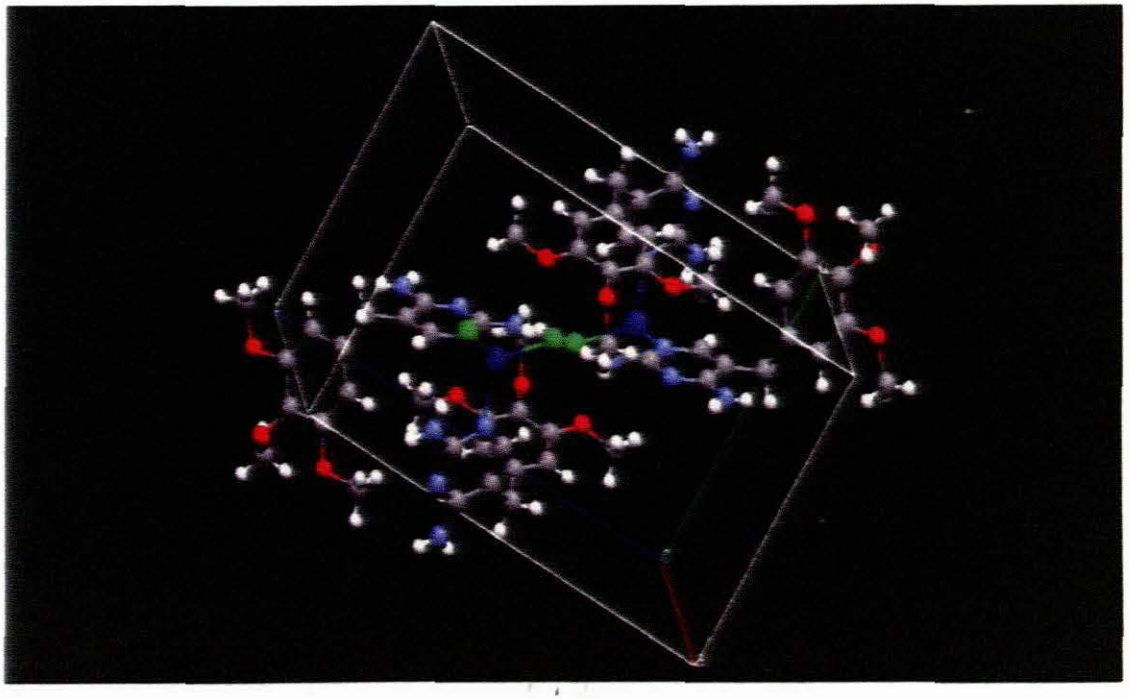

Figure 43: The Packing diagram for $[Co(TMP)_2Cl_2]$

Table 13: Hydrogen bonds for $[Co(TMP)_2Cl_2]$

D–H…A	d(D–H)	d(H…A)	d(D…A)	<(DHA)
N(3)–H(1N)…Cl(1)	0.84(2)	2.47(2)	3.2728(18)	163(2)
N(8)–H(7N)…Cl(1)#1	0.84(2)	2.85(2)	3.5474(17)	141.4(17)
N(7)–H(6N)…O(1)#2	0.84(2)	2.06(2)	2.894(2)	167(2)
N(7)–H(6N)…O(2)#2	0.84(2)	2.55(2)	3.089(2)	122.9(18)
N(7)–H(5N)…Cl(2)	0.83(2)	2.43(2)	3.2380(17)	165(2)
N(8)–H(8N)…O(5)#3	0.82(2)	2.15(2)	2.910(2)	155(2)
N(3)–H(2N)…O(4)#4	0.86(3)	2.17(3)	2.994(2)	160(2)

Symmetry transformations used to generate equivalent atoms:
#1 x, y +1, z #2 -x , -y+2, -z #3 -x + 1, -y + 2, -z + 1
#4 -x + 1, y + 1, -z + 1.

3.4.1.2: Cobalt(II) Complex of trimethoprim

Another cobalt(II) complex, obtained from cobalt(II) acetate, crystallized as a dimer. The single crystals suitable for X-ray analysis were obtained as highlighted in section 2.6.1.2. The crystal structure is formulated as $\{[Co_2(TMP)_2(CH_3COO)_4].2C_7H_8.(CH_3O)\}$ based on the empirical formula, $C_{51}H_{67}Co_2N_8O_{15}$ obtained from the X-ray structural parameters. Elemental analysis: [Found (Calc.)]: C, 52.53 (53.27); H, 5.87 (5.85), N, 9.82 (9.74); Co, 10.16 (10.25). The complex was further characterized by UV-Vis and IR spectroscopy. The molecular structure of the complex is shown in Figure 44 with the atom-numbering scheme used in Table 14, which also contains the most relevant bond distances and angles.

The crystals consist of packings of $[Co_2(TMP)_2(CH_3COO)_4]$ molecules with a molecule of toluene and a methoxy group clathrated in the molar ratio 1:2:1. The selected bond lengths and angles for the crystal is presented in Table 15. The crystals contain dimeric $\{[Co_2(TMP)_2(CH_3COO)_4]\cdot 2C_7H_8\cdot(CH_3O)\}$ molecules, packed with normal van der Waals interactions in crystallographic symmetry with inversion center lying on the midpoint of the Co···Co interactions so that only half of the molecule is crystallographically independent. The cobalt atoms are in a distorted octahedral environment in which each is bonded to trimethoprim, acting as a monodentate ligand through pyrimidinic nitrogen, N(1) position and two bridging acetate ligands. The Co—Co bond length of 2.6684(4) is at the extreme of the normal bond lengths obtained for acetate-bridged crystals. The four acetates are almost planar with dihedral bond angles of approximately 90°.

Table 14: Crystal data and structure refinement for $\{[Co_2(TMP)_2(CH_3COO)_4]\cdot 2C_7H_8\cdot(CH_3O)\}$

Empirical formula	$C_{51}H_{67}Co_2N_8O_{15}$
Formula weight	1149.99
Temperature	100(2)K
Wavelength	0.71073A
Crystal system	Monoclinic
Space group	C_2/c
Unit cell dimensions	
a (Å)	24.313(4)
b (Å)	15.321(3)
c (Å)	16.323(3)
β (°)	116.526(2)
γ (°)	90
Volume ($Å^3$)	5440.1(17)
Z	4
D_{calc} Mg/m^3	1.404
Absorption coefficient (mm^{-1})	0.683
F(000)	2412
Crystal size (mm)	0.30 × 0.20 × 0.05
Theta range (°)	1.63 to 25.02
Reflections collected	18581
Independent reflection	*4807 [R(int) =0.0867]*
Completeness to Θ = 26.40	99 %
Refinement method	Full-matrix least-squares on F^2
Data/restraints/parameters/	4807 / 4 / 357
Goodness-of-fit on F^2	0.967
Final R indices [I>2sigma(I)]	R1 = 0.0545, wR2 = 0.1392
R indices (all data)	R1 = 0.0951, wR2 = 0.1531
Largest diff. Peak and hole	0.931 and –0.630 e. $Å^{-3}$

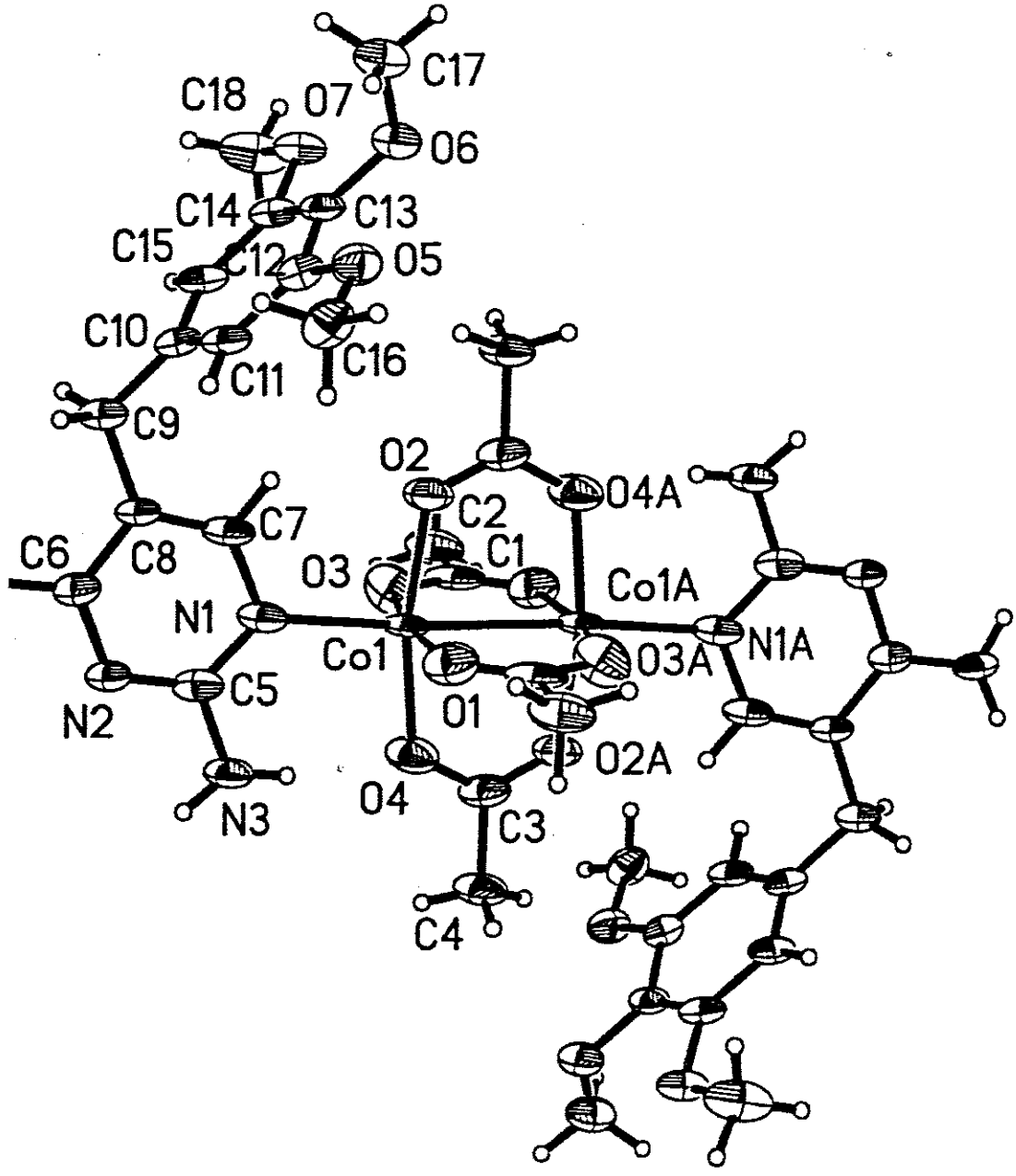

Figure 44: X-ray crystal structure of $\{[Co_2(TMP)_2(CH_3COO)_4]\cdot 2C_7H_8\cdot(CH_3O)\}$

Table 15: Selected bond length and angles for $\{[Co_2(TMP)_2(CH_3COO)_4]\cdot 2C_7H_8\cdot(CH_3O)\}$

Bond length		Bond angle	
Co(1)–O(1)	1.965(4)	O(1)–Co(1)–O(3)	167.06(16)
Co(1)–O(3)	1.971(4)	O(1)–Co(1)–O(2)	89.78(14)
Co(1)–O(2)	1.975(3)	O(3)–Co(1)–O(2)	89.01(15)
Co(1)–O(4)	1.997(3)	O(1)–Co(1)–O(4)	89.07(15)
Co(1)–N(1)	2.187(4)	O(3)–Co(1)–O(4)	89.25(15)
Co(1)–Co(1A)	2.6884(13)	O(2)–Co(1)–O(4)	167.12(15)
		O(1)–Co(1)–N(1)	94.16(15)
		O(3)–Co(1)–N(1)	98.76(15)
		O(2)–Co(1)–N(1)	92.16(14)
		O(4)–Co(1)–N(1)	100.72(14)
		O(1)–Co(1)–Co(1A)	82.55(12)
		O(3)–Co(1)–Co(1A)	84.52(12)
		O(2)–Co(1)–Co(1A)	83.46(11)
		O(4)–Co(1)–Co(1A)	83.67(11)
		N(1)–Co(1)–Co(1A)	174.50(10)
		C(1A)–O(1)–Co(1)	125.4(3)
		C(3A)–O(2)–Co(1)	124.9(3)
		C(3)–O(4)–Co(1)	122.9(4)
		C(5)–N(1)–Co(1)	128.2(3)
		C(1A)–Co(1)–Co(1)	118.0(3)

Symmetry transformation used to generate equivalent atoms:
#1 –x, -y + 1, -z #2 -x + 2, y, -z + ½ #3 -x + ½, -y + ½, -z +1

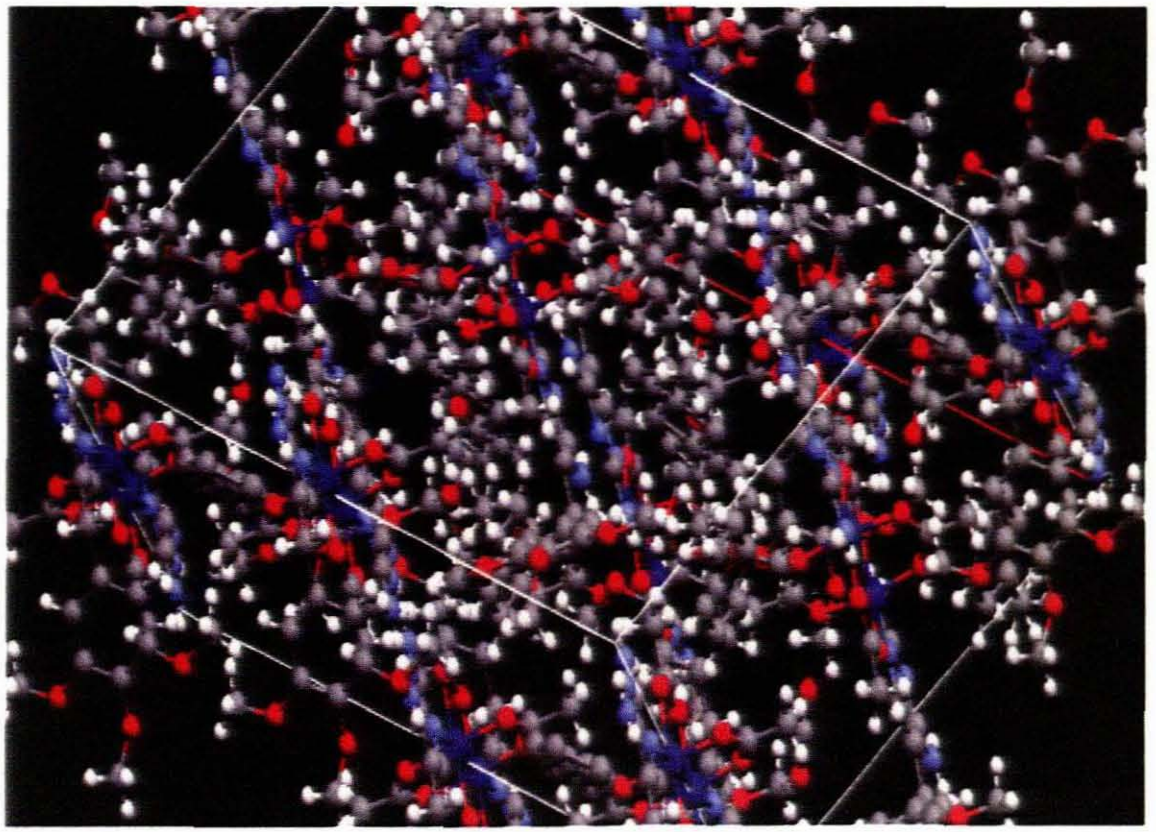

Figure 45: Crystal Packing for $\{[Co_2(TMP)_2(CH_3COO)_4].2C_7H_8.(CH_3O)\}$

Table 16: Hydrogen bonds for $\{[Co_2(TMP)_2(CH_3COO)_4]\cdot 2C_7H_8\cdot(CH3O)\}$

D–H…A	d (D-H)	d (H···A)	d (D···A)	‹(DHA)
N(4)–H(4N)…O(6)#4	0.860(19)	2.66(4)	3.274(5)	129(4)
N(4)–H(4N)…O(7)#4	0.860(19)	2.31(4)	3.000(5)	137(4)
N(4)–H(3N)…N(2)#5	0.859(19)	2.24(2)	3.080(6)	165(5)
N(3)–H(2N)…O(4)	0.88(2)	2.00(3)	2.865(6)	168(7)
N(3)–H(1N)…O(7)#6	0.88(2)	2.28(4)	3.076(5)	149(6)

Symmetry transformations used to generate equivalent atoms:

#1 –x, -y +1, -z #2 -x +2, y, -z + ½ #3 -x + ½, -y + ½, -z + 1

#4 -x + ½, y + ½, -z + ½ #5 -x, -y +2, -z #6 x-1/2, -y +3/2, z-½

The Co(1)—O(4) bond length of 1.997 Å is unusually long as compared to the other three Co—O bond lengths in the crystal structure with an average of 1.970 Å. The only probable explanation might be as a result of H—bonding (Table 16) within the crystal lattice. The packing diagram of the structure is shown in Figure 45. Each molecule is linked with four other molecules through intermolecular H—bonding.

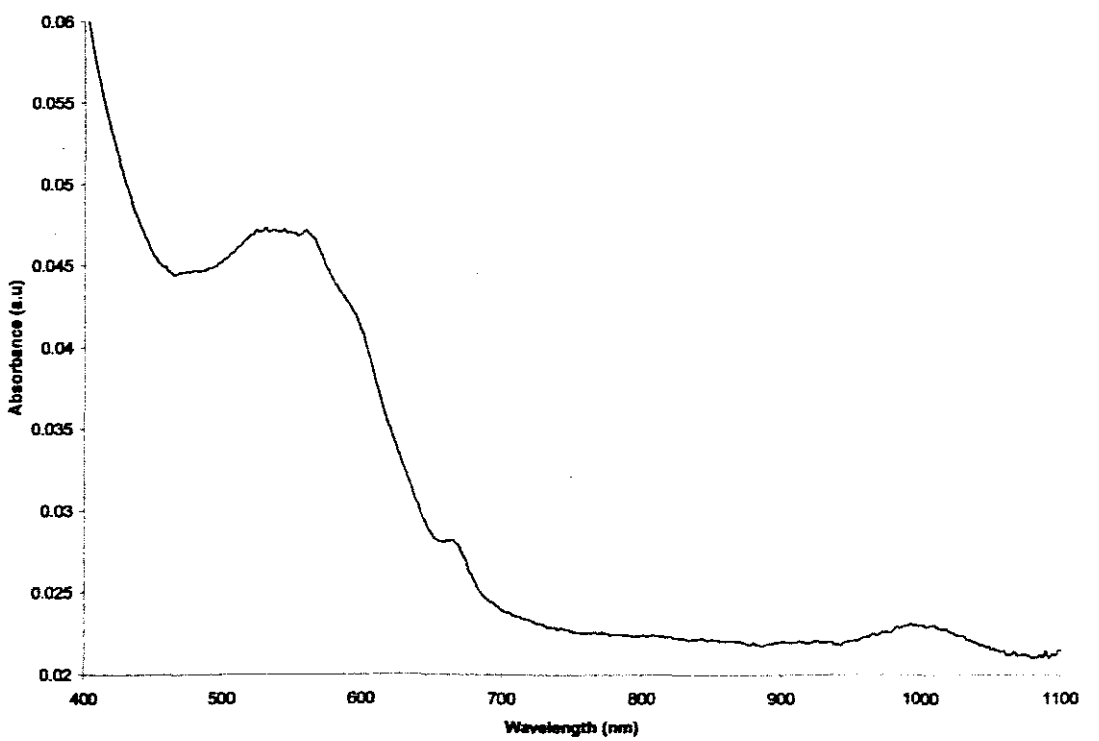

Figure 46: Solution Spectrum of $\{[Co_2(TMP)_2(CH_3COO)_4]\cdot 2C_7C_8\cdot(CH_3O)]\}$ in DMF

The electronic structure of the dimeric complex is shown in Figure 46. Three weak bands, typical of Co(II) octahedral complex, are observed. A band in the near infrared region at 10,030 cm^{-1} (997 nm) is assigned to $^4T_{1g}(F) \rightarrow {}^4T_{2g}(F)$, a shoulder occurs at 15,105 cm^{-1}

which is usually due to $^4T_{1g}(F) \rightarrow {}^4A_{2g}(F)$ and a more intense band at 18,656 cm^{-1} is assigned to $^4T_{1g}(F) \rightarrow {}^4T_{1g}(P)$. The fine structure around this band is probably due to spin-orbit coupling or overlaps due to the many metal centres within the crystal lattice.

3.4.2 Copper (II) complex of Trimethoprim

Two copper complexes were isolated. The green complex has a deep green colour and was characterised by elemental analysis, UV-Vis, IR, EPR and single crystals X-ray studies. Molecular formula of the compound is $Cu_2C_{51}H_{60}N_8O_{15}$, molar mass, 1152.17 while a second complex with a molecular formula of $Cu_2C_{52}H_{62}N_8O_{15}$, has molar mass of 1166.20. The two structures are typically the same. The molecular structures of the complexes are shown in Figs. 47 and 49 with the atom-numbering scheme in Table 17, which also contains the most relevant bond distances and angles.

The complexes belong to different space group. One belong to $P2(1)/c$ space group while the other belong to C_2/c. The crystals of the complexes consist of packing of two molecules of trimethoprim, and four acetate-bridged Cu—Cu bond, a molecule of methanol and toluene. The molecular formulae of the complexes do not fit any formulation, the closest is one containing two molecules of toluene but this will be short of 6 H atoms. The selected bond lengths and angles for the complexes are presented in Tables 18 and 19. Although the two complexes are in different space groups, the bond lengths and angles around the two Cu ions are essentially the same with very slight variations.

Table 17: Crystal data and structure refinement for $C_{51}H_{60}Cu_2N_8O_{15}$ and $C_{52}H_{62}Cu_2N_8O_{15}$

Empirical formula	$C_{51}H_{60}Cu_2N_8O_{15}$	$C_{52}H_{62}Cu_2N_8O_{15}$
Formula weight	1152.15	1166.18
Temperature	100(2)K	100(2) K
Wavelength	0.71073A	0.71073 A
Crystal system	Monoclinic	Monoclinic
Space group	P2(1)/c	C_2/c
Unit cell dimensions		
a (Å)	22.299(3)	24.136(3)
b (Å)	15.2270(17)	15.2365(19)
c (Å)	16.2410(18)	16.225(2)
β (°)	104.0990(18)	116.448(2)
γ (°)	90	90
Volume (Å ^{3})	5348.5(10)	5342.4(11)
Z	4	4
D_{calc} Mg/m^3	1.431	1.450
Absorption coefficient (mm^{-1})	0.870	0.872
F(000)	2400	2432
Crystal size (mm)	0.30 x 0.20 x 0.20	0.15 x 0.15 x 0.10
Theta range (°)	1.64 to 28.29	1.64 to 28.30
Index ranges	-29<=h<=29, -20<=k<=19, -21<=1<=21	-32<=h<=31, -20<=k<=20 -21<=1<=21
Reflection collected	45633	22960
Independent reflection	12713 [R(int) = 0.0523]	6357[R(int) = 0.0799]
Completeness to Θ = 26.40	95.7 %	95.7
Refinement method	Full-matrix least-squares on F^2	Full-matrix least-squares on F^2
Data/restraints/parameters/	12713 / 0 / 651	6357 / 0 /328
Goodness-of-fit on F^2	1.063	1.014
Final R indices [I>2sigma(I)]	R1 = 0.0558, wR2 = 0.1615	R1 = 0.0703 wR2 = 0.1776
R indices (all data)	R1 = 0.0720, wR2 = 0.1703	R1 = 0.1130 wR2 = 0.1978
Largest diff. Peak and hole	2.352 and –0.799 e. Å^{-3}	1.911 and -0.939

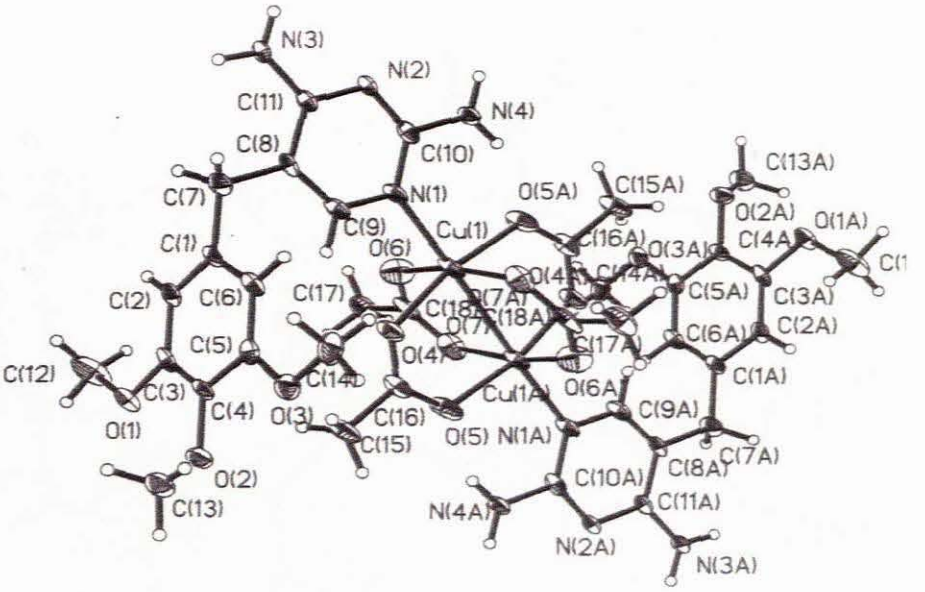

Figure 47: X-ray crystal structure of $C_{51}H_{60}Cu_2N_8O_{15}$

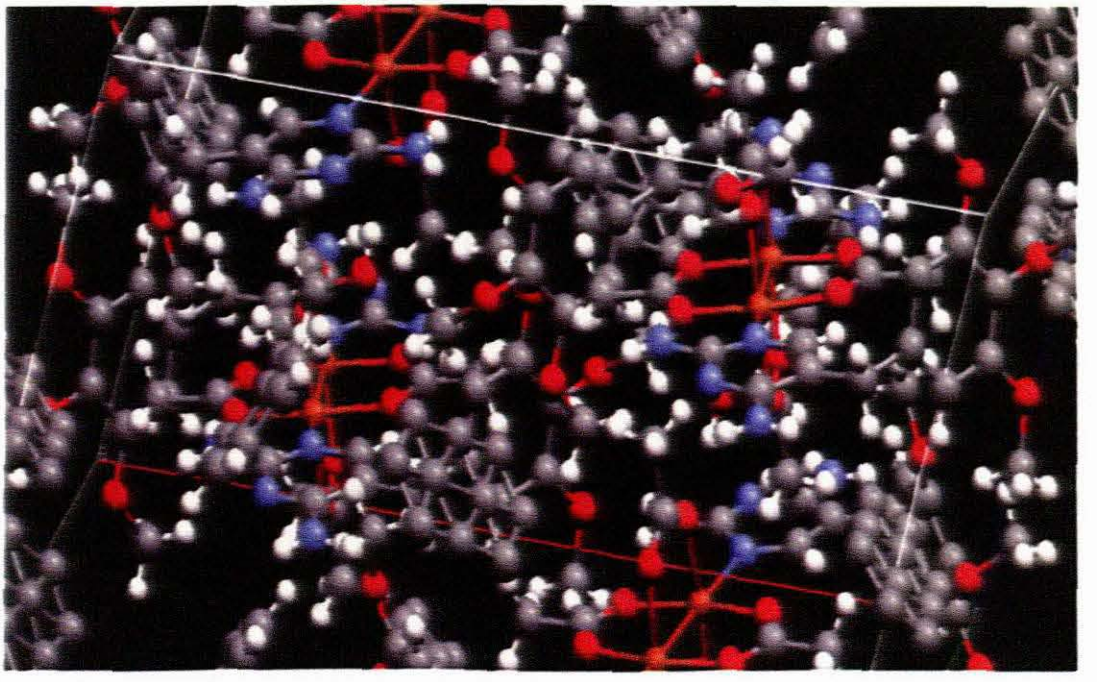

Figure 48: Crystal packing for $C_{51}H_{60}Cu_2N_8O_{15}$

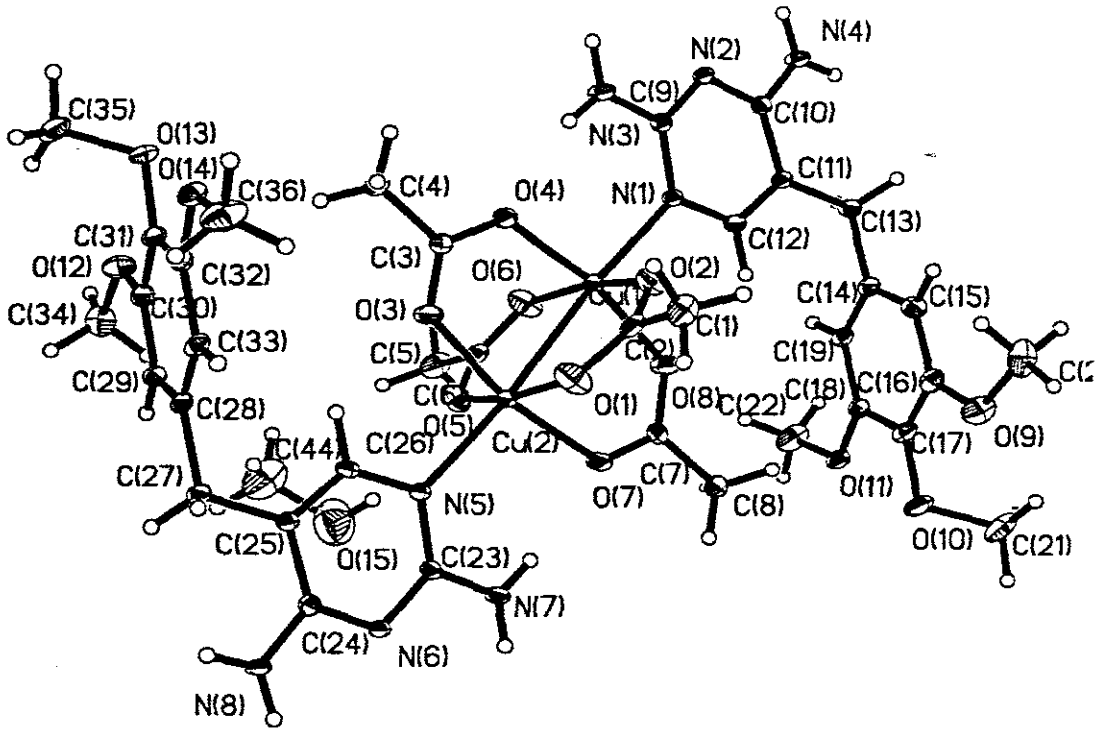

Figure 49: X-ray crystal structure of $C_{52}H_{62}Cu_2N_8O_{15}$

Table 18: Selected bond length for $C_{51}H_{60}Cu_2N_8O_{15}$ and $C_{52}H_{62}Cu_2N_8O_{15}$

$C_{51}H_{60}Cu_2N_8O_{15}$		$C_{52}H_{62}Cu_2N_8O_{15}$	
Cu(1)–O(6)	1.965(2)	Cu(1)–O(7)#3	1.958(4)
Cu(1)–O(2)	1.966(2)	Cu(1)–O(6)	1.971(4)
Cu(1)–O(8)	1.968(2)	Cu(1)–O(4)	1.973(3)
Cu(1)–O(4)	1.983(2)	Cu(1)–O(5)#3	1.988(3)
Cu(1)–N(1)	2.182(2)	Cu(1)–N(1)	2.183(4)
Cu(1)–Cu(2)	2.6756(6)	Cu(1)–Cu(1A)#3	2.6769(12)
Cu(2)–O(5)	1.968(2)	O(5)–Cu(1)#3	1.988(3)
Cu(2)–O(1)	1.9699(2)	O(7)–Cu(1)#3	1.958(4)
Cu(2)–O(3)	1.974(2)	O(8)–C(29)#4	1.257(13)
Cu(2)–O(7)	1.9819(2)	Cu–O(6)	
Cu(2)–N(5)	2.182(2)	Cu–O(6)	

Table 19: Selected bond angles for $C_{51}H_{60}Cu_2N_8O_{15}$ and $C_{52}H_{62}Cu_2N_8O_{15}$

$C_{51}H_{60}Cu_2N_8O_{15}$		$C_{52}H_{62}Cu_2N_8O_{15}$	
O(6)–Cu(1)–O(2)	166.27(9)	O(7)#3–Cu(1)–O(6)	166.84
O(6)–Cu(1)–O(8)	89.24(10)	O(7)–Cu(1)–O(4)	89.71(15)
O(6)–Cu(1)–N(1)	98.79(9)	O(6)–Cu(1)–N(1)	98.86(16)
O(4)–Cu(1)–N(1)	100.88(8)	O(5)#3–Cu(1)–N(1)	100.76(14)
O(2)–Cu(1)–Cu(2)	84.16(7)	O(4)–Cu(1)–Cu(1)	84.43(11)
N(1)–Cu(1)–Cu(2)	174.60(6)	N(1)–Cu(1)–Cu(2)	174.46(11)
O(5)–Cu(2)–O(1)	167.65(9)	O(4)–Cu(1)–O(5)#3	166.91(15)
C(9)–N(1)–C(12)	114.9(2)	C(10)–N(1)–C(9)	114.8(4)
C(9)–N(1)–Cu(1)	127.40(18)	C(10)–N(1)–Cu(1)	127.5(3)
C(12)–N(1)–Cu(1)	117.52(17)	C(9)–N(1)–Cu(1)	117.6(3)
C(3)–O(3)–Cu(2)	124.98(19)	C(16)–O(4)–Cu(1)	124.7(3)

The structures of the complexes are typically that of copper(II) carboxylates with empirical formula $[Cu(O_2CR)L)$ where L is an adduct such as water or pyridine[163]. It is well known that many compounds of this type are magnetically non-dilute, and are better formulated as $[Cu_2(O_2CR_4)L_2]$, with interaction between the two copper atoms, held together by bridging carboxylate groups. The coordination geometry around each copper atom in the two complexes, $C_{51}H_{60}Cu_2N_8O_{15}$ and $C_{52}H_{62}Cu_2N_8O_{15}$ closely resembles that found in the above cited complexes.

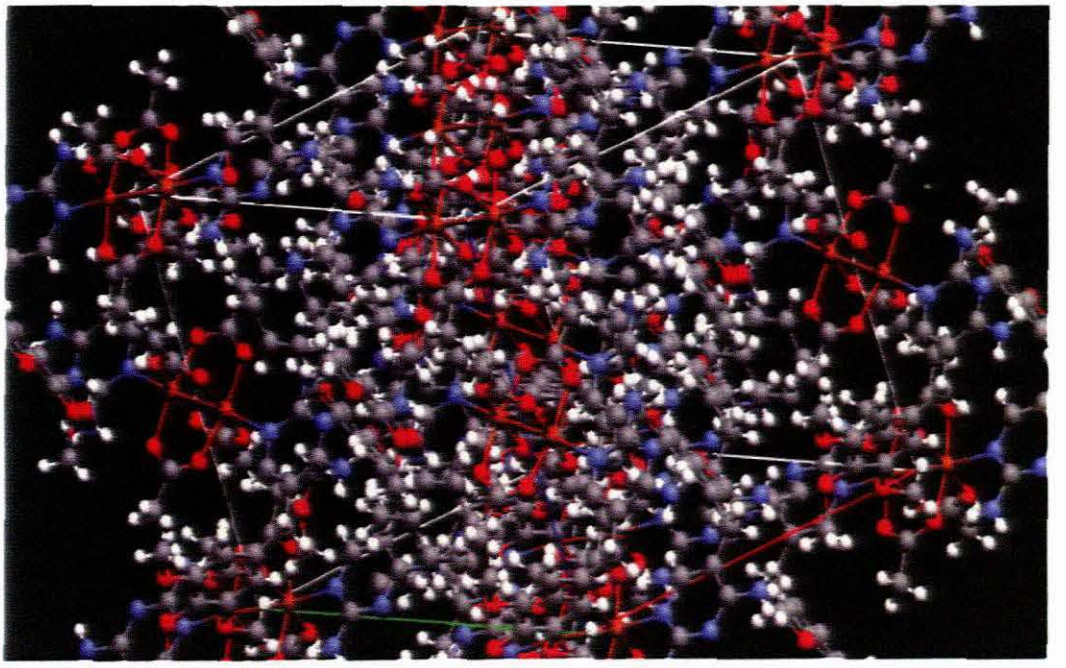

Figure 50: Packing diagram for $C_{52}H_{62}Cu_2N_8O_{15}$

Table 20: Hydrogen bond for $C_{51}H_{60}Cu_2N_8O_{15}$

D–H…A	d (D-H)	d (H···A)	d (D···A)	<(DHA)
O(15)–H(15A)…N(5)	0.84	2.58	3.190(4)	130.1
O(15)–H(15A)…O(5)	0.84	2.24	2.992(4)	148.7
N(8)–H(8E)…O(14)#3	0.88	2.24	2.960(3)	138.5
N(8)–H(8D)…N(2)#4	0.88	2.20	3.067(3)	167.5
N(7)–H(7B)…O(11)#5	0.88	2.27	3.066(3)	149.8
N(7)–H(7A)…O(7)	0.88	2.03	2.857(3)	155.4
N(4)–H(4E)…O(11)#6	0.88	2.26	2.988(3)	139.9
N(4)–H(4D)…N(6)#7	0.88	2.18	3.048(3)	171.2
N(3)–H(3B)…O(4)	0.88	2.02	2.849(3)	156.8
N(3)–H(3A)…O(14)#8	0.88	2.27	3.051(3)	148.1

Symmetry transformations used to generate equivalent atoms:
#1 -x + 2, -y +1, -z + 2 #2 -x +1, -y, -z + 1 # -x + 2, y +½, -z + 3/2
#4 x, y-1, z #5 -x + 1, y + ½, -z + 3/2 #6 -x + 1, y-½, -z +3/2
#7 x, y-1, z #8 -x + 2, y-½, -z +3/2

Table 21: Hydrogen bond for $C_{52}H_{62}Cu_2N_8O_{15}$

D–H...A	d (D-H)	d (H···A)	d (D···A)	<(DHA)
N(3)–H(3A)...N(2)#5	0.88	2.18	3.052(5)	169.8
N(3)–H(3B)...O(1)#6	0.88	2.25	2.971(5)	139.7
N(4)–H(4A)...O(1)#7	0.88	2.27	3.064(5)	149.5
N(4)–H(4B)...O(5)#3	0.88	2.03	2.854(5)	155.8

Symmetry transformations used to generate equivalent atoms:
#1 -x, y, -z + ½ #2 -x + ½, -z + 1 #3 -x, -y + 2, -z
#4 -x + 2, y, -z + ½ #5 -x, -y +1, -z #6 -x + ½, y-½, -z + ½
#7 x-½, -y + 3/2, z-½

The four bidentate acetate group bridge two copper atoms which are in a distorted octahedral environments with the carboxylic O atoms at the equatorial sites of the octahedron and the apical positions occupied by the pyrimidinyl N(1) of the trimethoprim and by the centrosymmetrically related copper atom. Each copper atom looks displaced from the plane of the four equatorial O atoms towards the N(1) and away from the other Cu atom. The Cu—O bond lengths are different, and this is most probably due to the effect of hydrogen bonding in the complexes (Table 20 and 21). The Cu—Cu bond length is in the range of those reported in the literature but slightly less than for copper trimethoprim complex reported by Naldini, *et al.*[113]. The packing diagrams for the complexes are shown in Figures 49 and 50. Each complex is surrounded by four other molecules in the crystal lattice, linked by H—bonding.

3.4.2.1 Electronic Spectra and Magnetic properties of the Cu complexes

The electronic spectrum of one of the crystals is shown in Figure 51. A single broad around 14,286 cm^{-1} (700 nm) characteristic of Cu^{2+} ion with hexa-coordinated geometry[163] which is in agreement with the data obtained from the X-ray diffraction for

the complex. A survey of copper(II) electronic spectroscopy presents difficulty because of the lack of definitive statements which can relate spectra with structure[111]. And since the ground state in an octahedral field is the Jahn-Teller unstable ^2E_g, very few regular octahedral copper(II) complexes exist. The X-ray single crystal of the complex showed that it is distorted octahedral. The shoulder at about 26,316 cm^{-1} (380 nm) is typical of dimeric copper(II) complexes[173] confirmed by the X-ray structural data. The distortion does not seem to be prominent because the band at 700 nm is not particularly unsymmetrical.

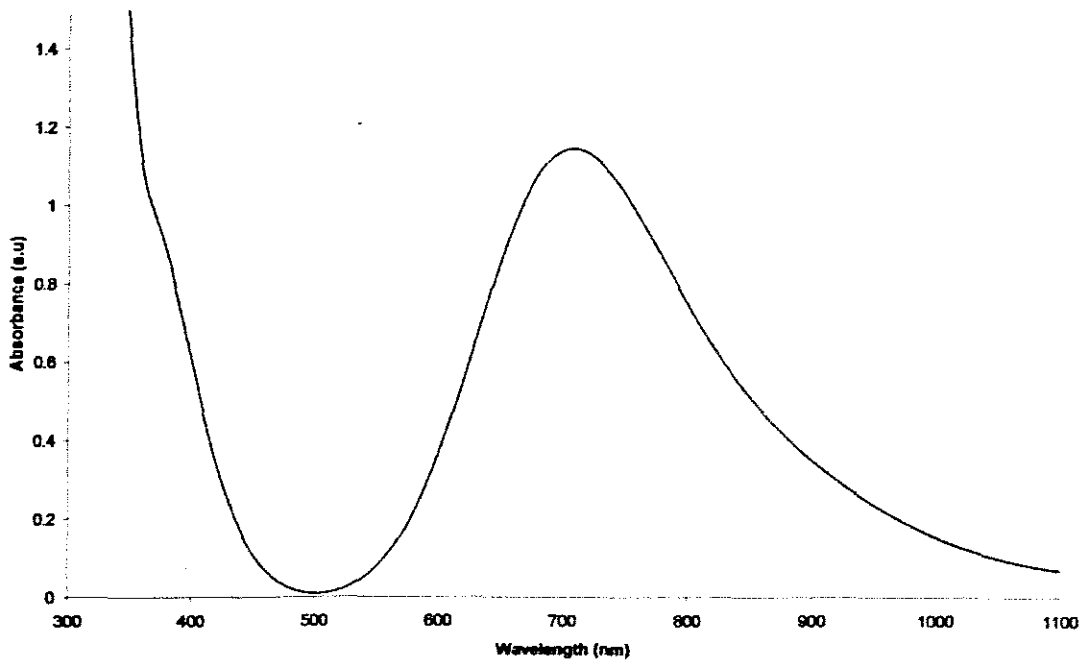

Figure 51: Electronic spectrum of $C_{52}H_{62}Cu_2N_8O_{15}$

The room temperature magnetic moments for the two complexes were expectedly sub-normal, at 1.27 B.M. for $C_{51}H_{60}Cu_2N_8O_{15}$ and 1.32 B.M. for $C_{52}H_{62}Cu_2N_8O_{15}$ much lower than the spin-only moment for magnetically dilute copper(II) complexes. The lower magnetic moment can be attributed to the dimeric structure in which two copper atoms interact anti-ferromagnetically to produce a low-lying singlet (diamagnetic) and an excited but thermally accessible triplet (paramagnetic) level[163]. In spite of a continuous flow of work on these types of compounds, there is still no general agreement as to the actual mechanism of the interaction or on possible correlations of its relevant properties of the carboxylate and axial ligands[174]. The most common interpretation assumes that the singlet and triplet levels arise from a single interaction between the unpaired spins of the copper atoms [175] which takes the form of δ overlap of the copper dx^2-y^2 orbital[176].

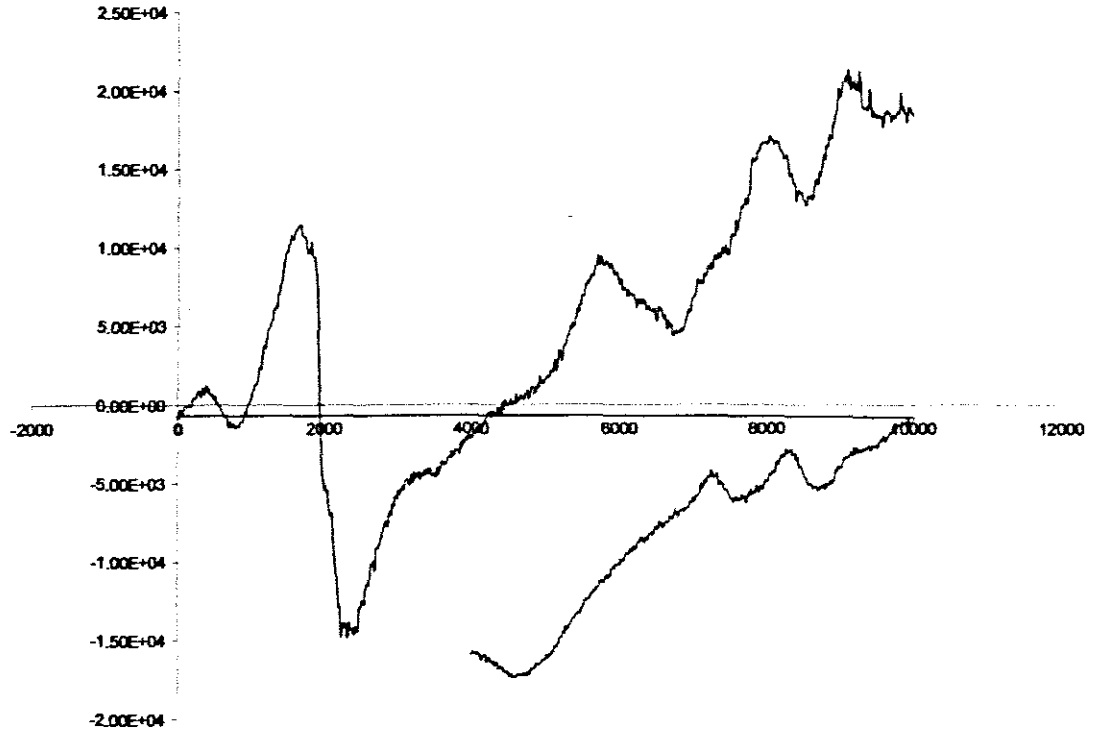

Figure 52: EPR spectra of one of the copper complexes

The EPR spectrum of the copper complex is shown in Figure 52. Using the X-band radiation at room temperature, three bands could be observed from the spectrum, g_1 = 2.34, $g_2 = g_3 = 2.06$, D = 1.159 cm^{-1}, E = 0.0412 cm^{-1}. These values are in agreement with binuclear copper(II) complexes. Thus, the result compliments the magnetic moments to support the binuclear nature of the complex as confirmed from the X-ray crystal structures.

3.4.2.2 Infrared Spectra for the complexes

A comparison of the infrared spectrum of the free trimethoprim ligand with the complexes showed that the absorption bands in the region 3467- 3174 cm^{-1} showed only very slight changes in the complexes which might be attributed to the fact that the NH_2 on the drug are not involved in direct bond formation with the metal ion. . The mode of coordination of carboxylate groups can be deduced from the magnitude of the observed separation (Δ) between $\nu_{as}(CO_2)$ and $\nu_s(CO_2)$. In binuclear complexes, the $\nu_{as}(CO_2)$ bands are expected to be at higher frequencies than that of the free ligand. The $\nu_{as}(CO_2)$ band occurs at 1667 cm^{-1} for $C_{51}H_{60}Cu_2N_8O_{15}$ and $C_{52}H_{62}Cu_2N_8O_{15}$ complexes compared to 1578 cm^{-1} for CH_3COONa and 1618 cm^{-1} for a reported Cu(II) complex of trimethoprim[113]. The $\nu_s(CO_2)$ for $C_{51}H_{60}Cu_2N_8O_{15}$ and $C_{52}H_{62}Cu_2N_8O_{15}$ also occurs at 1462 cm^{-1} compared to 1414 cm^{-1} for CH_3COONa. A very sharp band at 681 cm^{-1} is assigned to Cu—N while the bands at 404 cm^{-1} is assigned to Cu—O band. Other

Cu—O bands occur at 469 and 343 cm^{-1}. The multiple bands in the region 625 – 534 cm^{-1} can be attributed to the N— Cu—O interactions.

3.4.3 Platinum (II) and Palladium (II) complexes of Trimethoprim

The Pt(II) complex was synthesized as highlighted in section 2.6.3. The complex is formulated as $[Pt(TMP)(H_2O)Cl_2]\cdot H_2O$. Molar mass, 592.34; elemental analyses for $PtC_{14}H_{22}N_4O_5Cl_2$: [Found (Calc.)]: C, 28.13 (28.39); 3.34 (3.74); N, 9.30 (9.46). The product was yellow in colour. Yield: 39%.

The palladium complex was synthesized from $K_2[PdCl]_4$ and trimethoprim. A brown product was obtained. The complex is formulated as $[Pd(TMP)(H_2O)Cl_2]\cdot H_2O$; molar mass, 503.68, elemental analyses for $PdC_{14}H_{22}N_4O_5Cl_2$: [Found (Calc.)]: C, 33.17 (33.39); H, 4.23 (4.40); N, 10.97 (11.12); yield: 68%. The proposed structure for the complexes is shown in Figure 53.

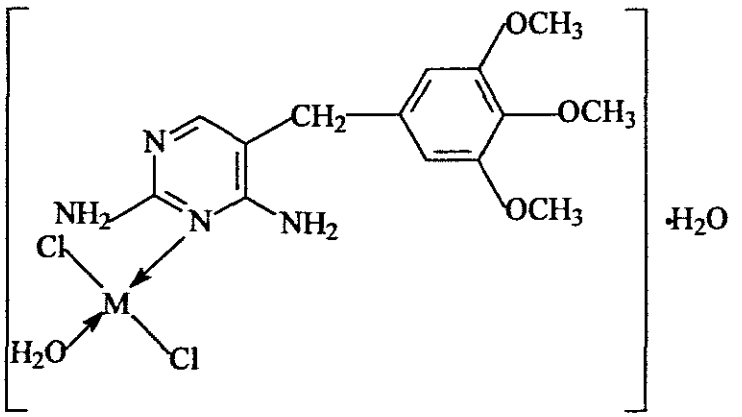

M = Pt, Pd

Figure 53: Proposed structure for Pt(II) and Pd(II) complexes of trimethoprim

3.4.3.1 Electronic Spectra of Pt(II) and Pd(II) trimethoprim complexes

The electronic spectra of the complexes are shown in Figure 54. The spectra are typical of square planar complexes which show little d—d absorption bands but gives a series of fragmented bands between 25,000-33,333 cm^{-1} (400 -300 nm) that can be attributed to high spin-orbit coupling. Magnetic moments of 0.34 B.M. for the Pt(II) and 0.24 BM for the Pd(II) complexes respectively confirm that the complexes are diamagnetic.

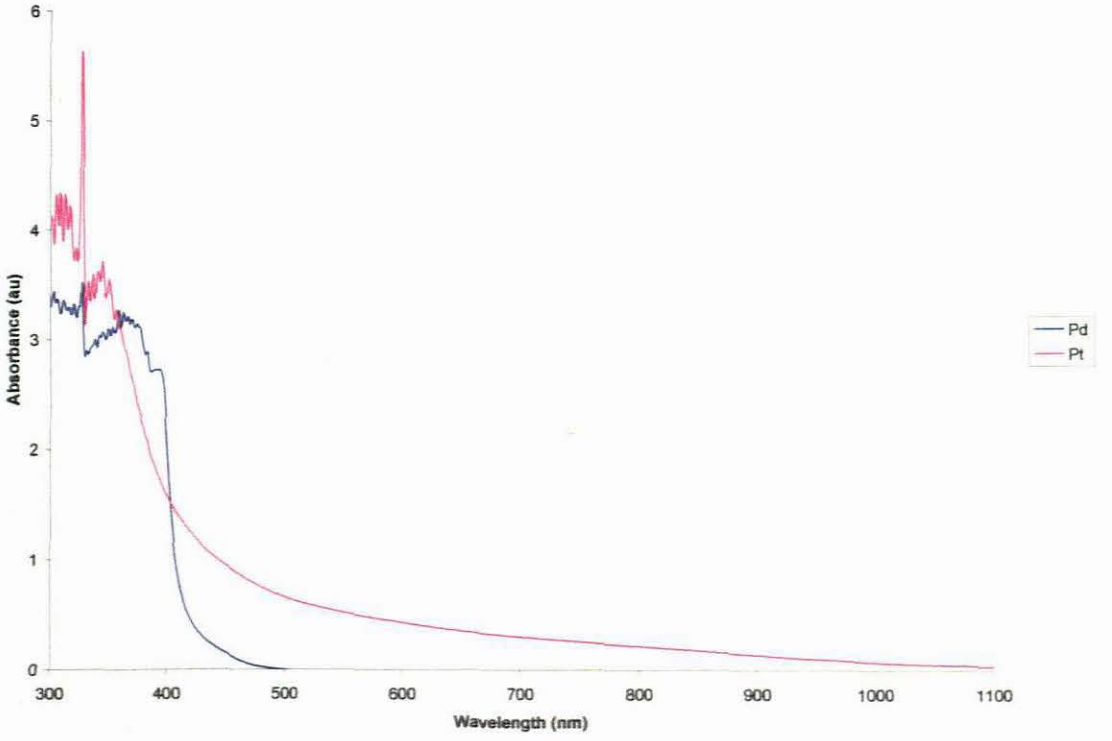

Figure 54: Solution Spectra of Pd(II) and Pt(II) complexes of trimethoprim in DMF

3.4.3.2 Infrared Spectra of Pt(II) and Pd(II) trimethoprim complexes

The IR spectrum of Pd(II) trimethoprim complex is presented in Figure 55. The infrared spectra of the complexes showed the NH_2 in the trimethoprim was not involved in coordination because of the little changes observed in the region 3450 – 3000 cm^{-1} of the complex when compared with that of the ligand. The rocking and wagging vibrations of the coordinated water, ρ_r (H_2O), occur at 589 (Pd) and 587 (Pt) while ρ_w (H_2O) are assigned to the bands at 845 and 810 cm^{-1} in both complexes respectively. The other vibrational bands are assigned thus, νM—N is assigned to the band at 778 cm^{-1} (Pd) and 776 cm^{-1} (Pt); νM—O bands occur at 528 cm^{-1} (Pd) and 512 cm^{-1} for Pt; νM—Cl bands is assigned to a single band at 256 cm^{-1} for both Pd and Pt.

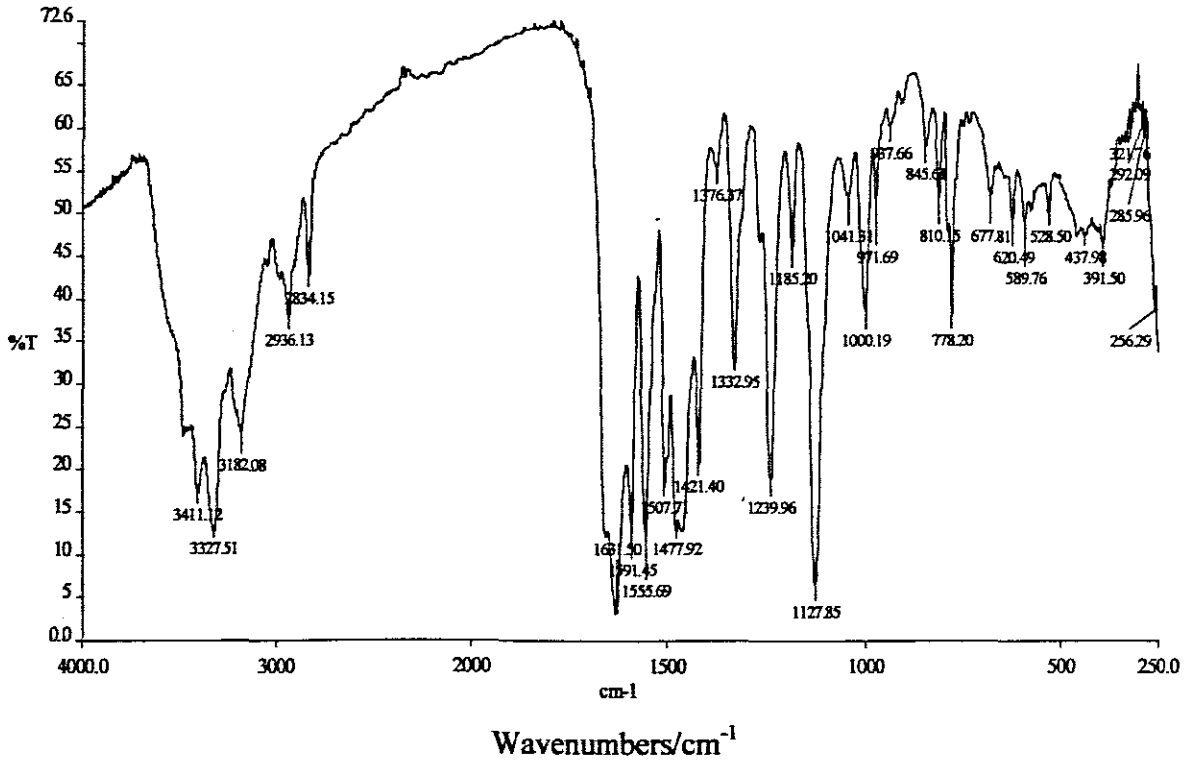

Wavenumbers/cm^{-1}

Figure 55: IR spectrum of Pd(II) complex of trimethoprim.

3.4.5 Nickel (II) complex of Trimethoprim

The Ni complexes were synthesized from the reaction between $[Ni(CH_3COO)_2]\cdot 4H_2O$ and trimethoprim in methanol. The green product obtained was characterized by single crystal X-ray structure, room temperature magnetic moment, IR and UV-Vis spectroscopy. The complex is formulated as $[Ni(TMP)_2(CH_3OH)_2(CH_3COO)_2]$. Elemental analyses for $NiC_{34}H_{50}N_8O_{12}$ [Found (Calc.)]: C, 49.56 (49.71); H, 5.94 (6.14); N, 13.46 (13.64), Ni, 7.02 (7.17).

3.4.5.1 X-ray crystal structures of $[Ni(TMP)_2(CH_3OH)_2(CH_3COO)_2]$

The green single crystal was used for X-ray diffraction measurements. The structure was solved by direct methods and refined on F^2 by full-matrix least-squares techniques. All non-hydrogen atoms were refined anisotropically. The selected data and details of the structure refinements are given in Table 22. Single X-ray crystal studies of compound was undertaken to elucidate the coordination sphere of Ni(II). The molecular structure of the complex with the atomic numbering scheme is shown in Figure 56 and selected bond length and angles are given in Table 23. The complex crystallized in the C_2/c space group. The Ni(II) atom is in an octahedral environments formed by two trimethoprim molecules that act as monodentate ligand and coordinate through the pyrimidinic N(1) atom with two acetates acting as monodentate ligands through oxygen and the octahedral geometry around the Ni(II) ions is completed by coordination to two methanol molecules.

The two Ni—N(1) bond length (2.101 Å) for the two trimethoprim molecules are similar and the four other bond lengths from the two acetate and methanol are essentially the

Table 22: Crystal Data and Structure Refinement for $[Ni(TMP)_2(CH_3OH)_2(CH_3COO)_2]$

Empirical formula	$C_{34}H_{50}N_8NiO_{12}$
Formula weight	821.53
Temperature	100(2)K
Wavelength	0.71069A
Crystal system	Monoclinic
Space group	C_2/c
Unit cell dimensions	
a (Å)	27.080(5)
b (Å)	9.0649(5)
c (Å)	20.416(5)
β (°)	128.663(5)
γ (°)	90.000(5)
Volume ($Å^3$)	3913(2)
Z	4
D_{calc} Mg/m^3	1.395
Absorption coefficient (mm^{-1})	0.566
F(000)	1736
Crystal size (mm)	0.40 x 0.40 x 0.40
Theta range (°)	1.93 to 26.39
Index ranges	-33<=h<=29, -8<=k<=11, -25<=l<=25
Reflections collected	10995
Independent reflections	3993 [R(int) =0.0354]
Refinement method	Full-matrix least-squares on F^2
Data/restraints/parameters/	3993 / 0 / 274
Goodness-of-fit on F^2	0.998
Final R indices [I>2sigma(I)]	R1 = 0.0314, wR2 = 0.0775
R indices (all data)	R1 = 0.0391, wR2 = 0.0796
Largest diff. Peak and hole	0.0391 and –0.231 e. $Å^{-3}$

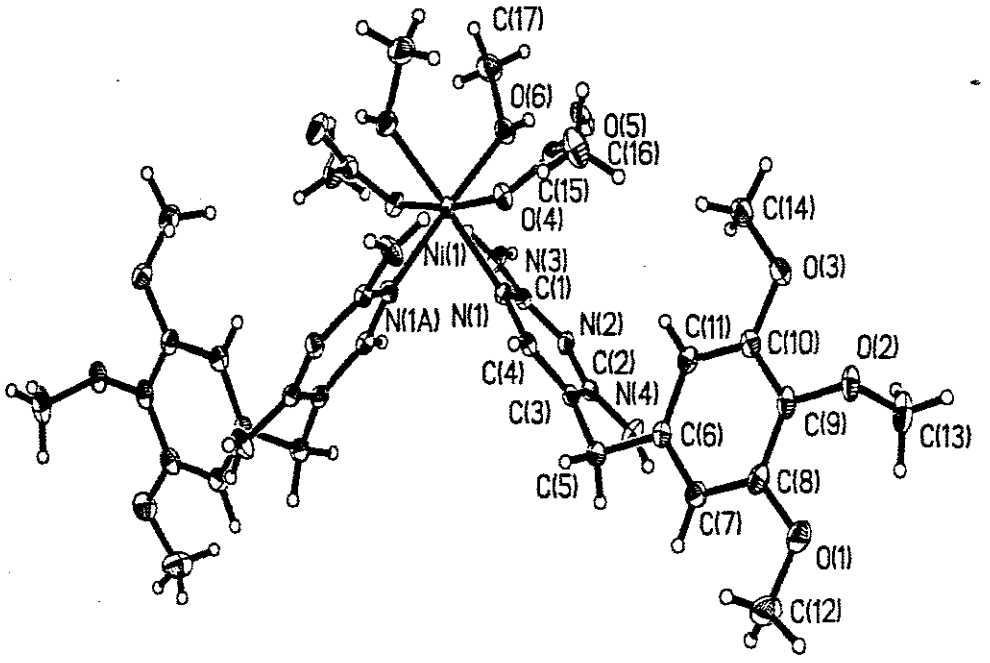

Figure 56: X-ray crystal structure of $[Ni(TMP)_2(CH_3OH)_2(CH_3COO)_2]$

same (2.072 Å) with only very slight variation (0.0001 Å) but longer than the Ni—N(1) bond length. Thus the coordination geometry around the Ni(II) atom is a distorted *octahedron*.

The distortion is further confirmed by the variations shown in the bond angles. The angles between Ni(II) and the methanol molecules, O(6)—Ni(1)—O(6)#1 is 93.54(8)°, greater than 90°. On the other hand, the angle between the Ni(II), methanol and acetate ion is less than 90°. Also, the angles between Ni(II), pyrimidinyl N(1) and methanol is different from their angle with the acetate; O(6)#1—Ni(1)—N(1)#1 is 88.79(6)° while

O(4)#1—Ni(1)—N(1)#1 is 92.84(5)°. The other angles between Ni, methanol and acetate ions are also less than the expected 180° and differ among each other; O(4)#1—Ni(1)—N(1) is 172.75(6)° while O(6)#1—Ni(1)—N(1)#1 is 177.64(5)°. The crystal structure consists of discrete $[Ni(TMP)_2(CH_3OH)_2(CH_3COO)_2]$ molecules linked to four other molecules by means of intermolecular hydrogen bonding (Table 24).

The packing of the $[Ni(TMP)_2(CH_3OH)_2(CH_3COO)_2]$ molecules in the crystal structure (Figure 57) consists of parallel chains formed by mutual interaction between molecules through intermolecular H-bonding. Each discrete molecule interacts with itself through four intramolecular H-bonding and interact with four neighbouring molecules through intermolecular H-bonding. The four intermolecular H-bonds are formed from one O-atom from the middle methoxy group on each trimethoprim and one of the NH_2 groups. Thus each molecule of trimethoprim acts as hydrogen-bond donor as well as acceptors. In this way, each discrete molecules of the complex contains two H-bond donors and acceptors. For the intramolecular H-bond, the NH_2 of the trimethoprim and methanol molecules are the donors while the acetate oxygen atoms are acceptors.

Table 23: Selected bond length and angles for $[Ni(TMP)_2(CH_3OH)_2(CH_3COO)_2]$

Bond length		Bond angles	
Ni–O(6)	2.0719(13)	O(6)–Ni(1)–O(6A)	93.54(8)
Ni–O(6A)	2.0720(13)	O(6)–Ni(1)–O(4A)	87.64(5)
Ni–O(4A)	2.0721(12)	O(6A)–Ni(1)–O(4A)	87.39(5)
Ni–O(4)	2.0721(12)	O(6)–Ni(1)–O(4)	87.39(5)
Ni–N(1)	2.1006(14)	O(6A)–Ni(1)–O(4)	172.75
Ni–N(1A)	2.1006(14)	O(6)–Ni(1)–N(1)	88.79
N(1)–C(4)	1.348(2)	O(6A)–Ni(1)–N(1)	177.64
N(1)–C(1)	1.353(2)	O(4A)–Ni(1)–N(1)	92.33
N(2)–C(2)	1.340(2)	O(4)–Ni(1)–N(1)	92.84(5)
N(3)–C(1)	1.344(2)	O(6)–Ni(1)–N(1A)	177.64(5)
N(3)–C(1)	1.337(2)	O(6A)–Ni(1)–N(1A)	88.79(6)
N(3)–H(3A)	0.86(2)	O(4A)–Ni(1)–N(1A)	92.84(5)
N(3)–H(3B)	0.80(2)	O(4)–Ni(1)–N(1A)	92.34(5)
N(4)–C(2)	1.340(2)	N(1)–Ni(1)–N(1A)	88.88(8)
N(4)–H(4A)	0.818(19)	C(15)–O(4)–Ni(1)	132.64(11)
N(4)–H(4B)	0.87(2)	C(17)–O(6)–Ni(1)	129.47(11)
C(2)–C(3)	1.423(2)	Ni(1)–O(6)–H(60)	105.1(16)
C(3)–C(4)	1.362(2)	C(1)–N(1)–Ni(1)	128.02(11)

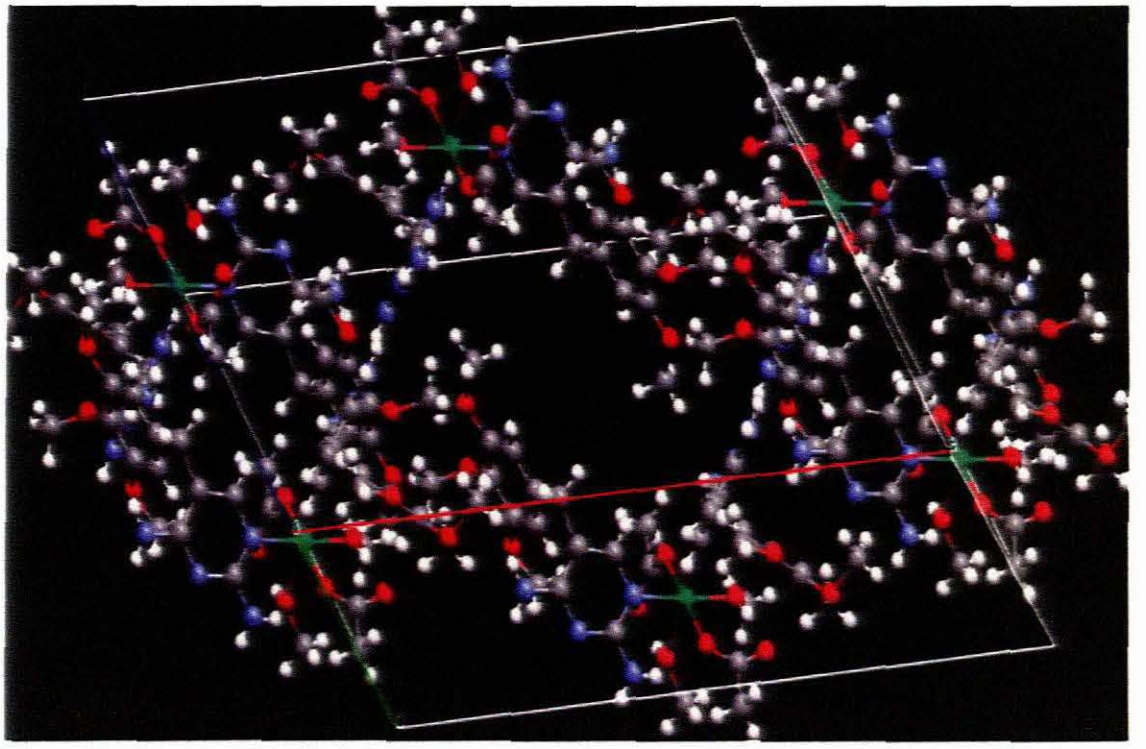

Figure 57: The crystal packing for $[Ni(TMP)_2(CH_3OH)_2(CH_3COO)_2]$

Table 24: Hydrogen bond for $[Ni(TMP)_2(CH_3OH)_2(CH_3COO)_2]$

D–H…A	d (D-H)	d (H···A)	d (D···A)	‹(DHA)
N(4)–H(4B)…N(2)#2	0.87(2)	2.24(2)	3.112(2)	179(2)
N(4)–H(4A)…O(3)#3	0.818(19)	2.473(19)	3.1063(19)	135.0(16)
N(3)–H(3B)…O(2)#4	0.80(2)	2.30(2)	2.925(2)	136(2)
N(3)–H(3A)…O(4)#1	0.86(2)	2.00(2)	2.790(2)	151.1(18)
O(6)–H(60)…O(5)	0.77(2)	1.85(2)	2.5969(18)	164(2)

Symmetry transformations used to generate equivalent atoms: #1 -x + 1, y , -z +3/2 #2 -x +1/2, -y +1/2, -z +1 #3 -x +1/2, -y +1/2, -z +3/2

3.4.5.2 Electronic spectrum and magnetic property of $[Ni(TMP)_2(CH_3OH)_2(CH_3COO)_2]$

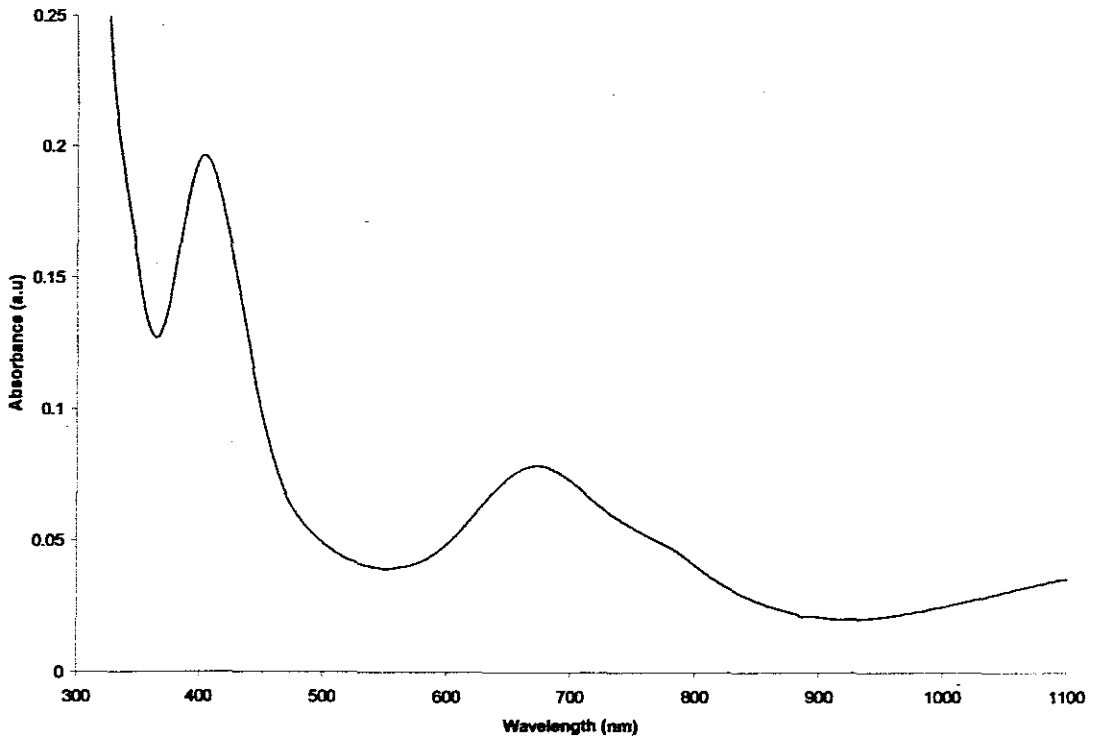

Figure 58: Electronic Spectrum of $[Ni(TMP)_2(CH_3OH)_2(CH_3COO)_2]$

The electronic spectrum of the complex in DMF is shown is Figure 58. The spectrum shows three absorption bands corresponding to the partly allowed electronic transitions for a d^8 ion in octahedral environment. The absorption band at 24,938 cm^{-1} (400 nm) is assigned to $^3A_{2g}(F) \rightarrow {}^3T_{1g}(P)$, a second band at 15,105 cm^{-1} (662 nm) is assigned to $^3A_{2g}(F) \rightarrow {}^3T_{1g}(F)$ with a weak shoulder at about 13,158 cm^{-1} (760 nm). The third absorption band can be assigned to a broad band due to $^3A_{2g}(F) \rightarrow {}^3T_{2g}(F)$ that start at about 9,524 cm^{-1} (1050 nm). The effective magnetic moments of 2.97 B.M. obtained for

the complex corroborates the octahedral geometry of the complex with two unpaired electrons.

3.4.5.3 Infrared Spectrum of $[Ni(TMP)_2(CH_3OH)_2(CH_3COO)_2]$

The vibration bands at 3460, 3369 and 3182 cm^{-1} confirm that the NH_2 on the trimethoprim ligand is not involved in coordination although they shift slightly in comparison to the free ligands. The presence of acetate in the coordination sphere of the metal is confirmed by the $\nu_{as}(CO^-_2)$ stretching frequency at 1630 cm^{-1} and the $\nu_s(CO^-_2)$ at 1471 cm^{-1}. The bands at 664 and 528 cm^{-1} are assigned to Ni—N stretching frequencies while the bands at 438 and 391 cm^{-1} are assigned to Ni—O.

3.4.6 Manganese(II) complex of Trimethoprim

The product was pale pink in colour and is formulated as $[Mn(TMP)(CH_3OH)Cl_2]$, $MnC_{15}H_{22}N_4O_4Cl_2$; molar mass, 448.21; yield, 48%. Elemental analysis, [Found (Calc.)]: C, 40.38 (40.20); H, 4.95 (5.10), N, 12.62 (12.50). The proposed structure of the complex is shown in Figure 59.

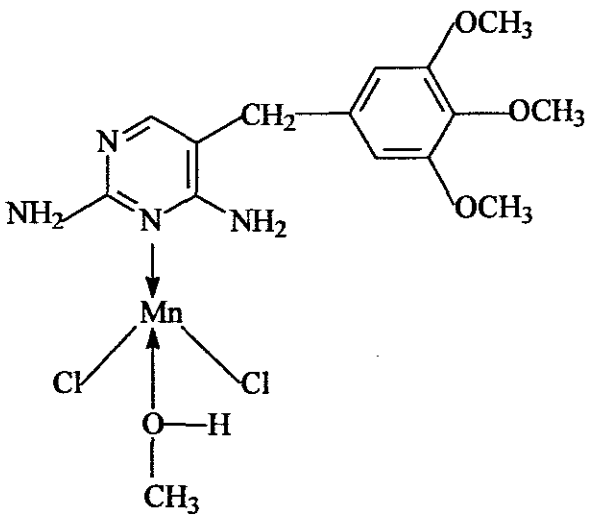

Figure 59: Proposed structure for [Mn(TMP)(CH_3OH)Cl_2]

3.4.6.1 Electronic Spectrum and Magnetic properties of [Mn(TMP)(CH_3OH)Cl_2]

The electronic spectrum of the Mn(II) trimethoprim complex is shown in Figure 60. The complex is formulated as a four-coordinate species. The spectra of tetrahedral manganese(II) complexes fall into three well-defined regions because of the fairly low D_q values involved. Thus transitions to the components of the ^4G term lie between 19,000–25,000 cm^{-1} (526–400 nm), those to ^4P and ^4D between 25,000–29,000 cm^{-1} (400–345 nm), and those to ^4F lie between 35,000–38,000 cm^{-1} (285–263 nm)[165]. From the electronic spectrum of the complex, the only observable transitions are those to ^4F between 310–260 nm.

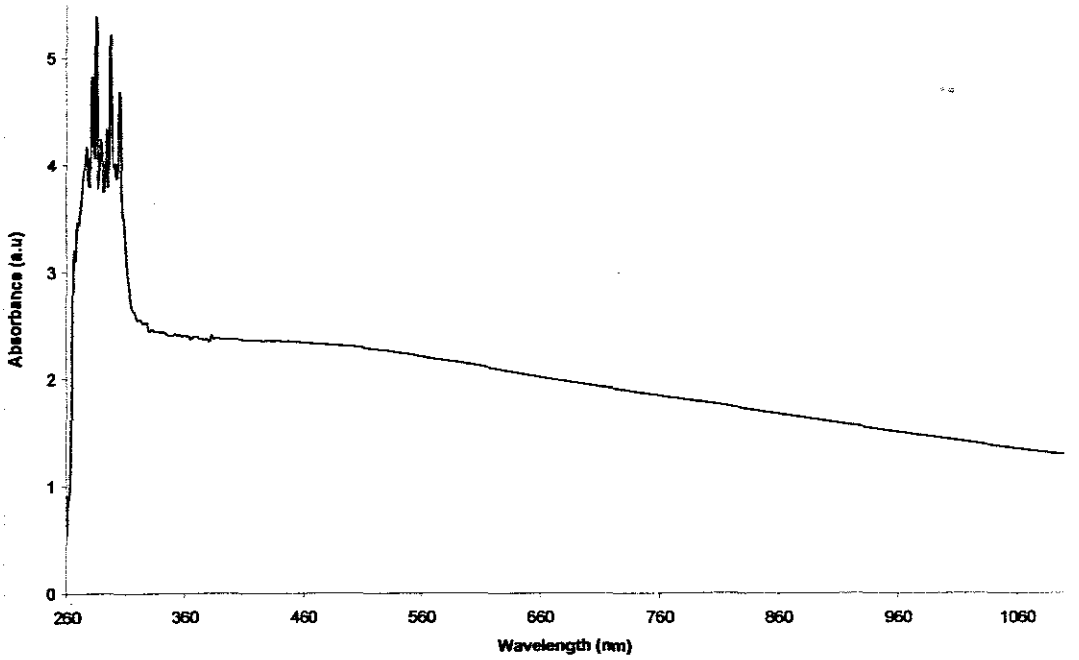

Figure 60: solution Spectrum of $[Mn(TMP)(CH_3OH)Cl_2]$ in DMF

3.4.6.2 Infrared Spectrum of $[Mn(TMP)(CH_3OH)Cl_2]$

The IR spectrum of the drug shows vibrational bands at 3408, 3324 and 3162 cm^{-1} that are assigned to the free NH_2 on trimethoprim. The spectrum of the complex (Figure 61) is similar to those of other trimethoprim complexes already discussed above. The bands at 511, 374 and 289 cm^{-1} are assigned to Mn—N, Mn—O and Mn—Cl stretching frequencies respectively.

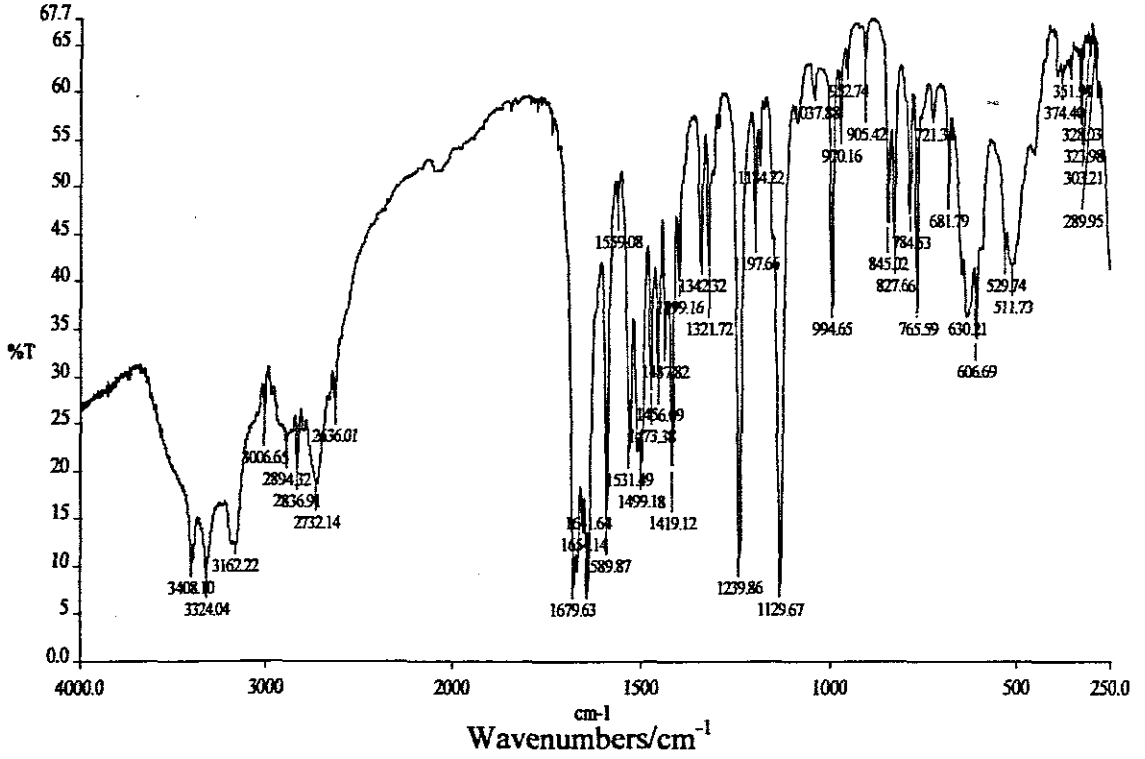

Figure 61: IR spectrum of $[Mn(TMP)(CH_3OH)Cl_2]$

3.5.0 Metal Complexes of Amodiaquine

3.5.1 Iron(III) complex of Amodiaquine with dithiocarbamate

The product was black in colour and is formulated as $[Fe(AQ)(C_3H_6NS_2)Cl_3]\cdot 3H_2O$, $FeC_{23}H_{36}N_4O_4S_2Cl_4$. Molar mass, 638.50; yield, 56%. Elemental analysis, [Found (Calc.)]: C, 43.85 (43.27); H, 5.97 (5.68); N, 8.49 (8.77). The proposed structure for the complex is shown in Figure 62.

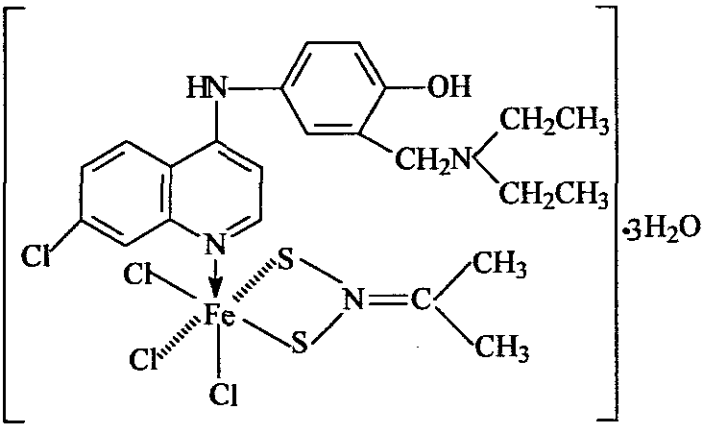

Figure 62: Proposed structure for $[Fe(AQ)(C_3H_6NS_2)Cl_3]\cdot 3H_2O$

3.5.1.1 Electronic and Magnetic properties of $[Fe(AQ)(C_3H_6NS_2)Cl_3]\cdot 3H_2O$

The electronic spectra of $[Fe(AQ)(C_3H_6NS_2)Cl_3]\cdot 3H_2O$ complex is shown in Figure 63. Charge transfer transitions in Fe(III) complexes occur between 26,000-45,000 cm^{-1} (384-222 nm). The absorption bands in this region in the spectrum can be attributed to L→M charge transfer. A number of closely spaced bands appear at 23,923–23,041 cm^{-1}, (418-434 nm) and is assigned to $t_{1g} \rightarrow t_{2g}$ charge transfer transition.

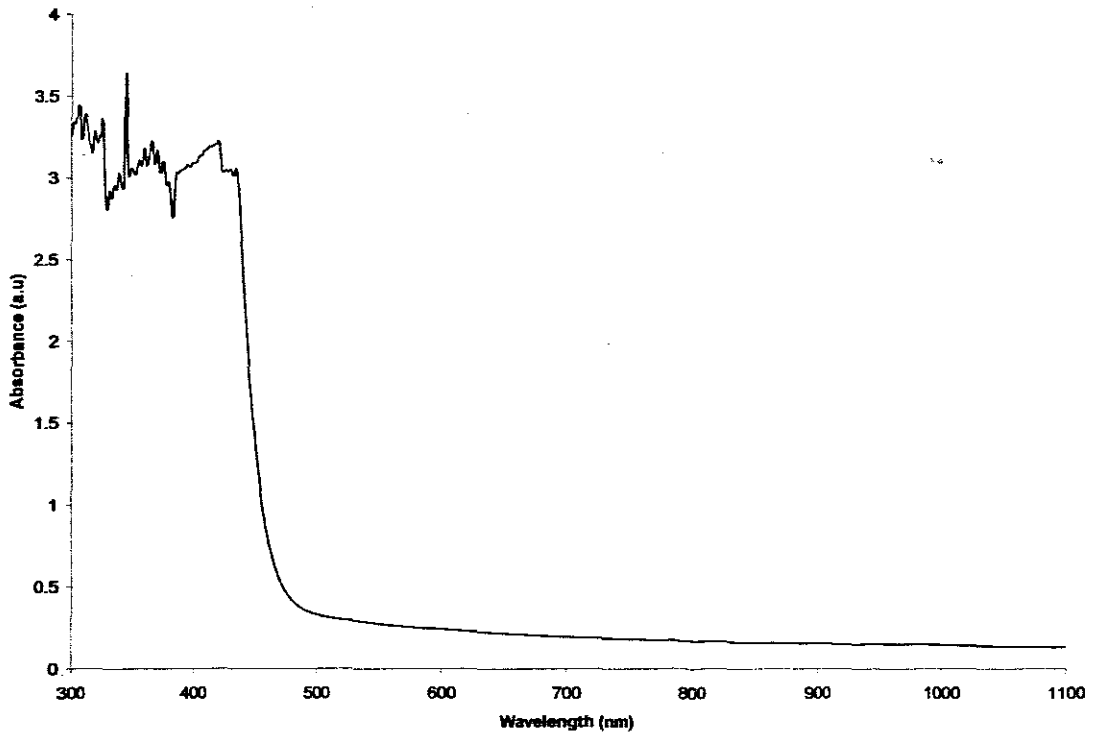

Figure 63: Solution spectrum of $[Fe(AQ)(C_3H_6NS_2)Cl_3]\cdot 3H_2O$

3.5.1.2 Infrared spectrum of $[Fe(AQ)(C_3H_6NS_2)Cl_3]\cdot 3H_2O$

The N—H stretching frequency occurs as a single broad band at 3429 cm^{-1} unlike in the free ligand where it occurs as a sharp band at 3421 cm^{-1}. The ν(C=N) which occurs at 1587 and 1618 cm^{-1} in the ligand occurs at 1586 and 1616 cm^{-1} in the complex. The N—S stretching frequency is assigned to the bands at 1096 cm^{-1} while Fe—N, Fe—S, and Fe—Cl stretching frequencies are assigned at 420, 384 and 278 cm^{-1} respectively.

3.5.2 Iron(III) complex of Amodiaquine with 2,2-bipyridine

The black complex analyzed as $[Fe(bipy)Cl_3]$, indicating that amodiaquine did not coordinate. The molecular formula of the complex formed is $FeC_{10}H_8N_2Cl_3$, molar mass,

318.39. Elemental analysis: [Found (Calc.)]: C, 39.79 (37.72); H, 2.81 (2.53), N, 9.28 (8.80). Further work on the complex was therefore suspended but reserved as a possible starting material for preparing other complexes of antimalarial drugs.

3.6 Platinum (II) complex of Chloroquine

The product was pale yellow and formulated as $Na_2[Pt(CQB)_2Cl_4]$, where CQB = chloroquine base ($C_{18}H_{26}N_3Cl$). The molecular formula of the complex is $Na_2PtC_{36}H_{56}N_6Cl_6$; molar mass, 1022.63. Elemental analysis, [Found (Calc.)]: C, 42.39 (42.28); H, 5.47 (5.13), N, 7.80 (8.22). The proposed structure, based on this formulation, is shown in Figure 64.

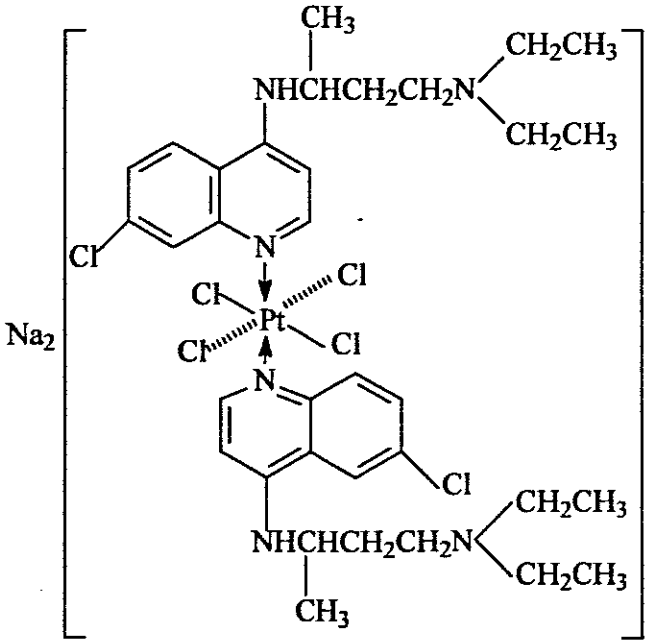

Figure 64: Proposed structure of $Na_2[Pt(CQ)_2Cl_4]$

3.6.1 Infrared Spectrum of $Na_2[Pt(CQB)_2Cl_4]$

Chloroquine base has three potential donor sites. The IR spectrum of the complex (Figure 65) and free chloroquine base were compared. Two bands at 3318 and 2968 cm^{-1} are assigned to N—H and C—H stretching frequencies of the chloroquine base. This observation was further strengthened by the sharp absorption band at 861 and 804 cm^{-1} due to N—H deformation. The broadening of the band at 3318 cm^{-1} is due to overlap of the N—H and H_2O motions. The ν(C=N), which occur at 1575 cm^{-1} with medium intensity in the chloroquine base, is shifted to a very sharp band at 1590 cm^{-1} in the complex. This shows that chloroquine bond preferentially to platinum through the quinoline N atom. The C—N band for the tertiary amino N atom that occur at 1365 cm^{-1} remain virtually unchanged in the complex. The Pt—N and Pt—Cl stretching frequencies are assigned to the bands at 539 and 324 cm^{-1} respectively. Thus, the IR spectrum showed that Pt preferentially bond to chloroquine base through the endocyclic N(1) of the quinoline ring like in the Co(III) chloroquine complex.

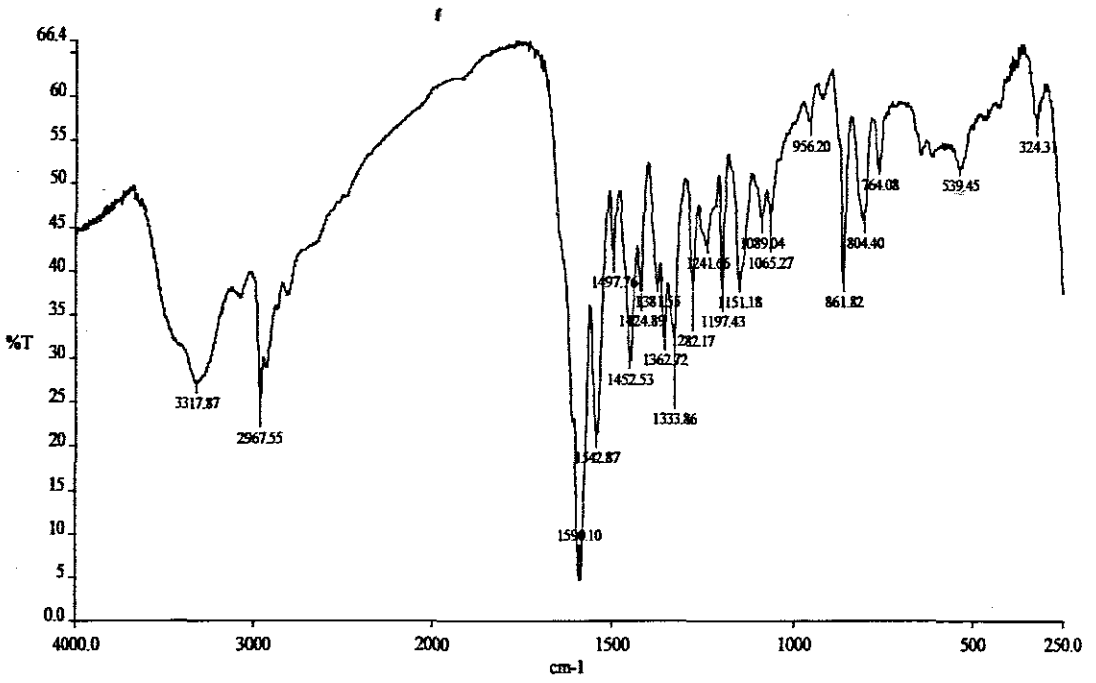

Figure 65: IR Spectrum of $Na_2[Pt(CQB)_2Cl_4]$

3.7 Iron(III) complex of pyrimethamine with dithiocarbamate

The product was brown in colour and is formulated as $[Fe(pyrm)_2(C_3H_6NS_2)Cl_2]$, pyrm = pyrimethamine, with molecular formula $FeC_{27}H_{32}N_9Cl_4S_2$. Molar mass, 744.39; yield: 57%; elemental analysis, [Found (Calc.)]: C, 44.04 (43.57); H, 4.59 (4.33), N, 17.09 (16.93). The proposed structure based on the microanalysis is given in Figure 66.

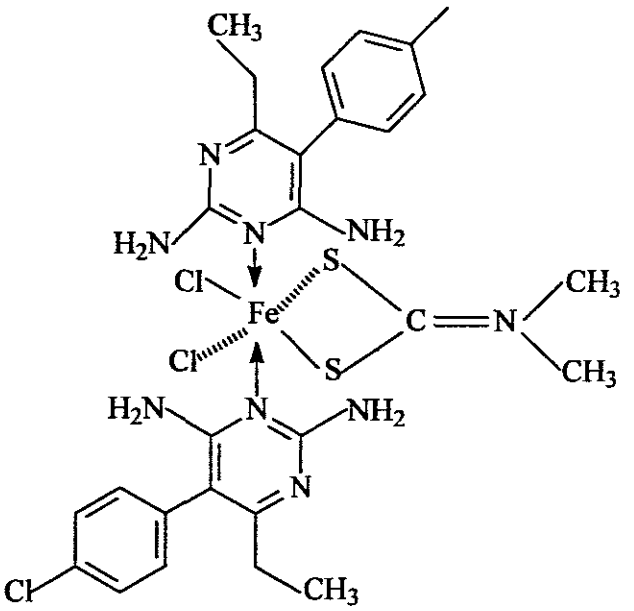

Figure 66: Proposed structure for $[Fe(pyrm)_2(C_3H_6NS_2)Cl_2]$

3.7.1 Electronic spectra and Magnetic Properties of $[Fe(pyrm)_2(C_3H_6NS_2)Cl_2]$

The electronic spectrum of the complex is given in Figure 67. Charge transfer transition in Fe(III) complexes occur between 26,000 - 45,000 cm^{-1} (384- 222 nm). The absorption band at about 27,027 cm^{-1} (370 nm) is attributed to L→M charge transfer. The effective magnetic moment of 5.3 BM confirms that the complex is a high-spin octahedral complex.

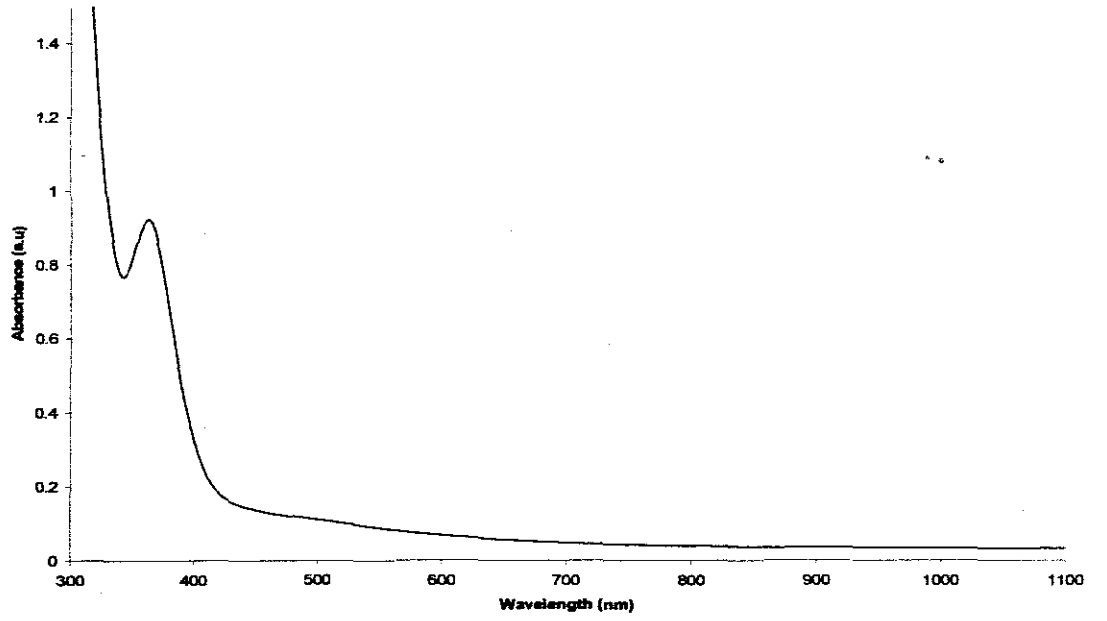

Figure 67: Electronic Spectrum of $[Fe(pyrm)_2(C_3H_6NS_2)Cl_2]$ in DMF

3.7.2 Infrared spectrum of $[Fe(pyrm)_2(C_3H_6NS_2)Cl_2]$

The infrared spectrum of the complex showed multiple bands in the region 2900-3400 cm^{-1}. These bands might be attributed to the presence of four free NH_2 group on the complex, thereby confirming the proposition that the metal preferentially coordinate to the drug through the N(1) atom. This is further confirmed by the substantial shift in the ν(C=N) stretching frequency which occur at 1664 and 1590 cm^{-1} in the complex as compared to 1676 and 1590 cm^{-1} in trimethoprim ligand. The N—S stretching frequency is assigned to the bands at 1102 cm^{-1} while Fe—N, Fe—S, and Fe—Cl stretching frequencies are assigned to the bands at 458, 364 and 272 cm^{-1} respectively.

3.8.1 Iron(III) complex of pyrimethamine with trimethoprim

The complex obtained was brown in colour and is formulated as $[Fe(pyrm)_2(TMP)Cl_3]\cdot CH_3OH$: $FeC_{39}H_{48}N_{12}O_5Cl_5$; molar mass, 998.96; yield, 63%. Elemental analysis, [Found (Calc.)]: C, 47.45 (46.94); H, 5.31 (4.85), N, 17.01 (16.84). The proposed structure is given in Figure 68. It consists of Fe bonded to two molecules of pyrimethamine, a molecule of trimethoprim and the octahedral arrangement around the metal ion is completed by coordination of three chloride ions, with a molecule of methanol in the crystal lattice. This constitutes the first mimic of a combination drug, templated on a metal centre, in this work.

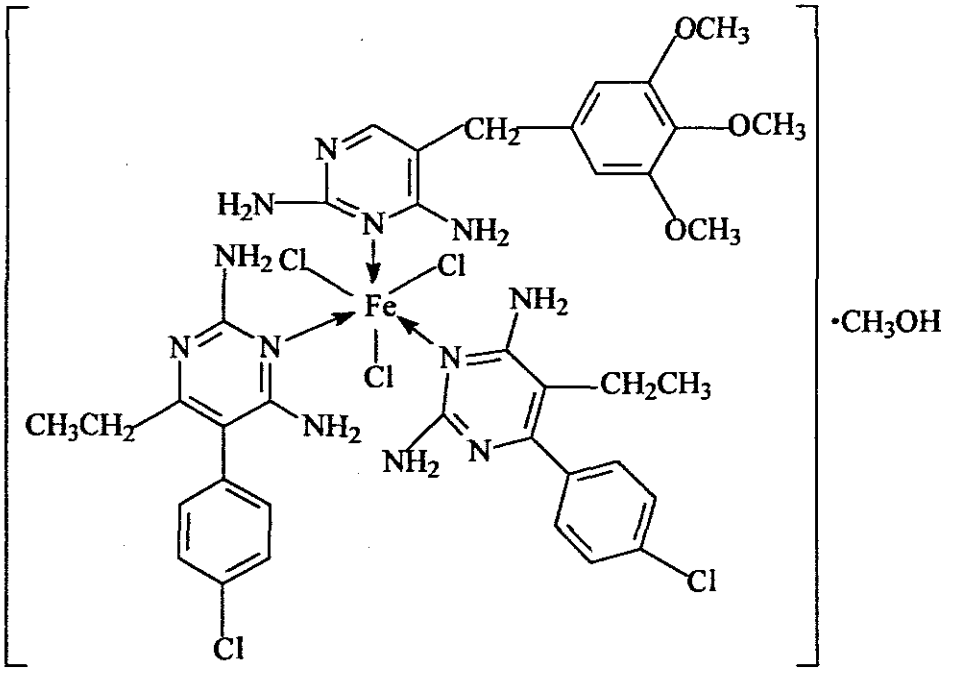

Figure 68: Proposed structure for $[Fe(pyrm)_2(TMP)Cl_3]\cdot CH_3OH$

3.8.1.1 Spectra and Magnetic properties of $[Fe(pyrm)_2(TMP)Cl_3]\cdot CH_3OH$

The electronic spectrum of the complex is given in Figure 69. Charge-transfer transition in Fe(III) complexes occur between 26,000 - 45,000 cm^{-1} (384- 222 nm). The absorption band at about 27,548 cm^{-1} (363 nm) in the spectrum is attributed to L→M charge transfer. Other charge-transfer transitions can be seen in the region 300-275 nm. Effective magnetic moment of 5.1 BM confirms that the complex is high spin octahedral complex with five unpaired electron.

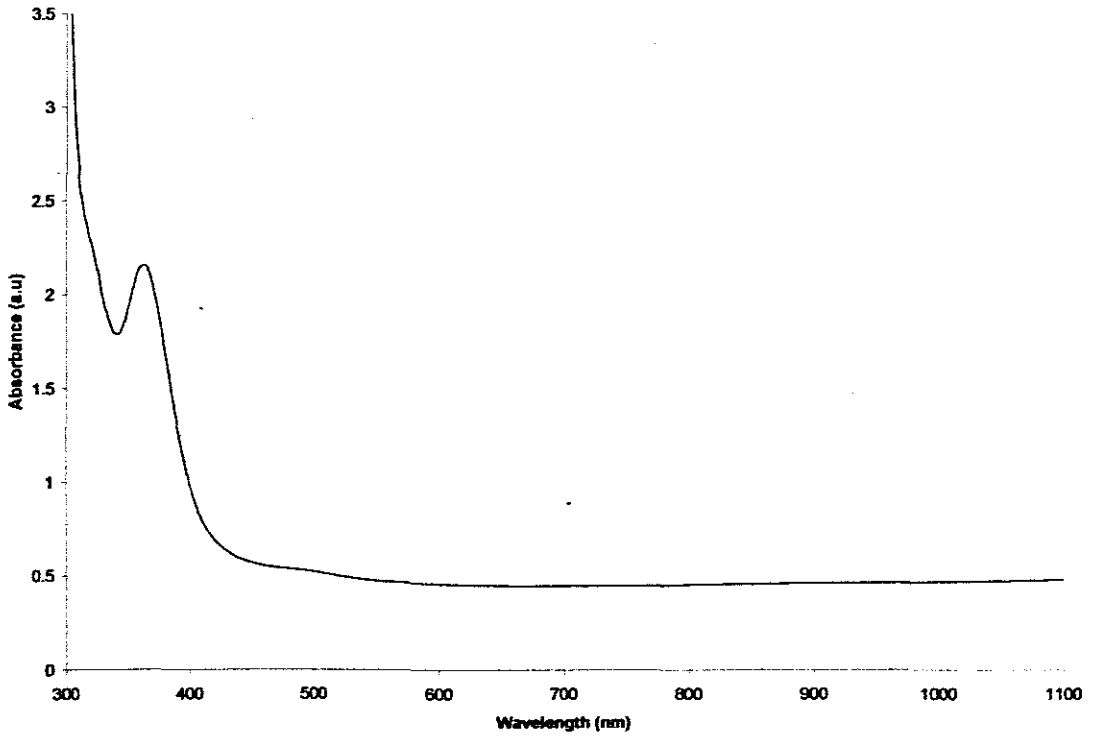

Figure 69: Solution spectrum of $[Fe(pyrm)_2(TMP)Cl_3]\cdot CH_3OH$

3.8.2 Cobalt(II) complex of pyrimethamine with trimethoprim

This synthesis was undertaken to synthesize a complex involving combination drugs as well but results from elemental analysis showed that the metal ion is coordinated

essentially to the trimethoprim while pyrimethamine crystallizes out from the filtrate. The product was pale pink and is formulated as $[Co(TMP)_2Cl_2(CH_3OH)_2]$, $CoC_{30}H_{44}N_8O_8Cl_2$. Molar mass, 774.57; elemental analysis, [Found (Calc.)]: C, 46.18 (46.52); H, 5.22 (5.73), N, 13.93 (14.47). The proposed structure of the complex is given in Figure 70. In the complex, cobalt coordinates to two molecules of trimethoprim, two chloride ions and the octahedral geometry of the cobalt ion is completed by coordination to two molecule of methanol used as the medium of preparation.

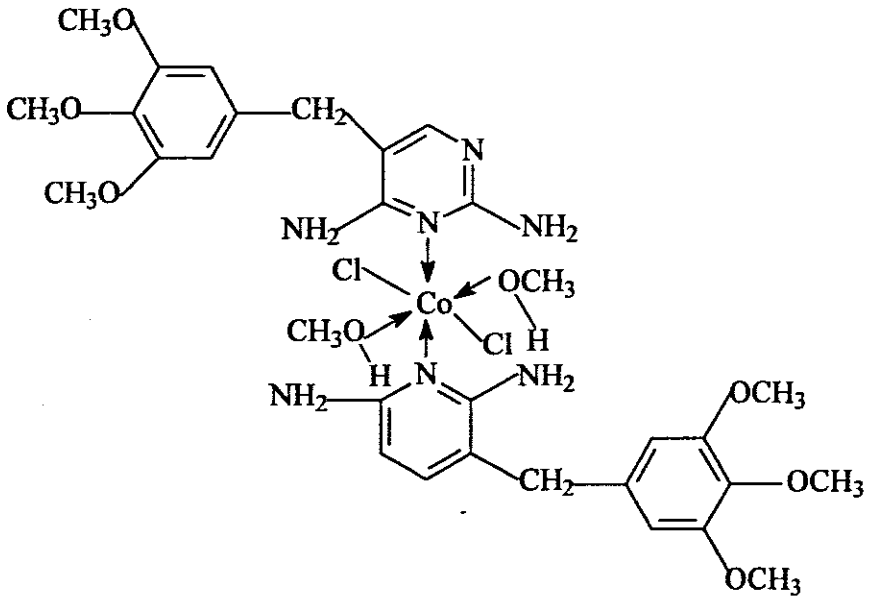

Figure 70 Proposed structure for $[Co(TMP)_2Cl_2(CH_3OH)_2]$

3.8.2.1 Electronic spectrum of $[Co(TMP)_2Cl_2(CH_3OH)_2]$

The electronic spectrum of $[Co(TMP)_2Cl_2(CH_3OH)_2]$ is shown in Figure 71.

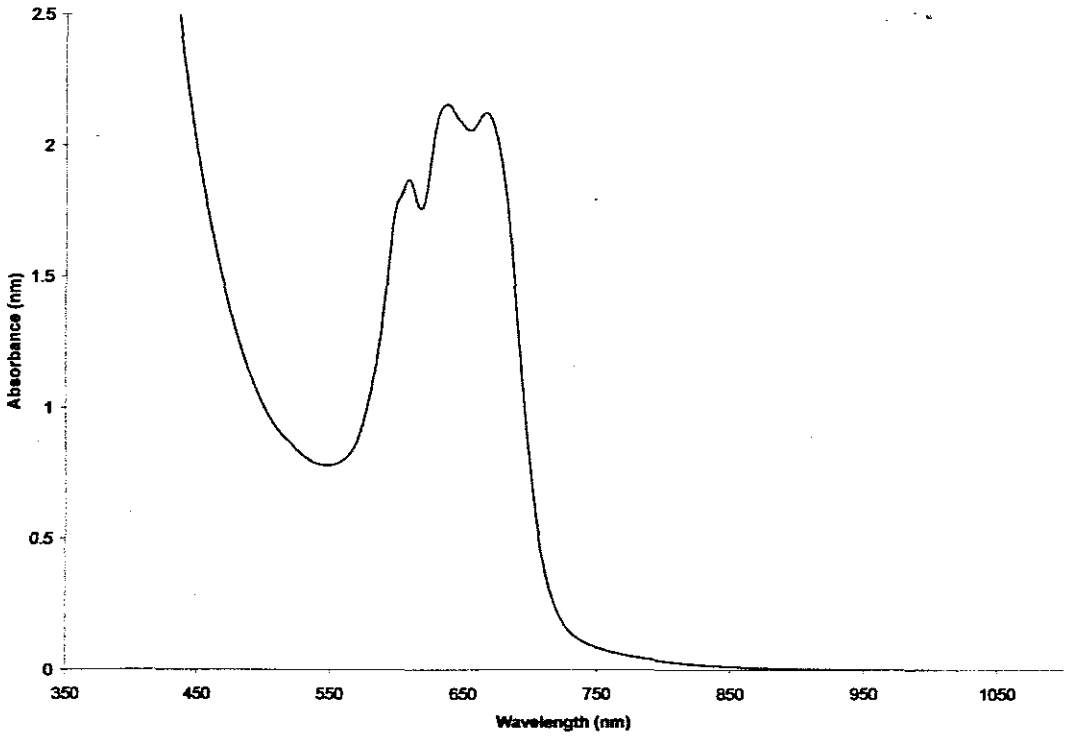

Figure 71: Solution spectrum of $[Co(TMP)_2Cl_2(CH_3OH)_2]$ in DMF

The spectrum in the visible region showed three bands. A broad band at about 15,385 cm^{-1} (650 nm) which split into two of almost equal intensity may be assigned to $^4T_{1g} \rightarrow {}^4T_{2g}$ while the band at 21,277 cm-1 (570 cm^{-1}) is assigned to the $^4T_{1g}(F) \rightarrow {}^4T_1(P)$ transitions. The assignment is in conformity with the proposed octahedral geometry for the complex.

CHAPTER FOUR

4.0 Biological Studies

4.1 Introduction

Biological studies in antimalarial chemotherapy involve investigations aimed at determining the activity of potential antimalarial drugs or resistance to drugs which are currently being used. It is part of the goal to develop safe and affordable new drugs to counter the spread of malaria parasites that are resistant to existing drugs. Efforts to discover and develop new antimalarial drugs have increased in recent years because of the recognition of the global importance of fighting malaria, and the dedicated public-private partnership strategy to discover, develop and deliver new drugs[177]. Current enthusiasm for combining scientific innovation with expertise in the drug discovery and development processes has influenced dramatically assay methods for potential antimalarial drugs. Drug efficacy, pharmacology and toxicity are important parameters in the selection of compounds for development but the process of evaluating new compounds on the path from drug discovery to development has not been standardized. Four basic methods are routinely used to study or measure antimalarial sensitivity or resistant. They are *in vitro*, *in vivo*, animal model studies and molecular techniques.

4.2 *In vitro* Studies

In vitro screens for activities of compounds, which constitute key component of a critical path for an antimalarial drug discovery programme, depend on the ability to culture *P. falciparum in vitro* in human erythrocytes. The process involves propagating parasites in leukocyte-free erythrocytes at 37 °C and between 2-5% heamatocritic under reduced

oxygen (typically 3-5% O_2, 5% CO_2, 90-92% N_2) in tissue culture media containing either human serum or Albumax[177]. Trager and Jensen[178] developed the technique for *in vitro* culture of *P. falciparum* that led to a better understanding of malaria biology. The assay is used to determine sensitivity/resistance of the parasites to antimalarial drugs. However, unlike antibiotic assays, the *in vitro* drug sensitivity test for antimalarial drug is not yet standardized. Two *in vitro* tests have been widely used. The microtest, which was developed by Richman and adopted by WHO for epidemiologic monitoring of drug–resistant malaria, requires a parasite count under the microscope to measure the capacity of antimalarial drugs to inhibit parasite maturation to the schizont stage[179]. The results are expressed as minimal inhibitory concentration (MIC).

The second test, the isotopic microtest developed by Desjardins [180], has been widely used in most research laboratories that work on antimalarial drugs. This assay measures the inhibition of the incorporation of radiolabelled DNA precursor into the parasites. The isotopic assay is less time consuming than Richman's assay but requires well-equipped laboratory with sterile hood, cell harvester, liquid scintillation counter, et cetera [181]. The semi–microtest, that is a variant of the microtest, is no longer in use for economic reasons[182].

The *in vitro* activity of the antimalarial complexes was assessed by using the procedures of Desjardins [180] and inhibition of uptake of radiolabel nuclei served as indicator of antimalarial activity.

Several alternative assays have also been developed; Gluzman, *et al.*[183] developed an assay system that requires only a few hours to obtain results. This principle is based on the fact that chloroquine-resistant parasites actively expel chloroquine, while chloroquine-sensitive parasites accumulate the drug[184]. Secondly, the addition of verapamil inhibits chloroquine efflux in chloroquine-resistant parasites, but not in chloroquine-sensitive parasites[185]. However, results have shown that this rapid assay is discordant with the *in vivo* and isotopic *in vitro* tests[186]. Makler, *et al.*[187] recently proposed a novel *in vitro* assay based on an enzymatic reaction that specifically detects the presence of malarial lactate dehydrogenase (LDH). Brockelman, *et al.*[188] developed a minor modification in culture media that allows a short-term *in vitro* culture for *P. vivax*. This technique is adapted to perform isotopic *in vitro* assays for *P. ovale* and *P. malariae*[189].

Parasites for malaria assay are original from infected patients but may be obtained from different laboratories working on malaria biology. They are classified into three groups: clones, strains (or lines) and isolates. A clone is genetically homogenous and obtained by either micromanipulation or limiting dilution. About ten reference clones are available in research laboratories in the world. The parasites stocks are cryo-preserved at the University of Edinburgh. Clones used ensure reproducible assay over time. The strains are parasites that are adapted to *in vitro* conditions but are not necessarily homogenous in genetic terms. Continuous culture may select subpopulations of parasites over time, leading to homogenous constitution of parasites. However, it is also possible that different aliquots of the original strain could diverge independently in different

laboratories. An isolate refers to a set of populations obtained from an infected person at a given time. The isolates represent the parasites existing in their natural state. Studies showed that a given isolate often consists of several subpopulations of genetically distinct parasites. The isolates are most useful for studies that aim to define the epidemiology of drug resistance and to analyse the relationship between the phenotype (drug sensitivity) and genotype (DNA sequence of established or candidate resistance genes). Isolates used for studies should always be obtained from patients who have not self-medicated with antimalarial drugs since the presence of drugs may modify the assay results.

There is no standardized protocol for procedures used for preparation of test compounds and coating the culture plates for the assay. The most commonly used solvents are distilled water, ethanol, methanol, and DMSO. Most of these solutions may be stocked at 4 °C for at least 3 months with the exception of DMSO. Test compounds should be distributed into culture plates just before the parasites are introduced to avoid the problems associated with solubility. For some compounds, the solutions may be distributed and air-dried, and the pre-coated plates may be stocked for several months depending on the shelf life of the test compounds[190].

In vitro assay may be carried out using fresh isolates or clones maintained in continuous culture. The two parameters that may influence assay results are the parasitaemia and heamatocritic. These refer to inadequate inhibition of parasite growth due to an excessive number of parasites as compared with the drug concentration. In addition, the varying concentrations of folic acid or para-aminobenzoic acid in the culture medium have

considerable effects on the activity of antifolate drugs. A prolonged incubation time lowers the 50% inhibitory concentration for drugs with either rapid or slow action. In some cases, homologous sera during the acute phase of malaria infection are used in some assay. Moreover, in radio-labelled isotopes, tritium-labelled hypoxanthine is most commonly used. The results from *in vitro* assay are expressed as the 50% inhibitory concentration (IC_{50}), which corresponds to the drug concentration at which 50% of parasite growth is inhibited. In addition to IC_{50}, IC_{90} and IC_{99} can be calculated using computer software that fit linear or non-linear regression curves.

4.2.1 Application of *in vitro* assay

Screening

In vitro assay is used for screening potential antimalarial drugs. Its advantages are the use of the same malarial species that infects human, the possibility to test several compounds simultaneously and at high concentrations, lower cost, rapidity, and exclusion of host-related factors. The activity of the test compounds is evaluated by comparison with that of either compounds belonging to the same chemical class or compounds from different chemical classes[191]. The limits of *in vitro* screening include the lack of information on drug metabolism, pharmacokinetics, and drug toxicity.

Cross-resistance

In vitro assays can determine the activity of several compounds simultaneously using the same isolate of *P. falciparum*. *In vitro* cross-resistance is measured by calculating the degree of correlation between IC_{50s} of two compounds.

Drug combinations

In vitro assays are used to evaluate synergistic, additive, or antagonistic nature of a given combination[192]. Since resistance to practically all available antimalarial drugs necessitates the use of drug combinations, *in vitro* studies is used to determine the synergistic combination between these drugs. *In vitro* assays is also used to study the capacity of certain drugs belonging to various chemical classes to modulate resistance to chloroquine and mefloquine[193], and to understand the mechanism of action of antimalarial drugs[194].

Epidemiology of drug resistance

In vitro drug sensitivity assays play an important role in describing the epidemiology of resistance to classical drugs. *In vitro* assays are thus important tools to establish the baseline data on drug sensitivity in a given endemic area, and to monitor the evolution of drug sensitivity over time.

4.3 *In Vivo* Studies

Plasmodium species that cause human disease are essentially unable to infect non-primate animal models with the exception of a complex immunocompromised mouse model that has been developed to sustain *P. falciparum*-parasitized human erythrocytes *in vivo*[195]. *In vivo* evaluation of antimalarial compounds begins with the use of rodent malaria parasites. The most widely used in drug discovery and early development are *P. berghei, P. yoelii, P. chabaudi,* and *P. vinckei*[196]. Rodent models have been validated through the identification of several antimalarials, e.g. mefloquine, halofantrine and more

recently artemisinin derivatives[197-200]. Individual species and strains have been well characterized, including duration of cycle, time of schizogony, syncronicity, drug sensitivity and course of infection in genetically defined mouse strains[201,202].

An *in vivo* test consists of the treatment of a group of symptomatic and parasitaemic individuals with known doses of drug and subsequent monitoring of the parasitological and/or clinical response over time. One of the key characteristics of *in vivo* tests is the interplay between host and parasite. *In vivo* test most closely reflects actual clinical or epidemiological situations[203]. The original methods for *in vivo* tests required prolonged periods of follow-up (minimum of 28 days) and seclusion of patients in screened rooms to prevent the possibility of reinfection. This method was modified to shorter period of 7 to 14 days without seclusion under the assumption that reappearance of parasites within 14 days of treatment is more likely due to recrudence than reinfection[204].

The method has further been modified to reflect the increased emphasis on clinical response in addition to parasitological response. Responses to treatment are categorized purely on parasitological grounds as sensitive, RI, RII, and RIII resistance respectively[205]. Further modification now combines, to varying extent, parasitological and clinical indicators[206]. *In vivo* studies are limited by the following factors: major differences in sample size, exclusion criteria, length and intensity of follow-up rates. In sub-Saharan Africa, the methodology currently being used and promoted is a system that emphasizes clinical response over parasitological response[207]. The WHO has developed guidelines for *in vivo* antimalarial drug efficacy testing for *P. falciparum* and *P. vivax* in areas with

low-to-moderate transmission[201]. These guidelines are used widely by ministries of health and national malaria control programme to assess the efficacy of their first-line and second-line drugs for the treatment of malaria and to provide the information necessary to update national malaria treatment policies.

4.4 Animal model studies

This study is essentially an *in vivo* test conducted in non-human animal model and, consequently influenced by the same extrinsic factors as *in vivo* tests. The influence of host immunity is minimized by using laboratory-reared animals or animal-parasite combination unlikely to occur in nature. These tests allow for the testing of parasites which cannot be adapted to *in vitro* environments and the testing of experimental drugs not yet approved for use in humans. The major disadvantage is that only parasites that can grow in, or adapted to non-human primates can be investigated.

4.5 Molecular Method

The molecular techniques are at developmental and validation stage. Molecular techniques, when fully developed, will serve as a valuable surveillance tool for monitoring the occurrence, spread, or intensification of drug resistance. Molecular techniques used polymerase chain reaction (PCR) to indicate the presence of mutations encoding biological resistance to antimalarial drugs[208]. The feasibility, high sensitivity, and high resolution of this technique prove that it will be practical and highly valuable in studies on drug resistance and vaccine efficacy as well as the testing of novel antimalarial drugs. These techniques require only small amounts of genetic material as opposed to live

parasites, independence of host and environmental factors, and the ability to conduct large numbers of tests in a relatively short period of time. The technique is limited by the obvious need for sophisticated equipment and training, and the fact that gene mutations that confer antimalarial drug resistance are currently known or debated for a limited number of drugs[209].

4.6 Screening of the metal complexes

The metal complexes for this study were screened at the Parasite Chemotherapy Laboratory of the Swiss Tropical Institute, Switzerland. The complexes were screened against four different isolates of *P. falciparum* at different stages of development. The parasites used and the stage of development are given in Table. 25.

Table 25: List of parasites used for the *in vitro* studies

Parasite	Strain	Stage	Standard
T. b. rhodesience	STIB 900	trypomastigotes	Melarsoprol
T. cruzi	Tulahuen C4	amastigotes	Benznidazole
L. donovani	MHOM-ET-67/L82	amastigotes	Miltefosine
P. falciparum	K1	IEF	Chloroquine
Cytotoxicity	L6		Podophyllotoxin

4.7 Results and Discussion

The results of the *in vitro* screening are presented in Table 26.

Table 26: Results of the *in vitro* screening of the metal complexes

Sample	T.b.rhod. IC_{50}	T. cruzi IC_{50}	L.don. Axen. IC_{50}	L. don. inf. mac. IC_{50}	P. falc. K1 IC_{50}	Cytotox. L6 IC_{50}
Sample	T.b.rhod. IC_{50}	T. cruzi IC_{50}	L.don. Axen. IC_{50}	L. don. inf. mac IC_{50}	P. falc. K1 IC_{50}	Cytotox. L6 IC_{50}
Standadrd	0.00376667	0.68	0.09	0.7	0.0743	0.009
$[Co_2(QNC)(en)_4Cl_6]\cdot 2HCl$	0.587	4.7	11.4	-	0.02115	7.264
$[Co(en)_2(AQ)Cl]Cl_2$	0.45	5	22.6	-	0.0102	43.25
$[Co(TMP)_2Cl_2]$	63.183	>30	>30	-	>5	>90
$[Co(SD)_2(H_2O)_2]$	50.501	>30	>30	-	>5	>90
$[Cu(SD)_2(H_2O)_2]$	15.063	>30	>30	-	>5	19.9
$[Fe(SD)_3].(H_2O)_3$	>90	>30	27.5	-	>5	>90
$[Zn(SD)_2(H_2O)_2]$	>90	>30	>30	-	>5	>90
$[Cu(TMP)_2(CH_3COO)_4]$	3.411	16.3	>30	-	3.7231	40.83
$[Co(en)_2(TMP)_2]Cl_3$	27.348	14.9	13.5	-	>5	41.98
$[Ni(SD)_2(H_2O)_2]\cdot 2H_2O$	>90	>30	>30	-	>5	>90
$[Mn(SD)_2(H_2O)_2]$	54.407	24.6	7.2	-	2.127	>90
$[Mn(TMP)(CH_3OH)Cl_2]$	7.832	5.85	6.87	-	1.130215	38.76
$[Pt(TMP)(H_2O)Cl_2].H_2O$	37.912	>30	11.9	-	>5	>90
$[Pd(TMP)(H_2O)Cl_2]\cdot H_2O$	43.641	>30	16.6	-	>5	>90
$[Fe(Py)_2TMP(CH_3O)Cl_2]\cdot 2H_2O$	3.1885	3.75	15.6	-	>5	2.681
$[Ru(SD)_2(H_2O)Cl]$	56.108	>30	17.9	-	>5	>90
$Na_2[Pt(CQB)_2Cl_4]$	4.5355	8.05	>30	-	0.15595	77.35
$[Co(TMP)_2Cl_2(CH_3OH)_2]$	5.394	6.35	22.3	-	>5	3.925
$Fe(Py)_2(C_3H_6NS_2)Cl_2]$	0.171	0.895	0.49	dnp	2.1935	0.8
$[Pd(SD)(H_2O)(CH_3OH)]$	35.331	>30	>30	-	>5	>90
$[Pt(SD)(H_2O)Cl]$	>90	>30	>30	-	>5	>90
$[Fe(AQ)(C_3H_3NS_2)Cl_3]\cdot 3H_2O$	0.52	10.2	8.1	-	0.0088	15.71
$[Co(en)_2(CQ)Cl]Cl_2$	36.737	>30	>30	-	4.4058	>90

The results indicated that the complexes showed degrees of activity. The effect of the new complexes on the proliferation of *in vitro* cultures of the trypomastigotes of *T. b. rhodesiene*, amastigotes of *T. cruzi* and *L. donovani* varied considerably. On the *Plasmodium falciparum*, the complexes also showed varied activity with three complexes

showing a more pronounced activity than chloroquine. The three complexes with enhanced activity than chloroquine are $[Co_2(QNC)(en)_4Cl_6]\cdot 2HCl$, $[Co(en)_2(AQ)Cl]Cl_2$, $[Fe(AQ)(C_3H_3NS_2)Cl_3]\cdot 3H_2O$ which are 3.5, 7.3 and 8.4 times more active than chloroquine.

In order to make a comparative analysis, the three most active complexes were screened *in vitro* with the corresponding drug against *P. falciparum* K1 at IEF stage and chloroquine was used as the reference drug. The cytotoxicity was done with the L6 strain using podophyllotoxin as reference. The results of this screening are presented in Table 27.

Table 27: *In vitro* antimalarial activity of the most active complexes and chloroquine as a reference drug against *P. falciparum* strains

Compound	P. falc. K1		Cytotox. L6	
	IC-50	Ref. drug	IC-50	Ref. drug
Sulfadizine	>5	0.0585	>90	0.009
Amodiaquine	0.0037	0.0408	15.032	0.009
Pyrimethamin	2.55	0.0585	5.35	0.009
Quinacrine	0.0072	0.0478	2.775	0.009
Trimethoprim	4.733	0.0725	46.474	0.009
$[Co_2(QNC)(en)_4Cl_6]\cdot 2HCl$	0.0138	0.023	-	-
$[Co(en)_2(AQ)Cl]Cl_2$	0.0091	0.0315	-	-
$[Fe(AQ)(C_3H_3NS_2)Cl_3]\cdot 3H_2O$	0.0074	0.0315	-	-

Cobalt(III) quinacrine complex

In this study, the result showed that quinacrine was about 6.6 times more active than chloroquine but the complex, $[Co_2(QNC)(en)_4Cl_6]\cdot 2HCl$ was about 1.6 times more active than chloroquine. A comparison between the quinacrine drug and the cobalt(III) complex

showed that coordination of the drug to the metal reduces its activity by almost 50%. The metal complex, however was more active than sulfadiazine, trimethoprim and pyrimethamine.

Cobalt(III) amodiaquine complex

The results indicate that amodiaquine was 11 times more active than chloroquine while the complex was 3.5 times more active than the chloroquine used as reference in the same circumstance. A comparison between the drug and its cobalt(III) complex showed that the drug was 2.5 times more active than the complex. Thus, coordination to the metal reduces the activity of the drug by almost 60%. A further comparison between the complex and the other drugs showed that the complex was slightly less active than quinacrine but more active than sulfadiazine, trimethoprim and pyrimethamine.

Iron(III) amodiaquine complex

Iron(III)amodiaquine complex was 4.3 times more active than chloroquine but less active than amodiaquine. Coordination of amodiaquine to iron(III) reduced the activity of the drug by about 50%. In comparison with other antimalarial drugs, the complex had the same activity as aquamarine, but much more active than sulfadiazine, trimethoprim and pyrimethamine. A comparison between the two amodiaquine complexes showed the iron(III) complex was slightly more active than its corresponding cobalt(III) complex.

Sulfadiazine complexes

In order to establish the general activity of the sulfadiazine series, the activities of the metal complexes of sulfadiazine were compared with that of sulfadiazine drug. The results are presented in Table 28.

Table 28: *In vitro* antimalarial activity of sulfadiazine and its metal complexes against *P. falciparum* strains

Sample	*P. falc.* K1 IC_{50}	Cytotox. L6 IC_{50}
Sulfadiazine	>5	0.009
$[Co(SD)_2(H2O)_2]$	>5	>90
$[Cu(SD)_2(H2O)_2]$	>5	19.9
$[Zn(SD)_2(H_2O)_2]$	>5	>90
$[Ni(SD)_2(H_2O)_2]$	>5	>90
$[Mn(SD)_2(H_2O)_2]$	2.127	>90
$[Ru(SD)_2(H_2O)Cl]$	>5	>90
$[Pd(SD)(H_2O)(CH_3OH)]$	>5	>90
$[Pt(TMP)(H_2O)Cl_2].H_2O$	>5	>90

A cursory look at Table 28 shows that all the metal complexes, with the exception of the Mn(II) complex, had about the same activity as sulfadiazine. The Mn(II) complex was about 2.4 times more active than sulfadiazine.

Trimethoprim complexes

Table 29 shows the results of the antimalarial activity of trimethoprim and its metal complexes. Trimethoprim was much more active than its metal complexes. Thus, coordination of the metal to trimethoprim reduced its antimalarial activity. Mn(II) and Cu(II) complexes of trimethoprim were the most active; trimethoprim was 15 times more

active than the Mn(II) complex and 50 times more active than the corresponding Cu(II) complex.

Table 29: *In vitro* antimalarial activity of trimethoprim and its metal complexes against *P. falciparum* strains

Sample	*P. falc.* K1 IC_{50}	Cytotox. L6 IC_{50}
Trimethoprim	0.0743	0.009
$[Co(TMP)_2Cl_2]$	>5	>90
$[Cu(TMP)_2(CH_3COO)_4]$	3.7231	40.83
$[Co(en)_2(TMP)_2]Cl_3$	>5	41.98
$[Mn(TMP)(CH_3OH)Cl_2]$	1.130215	38.76
$[Pt(TMP)(H_2O)Cl_2].H_2O$	>5	>90
$[Pd(TMP)(H_2O)Cl_2].H_2O$	>5	>90
$[Fe(Py)_2TMP(CH_3O)Cl_2]\cdot 2H_2O$	>5	2.681
$[Co(TMP)_2Cl_2(CH_3OH)_2]$	>5	3.925

Pyrimethamine complexes

The results presented in Table 30 show too that pyrimethamine was about 50% more active than its corresponding metal complexes. Also in two instances where pyrimethamine and trimethoprim were coordinated to the same metal complex, the complexes were less active than either pyrimethamine or trimethoprim and the combinations seems not to have any synergistic enhancement on the activity of the complex.

Table 30: *In vitro* antimalarial activity of trimethoprim and its metal complexes against *P. falciparum* strains

Sample	*P. falc.* K1 IC_{50}	Cytotox. L6 IC_{50}
Pyrimethamine	2.55	5.35
$Fe(Py)_2(C_3H_6NS_2)Cl_2]$	>5	2.681
$[Fe(Py)_2TMP(CH_3O)Cl_2]\cdot 2H_2O$	>5	3.925

Chapter Five

5.0 Conclusions and Recommendations

5.1 Summary of Results

Cobalt(III) complexes

Seven complexes of cobalt(III) were synthesized and characterized. The complexes comprise a chloroquine complex, an amodiaquine complex, a quinacrine complex and two complexes each of trimethoprim and tetracycline. All the complexes were made from either *trans* or *cis*–$[Co(en)_2Cl]Cl_2$. All the complexes have octahedral geometry and the amodiaquine and quinacrine complexes were more active than choloroquine. The chloroquine complex is 1.6 times more active than chloroquine while the quinacrine complex was 3.5 times more active than chlorquine.

Sulfadiazine complexes

Eleven metal complexes of sulfadiazine were isolated and characterised. The complexes contained the following metal ions: Co(II), Cu(II), Zn(II), Mn(II), Ni(II), Pt(II), Pd(II), Fe(III), Ru(III) and VO(II). A cobalt(II) complex, $[Co(SD)_2(CH_3OH)_2]$ and sulfadiazine were characterized by single crystal X-ray structures. In all the complexes, sulfadiazine acted as a bidentate ligand and coordinates the metal ions through the pyrimidinic N and sulfonic N atoms. The metal(II) complexes (Co, Cu, Zn, Mn, and Ni) have octahedral geometry containing two molecules of sulfadiazine and two molecules of the solvent used in the synthesis within the coordination spheres. The Ni(II) complex, $[Ni(SD)_2(H_2O)_2]\cdot(H_2O)_2$, in addition contains two lattice water molecules. Pd(II) and Pt(II) complexes have square planar geometry and formulated as $[Pd(SD)(H_2O)(CH_3O)]$

and [Pt(SD)(H_2O)Cl]. Fe(III) and Ru(III) complexes have octahedral geometry formulated as [Fe(SD)$_3$]·3H_2O and [Ru(SD)$_2$(H_2O)Cl] while the oxovanadium complex is formulated as [VO(SD)$_2$(H_2O)]·H_2O. The complexes are all insoluble in all major solvents, both polar and non-polar except strong donor solvents like DMF and DMSO.

Trimethoprim complexes

Twelve complexes of trimethoprim have been isolated and one of the complexes, [Fe(py)$_2$(tmp)(CH_3OH)Cl$_3$]·2H_2O, contains a combination of two molecules of pyrimethamine and a molecule of trimethoprim. Five of the complexes were characterized by single X-ray crystal structures. They are Co(II) complexes, two Cu(II) complexes and one Ni(II) complexes. One of the Co(II) complex is a 4-coordinate complex containing two molecules of trimethoprim and two chloride ions in a tetrahedral arrangement. The second Co(II) crystal structure, [Co_2(TMP)$_2$(OAc)$_4$·2C_7H_8·CH_3O] is a dinuclear complex containing two trimethoprim molecules and the Co ions are bridged by four acetate group. The entire structure is clathrated with two molecules of toluene and a methoxy group. Two dinuclear Cu(II) complexes were also isolated with structures similar to the dinuclear Co(II) complex. One of the crystals contains a molecule each of toluene and benzene instead of two molecules of toluene. The fifth crystal structure of trimethoprim is a Ni(II) complex, [Ni(TMP)$_2$(CH_3OH)$_2$(CH_3COO)$_2$]. The structure contains two molecules of trimethoprim that act as monodentate ligands, two acetate ions and the distorted octahedral geometry around the Ni(II) is completed by two molecules of methanol. All the trimethoprim complexes isolated have octahedral geometry except [Co(TMP)$_2$Cl$_2$] which is tetrahedral, and the Pt(II) and Pd(II) are square planar.

Chloroquine metal complexes

Two metal complexes of chloroquine were isolated and characterised. The complexes are: $[Co(en)_2(CQ)Cl]Cl_2$ and $Na_2[Pt(CQ)_2Cl_4]$. The Co(III) complex have an octahedral geometry while the Pt(II) is isolated as an anionic complex.

Amodiaquine complexes

Two complexes of amodiaquine, $[Co(en)_2(AQ)Cl]Cl_2$ and $[Fe(AQ)(C_3H_6NS_2)Cl_3]\cdot 3H_2O$ were isolated and characterised. The Co(III) complex was made from *trans*–$[Co(en)_2Cl]Cl_2$ while the Fe(III) complex was synthesized from a mixture of $FeCl_3\cdot 6H_2O$, dithiocarbamate and amodiaquine. The complexes have octahedral geometry.

Conclusion

The rapid spread of drug-resistant malaria worldwide has stimulated the search for new drugs to treat millions of people infected with the parasite. There is an urgent need for antimalarials with novel structures, modes of action, or both, to deal with the development of resistance to the drugs in current use. Previous research has shown that attaching organic drugs to metal-containing fragments could enhance their activity; for example, chloroquine for malaria and clotrimazole for chagas disease[106]. Although metals have been used in medicine for centuries, the success of *cis*-$[PtCl_2(NH_3)_2]$, (cisplatin), and related compounds as anticancer drugs has stimulated renew interest in metal-based chemotherapies.

This study deals with the synthesis, characterisation and *in vitro* studies of metal complexes of antimalarial drugs. The main objective of which is to contribute to efforts being made to search for novel chemotherapeutic drugs that can be used against the resistant strains of *P. falciparum*. Thirty-two metal complexes derived from chloroquine, amodiaquine, trimethoprim, sulfadiazine, tetracycline and pyrimethamine were synthesised. The complexes were characterised by melting point / decomposition temperatures, solubility, conductivity measurement, elemental analyses, UV-Vis and IR spectroscopy, mass spectrometry, magnetic susceptibility measurement and EPR. Six of the complexes and sulfadiazine ligand were also characterised by single crystal X-ray studies.

The complexes were screened *in vitro* against four isolates of *P. falciparum* at various stages of the parasites development. The results showed that three of the metal complexes; cobalt(III)amodiaquine, cobalt(III)quinacrine and iron(III)amodiaquine were more active *in vitro* against the parasites in comparison to chloroquine, the drug of choice for chloroquine falciparum malaria in Africa.

The results from the *in vitro* antimalarial activities of the metal complexes showed that in most instances, coordination of the drug to the metal ions somehow reduces their antimalarial activity. It is somehow surprising that even coordination of the highly toxic metal ions such as Pt and Pd to the antimalarial drugs subsequently leads to a reduced activity. This might indicate that the toxicity of the metal centre does not affect activity against the resistant parasite. The major advantage of this is that, drugs such has

amodiaquine and quinacrine whose usage has been discontinued because of high toxicity might be easily modified by coordination to a metal centre. There is a need to carry out further analysis on the active complexes, most especially in *in vivo* studies to deduce the activity in a medium that resembles epidemiological studies. In addition, the reasons behind the reduction in the activity of the metal complexes with respect to the parent drug need to be established.

Recommendation and Suggestions for further work

The ^{1}Hnmr and ^{13}Cnmr of the complexes should be carried out especially the Co(III), Pt(II) and Pd(II) complexes. This will help in ascertaining the arrangement of the ligands around the metal ions and thus help in confirming the proposed stereochemistry for those complexes whose X-ray structures were not determined. Also, it is imperative that the EPR studies of the dinuclear Co(II) complex be carried out to determine the extent of the metal-metal interaction.

The three complexes that are active *in vitro* should be screened *in vivo* since *in vivo* state resembles the actual parasitological state in humans. If the complexes are active *in vivo,* additional experiments should be done to better understand the target mechanism of selectivity and their bioavailability. It is interesting to note that the three complexes that are more active than chloroquine are in the oxidation state of three, octahedral in geometry and contains bases such as ethylenediamine and dithiocarbamate. There is a great potential to vary the bases that are co-complexed to some metal(III) ions and extended to a number of metals found in biological fluids. Once this is done, the interplay

between stereochemistry, oxidation state, metal ions and drug series could be studied in detail.

Conventionally, medicinal chemistry within the context of pharmaceutical research has been primarily focused on organic compounds with therapeutic efficacy. However, the emergence of drug resistance as a worldwide problem in several diseases, specifically in cancer and tropically diseases, make it mandatory for scientists to broaden the domain of available therapies and metal complexes provide diversity and unique scaffolds for potential exploitation.

References

1. World Health Organisation (W. H. O.) Fact Sheet, (1998), No 94 Geneva.

2. Winstanley, P. (2001). Modern chemotherapy options for malaria. *The Lancet Infect. Disease*, **1**, 242-250.

3. U.S. Department of Health and Human Services (2002). National Institute of Allergy and Infectious Diseases. NIH Publication, No 02-7139, 1-17.

4. Gardner, M. J., Hall, N., Fung, E., White, O., Berriman, M., Hyman, W. R., Cariton, J. M., Pain, A., Nelson, K. E., Bowman, S., Paulsen, I. T., James, K., Elsen, J. A., Rutherford, K., Salzberg, S. L., Craig, A., Kyes, S., Chan, M., Nene, V., Shallom, S. J., Suh, B., Peterson, J., Angiuoli, S., Pertea, M., Allen, J. Selengut, J., Haft, D., Mather, M. W., Vaiya, A. B., Martin, D. M. A., Fairlamb, A. H., Fraunholz, M. J., Roos, D. S., Ralph, S. A., McFadden, G. I., Cummings, L. M., Subramanian, G. M., Mungall, C., Venter, J. C., Carucci, D. J., Hoffman, S. L., Newbold, C., Davis, R. W., Fraser, C. M., Barrell, B. (2002). Genome sequence of the human malaria parasite *Plasmodium falciparum*, *Nature* **419**, 498-511.

5. W. H. O. (1969). Parasitology of malaria. World Health Technical report series. 437:57

6. Breman, G. J. (2001). The ears of Hippopotamus: Manifestations, determinants and estimates of the malaria burden. *Am. J. Trop. Med. Hyg.*, 64(1-2), 1-11.

7. Molineaux, L. (1988). The epidemiology of human malaria as an expression of its distribution including some implications for its control. Werndorfer, W. H., McGregor, I. A. eds. Malaria, Principles and Practice of Malariology. Vol. 2. London: Churchill Livingston, 913-998.

8. Pratt, W. B. (1977). Chemotherapy of infection. Oxford University Press; N. Y. 316-323.

9. Greenwood, B. M., Bojang, K., Whitty, C. J. M., Targett, G. A. T. (2005). Malaria. *The Lancet*, **365** (9469), 1487-1498.

10. White, N. J., Breman, J. G. (2001). Malaria and babesiosis caused by red blood cell parasites. Braunward, E., Fanci, A. S., Kasper, D. L., Hauser, S. L., Longo, D. L., Jameson, J. L., eds. Harrison's Principles of Internal Medicine. 15th eds. New York: McGraw-Hill, 1203-1213.

11. Mcgregor, I. A., Gilles, H. M. (1961). Studies on the significance of high serum gamma globulin concentrations in Gambian Africans II. Gamma-globulin concentrations of Gambia. *Ann. Trop. Med. Parasitol.*, **54**, 275.

12. Bruce-Chwatt, L. J. (1952). Malaria in African infants and children in Southern Nigeria. *Ann. Trop. Med. Parasitol.*, **46** (2), 173-200.

13. Modiano, D., Petrarca, V., Sirima, B. S., Luoni, G., Nebie, I., Ciallot, D. A., Esposito, F. Coluzzi M. (1996). Different response to *Plasmodium falciparum* in West African sympatric ethnic groups. *Proc. Natl. Acad. Sci.*, USA. **91**, 2415-2419.

14. Azuike, O. B. (1991). The diagnosis, treatment and prevention of malaria. *Medicine Today*, 26-30.

15. Desowitz, R. S., Saave, J. J. (1965). The application of haemagglutination test to a study of the immunity to malaria in protected and unprotected population groups of Australian New Guinea. *Bull. W. H. O.*, **32**, 149.

16. McGregor, I. A., Wilson, R. J. M. (1971). Precipitating antibodies and immunoglobulin in *Plasmodium falciparum* infections in the Gambia, West Africa. *Trans. Roy. Soc. Trop. Med. Hyg.*, **65**, 136.

17. Botchier, G. A., Cohen, S. (1972). Anogenic variation and protective immunity in *Plasmodium knowlesi* malaria. *Immunology*, **23**(4), 503.

18. Beat, E. A. (1946). Sickle-cell disease in the Balovale district of Northern Rhodesia. *E. Afri. Med. J.*, **23**, 75.

19. Allison, A. C. (1954). Protection afforded by sickle-cell against subtertian malaria infection. *Brit. Med.* L. I. 290.

20. Donno, L. (1989). Drug combinations in the treatment of malaria. *J Chemother.*, **1**(1), 52-58.

21. Ademowo G. O. (2000). Malaria-Africa's health challenge of the millennium. *J. Transfigural Mathematics*, **6**(1), 29-38.

22. Woodward, R. B.; Doering, W. E., (1945). The total synthesis of quinine. *J. Am. Chem. Soc.*, **67**(5), 860-874.

23. Steck, E. A. (1972). The chemotherapy of Protozoan Diseases, vol 3, section 4, Water Reed Army Institute of Research, Washington, D.C.

24. Balkovec, J. M., Dake, G. R., Fujimoto, A., Koft, E. R., Niu, D., Storck, G. Tata, J. R. (2001). The first stereoselective total synthesis of quinine. *J. Am. Chem. Soc.*, **123**, 3239-3242.

25. Greenwood, D. (1995). Conflicts of interest: the genesis of synthetic antimalarial agents in peace and war. *J. Antimicrobial Chemother.*, **36**, 857-872.

26. Krettli, A.V., Miller, L. H. (2001). Malaria: a sporozoites runs through it. *Current Biol.*, II, 409-412.

27. Fairley, N. H. (1945). Chemotherapy suppression and prophylaxis in malaria. An experimental investigation undertaken by medical research team in Australia. *Trans Roy. Soc. Trop. Med. Hyg.*, **38**(5), 311-365.

28. Andersag, H., Breitner, S. and Jung, H. (1939). *Ger. Pat.*, **638**, 692

29. Coatney, G. R., Cooper, W. C., Eddy, N. B., Greenbary, J. (1953). Survey of antimalarial agents. Public Health Monograph No 9, Government Printing Office, Washington DC.

30. Burckhalter, J.H., Tendwick, J. H.., Jones, F. H., Jones, P. A., Holdcombe, W. F., Rawlings, A. L. (1948). Aminoalkylphenols as antimalarial II. (heterocyclic-amino)–α–amino–O–cresols: the synthesis of camquine. *J. Am. Chem. Soc.*, **70**, 1363-1373.

31. Coatney, G. R. (1963). Pitfall in a discovery: the chronicle of chloroquine. *Am. J. Trop. Med. Hyg.* **12**, 121-128.

32. Albert, A. (1966). The Acridines, 2nd edn, Arnold, London.

33. Adams, A. R. (1959). Drug treatment of malaria. *Br Med. J.* **5145**, 183-188.

34. Peterson, D. S., Milhous, W. K., Wellens, T. E. (1990). Molecular basis of differential resistance to cycloguanil and pyrimethamine in *Plasmodium falciparum* malaria. *Proc. Natl. Acad. Sci.* **87**, 3018-3022

35. Falco, E. A., Goodwin, L.G., Hitchings, G. H., Rollo, I. M., Russel, P. B. (1951). 2,4-diaminopyridines – a new series of antimalarials. *Br. J. Pharmacol Chemother.*, **6** (2), 185.

36. Hitchings, G. H., Falco, E. A., Vanderwerff, H., Russell, P. B., Russel, P. B., Eion, G. B. (1952). Antagonists of nucleic acid derivatives. VII. 2,4-diaminopyridines. *J. Biol. Chem.*, **199**(1), 43-56.

37. Long, P. H., Bliss, E. A. (1939). The clinical and experimental use of sulfanilamide, sulfapyridine and allied compounds. New York, Macmillan Press

38. Roll, I. M. (1975). Antiplasmodial efficacy of 2,4-diaminopyrimidinesulfonamide combinations, especially against chloroquine-resistant malaria. *Can. Med. Assoc. J.*, **112**(13), 50-53.

39. Schmidt, L. H. (1979). Studies on the 2,4-diamino-6-substituted quinazolines III. The capacity of sulfadiazine to enhance the activity of WR-158,122 and WR-159,412 against infections with various drug-susceptible and drug-resistant strains of *P. falciparum* and *P. vivax* in owl monkey. *Am. J. Trop. Med. Hyg.*, **28**(5), 808-818.

40. Diggnis, F. W. (1979). The true history of the discovery of penicillin, with refutation of the misinformation in the literature. *Br. J. Biomed. Sci.*, **56**(2), 88-93.

41. Puri, S. K., Dutta, G. P. (1982). Antibiotics in the chemotherapy of malaria. *Prog. Drug Res.*, **26**, 167-205.

42. Coatney, G.R., Greenberg, J. (1952). The use of antibiotics in the treatment of malaria. *Ann. N. Y. Acad. Sci.*, **55**(6), 1075-1081.

43. Avery, M. A., Jenning-White, C., Chong, W. K. M. (1987). The total synthesis of (+)-artemisinin and (+)-a-desmethyltemesinin. *Tetrahedron Letters*, **28**, 4629-4632.

44. Zhou, W. S., (1972). *artemisii deri* (Chimica Sinica, **37**, 129).

45. Vietinck, A. J. (1987). Topics in Pharmaceutical Sciences. Breimer, D. D., Speiser, P. (Eds.) Elservier, 249-262.

46. Chan, K. L., O'Neill, M. J., Phillipson, J. D., Warhurst, D. C. (1986). Plants as sources of antimalarial drugs. Part 3. *Eurycoma longifolia. Planta Medica*, **53** (3), 105-107.

47. Farnsworth, N. R. (1966). Biological and phytochemical screening of plants. *J. Pharm. Sci.*, **55**, 225-276.

48. Facer, C. A., Tanner, M. (1997). Clinical trials of malaria vaccines: progress and prospects. *Adv. Parasitol.*, **39**: 1-68.

49. Richie, T. L., Saul, A. (2002). Progress and Challenges for malaria vaccines. *Nature*, **415**: 694-701.

50. Patarroyo, M. E., Amador, R. Clavijo, P. (1988). A synthetic vaccine protects humans against challenge with asexual blood stages of *Plasmodium falciparum* malaria. *Nature*, **332**, 158-161.

51. Bojang, K. A., Obaro, S. K., D'Alessandro, U. (1998). An efficacy trial of the malaria vaccine SPf66 in Gambian infants: second year of follow-up. *Vaccine*, **16**, 62-67.

52. Stoute, J. A., Sloui, M., Heppner, D, G. (1997). A preliminary evaluation of a recombinant circumsporozoite protein vaccine against *Plasmodium falciparum* malaria. *N. Engl. J. Med.*, **336**, 86-91.

53. Genton, B. Betuela, I., Felger, I. (2002). A recombinant blood-stage malaria vaccine reduces *Plasmodium falciparum* density and exerts selective pressure on parasite populations in a phase 1-2b trial in Papua New Guinea. *J. Infec. Dis.*, **185**, 820-827.

54. Moorthy, V. S., Good, M. F., Hill, A. V. S. (2004). Malaria vaccine developments. *Lancet*, **363**, 150-156.

55. Greenwood, B., Alonso, P. (2002). Malaria vaccine trials. *Chem. Immunol.*, **80**, 366-395.

56. Jaramillo-Arango, J. A. (1949). Critical review of the basic facts in the history of Cinchona, *J. Linnaen Soc.*, **53**, 1272-1309.

57. Lee, M. R. (2002). Plants against malaria. Part 1 & 2: Cinchona or the Peruvian bark. *J. R. Coll. Physicians Edinb.*, **32**, 189-196, 300-305.

58. Peters, W. (1987). Chemotherapy and Drug Resistance in Malaria. Vols I and II. Academic Press, London.

59. Schuleman, W. (1932). Synthetic antimalarial preparations. *Proceedings of the Royal Society of Medicine*, **25**, 897-905

60. Edgcomb, J. H., Arnold, J., Yount, E. H. Jr., Alving, A. S., Eichelberger, L., Jeffery, G. M., Eyles, D., Young, M. D. (1950). Primaquine, SN 13272, a new curative agent in vivax malaria, a preliminary report. *J. Natl. Malaria Soc.*, 9(4), 285-292.

61. Benazet, F. (1963). Pharmacology of 8-aminoquinolines and combination, of various synthetic antimalarials. *Med. Trop.*, **23**, 760-768.

62. Matsueda, S. Satomi, T., Otaki, Y., Sato, S., Sasaki, S. (1972). Studies on Sesquiterpene lactone 8. Chemical constitution of the Artemisia feddei collected in Kochi prefecture. *Yakugaku Zasshi*, **92**(12), 1564-1566.

63. White, N. J., Fosten, F., Looareesuwan, S., Watkins, W. M., Marsh, K., Snow, R. W., Kokwaro, G., Ouma, J., Hien, T. T., Molyneux, M. E., Taylor, T.

E., Newbold, T. E., Ruebush, C. I., Danis, T. K., Greenwood, B. M., Anderson, R. M., Olliaro, P. (1999). Averting a malaria disaster. *Lancet*, **353**, 1695-1967.

64. Pussard, E., Verdier, F. (1994). Antimalarial 4-aminoquinolines: mode of action and pharmacokinetics. *Fundam. Clin. Pharmacol.*, **8**(1): 1-17.

65. Mckerrow, J. H., Sin, E., Rosenthal, P. J., Bouvier, J. (1978). The protease and pathogenicity of parasitic protozoa. *Annu. Rev. Microbiol.*, **47**, 821-853.

66. Van den Berghe L. (1954). The history of the discovery of *Plasmodium berghei*. *Indian J. Malariol.*, **8**(4), 241-243.

67. Spangler, W.L., Gribble, D., Abildgaard, C., Harrison, J. (1978). *Plasmodium knowlesi* malaria in the Rhesus monkey. *Vet. Pathol.*, **15**(1), 83-91.

68. Bruce-Chatt, L. J. (1986). Chemotherapy of Malaria. W. H. O.

69. Lobel, H. O., Campbell, C. C. (1986). Malaria prophylaxis and distribution of drug resistance. *Clinics in Tropical Medicine and Communicable diseases*, **1**, 225-242.

70. Modell, W. (1968). Malaria and victory in Vietnam. The first battle against drug-resistant malignant malaria is described. *Science*, **162**(860), 1346-1352.

71. Thaithong, S. (1983). Clones of different sensitivities in drug resistant isolates of *Plasmodium falciparum*. *Bull. W. H. O.*, **61**, 709-712.

72. Foley, M., Tilley, L. (1997). Quinoline antimalarials: mechanisms of action and resistance. *Inter. J. Parasitol.*, **27**, 231-240.

73. Plowe, C. V., Kublin, J. G., Duombo, O. K. (1994). *P. falciparum* dihydrofolate reductase and dihydropteoroate synthase mutations: epidemiology and role in clinical resistance to antifoliates. Drug Resistance Updates,

74. Ittarat, I., Asawamahasakda, W., Meshwick, S. R. (1994). The effects of antimalarials on the *Plasmodium falciparum* dihydroorate dehydrogenase. *Experimental Parasitol.*, **79**, 50-56.

75. Wernsdorfer, W. H. (1991). The development and spread of drug resistant malaria. *Parasitol. Today*, **7**, 297-303.

76. Verdrager, J. (1986). Epidemiology of the emergence and spread of drug-resistant falciparum malaria in South-East Asia and Australasia. *J. Trop. Med. Hyg.*, **89**. 277-289.

77. White, N. J. (1997). Assessment of the pharmacodynamic properties of antimalarial drugs *in vivo*. *Anti. Agents Chemo.*, **41**, 1413-1422.

78. Baso, L. K. (1991). Inefficacy of amodiaquine against chloroquine-resistant malaria. *Lancet*, **338**, 1460-146.

79. Watkins W. M. (1997). The efficacy of antifolate antimalarial combinations in Africa: a predictive model based on pharmacodynamic and pharmacokinetic analyses. *Parasitol. Today*. **13**, 459-464.

80. Rathod, P. K., McErlean, T., Lee, P. C. (1997). Variations in frequencies of drug resistance in *Plasmodium falciparum*. *Proc. Natl. Aca. Sci.* USA. **94**, 9389-9393.

81. Watkins, W. M., Masobo, M. (1993). Treatment of *Plasmodium falciparum* malaria with pyrimethamine-sulfadoxine: selective pressure for resistance is a function of long elimination half-life. *Transc. Royal. Soc. Trop. Med. Hyg.*, **87**, 75-78.

82. Palmer, K. J., Holliday, S. M., Brogden, R. N. (1993). Mefloquine. A review of its antimalarial activity, pharmacokinetic properties and therapeutic efficacy. **45**, 430-475.

83. Wernsdorfer, W. H. (1994). Epidemiology of drug resistance in malaria. *Acta Tropica*, 56, 143-156.

84. Comer, R. D., Young, M. D., Porter, J. A. Jr., Gauld, J. R., Merritt, W. (1968). Chloroquine resistance in Plasmodium falciparum malaria on the Pacific coast of Colombia. *Am. J. Trop. Med. Hyg.*, **17**(6), 795-799.

85. Peters, W. (1998). Drug resistance in malaria parasites of animals and man. *Adv. Parasitol.*, **41**, 1-62.

86. White, N. J. (1998). Drug resistance in malaria. *Br. Med. Bull.*, **54** (3), 703-715.

87. Mokehanpt, F. (1995). Mefloquine resistance in *Plasmodium falciparum* *Parasitol. Today*, **11**, 248-253.

88. Wongsrichanalai, C., Pickard, A. L., Wernsdorfer, W. H., Meshnick, S. R. (2002). Epidemiology of drug-resistant malaria. *The Lancet. Infect. Dis.* **2**: 209-218.

89. Campbell, C. C., Chin, W., Collins, E., Teutsch, S. M., Moss, D. M. (1979). Chloroquine-resistant *Plasmodium falciparum* from East Africa: cultivation and

drug sensitivity of the Tanzanian I/CDC strain from an American tourist. *Lancet*, **2**, 1151-1154.

90. Sansonetti, P. J., LeBras, C., Verdier, F., Charmot, G., Dupont, B., Lapresle, C., (1985). Chloroquine-resistant *Plasmodium falciparum* in Cameroon. *Lancet*, **1**, 1154-1155.

91. LeBras, J., Hattin, I., Bopuree, P., Coco-cianci, O., Garin, J., Rey, M., Charmot, G., Roue, R. (1986). Chloroquine-resistant malaria in Benin. *Lancet*, **2**, 1043-1044.

92. Salako, L. A., Aderounmi, F. A. (1987). *In vitro* chloroquine and mefloquine-resistant *Plasmodium falciparum* in Nigeria. *Lancet*, **1**, 572-573.

93. Sowunmi, A., Salako, L. A., Walker, O., Ogundahunsi, O. A. T.(1990). Clinical efficacy of mefloquine in children suffering from chloroquine-resistant *Plasmodium falciparum* malaria in Nigeria. *Trans. Royal Soc. Trop. Med. Hyg.*, **84** (6), 761-764.

94. Barnes, A. J., Ong, E. L., Dunbar, E. M., Mandal, B. K., Wilkins. E. G. (1991). Failure of chloroquine and proguanil prophylaxis in travellers to Kenya. *Lancet*, **338**, 1338-1339.

95. Basko, L. K., LeBras, J., Gillotui C. Ringwald P., Rabenfarson, E., Gimenez, F., Bonchand, O., Farinotti, R., Couland, J. P. (**1991**). Type RI resistance to halofantrine in West Africa. *Trop. Med. Parasitol.*, 42, 413-414.

96. Jelinek, T., Schelbert, P., Loescher, T. (1995). Eichenlamb, D. *Trop. Med. Parasitol.*, **116**, 211-217.

97. Solomons, T. W. G. (1996). Organic Chemistry, 6th Edition. John Wileys and Sons, New York, 934.

98. Howard-Lock, H. E., Lock, H. E., Lock, C. J., Mewa, A., Kean, W. F. (1986). D-penicillamine: chemistry and clinical use in rheumatic disease. *Semi Arthritis Rheum.*, 15(4), 261-281.

99. Lebwohl, D., Canetta, R. (1998). Clinical development of platinum complexes in cancer therapy: a Historical perspective and an update. *European J. of Cancer*, **34**(10), 1522-1534.

100. Harrap, K. R., Kellam, L. R., Jones, M., Goddard, P. M., Morgan, S. E., Murrer, B. A., Abrams, M. J., Giandomenico, C. M., Cobbleigh, T. (1991). Platinum coordination complexes which circumvent *cis*-platin resistance. *Adv. Enzyme Rugul.*, **31**, 31-43.

101. Orvig, C., Abrams, M. J., Eds. (1999). Medicinal inorganic chemistry. *Chem. Rev.*, **99** (9), 2201-2842.

102. Guo, Z., Sadler, P. J. (1999). Metals in medicine. *Angew Chem. Int. Ed. Engl.*, **38** (11), 1512-1531

103. Abrams, M. J., Murrer, B. A. (1993). Metal compounds in therapy and diagnosis. *Science*, **261**, 725-730.

104. Sanchez-Delgado, R. A., Navarro, M., Perez, H., Urbina, J. A. (1996). Towards a novel metal-based chemotherapy against tropical disease. 2. Synthesis and antimalarial activity *in vitro* and *in vivo* of new ruthenium- and rhodium-chloroquine complexes. *J. Med. Chem.*, **39**(5), 1095-1099.

105. Dudeja, M., Singh, J. P., Sangucin, N. K., Dhindsa, K. S. (1993). Coordination behaviour of chloroquine towards some biologically significant metal ions. *J. Indian Chem. Soc.*, **70**(2), 159-161.

106. Navarro, M., Vasquez, F., Sanchez-Delgado, R. A., Perez, H., Sinou, V., Schrevel, J. (2004). Toward a novel metal-based chemotherapy against tropical diseases.7. Synthesis and *in vitro* antimalarial activity of new gold-chloroquine complexes. *J. Med. Chem.*, **47**(21), 5204-5209.

107. Navarro, M., Perez, H., Navarro. M., Perez, H., Sanchez – Delgado, R. A. (1997). Toward a novel metal-based chemotherapy against tropical diseases.3. Synthesis and antimalarial activity *in vitro* and *in vivo* of the new gold-chloroquine complex $[Au(PPh_3)(CQ)]PF_6$. *J. Med. Chem.*, **40**(12), 1937 – 1939.

108. Dadacova, E. (1999). Preparation of $^{198}Au(1)$-labelled gold-chloroquine complex $[^{198}Au(PPh_3)(CQ)]PF_6$ as a potential antimalarial agent. *J. Labelled compounds and Radiopharmaceuticals*, **42** (3), 287 – 292.

109. Obaleye, J. A., Balogun, E. A., Adeyemi, O. G. (1999). Synthesis and *in vivo* effect of some metal drug complexes on malaria parasites. *Biokemistri*, **9**(1), 23 – 27.

110. Wasi, N., Singh, H. B., Gajanana, A., Raichowdhary, A. N. (1987). Synthesis of metal complexes of antimalarial drugs and *in vitro* evaluation of their activity against *Plasmodium falciparum. Inorg. Chim. Acta,* **135**(2), 133 – 137.

111. Wasi, N., Singh, H. B. (1988). Coordination complexes of drugs-preparation and characterization of metal complexes of amodiaquine-an antimalarial. *Synth. React. Inorg. Metal-Organic Chem.*, **18**(5), 473-485.

112. Dermatin, F., Manassero, M., Naldini, L., Zoroddu, M. A. (1983). Metal complexes of 2,4-diamino-5-(3',4',5'-trimethoxybenzyl)pyrimidine, (trimethoprim). Part I. Synthesis and crystal structure of $CoCl_2$-(trimethoprim)$_2$. *Inorg. Chim. Acta.* 77(6), L213-L214.

113. Naldini, L Cabras, M. A., Zoroddu, M. A., Dermaitn, F., Manassero, M., Sansoni, M. (1984). Metal complexes of 2,4-diamino-5-(3',4',5'-trimethoxybenzyl)pyrimidine, (trimethoprim).Part II. Synthesis, magnetic characterisation and X-ray structure of $[Cu_2(O_2CCH_3)_4$(trimethoprim)$_2].2C_6H_6.CH_3OH$. *Inorg. Chim. Acta*, **88**(1), 45-50.

114. Zoroddu, M. A; Naldini, L., Demartion, F., Masciochhi, N. (1987). Metal complexes of 2,4-diamino-5-(3',4',5'-trimethoxylbenzyl)pyrimidine(Trimethoprim) and 2,4-diamino-5-(p-chlorophenyl)-6-ethylpyrimidine(pyrimethamine). Part III. Syntheses and x-ray structures of $[Rh_2(O_2CCH_3)_4$(Trimethoprim)$_2]\cdot 2C_6H_6\cdot CH_3OH$ and $[Rh_2(O_2CCH_3)_4$(Pyrimethamine)$_2]$. *Inorg. Chim. Acta*, **128**(2), 179-83.

115. Muthiah, P.T., Robbert, J. J. (1999). Metal-pyrimidine interaction: synthesis and crystal structure of a cadmium complex of trimethoprim $([CdBr_2(TMP)_2(H_2O)_2]\cdot H_2O$ *J. Chem. Crystall.*, **29**(2), 223 – 226.

116. Simo, B., Perello, L., Ortiz, R., Castineiras, A., Latorre, J., Canton, E. (2000). Interaction of metal ions with a 2,4-diaminopyrimidine derivative (trimethoprim). Antibacterial studies. *J. Inorg. Biochem.* **81**(4), 275-283

117. Yamashita, S.; Seyama, Y., Ishikawa, N. (1978). Antimicrobial activity of metal derivatives of sulfonamides, *Experienta*, **34**(4), 472-3.

118. Lal, Keemti. (1978). Formation constant of some metal complexes with three sulfa drugs. *Chemical* era, **14**(5), 170-2.

119. El Guindi, N. M, Abdel Geward, F. M. (1988). Chelating tendencies of some sulfa drugs. *Egypt. J. Pharm. Sci.*, **29**(1-4), 457-63.

120. El Guinch, N. M., Abdel – Geward, F. M. (1989). Thermodynamic studies on the complexes between transitions metal ions and heterocyclic sulfonamides. *J. Med. Chem.*, 30(1-4), 29-34.

121. Goel, S., Lal, K. (1990). Studies on metal complexes of Schiff bases derived from sulfadiazine and sulfadimine with 5-substituted salicylaldehydes. *Asian J. Chem.*, **2**(3), 271-4.

122. Menabue, Sladini, M. (1993). Coordination behaviour of sulfa-drugs: synthesis, structural and spectroscopic investigation of M(II) (N1-pyrimidin-2yl-sulfanilamido)$_2\cdot xH_2O$. *J. Inorg. Biochem.*, **49**(3), 201 – 7.

123. Mukherjee, G. N., Bash, U., Ghosh, T. (1982). Studies on the interactions of biological metal ions with some sulfonamide drugs. Part 1. Equilibrium study on the complex formation of cobalt(II), nickel(II), copper(II) and zinc(II) with sulfapyridine, sulfadiazine and sulfathiozole. *J. Ind. Chem. Soc.*, **25**(3), 275 – 81.

124. Pandey, A. K., Mishra, L., Singh, V. K. (1996). Synthesis and structural characterisation of cobalt(II), nickel(II), copper(II) and zinc(II) complexes of Schiff base derived from sulfadiazine and pyridine-2-carboxaldehyde. *Asian J. Chem.*, **8**(3), 353-356.

125. Omar, M. M. (2002). Potentiometric and thermogravimetric studies on some metal-oxine-sulpha drug ternary complexes. *J. Therm. Analy. Calor.*, **68**(3), 1003 – 1015.

126. Tsumaki, T., Yoshino, T., Tanaka, T., Watanabe, I. (1952). Some quinine derivatives and their metallic complex salts. *Nippon Kagaku Zasshi,* **73**, 94-6.

127. Niyoki, S. K., Rieders, F. J. (1966). Further studies on chelation as a method of exclusion screening for drugs. *J. Forensic Sci.,* **11**(1), 105-8.

128. Tsangaris, J.M., Baxevanidis, G. T. Zeitschrift Naturforschumg, Teil Bi (1974). Complexes of quinine with copper(II), nickel(II), cobalt(II) and chromium(III) chlorides. *Zeitschrift fuer Naturforschung*, **29**(7/8), 532-7.

129. Farooz, O., Malik, A. (1975).Interaction of transition metals with some alkaloids. Metal complexes of quinaldine, quinine, brucine, and codeine. *Acta Chimica Academiae Scientiarum Hungaricae*, **85**(40), 389 – 94.

130. Gupta, S. S., Bhardwej, S. K., Kanshal, R. (1982). Study of the IR spectra of quinine-metal complexes. *Vijana Parishad Anu Sandhan Patrika.*, **25**(3), 269-73

131. Dudeja, M.; Suigh, J.P., Sangwan, N.K., Dhindsa, K. S. (1990). Synthesis and characterization of vanadyl(IV), iron(II), cobalt(II), nickel(II), and copper(II) complexes of cinchona alkaloids. *Chimica Acta Turcica*, **18**(3), 359-64.

132. Missling, C.; Mihan, S.; Polborn, K., Beck, W. (1996). Metal complexes of biologically important ligands. Part 86. Organometallic complexes of ruthenium(II), rhodium(III), iridium(III), and gold(I) with cinchona alkaloids. *Chemische Berichte*, **129**(3), 331-5.

133. Hubel, R., Polborn, K., Beck, W. (1999). Metal complexes of biologically important ligands. Part 113. Cinchona Alkaloids as versatile ambivalent ligands. Coordination of transition metals to the four potential donor sites of quinine. *Eur. J. Inorg. Chem.*, **3**, 471 – 482.

134. Hubel, R.; Jelinek, T.; Beck, W. (2000). Metal complexes of important ligands. Part 125. Palladium(II) and Platinum(II) complexes of quinine derivatives and *in vitro* tests. Zeitscnift fuer Naturforschung, B. *Chem. Sci.*, **5**(9), 821-833.

135. Biot, C., Glorian, G., Maciejewski, L. A., Brocard, J. S. (1997). Synthesis and antimalarial activity *in vitro* and *in vivo* of a new ferrocene-chloroquine analogue. *J. Med. Chem.* **40**, 3715-3718.

136. Biot, C., Delhaes, L., N'Diaye, C. M., Maciejewski, L. A., Camus, D., Dive, D., Brocard, J. S. (1999). Synthesis and antimalarial activity in vitro of ferrochlorochloroquine and related compounds. *Bioorg. Med. Chem.*, **7**, 2843-2847.

137. Biot, C., Delhaes, L., Abessolo, H., Domarle, O., Maciejewski, L. A., Delcourt, P., Deloron, P., Camus, D., Dive, D., Brocard, J. S. (1999). Novel metallocenic compounds as antimalarial agents. Study of the position of ferrocene in chloroquine. *J. Organom. Chem.*, **589**, 59-65.

138. Biot, C., Delhaes, L., Maciejewski, L. A., Mortuarie, M., Camus, D., Dive, D., Brocard, J. S. (2000). Synthetic ferrocenic mefloquine and quinine analogues as potential antimalarial agents. *J. Med. Chem.*, **35**, 707-714.

139. Itoh, T., Shirakami, S., Ishida, N., Yamashita, T. Y., Kim, H., Wataya, Y., (2000). Synthesis of novel ferrocenyl sugars and their antimalarial activities. *Biorg. Med. Chem. Lett.*, **10**, 1657-1659.

140. Delhaes, L., Biot, C., Berry, L., Maciejewski, L. A., Camus, D., Brocard, J. S., Dive, D. (2000). Novel ferrocenic artemisinin derivatives: Synthesis, *in vitro* antimalarial activity and affinity of binding with ferroprotoporphyrins IX. *Biorg. Med. Chem. Lett.* **8**, 2739-2745.

141. Delhaes, L., Abessolo, H., Biot, C., Berry, L., Delcourt, P., Maciejewski, L. A., Camus, D., Brocard, J. S., Dive, D. (2001). *In vitro* and *in vivo* antimalarial activity of ferrochloroquine, a ferrocenyl analogue of chloroquine against chloroquine-resistant malaria parasite. *Parasitol. Res.*, **87**, 239-244.

142. Blackie, M. A. L., Beagley, P., Chibale, K., Clarkson, C., Moss, J. R., Smith, P. J. (2003). Synthesis and antimalarial activity *in vitro* of new heterobimetallic complexes: Rh and Au derivatives of chloroquine and a series of ferrocenyl-4-amino-7-chloroquinolines. *J. Organo. Chem.*, **688**, 144-152.

143. Scheibel L. W., Stanton G. G. (1986). Antimalarial activity of selected aromatic chelator IV. Cation uptake in the presence of *Plasmodium falciparum* in the presence of oxines and siderochromes *Mol. Pharmacol.*, **30**(4), 364 – 369.

144. Sharma, V., Beatly, A., Goldberg, D. E., Piwnica-Worms, D. (1997). Structure of a novel gallium(III) complex with selective activity against chloroquine-resistant *Plasmodium falciparum*. *Chem. Comms.*, **No 22**, 2223-2224.

145. Tsfack, A., Loyevsky, M., Ponka, P., Cabantchik, Z. I. (1996). Modes of action of iron(III) chelators as antimalarials. 4. Potentiation of desferal action by benzoyl and isonocatinoyl hydrazone derivatives. *J. Lab. Clin. Med.*, **127**(6), 574-582.

146. Cole, K. A., Ziegler, J., Evans, C. A., Wright, D. W. (2000). Metalloporphyrins inhibit beta-haematin (hemozoin) formation. *J. Inorg. Biochem.*, **78**(2), 109 –115

147. Goldberg, D. E., Sharma, V., Oksman, A., Gluzman, I. Y., Wellems, T. E., Piwinica-Worms, D. (1996). Probing the locus of chloroquine resistance locus of *Plasmodium falciparum* with a Novel class of multidentate metal(III) coordination complexes. *J. Biol. Chem.*, **272**(10), 6567-6572.

148. Russell, P. F. (1955). Man's mastery of malaria. London: Oxford University Press.

149. Moorthy, V. S., Good, M. F., Hill, A. V. S. (2004). Malaria vaccine developments, *The Lancet*, **363**, 1-156

150. WHO (2000). Malaria – a global crisis. Geneva

151. Shanks, G. D., Biomndo, K., Hay S. I., Snow, R. W. (2000). Changing patterns of clinical malaria since 1965 among a tea population located in Kenyans highlands. *Trans R Soc Trop Med Hyg*, **94**, 253-255.

152. le Sueur, D., Sharp, B. L., Gouws, E., Ngxongo, S. (1996). Malaria in South Africa. *S. Afr Med J*; **86**, 936-939.

153. Greenwood, B., Mutabingwa, T. (2002). Malaria in 2002. *Nature*, **415**, 670-672.

154. Hemingway, J., Field, L., Vontas, J. (2002). An overview of insecticides resistance. *Science*, **298**, 96-97.

155. Guerin, P. J., Olliaro, P., Nosten, F. et al. (2002). Malaria: current status of control, diagnosis, treatment, and a proposed agenda for research and development. *Lancet Infect Dis.*, **2**, 564-573.

156. Martens, P., Hall, L., (2000). Malaria on the move: human population movement and malaria transmission. *Emerg. Infect Dis.*, **6**, 103-109.5

157. Muentener, P., Schlagenhauf, P., Steffen, R. (1999). Imported malaria (1985-1995): Trends and perspectives. *Bull. W. H. O.*, 77(7), 560-6.

158. Snow, R. W., Trape, J. F., Marsh, K. (2001). The past, present and future of childhood malaria mortality in Africa. *Trends Parasitol.*, **17**, 593-597.

159. Mabbs, F. E. Machin, D. J. (1973) Magnetism and Transition Metal Complexes, London, Chapman and Hall, 5

160. SMART (Version 5.625), SADABS (Version 2.03a) and SHELXTL (Version 6.12), Bruker, 2001, Bruker AXS Inc., Madison, Wisconsin, USA.

161. Conard, F. W. (1946). Inorganic syntheses, Vol. II, 221. McGraw-Hill Book company inc.

162. Sharma, V., Oksman, A., Gluzman, I. Y., Wellems, T. E.(1998). Book of abstracts, 216th ACS meeting, Boston.

163. Hathaway, B. J., Billing, D. E. (1970). The electronic properties and stereochemistry of mono-nuclear complexes of copper(II) ions. *Coord. Chem. Rev.*, **5**(2), 143-207.

164. Jorgensen, C. K. (1964). *Adv. Chem. Phys.*, **5**, 33.

165. Lever, A. B. P. (1984). Inorganic Electronic Spectroscopy. Elsevier, Amsterdam.

166. Rigg, J. M.; Sherwin, E. J. (1971). *Inorg. Nucl. Chem.*, **10**, 817.

167. Nakamato, K. Infrared and Raman Spectra of Inorganic and Coordination Compounds. 4th Edition. John Wiley and Sons, New York.

168. de Paula, F. C. S., Carvalho, S., Duarte, H. A., Baniago, E. B., Mangrich, A. S., Pereira-Maia, E. C. (1999). A physicochemical study of tetracycline coordination to oxovanadium(IV). *J. Inorg. Biochem.*, **76**, 221-230.

169. Seblin, J., Ortolano, T. R., Macglynn, S. P. (1964). Electronic spectra of vanadyl complexes. *J. Phy. Chem.*, **41**, 262-268

170. Balhausen, C. J., Gray, H. B. (1962). The molecular orbital treatment of $[VO(H_2O)_5]^{2+}$. *Inorg. Chem.*, **1**, 111-112.

171. Clark, R. J. H. (1973). Vanadium. *Comprehensive Inorganic Chemistry*, **3**, 514-518

172. Selbin, J. (1966). Oxovanadium(IV) complexes. *Coord. Chem. Rev.*, **1**, 293-314.

173. Kolawole, G. A., Adeyemo, A. O. (1992). Copper(II) complexes of vitamin B1 analogues and those of structurally related ligands. *Synth. Reac. Inorg. Met-Org. Chem.* **22**(5), 631-651.

174. Greenwood, N. N., Earnshaw, A. Chemistry of the elements. Pergamon Press, first edition, (1985).

175. Bleaney, B., Bowers, K. D. (1952). Anomalous paramagnetism of copper acetate; *Proc. Roy. Soc.*, **214**, 451-465.

176. Figgis, B. N., Martin, R. L. (1956). Magnetic studies with copper(II) salts. Part 1. Anomalous paramagnetism and δ-bonding in anhydrous and hydrated copper(II)acetate. *J. Chem. Soc.*, 3837-3846.

177. Fidock, D. A., Rosenthal, P. J., Croft, S. L., Brun, R., Nwaka, S. (2004). Antimalarial drug discovery: efficacy models for compound screening. *Nature Review: Drug discovery*, **3**, 509-520.

178. Trager, W., Jensen, J. B. (1976) Human malaria parasites in continuous culture. *Science*, **193**, 673-675

179. Riekmann, K. H., Campbell, G. H., Sax, L. J., Mrena, J. E. (1979) Drug sensitivity of *Plasmodium falciparum*, *Lancet*, **i**, 22-23

180. Desjardins, R. E., Canfield, C. J., Haynes, J. D., Chulay, J. D. (1979) Quantitative assessment of antimalarial activity in vitro by a semi-automated microdilution technique. *Anti. Agents Chemother.*, **16**, 710-718.

181. LeBras, J., Deloron, P. (1983) *Am. J. Trop. Med. Hyg.*, **32**, 447-451.

182. White, N. J. (1997). *Anti. Agents Chemother.*, **41**, 1413-1422

183. Gluzman, I. Y., Krogstad, D. J., Orjih, A. U., Nkangineme, K., Wellem, T. E., Martin, J. T., Schlesinger, P. H. (1990) A rapid in vitro test for chloroquine-resistant *Plasmodium falciparum*. *Am. J. Trop. Med. Hyg.*, **42**, 521-526.

184. Krogstad, D. J., Gluzman, I. Y., Kyle, D. E., Oduola, A. M. J., Martin, S. K., Milhous, W. K., Schlesinger, P. H. (1987) Efflux of chloroquine from *Plasmodium falciparum*: Mechanism of chloroquine resistance. *Science*, **238** (4831), 1283-1285.

185. Martin, S. K., Oduola, A. M. J., Milhous, W. K. (1987) Reversal of chloroquine in *Plasmodium falciparum* by verapamil. *Science*, **235**, 899-901.

186. Bickii, J., Basco, L. K., Ringwald, P. (1998) Assessment of three in vitro tests and an in vivo test for chloroquine resistance in Plasmodium falciparum clinical isolates. *J. Clin. Microbiol.*, **36**, 243-247.

187. Makler, M. T., Ries, J. M., Bancroft, J. E., Piper, R. C., Gibbins, B. L., Hinrichs, D. J. (1993) Parasite lactate dehydrogenase as an assay for Plasmodium falciparum drug sensitivity. *Am. J. Trop. Med. Hyg.*, **48**, 739-741.

188. Brockelman, C. R., Tan-Ariya, P. Bunnang, D. (1989) Development of in vitro microtest assessment for *Plasmodium vivax* sensitivity to chloroquine. *South East Asian J. Trop. Med. Public Health*, **20**, 2347-2351.

189. Ringwald, P., Bickii, J., Basco, L. (1997). Pyronaridine for treatment of Plasmodium ovale and Plasmodium malariae infections. *Antimicrobial Agents and Chemotherapy*, **41**, 2317-2319.

190. Ringwald, P., Basco, L. (2003). *In vitro* and *in vivo* drug sensitivity test for malaria. Drugs against parasitic diseases: R&D methodologies and issues, edited by Fairlamb, A. H., Ridley, R. G., Vial, H. J. TDR special programme for research and training in tropical diseases, section III, 185-192.

191. Basco, L. K., Bickii, J., Ringwald, P. (1998). *In vitro* activity of lumefantrine (benfumetol) against clinical isolates of Plasmodium falciparum in Younde, Cameroon. *Antimicrobial Agents and Chemotherapy*, **42**, 2347-2351.

192. Canfield, C. J., Pudney, M., Gutteridge, W. E. (1995) Interactions of atovaquone with other antimalarial drugs against *Plasmodium falciparum in vitro*. *Experimental Parasitol.*, **80**, 373-381.

193. Batra, S., Bhaduri, A. P. (1997) Reversal of chloroquine resistance in malaria: A new concept of chemotherapy. *Advances in Drug Research*, **30**, 201-232

194. Sowunmi, A., Oduola, A. M. J. (1997) Comparative efficacy of chloroquine/chlorpheniramine combination and mefloquine for the treatment of chloroquine-resistant Plasmodium falciparum malaria in Nigerian children. *Trans. Roy. Soc. Trop. Med. Hyg.*, **91**, 689-693.

195. Moreno, A., Badeli, E., Van Rooijen, N., Druihe, P. (2001) Human malaria in immunocompromised mice: new *in vivo* model for chemotherapy studies. *Antimicrob. Agents Chemother.* **45**, 1847-1853.

196. Childs, G. E. et al. (1984) Comparison of in vitro and in vivo antimalarial activities of 9-phenanthrenecarbinols. *Ann. Trop. Med. Parasitol.*, **78**, 13-20.

197. Peters, W. (1977). The chemotherapy of rodent malaria. XXVII. Studies on mefloquine (WR 142,490). *Ann. Trop. Med. Parasitol.*, **71**, 407-418.

198. Peters, W., Robinson, B. L., Ellis, D. S. (1987). The chemotherapy of rodent malaria. XLII. Halofantrine and Halofantrine resistance. *Ann. Trop. Med. Parasitol.*, **81**, 639-646.

199. Vennerstrom, J. L. (2000). Synthesis and antimalarial activity of sixteen dispiro-1,2,4,5-te traoxanes: alkyl-substituted 7,8,15,16-tetraoxadispiro[5.2.5.2]hexadecanes. *J. Med. Chem.*, **43**, 2753-2758.

200. Postner, G. (2003). Orally active, antimalarial, anticancer, artemisinin-derived trioxane dimmers with high stability and efficacy. *J. Med. Chem.*, **46**, 1060-1065.

201. Peters, W., Robinson, B. L. (1999). The chemotherapy of rodent malaria. LVI. Studies on the development of resistance to natural and synthetic endoperoxides. *Ann. Trop. Med. Parasitol.*, **93**, 325-329.

202. Sanni, L. A., Fonseca, L. F., Langhorne, J. (2002) Mouse models for erythrocytic-stage malaria. *Methods Mol. Med.*, **72**, 57-76.

203. Bloland, P. B. (2001). Drug Resistance in malaria. WHO/CDS/DRS/2001.4, 16.

204. Schapira A. (1988). The *Plasmodium falciparum* chloroquine *in vivo* test: extended follow-up is more important than parasite counting. *Trans. Royal Soc. Trop. Med. Hyg.*, **82**, 39-43.

205. Bruce-Chwatt, L. J. (1986). Chemotherapy of malaria, 2nd ed. Geneva, WHO Monograph Series No 27.

206. Brandling-Bennett, A. D., Oloo, A. J., Watkins, W. M., Boriga, D. A., Kariuki, D. M., Collins, W. E. (1988). Chloroquine treatment of falciparum malaria in an area of Kenya of intermediate chloroquine resistance. *Trans. Royal Soc. Trop. Med. Hyg.* **82**, 833-837.

207. WHO (1996). Assessment of therapeutic efficacy of antimalarial drugs for uncomplicated falciparum malaria in area with intense transmission. WHO/MAL/96.1077.

208. Plowe, C. V. (1995). Pyrimethamine and proguanil resistance-conferring mutations in *Plasmodium falciparum* dihydrofolate reductase: polymerase chain reaction methods for surveillance in Africa. *Am. J. Trop. Med. Hyg.* **52**, 565-568.

209. Su X. (1997). Complex polymorphisms in an approximately kDa protein are linked to chloroquine-resistant *P. falciparum* in Southeast Asia and Africa. *Cell*, **91**, 593-603.

Appendix

Table 31: Analytical Data for the complexes

Formulation	Empirical formula	Molar mass	% C	% H	% N	% M
trans-$[Co(en)_2Cl_2]Cl$	$CoC_4H_{16}N_4Cl_3$	285.49	16.85 (16.83)	5.69 (5.65)	19.68 (19.63)	21.17 (20.64)
cis–$[Co(en)_2Cl_2]Cl$	$CoC_4H_{16}N_4Cl_3$	285.49	16.85 (16.45)	5.69 (6.28)	19.68 (19.07)	21.17 (20.94)
$[Co(en)_2(CQ)Cl]Cl_2$	$CoC_{22}H_{34}N_7Cl_4$	597.30	43.01 (43.65)	6.31 (6.99)	16.50 (16.20)	9.29 (9.87)
$[Co(en)_2(AQ)Cl]Cl_2$	$CoC_{24}H_{38}N_7OCl$	641.36	45.52 (44.95)	5.78 (5.97)	15.22 (15.29)	9.37 (9.19)
$[Co(en)_2(TMP)_2]Cl_3$	$CoC_{32}H_{52}N_{12}O_6Cl_3$	866.13	44.56 (44.38)	6.00 (6.05)	19.12 (19.41)	6.80 (7.50)
$[Co(en)_2(TMP)Cl]Cl_2$	$CoC_{18}H_{34}N_8O_3Cl_3$	575.81	37.13 (37.55)	5.98 (5.95)	17.39 (19.46)	(10.2)
$[Co(en)_2(TCQ)Cl]Cl_2$	$CoC_{26}H_{40}N_6Cl_3O_8$	729.93	40.76 (42.78)	5.63 (5.52)	9.54 (11.53)	8.07 (8.07)
$[Co(en)_2(TCQ)Cl]Cl_2$	$CoC_{26}H_{40}N_6Cl_3O_8$	729.93	41.45 (42.78)	5.58 (5.52)	8.38 (11.53)	8.41 (8.07)
$[Co_2(QNC)(en)_4Cl_6]\cdot 2HCl$	$Co_2C_{31}H_{64}Cl_9N_{11}O$	1043.9	34.62 (35.67)	5.94 (6.18)	14.82 (14.76)	11.83 (11.29)
$[Co(SD)_2(H_2O)_2]$	$CoC_{20}H_{24}N_8O_6S_2$	595.91	40.07 (40.33)	3.92 (4.06)	18.76 (18.82)	9.62 (9.90)
$[Co(SD)_2(CH_3OH)_2]$	$CoC_{22}H_{26}N_8O_8S_2$	653.55	42.44 (42.51)	4.01 (4.22)	17.92 (18.02)	9.35 (9.48)
$[Cu(SD)_2(H_2O)_2]$	$CuC_{20}H_{22}N_8S_2O_6$	598.11	40.56 (40.16)	3.37 (3.71)	18.78 (18.73)	10.64 (10.62)
$[Zn(SD)_2(H_2O)_2]$	$ZnC_{20}H_{22}N_8O_6S_2$	599.94	39.85 (40.04)	3.45 (3.70)	18.25 (18.68)	(10.9)
$[Fe(SD)_3].(H_2O)_3$	$FeC_{30}H_{33}N_{12}O_9S_3$	857.71	42.46 (42.01)	3.56 (3.88)	19.23 (19.60)	6.48 (6.51)
$[Mn(SD)_2(H_2O)_2]$	$MnC_{20}H_{22}N_8O_6S_2$	589.50	39.58 (40.75)	3.62 (3.76)	18.53 (19.01)	(9.32)
$[Pd(SD)(H_2O)(CH_3OH)]$	$PdC_{11}H_{15}N_4O_4S$	405.74	32.42 (32.56)	3.51 (3.73)	13.60 (13.81)	(26.2)
$[Pt(SD)(H_2O)Cl]$	$PtC_{10}H_{11}N_4O_3SCl$	497.82	23.84 (24.13)	2.84 (2.23)	10.77 (11.25)	(39.1)
$[Ru(SD)_2(H_2O)Cl]$	$RuC_{20}H_{20}N_8O_5S_2Cl$	653.07	37.14 (36.78)	3.59 (3.09)	17.21 (17.16)	(15.0)
$[Ni(SD)_2(H_2O)_2]\cdot 2H_2O$	$NiC_{20}H_{26}N_8O_8S_2$	629.29	38.44 (38.17)	3.63 (4.16)	17.94 (17.81)	(9.33)
$[VO(SD)_2](H_2O)_2$	$VOC_{20}H_{22}N_8O_6S_2$	601.51	40.56 (39.94)	3.56 (3.69)	18.05 (18.63)	(8.47)
$[Co(TMP)_2Cl_2]$	$CoC_{28}H_{36}N_8O_6Cl_2$	710.48	47.24 (47.34)	5.01 (5.11)	15.81 (15.77)	8.35 (8.29)
$[Co_2(TMP)_2(OAc)_4\cdot$	$Co_2C_{51}H_{67}N_8O_{15}$	1150.0	52.53	5.87	9.82	10.16

$2C_7H_8{\cdot}CH_3O$]			(53.27)	(5.85)	(9.74)	(10.25
[Pt(TMP)(H_2O)Cl_2]·H_2O	$PtC_{14}H_{22}N_4O_5Cl_2$	592.34	28.13	3.34	9.30	(32.9)
			(28.39)	(3.74)	(9.46)	
[Pd(TMP)(H_2O)Cl_2]	$PdC_{14}H_{22}N_4O_5Cl_2$	503.68	33.17	4.23	10.97	(21.1)
·H_2O			(33.39)	(4.40)	(11.12)	
[Ni(TMP)$_2$(CH_3OH)$_2$	$NiC_{34}H_{50}N_8O_{12}$	821.53	49.56	5.94	13.46	7.02
(OAc)$_2$]			(49.71)	(6.14)	(13.64)	(7.17)
[Mn(TMP)(CH_3OH)Cl_2]	$MnC_{15}H_{22}N_4O_4Cl_2$	448.21	40.38	4.95	12.62	(12.2)
			(40.20)	(5.10)	(12.50)	
[Fe(AQ)($C_3H_6NS_2$)Cl_3]	$FeC_{23}H_{40}N_4O_7S_2Cl_4$	746.37	35.85	4.97	6.49	(7.4)
·$3H_2O$			(37.01)	(5.40)	(7.51)	
Na_2[Pt(CQB)$_2$$Cl_4$]	$PtC_{36}H_{56}N_6Cl_6O_2$	976.65	42.39	5.47	7.80	(19.3)
			(42.70)	(5.57)	(8.30)	
[Fe(Prym)$_2$($C_3H_6NS_2$)Cl_2]	$FeC_{27}H_{32}N_9Cl_4S_2$	744.57	44.04	4.59	17.09	(7.50)
			(43.57)	(4.33)	(16.93)	
[Fe(Prym)$_2$(TMP)Cl_3]·CH_3	$FeC_{39}H_{52}N_{12}O_6Cl_4$	982.58	47.45	5.31	17.01	(5.68)
OH			(47.67)	(5.33)	(17.11)	
[Co(TMP)$_2$$Cl_2$($CH_3OH$)$_2$]	$CoC_{30}H_{44}N_8O_8Cl_2$	774.57	46.18	5.22	13.93	(7.61)
			(46.52)	(5.73)	(14.47)	

Found (Expected)

Table 32: Some physical properties of the complexes

Formulation	Empirical formula	Molar mass	Colour	M. Pt (° C)	% Yield	μ (BM)
trans-$[Co(en)_2Cl_2]Cl$	$CoC_4H_{16}N_4Cl_3$	285.49	Green		78	0.59
cis-$[Co(en)_2Cl_2]Cl$	$CoC_4H_{16}N_4Cl_3$	285.49	Green		89	0.45
$[Co(en)_2(CQ)Cl]Cl_2$	$CoC_{22}H_{34}N_7Cl_4$	597.30	Green	246	48	0.47
$[Co(en)_2(AQ)Cl]Cl_2$	$CoC_{24}H_{38}N_7OCl$	641.36	Green	236	67	
$[Co(en)_2(TMP)_2]Cl_3$	$CoC_{32}H_{52}N_{12}O_6Cl_3$	866.13	Green	228	72	0.32
$[Co(en)_2(TMP)Cl]Cl_2$	$CoC_{18}H_{34}N_8O_3Cl_3$	575.81	Green	224	37	0.56
$[Co(en)_2(TCQ)Cl]Cl_2$	$CoC_{26}H_{40}N_6Cl_3O_8$	729.93	Brown	218	56	0.44
$[Co(en)_2(TCQ)Cl]Cl_2$	$CoC_{26}H_{40}N_6Cl_3O_8$	729.93	Brown	241	54	0.52
$[Co_2(QNC)(en)_4Cl_6]\cdot 2HCl$	$Co_2C_{31}H_{64}Cl_9N_{11}O$	1043.9	Light green	334	68	
$[Co(SD)_2(H_2O)_2]$	$CoC_{20}H_{24}N_8O_6S_2$	595.91	Pink	334	89	4.86
$[Co(SD)_2(CH_3OH)_2]$	$CoC_{22}H_{26}N_8O_8S_2$	653.55	Pink	345	75	4.93
$[Cu(SD)_2(H_2O)_2]$	$CuC_{20}H_{22}N_8S_2O_6$	598.11	Brown	247	76	1.88
$[Zn(SD)_2(H_2O)_2]$	$ZnC_{20}H_{22}N_8O_6S_2$	599.94	White	236	87	
$[Fe(SD)_3].(H_2O)_3$	$FeC_{30}H_{33}N_{12}O_9S_3$	857.71	Light brown	247	79	5.4
$[Mn(SD)_2(H_2O)_2]$	$MnC_{20}H_{22}N_8O_6S_2$	589.50	Cream	234	64	5.86
$[Pd(SD)(H_2O)(CH_3OH)]$	$PdC_{11}H_{15}N_4O_4S$	405.74	Brown	211	67	0.24
$[Pt(SD)(H_2O)Cl]$	$PtC_{10}H_{11}N_4O_3SCl$	497.82	Yellow	235	76	0.32
$[Ru(SD)_2(H_2O)Cl]$	$RuC_{20}H_{20}N_8O_5S_2Cl$	653.07	Dark brown	224	85	1.89
$[Ni(SD)_2(H_2O)_2]\cdot 2H_2O$	$NiC_{20}H_{26}N_8O_8S_2$	629.29	Green	228	78	2.98
$[VO(SD)_2](H_2O)_2$	$VOC_{20}H_{22}N_8O_6S_2$	601.51	Blue			
$[Pt(TMP)(H_2O)Cl_2]\cdot H_2O$	$PtC_{14}H_{22}N_4O_5Cl_2$	592.34	Yellow	214	39	0.34
$[Pd(TMP)(H_2O)Cl_2]\cdot H_2O$	$PdC_{14}H_{22}N_4O_5Cl_2$	503.68	Brown	237	68	0.24
$[Mn(TMP)(CH_3OH)Cl_2]$	$MnC_{15}H_{22}N_4O_4Cl_2$	448.21	Cream	231	48	
$[Fe(AQ)(C_3H_6NS_2)Cl_3]\cdot 3H_2O$	$FeC_{23}H_{40}N_4O_7S_2Cl_4$	746.37	Dark brown	256	56	
$Na_2[Pt(CQB)_2Cl_4]$	$PtC_{36}H_{56}N_6Cl_6O_2$	976.65	Yellow	213	32	
$[Fe(PY)_2(C_3H_6NS_2)Cl_2]$	$FeC_{27}H_{32}N_9Cl_4S_2$	744.57	Brown	223	57	5.3
$[Fe(PY)_2TMP(CH_3OH)Cl_2].2H_2O$	$FeC_{39}H_{52}N_{12}O_6Cl_4$	982.58	Brown	212	63	5.1

Table 36. Selected IR data (cm^{-1}) for sulfadiazine and the complexes

Formulation	$\nu(NH_2)$	$\nu(C=N)$	$\nu(SO_2)$ asym.	$\nu(SO_2)$ sym.	$\nu(SN)$	$\nu(MN)$	$\nu(MO)$
Sulfadiazine	3422vs 3355vs	1652vs	1325vs	1157vs	942s		
$[Co(SD)_2(CH_3OH)_2]$	3437vs 3347s	1625w	1267s	1129vs	987vs	596vs	390s
$[Co(SD)_2(H_2O)_2]$	3480vs 3248m	1652w 1621s	1263vs 1240vs	1124s	989	588vs	426s 390s
$[Cu(SD)_2(H_2O)_2]$	3448s 3368s	1631vs	1277ms	1126	971	526s	412s
$[Zn(SD)_2(H_2O)_2]$	3423vs 3355vs	1628s	1325vs 1264ms	1133s 1079s	977vs	388s	288s
$[Mn(SD)_2(H_2O)_2]$	3454s 3176s	1654vs	1326vs 1264s	1132s	946vs	345s	278s
$[Ni(SD)_2(H_2O)_2]\cdot 2H_2O$	3468s 3369s	1630vs	1263ms	1125ms	966s	378s	342w
$[Pd(SD)_2(H_2O)_2]$	3342s 3322s	1630s	1258ms	1124s	970vs	511s	409s
$[Pt(SD)_2(H_2O)_2]$	3417s 3318s	1631vs	1260s	1124s	968vs	512s	423s

Abbreviations: v = very; s = strong; m = medium; w = weak.

IR spectrum of $[Ru(SD)_2(H_2O)Cl]$

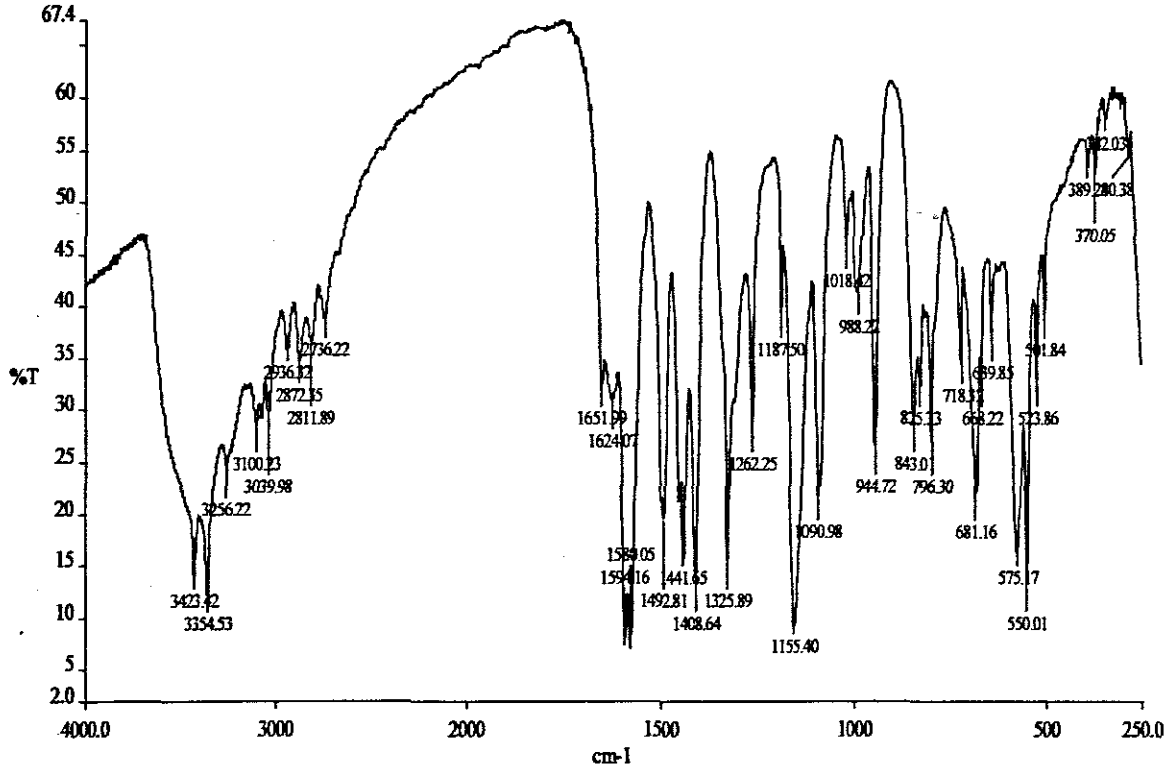

Wavenumbers/cm^{-1}

IR Spectrum of sulfadiazine

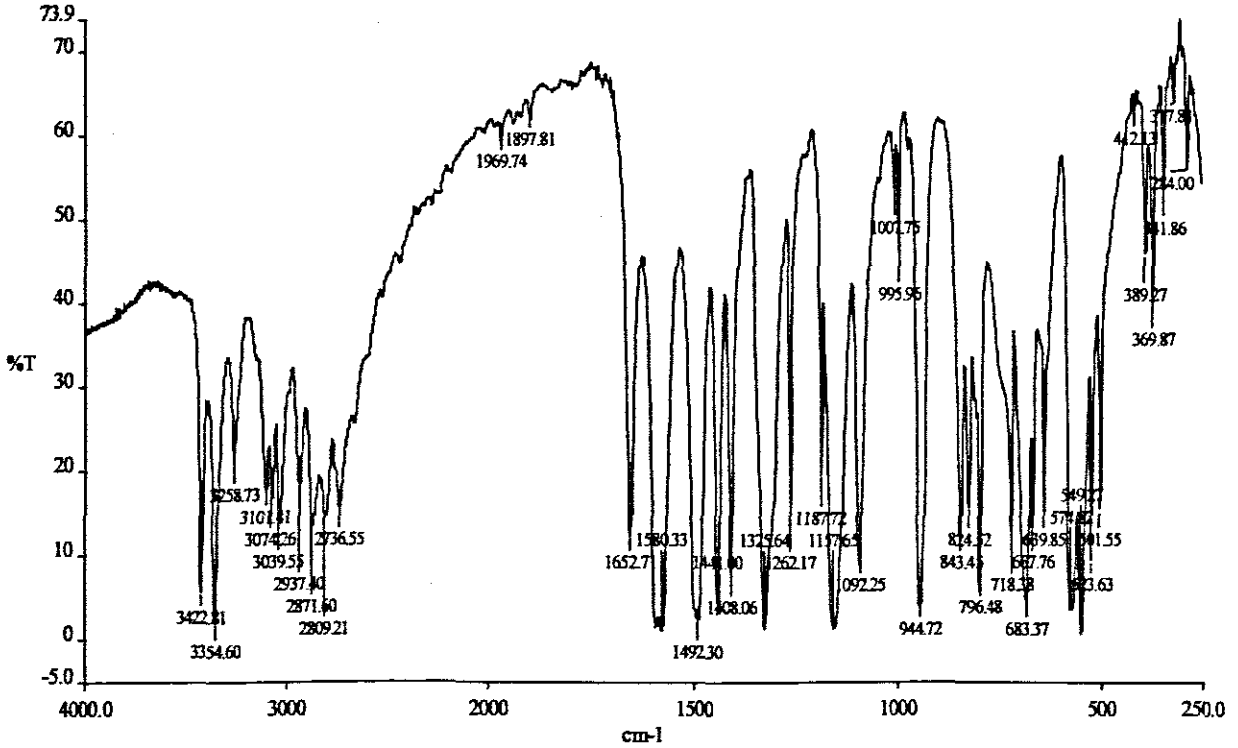

Wavenumbers/cm^{-1}

IR Spectrum of $Na_2[Pt(CQ)_2Cl_4]$

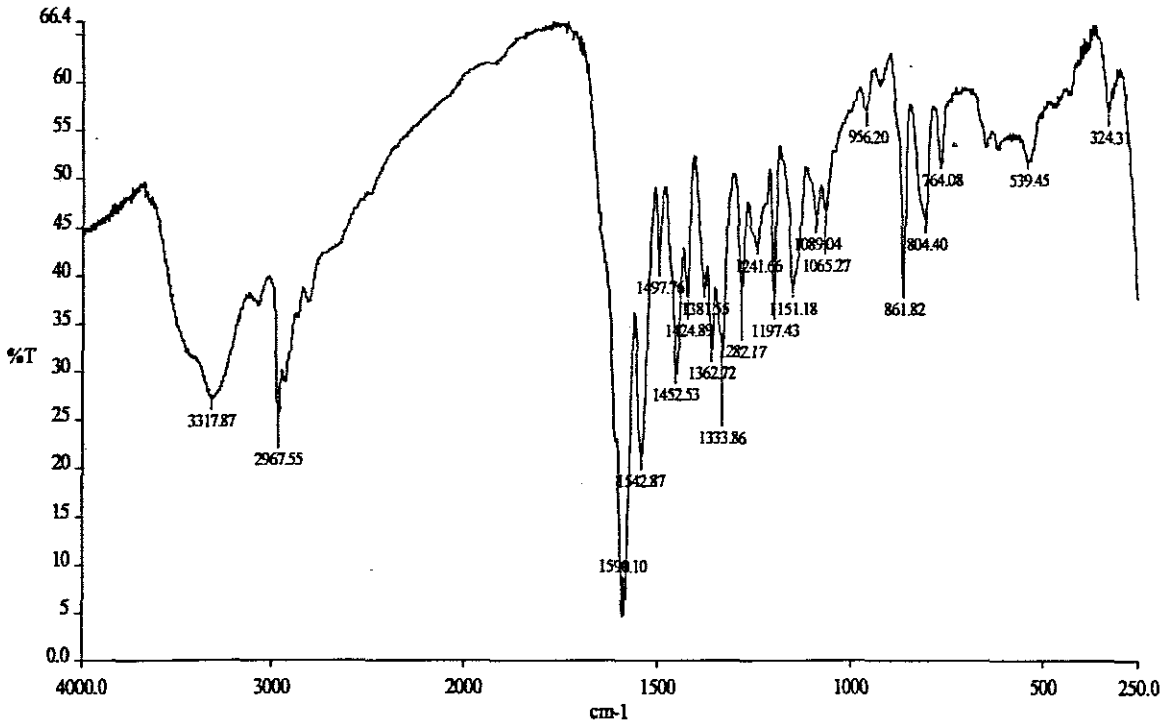

Wavenumbers/cm^{-1}

IR Spectrum of $[Co(en)_2(CQ)Cl_2]Cl$

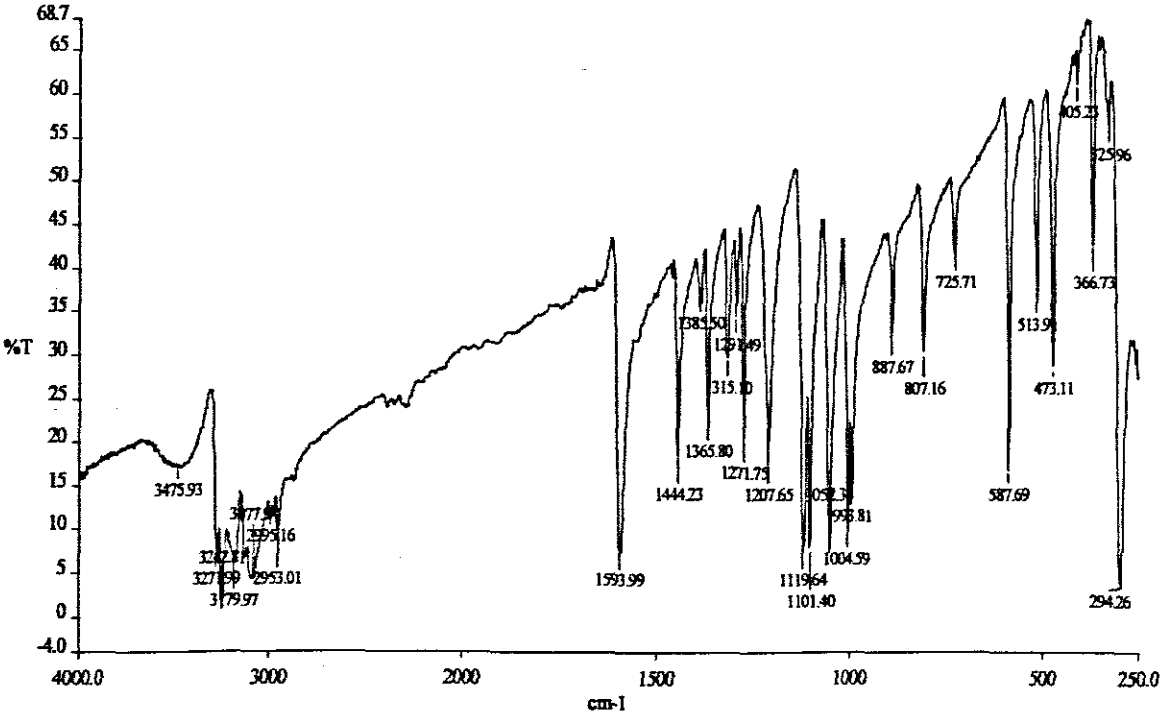

Wavenumbers/cm^{-1}

IR Spectrum of $[Fe(Py)_2(TMP)(CH_3OH)Cl_2]\cdot 2H_2O$

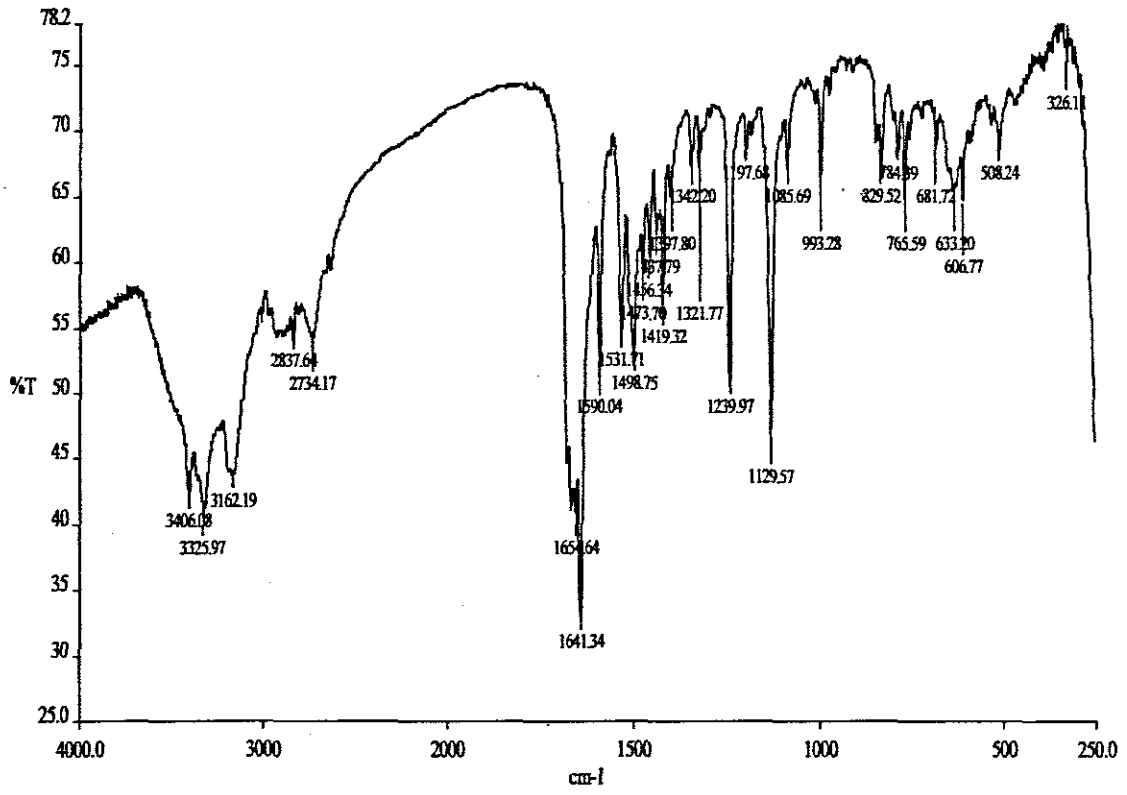

Wavenumbers/cm^{-1}

IR Spectrum of $[Cu(TMP)_2(CH_3COO)_4]\cdot 2C_6H_8.CH_3OH$

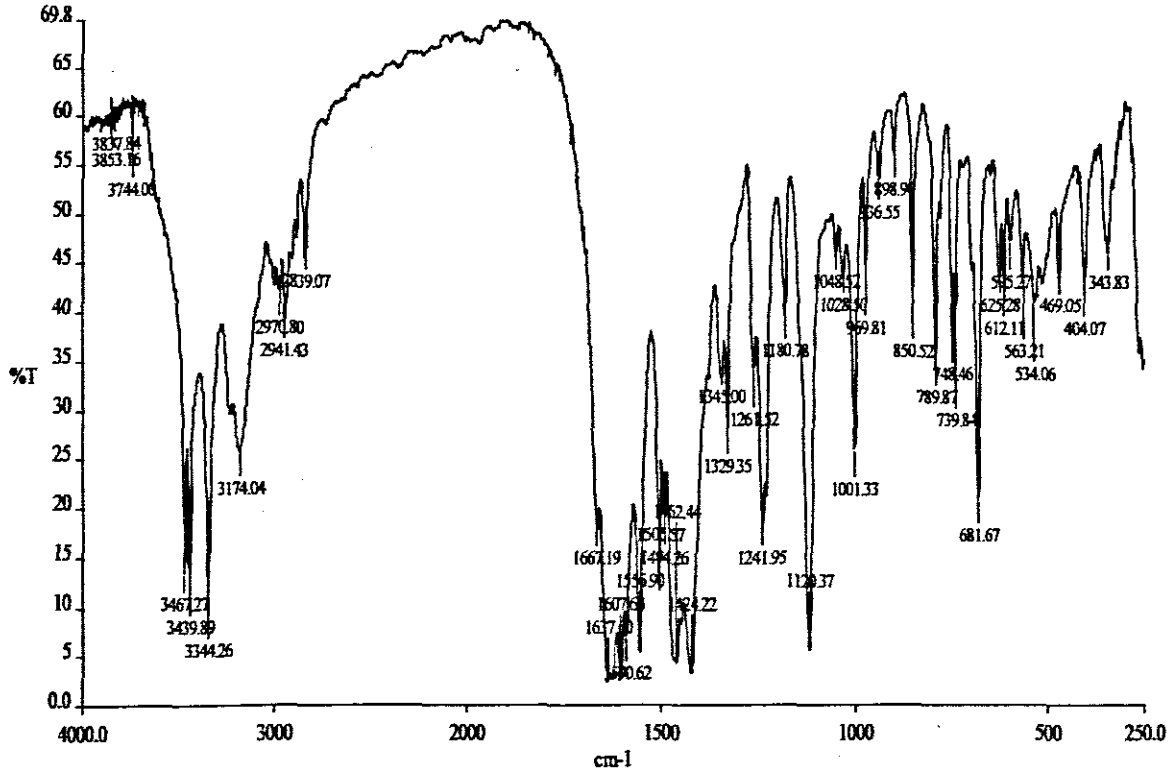

Wavenumbers/cm^{-1}

IR Spectrum of $[Mn(TMP)(CH_3OH)Cl_2]$

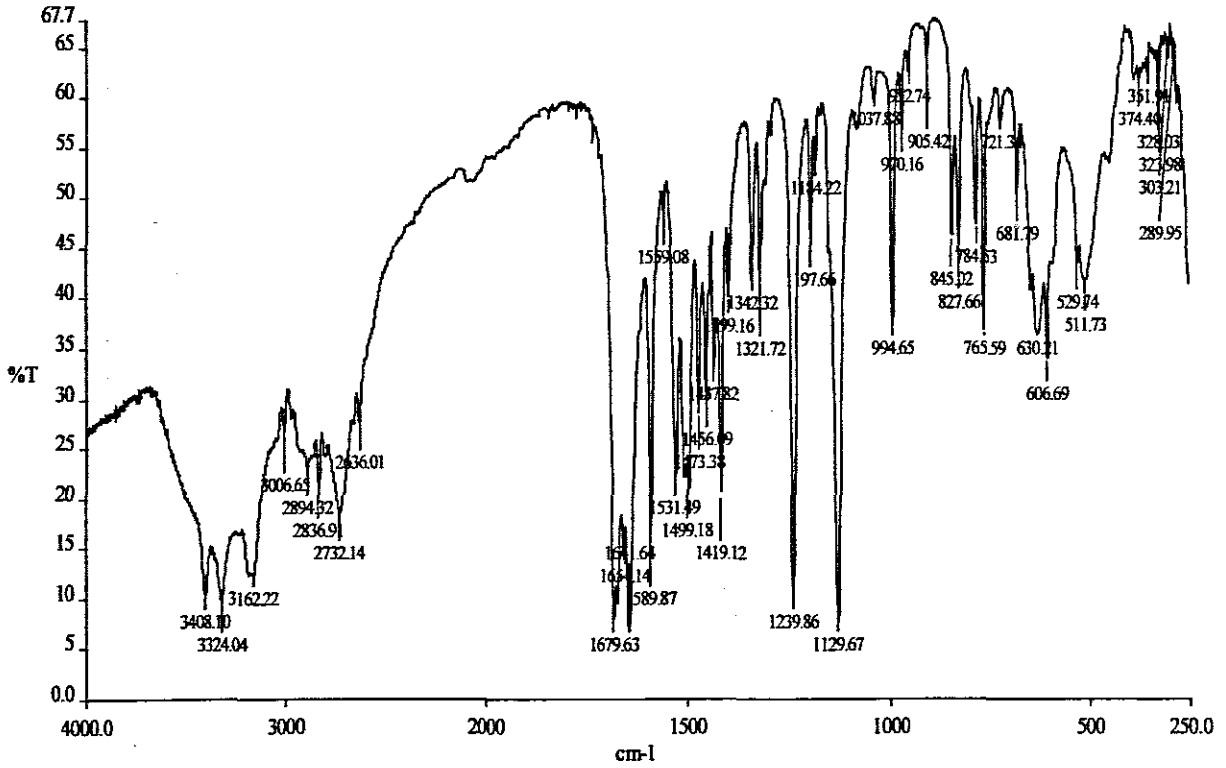

Wavenumbers/cm^{-1}

IR Spectrum of $[Pd(TMP)(H_2O)Cl_2]\cdot H_2O$

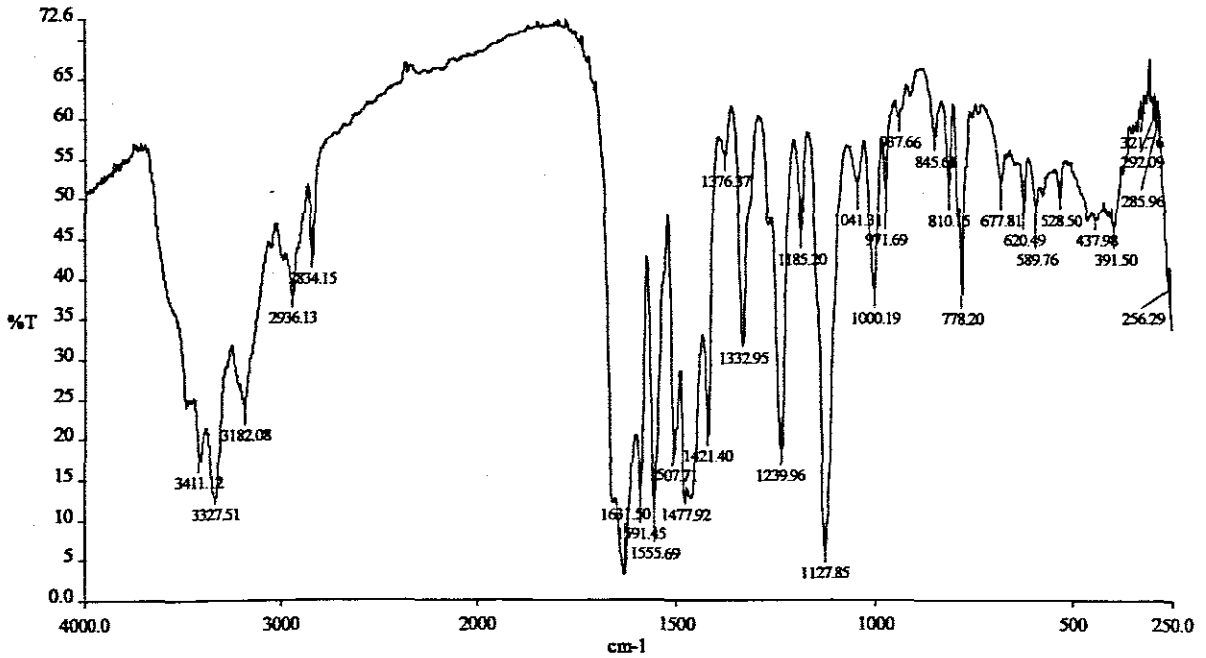

Wavenumbers/cm^{-1}

IR Spectrum of [Ni(TMP)2(CH3OH)(CH3O)]

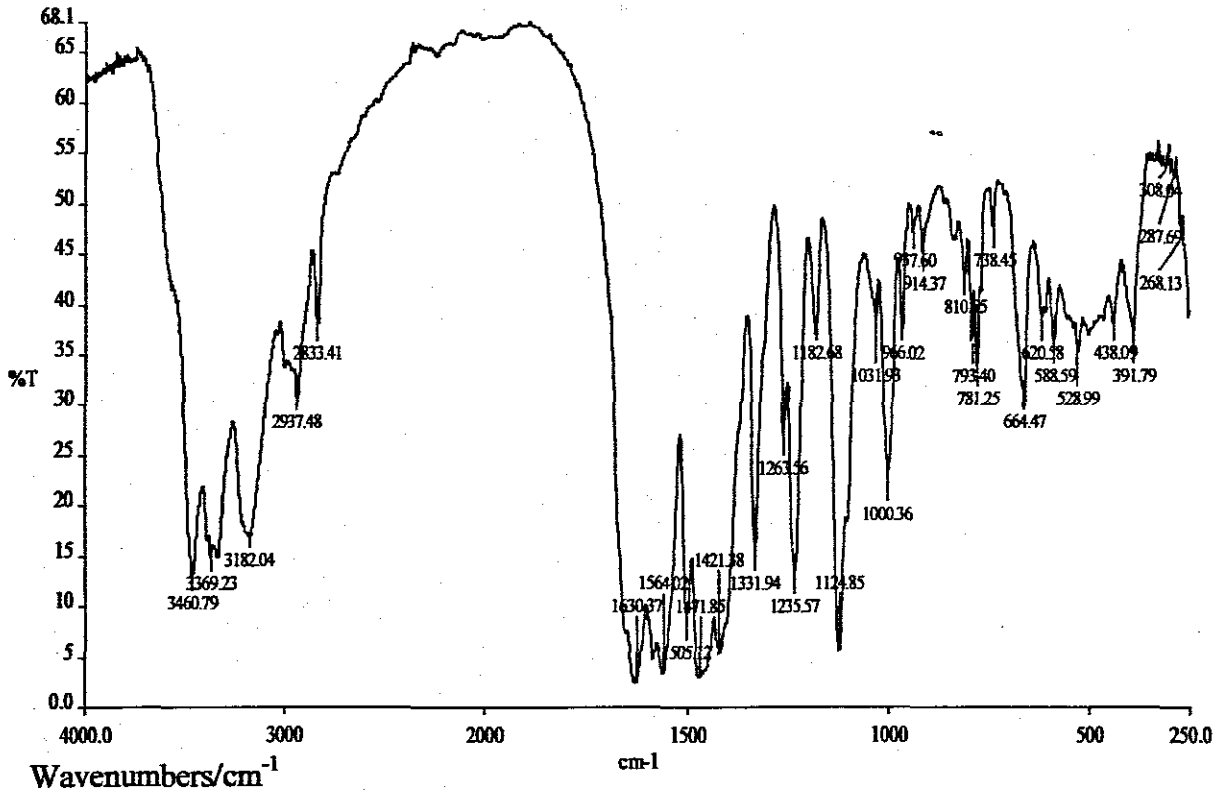

IR Spectrum of $[Co(en)_2(TMP)Cl]Cl_2$

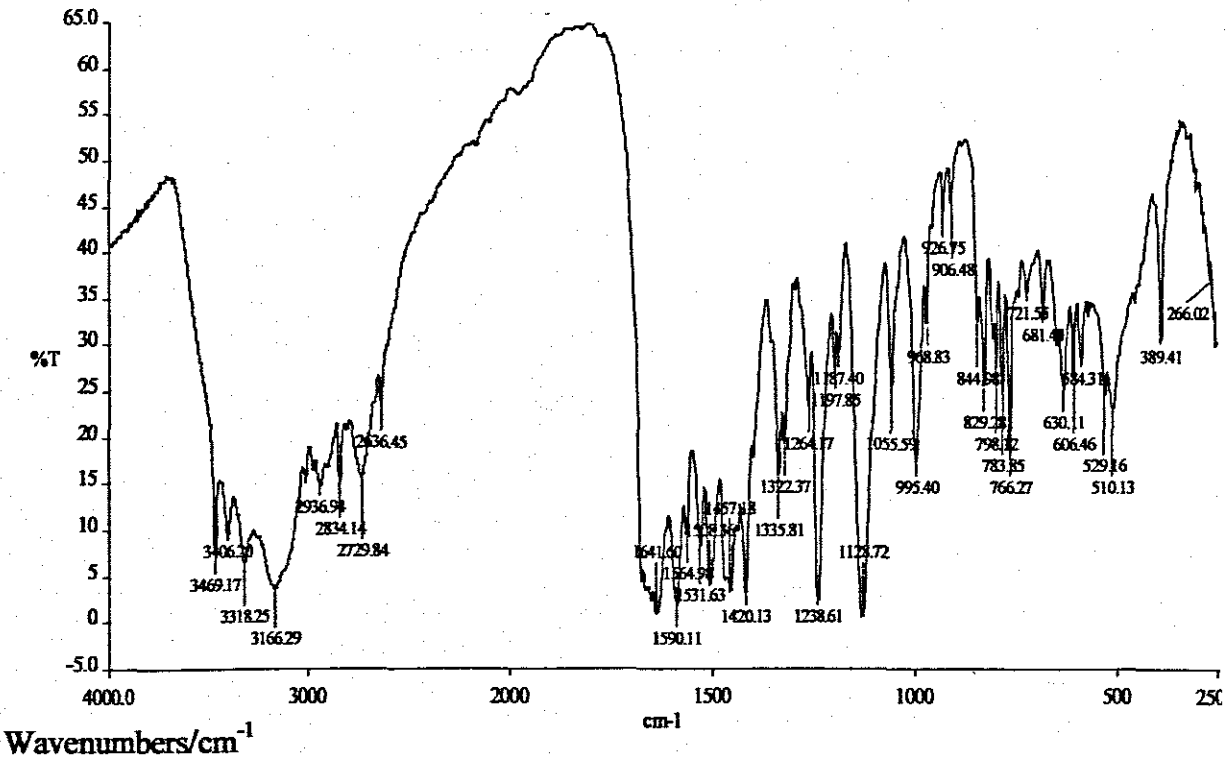

IR Spectrum of Amodiaquine

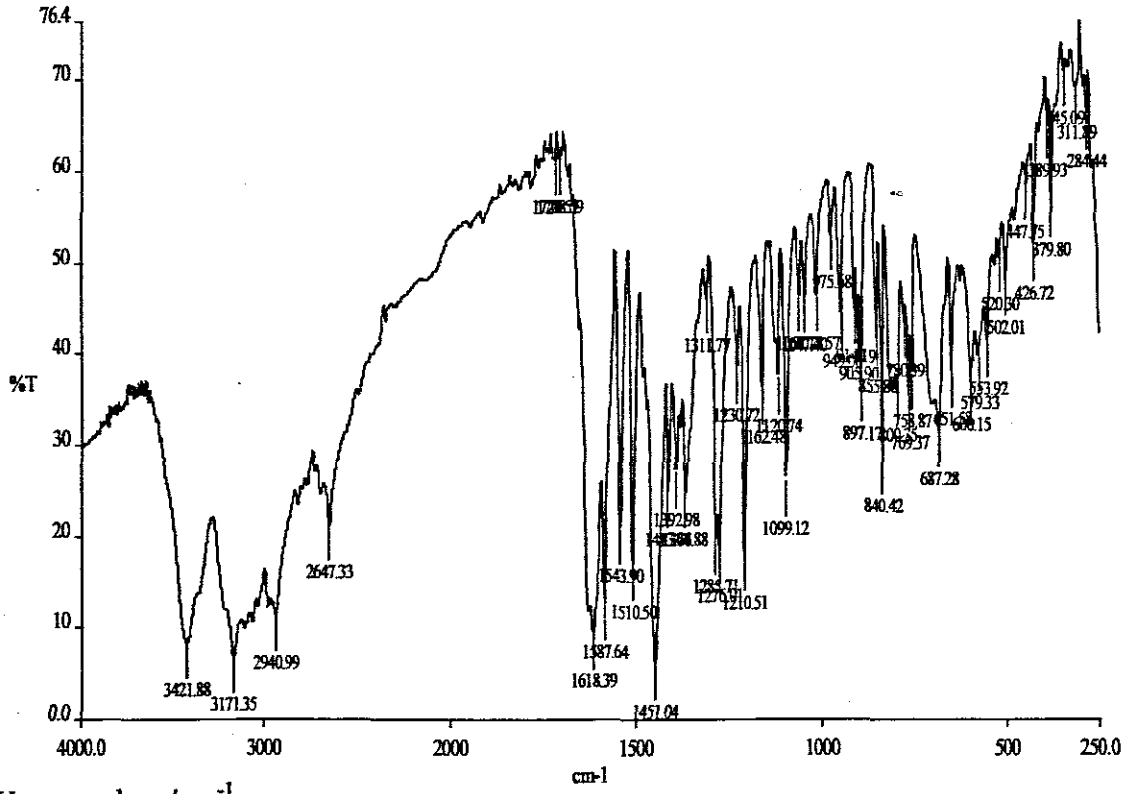

Wavenumbers/cm^{-1}

IR Spectrum of $[Fe(AQ)(C_3H_6NS_2)Cl_2]\cdot 3H_2O$

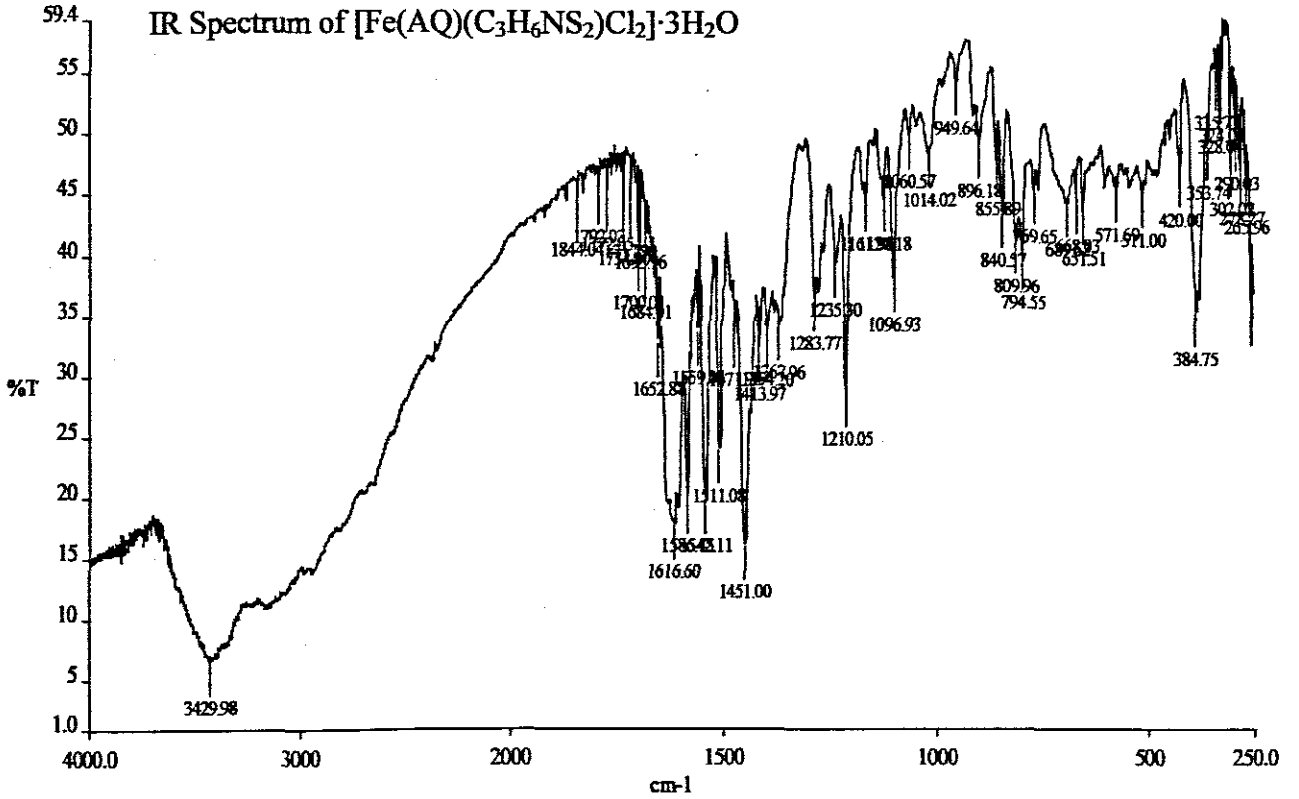

Wavenumbers/cm^{-1}

IR Spectra of *cis/trans* Co(III) amodiaquine complexes